

**DEVELOPMENT OF AN ANISOTROPIC SWELLING HYDROGEL
FOR TISSUE EXPANSION: CONTROL OVER THE DEGREE,
RATE AND DIRECTION OF HYDROGEL SWELLING**

A Dissertation
Presented to
The Academic Faculty

by

Jinhyun Lee

In Partial Fulfillment
of the Requirements for the Degree
Doctor of Philosophy in the
School of Polymer, Textile and Fiber Engineering

Georgia Institute of Technology
December 2008

Copyright 2008 by Jinhyun Lee

**DEVELOPMENT OF AN ANISOTROPIC SWELLING HYDROGEL
FOR TISSUE EXPANSION: CONTROL OVER THE DEGREE,
RATE AND DIRECTION OF HYDROGEL SWELLING**

Approved by:

Dr. David G. Bucknall, Advisor
School of Polymer, Textile & Fiber
Engineering
Georgia Institute of Technology

Dr. L. Andrew Lyon
School of Chemistry and Biochemistry
Georgia Institute of Technology

Dr. Haskell Beckham
School of Polymer, Textile & Fiber
Engineering
Georgia Institute of Technology

Dr. Yonathan S. Thio
School of Polymer, Textile & Fiber
Engineering
Georgia Institute of Technology

Dr. Yadong Wang
Department of Bioengineering and The
McGowan Institute for Regenerative
Medicine
University of Pittsburgh

Date Approved: November 4, 2008

나의 아버지 이 윤택 님과
나의 어머니 서 옥주 님께
바칩니다.

dedicated to

my father
YOON-TAEK LEE

and

my mother
OK-JOO SEO

ACKNOWLEDGEMENTS

First, I would like to thank God who always gives me infinite love and strength and leads me to the brightest and best way.

I would like to express my sincere gratitude to my advisor, Prof. David G. Bucknall for his support, guidance, and encouragement to achieve my goal over the past four years at Georgia Institute of Technology. I have felt lucky to have him as my thesis advisor who has listened to me and given me the freedom to pursue and explore this research, thus I could have more enjoyed working on this research. Without him, I could not have accomplished this research work about this much. It was a privilege to be his student.

I wish to thank my committee members, Prof. Haskell Beckham, Prof. L. Andrew Lyon, Prof. Yonathan S. Thio, and Prof. Yadong Wang for their valuable suggestion, critique, and advice of my work. I would also like to thank Prof. Anselm Griffin and Prof. Karl Jacob, Prof. Seung Soon Jang and his group, especially Seung Geol Lee, and Dr. Marc C. Swan for their valuable discussion.

I am grateful to Prof. Andrew Lyon's group, especially Dr. Neetu Singh, Prof. Mohan Srinivasarao and his group, especially Dr. Jung Ok Park, and Matija Crne, Prof. Meisha Shofner and his group, especially Jasmeet Kaur, Prof. Ken Gall and his group, especially Matthew DiPrima, and Prof. Haskell Beckham's group, especially Dr. Marcus Foston and Ryan Kincer for sharing their instruments and labs and assisting with their instruments.

I would also like to acknowledge Dr. Johannes Leisen for providing help with much of magnetic resonance imaging, Dr. Shanju Zhang for helping with scanning electron microscope and Dr. Kunsang Yoon for his guidance about how to purify monomers and the understanding of chemical reactions.

I must thank Prof. David Bucknall's group members, Bilge Hatiboglu, Katie Campbell, Zhan (Jennifer) Liu, and Dr. Xi Wang for not only making my laboratory and office enjoyable and exciting but also supporting me with kind and warm cheers.

I would like to thank my friends, Kishor Kumar Gupta, Vibhor Jain, Shamal Mhetre, and Mihir Anil Oka who came to PTFE at Georgia Tech at the same time and went through all courses of PhD program together for sharing time with me and giving me full of memories.

I would like to express my appreciation to Dr. Kyoungweon Park, Dr. Sunghyun Nam, and Dr. Han Gi Chae for guiding and adjusting me to the life in PTFE at Georgia Tech.

I must thank Prof. Steven Boggs who trusted and helped me to pursue my goal continuously in the USA and my former advisor Prof. Patrick T. Mather who have given me continuous advice and concern on my career.

I would like to thank my former advisor Prof. Hyoung Jin Choi who made me awaken to study in polymers and has continuously advised, Prof. In-Joo Chin who has always encouraged me for study, Prof. Soon-Ja Choi who also inspired me to be a good female scientist, and Dr. Young-Chang Noh who let me have great interest in hydrogels.

I also thank the members of the Sugarloaf Korean Baptist Church and the Open

Community Church for their love and prayer. I would like to thank Sungmin Kim, Myongsub Kim, Jonghan Lee, Sungho Kim, Sangmin Lee, Hyojin Kwon, Hyemi Kim, and YooJin Kim for making my Atlanta life lovely, enjoyable and unforgettable and for supporting with warm cheers.

I also thank my friends, Smita, Janet, Emma, Arun, Jinhee and Yookang for cheering me all the time and my friends in South Korea, Hyoungmin, Miyoung, Soyoung, Buyoun, and Sunghye for their care and love for long time.

Finally, I am deeply grateful to my family. I enormously thank my parents, Yoon-Taek Lee and Ok-Joo Seo who have showed me their vision of the future and respectful philosophy of life for their bottomless love, support, understanding, and encouragement for many years. I also thank my sisters, Jin-Sook and Sook-Hyun and my brother, Jin-Kyoo for their endless love and precious prayer and support. I would like to genuinely thank my grandmother, Nami Jang in heaven who loved and encouraged me to be bright and dignified and still help me to be robust.

TABLE OF CONTENTS

	Page
ACKNOWLEDGEMENTS	iv
LIST OF TABLES	xiv
LIST OF FIGURES	xvi
LIST OF SYMBOLS AND ABBREVIATIONS	xxvi
SUMMARY	xxxv
 <u>CHAPTER I. INTRODUCTION</u>	 1
 <u>CHAPTER II. BACKGROUND</u>	 4
2.1. Tissue Expanders	4
2.1.1. History of Tissue Expanders	4
2.1.2. Polymers for Hydrogel Tissue Expanders	8
2.1.3. In Vitro/In-Vivo Swelling and Biocompatibility of Hydrogel Tissue Expander	9
2.2. Hydrogels	11
2.2.1. Classification and Applications	11
2.2.2. Synthesis	12
2.2.3. Characterization of Gels	13
2.2.3.1. Gel Fraction, GF	13
2.2.3.2. Gel Composition and Chemical Structure	14
2.2.3.3. Thermal Properties of gels	14
2.2.3.4. Gels Swelling	15
2.2.3.5. Mechanical Properties of Hydrogels	17

2.2.3.6. Hydrogel Internal Morphology	18
2.2.3.7. Biocompatibility of Hydrogels	19
2.2.4. Swelling Behavior of Hydrogels	21
2.2.4.1. Thermodynamics of Hydrogel Swelling	21
2.2.4.2. Kinetics of Hydrogel Swelling: Penetrant Diffusion in Hydrogels	27
2.2.4.3. Change in Transparency During Swelling	29
2.2.5. Mechanical Properties	30
2.2.6. Network Structure Characteristics	32
2.2.7. Parameters Affecting on Swelling and Network Structure	34
2.2.7.1. Control in the Structure of Hydrogels	35
2.2.7.1.1. Type and Composition of Feed Monomers	35
2.2.7.1.2. Type and Concentration of Initiator	36
2.2.7.1.3. Type and Concentration of Crosslinker	37
2.2.7.1.4. Intensity of UV Irradiation	39
2.2.7.1.5. Hydrophobicity	40
2.2.7.1.6. Inclusions	41
2.2.7.2. External Conditions	42
2.2.7.2.1. Temperature of Swelling	42
2.2.7.1.2. pH	43
2.2.7.1.3. Penetrant	46
2.2.7.1.4. Applied Electric or Magnetic fields	48
2.3. Anisotropic Swelling of Hydrogels	50
References	55
 <u>CHAPTER III. EXPERIMENTS</u>	 69

3.1. Preparation of Hydrogel Systems	69
3.1.1. Synthesis of VP/HEMA Gels	69
3.1.2. Synthesis of VP/AA Gels	73
3.1.2.1. Isotropic VP/AA Gel Systems	73
3.1.2.2. The Optimization of Gel Systems for Anisotropic Swelling Studies	74
3.1.3. Synthesis of VP/ <i>n</i> MA (<i>n</i> series methacrylate) Gels	76
3.1.4. Silver Nanoparticles-Gel Composite	77
3.1.5. Encapsulation of Gels	78
3.1.6. Multilayer of Gels and Elastomers (GE-MULTI)	79
3.1.7. Anisotropic Swelling Hydrogels	80
3.1.7.1. Morphologically Gradient-Induced Anisotropic Swelling Hydrogels	80
3.1.7.2. Compressive Stress-Induced Anisotropic Swelling Hydrogels	80
3.2. Characterization of Gels and Hydrogels	83
3.2.1. Gelation Percent	83
3.2.2. Infrared Spectroscopy of Xerogels	83
3.2.3. Thermal properties of Xerogels	84
3.2.4. Internal Structure of Xerogels and Gels	84
3.2.5. Opaque Color Shown in Heated Gels/Compressed Gel: Optical Microscopy	85
3.2.6. Anisotropy of the compressed gels: Birefringence	85
3.2.7. Swelling Behavior of Gels	86
3.1.7.1. Swelling Ratio (<i>q</i>)	86
3.1.7.2. The Swelling Rate	87
3.2.8. Mechanical Properties of Hydrogels and Gels	88

3.2.9. Structural Characteristics M_c & v_e and Interaction Parameter, χ of Hydrogel	89
3.1.9.1. VP/HEMA hydrogels	89
3.1.9.2. VP/AA hydrogels	89
Reference	90

CHAPTER IV. CONTROL OVER SWELLING DEGREE AND RATE OF NEUTRAL HYDROGEL OF VP/HEMA COPOLYMER

4.1. UV-Polymerized VP/HEMA Gels	93
4.1.1. Composition of Xerogels	93
4.1.2. Gelation of Xerogels	97
4.1.3. Thermal Analysis	99
4.1.4. Color Changes in Gels	103
4.1.5. Swelling Kinetics of Gels	103
4.1.6. Characteristics of VH/HEMA hydrogels	108
4.1.6.1. Effect of Feed Ratio of VP and HEMA	108
4.1.6.2. Effect of Initiator Concentration (C_I)	110
4.1.6.3 Effect of UV irradiation Intensity (I_{UV})	112
4.1.6.4. Molecular Network Structure of UVHIB Hydrogels	114
4.1.6.5. Effect of Crosslinker Concentration (C_C) and Type	115
4.2. Thermal Polymerized VP/HEMA Gels	125
4.2.1. The Gelation and Composition of Gel	125
4.2.2. Glass Transition Temperature, T_g	126
4.2.3. Morphology	127
4.2.4. Swelling Studies	128
4.3. Conclusions	133

References	136
 <u>CHAPTER V. CONTROL OVER SWELLING DEGREE AND RATE OF IONIC HYDROGEL OF VP/AA COPOLYMER</u>	 142
5.1. Comparison of swelling behavior of VP/HEMA gels and VP/AA gels	142
5.2. UV-Polymerized VP/AA Gels with Various Ratios of Monomers	144
5.2.1. Swelling Behavior	144
5.2.2. Mechanical Stiffness of VP/AA Hydrogels	150
5.2.3. pH-Dependent Swelling Behavior	151
5.2.4. Structure Parameters, M_c & v_e and Interaction Parameter, χ	152
5.2.5. Temperature-Dependent Swelling Behavior	155
5.2.6. Gelation Percent of VP/AA Xerogels	156
5.2.7. Glass Transition Temperature, T_g	157
5.2.8. IR Spectroscopy of VP/AA Xerogels	159
5.2.9. Possible Explanations of Anomalous Composition-Dependent Swelling Behavior	162
5.3. Effect of Crosslinker Concentration (C_C) and Type on VP/AA Hydrogel	164
5.4. Final Optimization of the VP/AA Gel System for Anisotropic Swelling: Effect of C_I on the Swelling of the Gels by UV-Initiated or Thermal Polymerization	167
5.5. Conclusion	174
References	176
 <u>CHAPTER VI. CONTROL OVER SWELLING RATE OF OTHER GEL SYSTEMS</u>	 179
6.1. VP Based Gels with Hydrophobic Species	179
6.1.1. Swelling Studies	181
6.1.2. Mechanical Stiffness and Structural Parameters (M_c and v_e)	185

6.2. VP/HEMA Gel Composites with Silver Nanoparticles	187
6.2.1. Preparation and Swelling Studies	187
6.3. VP/HEMA Gels Encapsulated by Elastomer films	190
6.3.1. Elastomeric Films to Encapsulate Gels	190
6.3.2. Swelling Studies	193
6.4. Multilayer of Elastomer and Hydrogels	196
6.4.1. Preparation and Swelling Studies	196
6.5. Conclusions	199
References	201
 <u>CHAPTER VII. CONTROL OVER SWLLING DIRECTION- CONTROLLED ANISOTROPIC SWELLING</u>	 204
7.1. Swelling of Gradient Hydrogels	205
7.1.1. Assumption of Gradient Morphology-Induced Anisotropic Swelling	205
7.1.2. Swelling Studies	207
7.2. Compressed Force Induced Anisotropic Swelling of Gels	212
7.2.1. VP/AA Gels Compressing Conditions	212
7.2.2. Gel Network Structure Change under Applied Compression	215
7.2.3. Fixicity of Gels	216
7.2.4. Morphology	218
7.2.5. Birefringence of the Compressed Gels	227
7.2.6. Thermomechanic Cycle of Compression, Anisotropic Swelling, and Deswelling of Gels	229
7.2.7. Swelling Studies-Anisotropic Swelling	231
7.3. Conclusions	242
References	245

<u>CHAPTER VIII. CONCLUDING REMARKS AND FUTURE WORK</u>	248
APPENDIX A: Development of Photomasks	250
APPENDIX B: Spatial Distribution of Self-Diffusion Coefficients (D_s) of Water in Gradient Hydrogels	254

LIST OF TABLES

	Page
Table 2.1. Swelling of AAc/MBI Hydrogel in various solvents	46
Table 3.1. Conditions of UV initiated synthesis for VP/HEMA gels crosslinked with BIS65	70
Table 3.2. VP/HEMA gels UV initiated synthesized with various concentrations of GLY and DEGDA with feed VP:HEMA weigh ratio of 9:1, 0.8 wt. % Irgacure 651 and Mask3	72
Table 3.3. Feed monomer ratio of VP/HEMA gels thermal synthesized with 0.35 wt. % AIBN and 0.2 wt. % BIS	73
Table 3.4. Monomer feed ratio of VP/HEMA gels synthesized with various feed monomer ratio using 0.8 wt. % Irgacure 651, 0.2 wt. % BIS and Mask 3	74
Table 3.5. Synthesis Conditions for VP/AA gels	75
Table 3.6. VP/ <i>n</i> MA gels photo-polymerized with 0.8 wt % Irgacure 651, 0.2 wt.% BIS, and Mask3	76
Table 3.7. The conditions of preparing PDMS and PB elastomer films with various thickness	78
Table 3.8. Thickness of UVHIB 3 and PB rubber layers	79
Table 3.9. The processing conditions of compression for the compressed TVAAB5 <i>b</i> gels	82
Table 4.1. Composition Ratios of VP and HEMA units in photo-polymerized VP/HEMA gels	95
Table 4.2. The fitting coefficients a_1 , a_2 , and a_3 for BIS, DEGDA and GLY	119
Table 4.3. The fitting coefficients, B_1 and B_2 for BIS, DEGDA and GLY	122
Table 4.4. Hansen solubility parameters for VP, HEMA, BIS, GLY, DEGDA, and water	123
Table 4.5. Difference between each Hansen solubility parameters of VP and crosslinker	124
Table 4.6. Characteristics of for VP/HEMA gels thermally synthesized	126
Table 5.1. The fitting coefficients a_1 , a_2 , and a_3 and r-square for UVAIB hydrogels prepared with various C_{AA}	146

Table 5.2. The R_s and t_{\max} of UVAIB hydrogels prepared with various C_{AA}	147
Table 5.3. Characteristics of for VP/AA gels photo-polymerized with 0.1 and 0.2 wt. % BIS and 0.1 wt. % DEGDA	165
Table 5.4. Hansen solubility parameters for VP, AA, BIS, and DEGDA	166
Table 5.5. Difference between each Hansen solubility parameter of VP and crosslinker (BIS and DEGDA) and AA and crosslinker (BIS and DEGDA)	166
Table 5.6. The Synthesis conditions and characteristic properties of the optimized gel system, TVAAB5b gel	173
Table 6.1. Mechanical Properties of PDMS Elastomer Films	191
Table A1. Characteristics of the photomasks used	252

LIST OF FIGURES

	Page
Figure 2.1. Schematic diagram of skin expander using an inflatable balloon. US Federal Government Public domain image. Source NIH (national institutes of health) (Reproduced from [9]).	5
Figure 2.2. Effect of osmotic pressure, produced by a solution with different solute concentrations on the blood cells (Reproduced from [14]).	6
Figure 2.3. A conventional silicon balloon expander (left) and a hydrogel expander (right) with the same nominal final filling volume (scale in cm) (Reproduced from [13]).	6
Figure 2.4. (Above, left) Unilateral incomplete cleft palate before treatment. (Above, center) Expanded mucoperiosteal tissue almost closing hard palate gap. (Above, right), Hydrogel expanders before and after swelling. (Below, left) Note exposed Expander after the expansion of 4 expanders. (Below, left center) Swelled cylinder-like expanders against the background of the palate. Immediate Result (Below, center right) and final outcome of palatoplasty without any relaxing incisions (Below, right) (Reproduced from [2]).	7
Figure 2.5. Schematic drawing of the pressure registration unit: (1) perforated piston with peripheral rubber sealing and lockable piston rod; (2) chamber with 0.9% NaCl-solution; (3) folded, waterproof membrane; (4) gel cylinder in expansion chamber; (5) measuring chamber; (6) triple way stopcock to evacuate the measuring chamber and approximate the membrane to the gel cylinder; (7) pressure transducer and (8) monitoring and recording system [Redrawn from [12]].	10
Figure 2.6. MRI images corresponding to the dynamic swelling isotherms of P(MAA) hydrogels in an aqueous solution at pH 7 and 25 °C. Prior to these measurements the gels had been soaked at pH 2 (Reproduced from [21]).	17
Figure 2.7. SEM images of sandwich-like IPN hydrogel having PNIPAAm inside PAAm networks. Micrographs of fractured hydrogel freeze-dried after swelling at 40 °C (a) external layer and (b) internal layer (Reproduced from [81]).	19
Figure 2.8. (a) the change of the end to end vector from \vec{r}_0 to \vec{r} of a polymer chain under a constant load, and (b) change in vector of a chain between two crosslinking junctions in a polymer network under the same condition as the applied to a polymer chain.	22

- Figure 2.9. The curves of τ_{eng} versus λ , obtained using the theoretical thermodynamic equation and by the deformation experiments in uniaxial direction for hydrogels. 32
- Figure 2.10. Water uptake measurements for BMA/HEMA copolymers of mole fraction of BMA (F_{BMA}): $F_{BMA} = 0.0$ (a); $F_{BMA} = 0.025$ (b); $F_{BMA} = 0.05$ (c), $F_{BMA} = 0.075$ (d); $F_{BMA} = 0.1$ (e); and $F_{BMA} = 0.15$ (f) (Reproduced from [115]). 36
- Figure 2.11. The swelling % of MAAm/MAA hydrogels as a function of initiator (KPS) concentration (Reproduced from [107]). 37
- Figure 2.12. The swelling ratio of SSS-co-VBT gel vs. time for two total dose (a) 5 kGy and (b) 10 kGy (Reproduced from [45]). 39
- Figure 2.13. Temperature dependence of normalized volume V/V_{65} of PNIPA gel 1, 2, and 3 crosslinked with different monomer/cross-linker molar ratio of 20, 60, and 80, respectively. Here, V_{65} represents V of each gel at 65 °C. The inset shows the enlargement around 35 °C (Reproduced from [121]). 42
- Figure 2.14. The q of VP/HEMA copolymers crosslinked with MAAm as a crosslinker as a function of pH in PB solutions at 25 °C (Reproduced from [57]). 44
- Figure 2.15. Effect of pH on swelling of SSS/VBT polyampholytic gels: (a) 10 mM, (b) 25 mM and (c) 50 mM concentration of BIS (Reproduced from [45]). 44
- Figure 2.16. (a) Cross-sectional schematic of the cantilever/polymer structure and (b). Equilibrium cantilever deflection as a function of pH around the polymer. The solid line is experimental results. The dotted line is obtained with the cantilever and polymer modeled as a composite beam with no slip at the boundary. The inset shows three dimensional plot of the deflection of the cantilever/polymer at pH=7.0, obtained from the model (Reproduced from [28]) 45
- Figure 2.17. SEM images of equilibrated swollen NDF hydrogels (size of the bar is 10 μ m) ($\times 800$). (NDF-1, 75 : 25 vol % DMF/distilled water; NDF-2, 62.5 : 37.5; NDF-3, 50 : 50; NDF-4, 37.5 : 62.5; NDF-5, 25 : 75; NDF-6, 12.5 : 87.5) (Reproduced from [124]). 47
- Figure 2.18. Equilibrium swelling ratios of NDF 1-6 hydrogels (Reproduced from [124]) 47
- Figure 2.19. Photographic sequence showing how the volume of a 3-cm PAAm hydrogel immersed in 50 % acetone/water mixture diminishes with increasing applied electric field (0 ~2.5 V) (Reproduced from [125]). 48

Figure 2.20. Elongation of a ferrogel under (a) no magnetic field and (b) maximal magnetic field at the lower end of the ferrogel [40].	49
Figure 2.21. A schematic description of a diffusion process of ink molecules in (a) water and (b) the gel swelling process. For the former, the relative change of the length is negligible compared with that of the diameter. In the swelling of a long cylindrical gel, the relative change of the length and the diameter are the same (Redrawn from [129]).	50
Figure 2.22. Depiction of polymer relaxation during water sorption into a slab geometry (A) and on the molecular level (B). Shaded area represents glassy polymer regions (Reproduced from [73]).	51
Figure 2.23. The hydrogel layer is cross-linked in some reference state (B), and the gel at the substrate remains in this reference state. The elastic energy of the network acts as compression when the gel layer is swollen (C) relative to the reference state and as elongation when the gel layer is collapsed (A) relative to the reference state. The compression or elongation increases monotonically and is greatest at the free surface of the gel. Our measurements are for infinitely wide films, but the exact shape of the gel with lateral swelling depends on both the film thickness and the aspect ratio of the gel layer (Reproduced from [134]).	53
Figure 3.1. Chemical Structures of monomers of VP, HEMA, and AA, cross-linkers of BIS, DEGDA, and GLY, and initiators of AIBN and Irgacure 651.	71
Figure 3.2. The schematic of an assembled device for UV-initiated polymerization [1].	72
Figure 3.3. Chemical Structure of MMA, BMA, OMA, and LMA	76
Figure 3.4. The synthesis of silver nanoparticles in aqueous solution (a) and the synthesis process of the silver nanoparticles-UVHIB 3 gel composite (b).	77
Figure 3.5. The schematic of a GE-MULTI made of three layers of UVHIB 3 gel and PB elastomer membrane on the silicon wafer	79
Figure 3.6. The schematic of experimental setup of polarized optical microscopy	85
Figure 3.7. Mass swelling ratio (q_m) of gel as a function of time	87
Figure 4.1. The IR spectra of VP:HEMA xerogels with various comonomer ratios (VHIB1= 70:30, UVHIB2= 80:20, UVHIB3= 90:10, and UVHIB4= 99:01 of VP: HEMA).	94
Figure 4.2. The IR spectra of VP/HEMA xerogels with various I_{UV} (UVHIB3= 0.238, UVHIB3c=0.92, UVHIB3d=1.63, and UVHIB3e=2.65 mW/cm ²) (a) and with different C_I (UVHIB3 =0.8, UVHIB3g =0.5, UVHIB3h = 0.2 wt %) (b).	96

- Figure 4.3. UV Spectra of UVHIB1 pregel mixture during its polymerization at certain time interval. 97
- Figure 4.4. Gelation Percent of UVHIB1 gels irradiated by UV for different exposure times 98
- Figure 4.5. The effect of (a) VP content in the gels obtained by UV (\square) and thermal (\blacksquare) polymerization, (b) UV light intensity and (c) initiator concentration on the T_g of V/PHEMA gels. Predicted values for T_g are plotted in (a) using the Gordon-Taylor equation (i), as well as the Kwei equation, when (ii) $\alpha = 1$ and $\beta = 50$ and (iii) $\alpha = 14$ and $\beta = 30$. 101
- Figure 4.6. TGA diagrams of UVHIB gels synthesized with various (a) feed monomer ratios (b) UV irradiation intensities, and (c) initiator concentrations. 102
- Figure 4.7. Swelling behavior of various UVHIB3 gels polymerized using different photomasks (UV intensities); (∇) mask1, (\bigcirc) mask2, (\bullet) mask3, (\blacktriangledown) mask4, (\blacksquare) mask5 and (\blacklozenge) mask6 (Each q_m point is the averaged one of three measured values). Pictures are VH 3 hydrogels taken at 0, 40, 120 and 480 min during the swelling measurement. 104
- Figure 4.8. Swelling behavior of various (a) UVHIB gels polymerized with different feed monomer ratios and (b) UVHIB3 gels synthesized with different C_I s (Each q_m point is the averaged one of three measured values). 105
- Figure 4.9. Effect of (a) VP content in VP/HEMA gel and (b) UV intensity on penetrant diffusion coefficient (D). 107
- Figure 4.10. Effect of VP content (C_{VP}) in VP/HEMA gels on (a) measured equilibrium volume swelling ratio (q_{ve}) and compression modulus (G) and (b) calculated effective cross-link density (ν_e) and average molecular weight between cross-links (M_c). 109
- Figure 4.11. Effect of initiator concentration (C_I) on (a) measured equilibrium volume swelling ratio (q_{ve}) and compression modulus (G) and (b) calculated effective cross-link density (ν_e) and average molecular weight between cross-links (M_c) of VP/HEMA hydrogels. 111
- Figure 4.12. Effect of UV intensity (I_{UV}) on (a) measured equilibrium volume swelling ratio (q_{ve}) and compression modulus (G) and (b) calculated effective cross-link density (ν_e) and average molecular weight between cross-links (M_c) of VP/HEMA hydrogels. 113
- Figure 4.13. Schematic network structure at fully swollen state of hydrogels prepared at (a) lower and (b) higher UV intensity/initiator concentration. The average

molecular weight between two cross-links making a complete mesh (M_c) increases (as shown by the arrows) with increasing UV intensity/initiator concentration. 114

Figure 4.14. (a) q_{ve} and G of the UV-polymerized VP/HEMA gels synthesized with various crosslinkers (BIS, DEGDMA and GLY) at different crosslinker concentrations. 117

Figure 4.15. (a) v_e and M_c of the UV-polymerized VP/HEMA gels synthesized with various crosslinkers (BIS, DEGDMA and GLY) at different crosslinker concentrations. 118

Figure 4.16. The χ of the UV-polymerized VP/HEMA gels synthesized as a function of (a) C_C and (b) q_{ve} for three different crosslinkers (BIS, DEGDMA and GLY). 121

Figure 4.17. The IR spectra of VP:HEMA xerogels thermally synthesized with various comonomer ratios (TVHAB1= 70:30, TVHAB2= 80:20, TVHAB3= 90:10, and TVHAB4= 99:01 of VP: HEMA). 125

Figure 4.18. LVEM images of VP/HEMA copolymeric hydrogels with various compositions of monomer units (See Table 4) 127

Figure 4.19. Swelling behavior of thermally polymerized VP/HEMA gels with various compositions; (■) TBHAB1, (▽)TBHAB2, (◆) TBHAB3, and (○) TBHAB4 (Each q_m point is the averaged one of three measured values). Pictures are TBHAB3 hydrogels taken at 0, 200, 400, and 600 min during the swelling measurement (The size of white bar: 2.54 cm). 128

Figure 4.20. Initial Swelling rate (Rs) of thermally polymerized VP/HEMA (TVHAB) gels (●) and photo-polymerized VP/HEMA (UVHIB) gels (o) as a function of VP feed weight %. 130

Figure 4.21. Penetrant diffusion coefficient (D) as a function of VP content in thermally synthesized VP/HEMA gels (Each point is the averaged one of three measured values) 131

Figure 5.1. The mass swelling ratio (q_m) of VP/AA gels and VP/HEMA gels prepared with VP:HEMA and VP:AA of 90:10, respectively 143

Figure 5.2. The equilibrium volume swelling ratio (q_{ve}) of VP/AA hydrogels as a function of the feed weight % of AA (C_{AA}) 144

Figure 5.3. The mass swelling ratio (q_m) with time for fully swollen VP/AA hydrogels prepared with different AA feed content (C_{AA}). 146

Figure 5.4. The R_s and t_{\max} of UVAIB gels as a function of q_{ve}	147
Figure 5.5. The D of saline solution diffusing into UVAIB hydrogels as a function of the feed weight % of AA (C_{AA})	149
Figure 5.6. The G of fully swollen VP/AA hydrogels prepared with different C_{AA} (Two deviated values were not used for fitting the modulus values).	150
Figure 5.7. The equilibrium volume swelling ratio (q_{ve}) of VP/AA hydrogels determined at different pH for 8 different hydrogels obtained with various feed weight ratio of VP:AA.	152
Figure 5.8. The molecular weight between crosslinks (M_c) and crosslink density (v_e) of UVAIB hydrogels prepared with different feed weight % of AA (C_{AA}).	153
Figure 5.9. The χ of the UVAIB hydrogels as a function of (a) C_{AA} and (b) q_{ve}	154
Figure 5.10. The equilibrium volume swelling ratio (q_{ve}) of fully swollen VP/AA hydrogels prepared with different AA feed content (C_{AA}) for three different temperatures	155
Figure 5.11. The gelation percent of VP/AA gels synthesized with different AA feed content (C_{AA}) by UV-initiated polymerization	157
Figure 5.12. The measured values of glass transition temperature (\bullet) of VP/AA xerogels prepared with different AA feed content (C_{AA}) and predicted values for T_g are plotted using the Flory-Fox equation (---), the Gordon-Taylor equation (.....), as well as the Kwei equation (—, $\alpha = 1$ and $\beta = 50$).	158
Figure 5.13. The IR Spectra of UVAIB2 (90:10 feed ratio of VP:AA), UVAIB5 (60:40), UVAIB10 (10:90), UVAIB11 (0:100) xerogels	160
Figure 5.14. The IR Spectra of the UVAIB11 xerogel (0:100 feed ratio of VP:AA) before and after the hydrolysis preformed at 100 °C for 2 hours	161
Figure 5.15. A schematic of (a) the molecular structures of the VP/AA gel synthesized with lower C_{AA} (less than 40~50 wt. %) and of the gel after the swelling, and (b) the formation of anhydride group during the synthesis of the gel with higher C_{AA} (higher than 40~50 wt. %) in their network (For easy understanding, only COOH groups are denoted on the chains).	163
Figure 5.16. The mass swelling ratio of the VP/AA gels synthesized with BIS of 0.05, 0.1, and 0.2 wt. % and DEGDA of 0.1 wt. % as a function of time	164
Figure 5.17. The mass swelling ratio (q_m) of the VP/AA gels synthesized with AIBN and Irgacure 651 of 0.8 wt. % as a function of time	168

Figure 5.18. The mass swelling ratio (q_m) of the VP/AA gels synthesized with various weight % of initiator (AIBN) by UV-initiated (UV) and thermal (Heat) polymerizations	169
Figure 5.19. The q_{ve} of VP/AA gels UV-initiated (UV) and thermally (Heat) polymerized with initiator concentration of 0.2, 0.4, and 0.8 weight %	170
Figure 5.20. The (a) R_s and (b) t_{max} of VP/AA gels UV-initiated (UV) and thermally (Heat) polymerized with initiator concentration of 0.2, 0.4, and 0.8 weight %	171
Figure 5.21. Toughness and Modulus of TVAAB gels thermally polymerized with initiator concentration of 0.2, 0.4, and 0.8 weight %	172
Figure 6.1. The mass swelling ratio (q_m) of UVMIB3, UVBIB3, UVOIB3, UVLIB3, and UVHIB3 as a function of swelling time (the inserted figure shows the enlarged initial swelling behavior of the gels up to the swelling time 150 min.).	181
Figure 6.2. The q_{ve} and G of VP/MA hydrogels as a function of the number of carbon (C) in the alkyl group of each methacrylate	182
Figure 6.3. The R_s (●) and t_{max} (o) of VP/MA hydrogels as a function of the number of carbon (C) in the alkyl group of each methacrylate.	183
Figure 6.4. The q_{ve} of VP/MA hydrogels as a function of the number of carbon (C) in the alkyl group of each methacrylate	184
Figure 6.5. The G of VP/MA hydrogels as a function of the number of carbon (C) in the alkyl group of each methacrylate	185
Figure 6.6. The M_c (●) and v_e (o) of VP/MA hydrogels as a function of the number of carbon (C) in the alkyl group of each methacrylate	186
Figure 6.7. Mass swelling ratio (q_m) of the semi-interpenetrating Ag-UVAIB3 gel composite and UVHIB3 gel as a function of time	188
Figure 6.8. The R_s (□) and t_{max} (⊠) of both semi-interpenetrating Ag-UVAIB3 gel composites and UVHIB3 gels	189
Figure 6.9. The (a) <i>toughness</i> and (b) ε_b of PDMS films as a function of film thickness for three different F_{PC} used for making films	192

Figure 6.10. Mass swelling ratio (q_m) of the UVAIB3 gels encapsulated with different PB films with different d_e values or PDMS2e of 600 μm film thickness (Legend denotes the gels and the elastomer film type and the film thickness).	193
Figure 6.11 The R_s (●) and t_{max} (o) of the UVAIB3 gels encapsulated with different PB films with different d_e values	195
Figure 6.12. The schematic of a swelling measurement setup for a (GE) _m made of UVHIB3 gel and PB rubber layers	197
Figure 6.13. The q_m of two (GE) _m s as a function of time (The diffusion rate of a saline solution of (GE) _m 1 and (GE) _m 2 is $2.49 \times 10^{-3} \text{ mgH}_2\text{O}/\text{cm}^2 \cdot \text{sec}$ and $6.34 \times 10^{-4} \text{ mgH}_2\text{O}/\text{cm}^2 \cdot \text{sec}$, respectively).	198
Figure 7.1. The schematic of expected structural gradient in a gel (left) obtained using a DGrad-Mask 1 and its fully swollen state (right)	206
Figure 7.2. The mass swelling ratio (q_m) of DGrad-UVHIB3 gel and UVHIB3 gel as a function of time	208
Figure 7.3. The R_s (□) and t_{max} (▣) of DGrad-UVHIB3 gels and UVHIB3 gels	208
Figure 7.4. The picture of fully swollen DGrad-UVHIB3 hydrogels taken by stereo-optical microscopy	210
Figure 7.5. The $D_s(x)$ images of (a) the cross-sectional view and (b) the planar view of the DGrad3-UVHIB3 gel determined by MRI technique. The diffusion coefficient is encoded by the grayscale (light: high D_s and dark: low D_s).	211
Figure 7.6. Second heating DSC curve of the TVAAB5b gel with a heating rate of 10 $^{\circ}\text{C}/\text{min}$ under nitrogen gas	214
Figure 7.7. The compression and recovery curve of TVAAB5b gel at 130 $^{\circ}\text{C}$ and with the strain rate of 0.001 s^{-1} (first loading and unloading cycle (—) and second cycle (---))	214
Figure 7.8. Assumed model for the ideal network structure of a gel and the intermediate and fully compressed network structure of the partial gel part (the chain in dotted circle shows slippage due to the friction occurred on the surface)	215
Figure 7.9. The fixicity of TVAAB5b gels compressed at strain rate 0.001 s^{-1} and strain 90 % as a function of temperature	216
Figure 7.10. The fixicity of TVAAB5b gels compressed (a) at temperature 110 $^{\circ}\text{C}$ and strain rate 0.001 s^{-1} a function of strain and (b) at temperature 110 $^{\circ}\text{C}$ and strain 90 % as a function of strain rate	217

- Figure 7.11. WAXS diffraction patterns and their intensity versus 2θ for the transparent and opaque parts of TVAAB5b-2 gel 219
- Figure 7.12. OM images of (a) center part, (b) boundary between center and edge, (c) edge part, and (d) magnification of edge part of compressed TVAAB5b-2 gel (scale bars in (a), (b), and (c) images indicate 100 μm and in (d) 20 μm) 220
- Figure 7.13. SEM micrographs of a TVAAB5 gel before (a) and after (b) the annealing at 110 $^{\circ}\text{C}$ for 1 hour. 221
- Figure 7.14. SEM micrographs of (a) cross-sectional view of compressed TVAAB5b_2 gel, (b) transparent part, (c) the boundary part between edge and center parts, and (d, e, f, g & h) the edge parts of the compressed gel 222
- Figure 7.15. The schematics for the formation and evolution of voids in a cylindrical shape gel by annealing process and the extermination and deformation of voids in the center (part I: stationary zone and part II: moving zone), boundary and edge parts of the gel by compression process under no slip condition. The expected normal stress σ_{rr} and σ_{zz} and shear stress (σ_{rz}) profiles along the r direction at $z=0$. 224
- Figure 7.16. (a) Velocity field and velocity component fields (left side) and the pressure distribution (right side, darker regions corresponding to higher values of the pressure) in no slip squeeze flow according to a theoretical equation (Reproduced from [20]). (b) The computed displacement fields for a 29 % compressive deformation under no slip wall boundary condition (Reproduced from [21]). 226
- Figure 7.17. Birefringence images of the compressed TVAAB5b gel obtained between (a) crossed polarizers and (b) parallel polarizers at room temperature (light propagates along z axis) (with schematic gel with transparent and opaque parts as well as stationary zone). Arrows note the corresponding part and zone 228
- Figure 7.18. The thermomechanic cycle for compression, anisotropic swelling and deswelling of compressed gels (G1-G5 are the gels before and after the compression and H1 is the fully swollen hydrogel) 229
- Figure 7.19. The q_{me} and q_{ve} of various TVAAB5b gels compressed at various temperatures of 100 $^{\circ}\text{C}$, 110 $^{\circ}\text{C}$, 120 $^{\circ}\text{C}$, 130 $^{\circ}\text{C}$, 140 $^{\circ}\text{C}$ and 150 $^{\circ}\text{C}$ (the used $\dot{\epsilon}_c$ and ϵ_c are 0.001 s^{-1} and 90 %, respectively). 232
- Figure 7.20. (a) the q_{De} and q_{He} and (b) $DSA (= q_{He}/q_{De})$ of various TVAAB5b gels compressed at the temperature of 100 $^{\circ}\text{C}$, 110 $^{\circ}\text{C}$, 120 $^{\circ}\text{C}$, 130 $^{\circ}\text{C}$, 140 $^{\circ}\text{C}$ and 150 $^{\circ}\text{C}$ (the used $\dot{\epsilon}_c$ and ϵ_c are 0.001 s^{-1} and 90 %, respectively). 233

- Figure 7.21. The q_{me} and q_{ve} of various TVAAB5b gels compressed up to the strain of 70 %, 80 %, 90 % and 95 % (the used $\dot{\epsilon}_c$ and T_c are 0.001 s^{-1} and $110 \text{ }^{\circ}\text{C}$, respectively). 234
- Figure 7.22. (a) the q_{De} and q_{He} and (b) DSA of various TVAAB5b gels compressed up to the strain of 70 %, 80 %, 90 % and 95 % (the used $\dot{\epsilon}_c$ and T_c are 0.001 s^{-1} and $110 \text{ }^{\circ}\text{C}$, respectively). 235
- Figure 7.23. The q_{me} and q_{ve} of various TVAAB5b gels compressed with the $\dot{\epsilon}_c$ of 0.0001 s^{-1} , 0.0002 s^{-1} , 0.001 s^{-1} , and 0.01 s^{-1} (the used ϵ_c and T_c are 0.001 s^{-1} and $110 \text{ }^{\circ}\text{C}$, respectively). 236
- Figure 7.24. (a) the q_{De} and q_{He} and (b) DSA of various TVAAB5b gels compressed with the $\dot{\epsilon}_c$ of 0.0001 s^{-1} , 0.0002 s^{-1} , 0.001 s^{-1} , and 0.01 s^{-1} (the used ϵ_c and T_c are 0.001 s^{-1} and $110 \text{ }^{\circ}\text{C}$, respectively). 237
- Figure 7.25. The TVAAB5b gel compressed with 0.0001 s^{-1} at $110 \text{ }^{\circ}\text{C}$ up to 90 % (left) and the hydrogel fully swollen in saline solution at room temperature for 14.4 days (right). 238
- Figure 7.26. The R_s and t_{max} of various TVAAB5b gels compressed (a) at various T_c (with the $\dot{\epsilon}_c$ of 0.001 s^{-1} and up to the ϵ_c of 90 %), (b) up to various ϵ_c (with the $\dot{\epsilon}_c$ of 0.001 s^{-1} and at T_c of $110 \text{ }^{\circ}\text{C}$), and (c) with various $\dot{\epsilon}_c$ (at T_c of $110 \text{ }^{\circ}\text{C}$ and up to the ϵ_c of 90 %). 240
- Figure A1. Various photomasks with different UV transmittance from 0 % to 100 % (from Mask E to Mask A) 250
- Figure A2. UV spectra of photoinitiator (Irgacure 615), monomer mixture of VP/HEMA, standard slide glass, and photomasks A-E. 251
- Figure A3. The schematic of the discrete gradient photomask (DGrad-Mask1) developed in our lab and the UV irradiation intensity through each section in the mask. 252
- Figure A4. The schematic of three discrete gradient photomask (Dgrad-Mask2) developed in our lab and the UV irradiation intensity through each section in the mask 252
- Figure B1. Schematic diagram of DGrad3-UVHIB3 gel (right) obtained by UV initiated polymerization using the photomask Dgrad-Mask2 (left). 254
- Figure B2. The D_s values of water in material having anisotropic structure along the x, y, and z directions ($D_s(x)$, $D_s(y)$ and $D_s(z)$, respectively) determined by diffusion tensor MRI (DTI, Redrawn from [3]). 255

LIST OF SYMBOLS

A	Absorbance
C_I	Initiator Concentration
C_C	Crosslinker Concentration
C_{AA}	Concentration of Acrylic Acid (AA)
C_{VP}	Concentration of Vinyl Pyrrolidone (VP)
d	Diameter of Films of Hydrogels
d_e	The Thickness of Elastomer Films or Membrane
D	Diffusion Coefficient
D_c	Cooperative Diffusion Coefficient
d_e	Film Thickness
D_s	Self Diffusion Coefficient
E	Elastic Modulus
E_{coh}	Cohesive Energy (or Total Cohesive Energy)
E_d	The energy of dispersion bonds
E_h	The energy of hydrogen bonds
E_p	The energy of polar bonds
G	Shear Modulus or Compressive Modulus
GF	Gel Fraction
F	Molar Attraction Constant
F_{di}	The Molar Attraction Constant for Dispersion Forces per Structural Group
F_m	Feed Monomer Weight Ratio

F_{pi}	The Molar Attraction Constant for Polar Forces per Structural Group
F_{PC}	The Ratio of PDMS pregel and Crosslinker
I_{CUV}	The Critical UV Intensity
I_0	The Light Intensity of Incident Light
I_1	The Light Intensity After Passing the Medium Material
I_{UV}	UV Intensity
k	The Swelling Rate Constant
k_B	Boltzmann's Constant
l	The Film Thickness
l_{ma}	The length of major axis in ellipsoid
l_{mi}	The length of minor axis in ellipsoid
M_c	The Molecular Weight between Crosslinking Junctions
n	The Characteristic Exponent Which Implies the Type of Transport Mechanism (or Called Diffusion Mode)
P	The Swelling Pressure
P	The Elastic Contractibility of Extended Chains
Q	Swelling Ratio
q_D	Diameter Swelling Ratio
q_{De}	Equilibrium Swelling Ratio in Terms of Diameter
q_e	Equilibrium Swelling Ratio
q_H	Height Swelling Ratio
q_{He}	Equilibrium Swelling Ratio in Terms of Height
q_m	Mass Swelling Ratio
q_{me}	Equilibrium Swelling Ratio in Terms of Mass

q_{t60}	Swelling Ratio at Initial 60% Increase in Swelling Ratio
q_v	Volume Swelling Ratio
q_{ve}	Equilibrium Swelling Ratio in Terms of Volume
$\sqrt{\bar{r}_0^2}$	The End-to-End Distance in the Unperturbed State
R	The Gas Constant
R_g	The Radius of Gyration of a Molecule
R_S	Gel Initial Swelling Rate from the Time Zero to the Time at Initial 60% Increase in Swelling Ratio (t_{60})
T	Temperature
T	Transmittance (T %: transmittance Percent)
T_c	Compression Temperature or (Critical Temperature)
T_g	Glass Transition Temperature
t	Time
t_{60}	Time at Initial 60% Increase in Swelling Ratio
t_{max}	Time Reaching to Maximum Expansion of Hydrogel System
V	Molar Volume
V_∞ and V_d	The Volume of an Equilibrium Swollen Hydrogel Sample and the Gel Volume Before Swelling, Respectively
W_0 and W_f	The Weights of the Gel Before and After Extraction or Swelling, Respectively
W_t and W_∞	Weight of Solvent Uptake of Hydrogel at Time t and at Equilibrium Time t_∞ , Respectively
χ	The Flory-Huggins Interaction Parameter
δ_t	Total Solubility Parameter
δ_d	The Solubility Parameter for Dispersion Forces

δ_h	The Solubility Parameter for Hydrogen Bonding Forces
δ_p	The Solubility Parameter for Polar Forces
ε	Strain
ε_b	Strain at Break
ε_c	Applied Compression Strain
ε_r	Residual or Remained Strain (or Resulting Compressed Strain)
$\dot{\varepsilon}$	Strain Rate
$\dot{\varepsilon}_c$	Compression Strain Rate
ϕ_∞	The Volume Fraction of Polymer at Equilibrium
η	The Viscosity of Fluid
λ	The UV wavelength
λ_{max}	The wavelength showing maximum UV absorption peak
λ_p	The wavelength showing maximum UV absorption peak in the range interested
ν_e	The Effective Crosslinking Density of Hydrogel
π	Osmotic Pressure
ρ	The Density of Gel
ρ_p and ρ_s	The Densities of Gel and Solvent, Respectively
σ	Stress
σ_b	Stress at Break
σ_{rr}	Normal Stress in the r Direction
σ_{zz}	Normal Stress in the z Direction

σ_{rz}	Shear Stress of z direction in r area
ξ	Mesh Size
ξ_H	The Hydrodynamic Correlation Length

LIST OF ABBREVIATIONS

AA	Acrylic Acid
AFM	Atomic Force Microscopy
AIBN	Azo-Isobutyronitrile
AAmPA	Acidic 3-Acryloylamino-Propionic Acid
AN	Acrylonitrile
ATP	Adenosine Triphosphate
ATR-FTIR	Attenuated Total Reflectance-Fourier Transform Infrared
BIS	N, N-methylene Bisacrylamide, Tetra-functionality
BMA	Butyl Methacrylate
CAM	Calcein-Acetoxy Methyl Ester
CGrad-Mask	Continuous Gradient Photomask
DEAAm	N, N-Diethylacrylamide
DEGDA	Diethylene Glycol Diacrylate
Dex	Dextran
DGrad-Mask	Discrete Gradient Photomask
DLS	Dynamic Light Scattering
DMA	Dynamic Mechanical Analysis
DMAAm	N, N-Dimethyl Acrylamide
DMIAAm	2-(Dimethylmaleimido)-N-Ethyl-Acrylamide
DNF	dextran-maleic acid (Dex-MA)/NIPAAm copolymer
DSA	Degree of Swelling Anisotropy

DSC	Differential Scanning Calorimetry
DTI	Diffusion Tensor MRI
E-beam (e-beam)	Electron Beam
EF	Electric Field
ECM	Extracellular Matrix
EGDMA	Ethylene Glycol Dimethacrylate
ESEM	Environmental Scanning Electron Microscopy
EWC	Equilibrium Water Content
FTIR	Fourier Transform Infrared
(GE) _m	Multilayer of Alternating Gels and Elastomers Membranes
GF	Gelation Fraction
GLY	Glyoxyl Bis(Diallylacetal), Octafunctionality
Grad-H	A Hydrogel System with Gradient Network (ex: Grad-VH 3: VH 3 with Gradient Network)
HaCaT cells	Human Epidermal Keratinocyte Cells
HEMA	2-hydroxyethyl Methacrylate
HMMI	N-hydroxymethyl Maleimide
Irgacure 651	2,2-Dimethoxy-2-Phenylacetophenone
LCST	Low Critical Solution Temperature
LMA	n-Lauryl Methacrylate (or n-Dodecyl Methacrylate)
MAA	Methacrylic Acid
MAAm	Methacrylamide
MDSC	Modulated DSC
MF	Magnetic Field

MLR	Mixed Lymphocytes Reaction
MMA	Methyl Methacrylate
MRI	Magnetic Resonance Imaging
MTT	3-(4,5-Dimethylthiazol-2-yl)-2,5-Diphenyltetrazolium Bromide, a Tetrazole
NIH	National Institutes of Health
NIPAAm	N-isopropylacrylamide
NMR	Nuclear Magnetic Resonance
OMA	Octyl Methacrylate
PANI	Polyaniline
PAAm	Poly (Acryl Amide)
Pas Cells	Preadipocytes Cells
PB	Polybutadiene
PDMS	Polydimethylsiloxane
PEG	Poly(Ethylene Glycol)
PEGMEA	Poly(Ethylene Glycol Methyl Ether Acrylate)
PEGTMO	Poly(Ethylene Glycon-b-Tetramethylene Oxide)
PEO	Poly(Ethylene Oxide)
PHEMA	Poly(2-Hydroxyethyl Methacrylate)
PMMA	Poly(Methyl Methacrylate)
PNIPAAm	Poly(N-Isopropylacrylamide)
PVA	Poly(vinyl Alcohol)
PVP	Poly(N-Vinylpyrrolidone)
SA	Stearic Acrylate

SANS	Small Angle Neutron Scattering
SAXS	Small Angle X-ray Scattering
SEM	Scanning Electron Microscopy
SSS	<i>p</i> -Sodium Styrene Sulfonate
SPHs	Superporous Hydrogels
TGA	Thermogravimetric Analysis
TPT	1,1-Trimethylolpropane Dimethacrylate
UV	Ultraviolet
VA	N-vinyl-2-pyrrolidinone (VP)/Acrylic Acid (AA)
VBt	vinyl benzyl trimethylammoniumchloride
VH	N-vinyl-2-pyrrolidinone (VP) /2-Hydroxyethyl Methacrylate (HEMA)
THFMA	Tetrahydrofurfuryl Methacrylate
VSA	Vinylsulfonic Acid
VP	N-Vinyl-2-Pyrrolidinone or 1-Vinyl-2-Pyrrolidinone
WAXS	Wide Angle x-Ray Scattering

Decoding the name of ABCDE gel

A indicates polymerization method (T: thermal polymerization and U: UV-initiated polymerization)

B indicates main monomer (V: VP)

C indicates comonomer (H: HEMA and A: AA)

D indicates initiator type (I: Irgacure 651 and A: AIBN)

E indicates crosslinker type (B:BIS, G:GLY, and D:DEGDA)

SUMMARY

Hydrogels are polymeric materials with chemically, physically or topologically crosslinked networks which have a capacity to absorb and retain water. They have been frequently used for many medical applications because of their useful physical properties such as oxygen permeability and excellent compatibility with living tissue and blood. The long term goal of our research is to develop a hydrogel system for use in reconstructive and plastic surgeries such as the closure of cleft palate defects and syndactyly (congenitally fused fingers or toes) repair. The medical requirements are not only well controlled (or defined) swelling behavior such as high degree of swelling, slow swelling rate and anisotropic swelling, but also appropriate mechanical strength in addition to being bio-benign. In this work, to facilitate the development of useful device an attempt was made to understand the swelling and mechanical properties of the hydrogels as a function of certain key parameters and investigated the effect of these parameters on the properties. Two known biocompatible (and FDA approved) hydrogel systems were prepared using thermal polymerization or UV-initiated polymerization. One system is the neutral hydrogel of N-vinyl-2-pyrrolidinone (VP) and 2-hydroxyethyl methacrylate (HEMA) copolymer and the other system is the ionic hydrogel system of N-vinyl-2-pyrrolidinone (VP) and acrylic acid (AA) copolymer. The systematic control over the degree, rate, and direction (anisotropy) of swelling of the hydrogels was focused to study. The control of gel swelling was achieved by regulating the network structure and composition of gels as well as environmental conditions. The xerogels were characterized by measuring the gelation point and percent, analyzing thermal properties obtained by differential scanning calorimetry (DSC) and thermogravimetric analysis (TGA), and evaluating the gel composition determined by Fourier transform infrared (FTIR) spectroscopy. Swelling measurements and dynamic mechanical analysis (DMA)

of the hydrogels have also been carried out to study their swelling behavior and mechanical properties. Based on these results, their network structure characteristics were evaluated using known thermodynamic and kinetic equations known for hydrogels.

Using VP/HEMA hydrogels, the effect of comonomer composition, ultraviolet (UV) irradiation intensity controlled by using the photomasks developed in this lab, concentration of photoinitiator (2,2-Dimethoxy-2-phenylacetophenone (Irgacure 651)) and cross-linker (N, N-methylene bisacrylamide (BIS)), the type of crosslinker as well as polymerization methods on the swelling degree and kinetics, structural characteristics, and mechanical modulus of a neutral hydrogel were investigated. Additionally, the ionizable moieties of AA instead of neutral species of HEMA were incorporated into the gel network, and the obtained ionic VP/AA hydrogel displayed a much improved degree of swelling. Using the VP/AA hydrogels, the swelling behavior, structure and mechanical modulus of the hydrogels were investigated as a function of concentration of ionizable AA species (C_{AA}), and the effects of pH and temperature on their equilibrium swelling ratios were analyzed. Through these experimental performances and characterizations of gel/hydrogel systems, the hydrogel system producing the maximum equilibrium swelling ratio and slow enough swelling rate was determined to be UV-initiated polymerized VP/AA gel with the C_{AA} of 40 wt. %. Moreover, by investigating the effect of crosslinker concentration and type, initiator concentration and type, and polymerization method on the degree and kinetics of swelling and mechanical properties of the VP/AA hydrogel with the C_{AA} of 40 wt. %, the optimized gel system was obtained to be the VP/AA gel crosslinked by thermal polymerization with the VP:AA feed weight ratio of 6:4, with the initiator AIBN of 0.4 wt. % with the crosslinker BIS of 0.2 wt. %, (TVAAB5b gel), which was used for anisotropic swelling studies.

Investigations into the swelling rate of some other systems were performed based on the VP/HEMA gels. Four different systems such as the multilayers of alternating elastomer films (polybutadiene (PB) or polydimethylsiloxane (PDMS)) and gels, the gels

encapsulated with the elastomer films, the gel composite with silver nanoparticles, and the gels of VP and methacrylate with increasing the length of hydrophobic groups have been prepared and their swelling behavior was studied.

Some reports of the observations on anisotropic swelling of gels have been presented. However, this has been not researched intensively and indeed systematic studies on control over the anisotropic swelling of hydrogels have not been reported. In this thesis, two novel methods to prepare the gel system showing controlled anisotropic swelling are presented. One method is to induce anisotropic swelling through a structural gradient VP/HEMA gels synthesized by UV polymerization using gradient photomasks. The other method is to obtain compressive stress induced anisotropic swelling. The cylindrical gels were compressed by controlling strain from 70 % to 95 %, strain rate from 0.0001 s^{-1} to 0.001 s^{-1} and temperature from 100 °C to 150 °C. Controlled anisotropic swelling of compressed gels was successfully obtained and the achieved maximum swelling anisotropy (*DSA*), which is ratio of the equilibrium height swelling ratio to equilibrium diameter swelling ratio, was 25 ± 3.2 . Among the tens of hydrogel systems developed for the use of applications such as cleft palate or syndactyly surgeries, TVAAB5b gel was decided to be the optimal gel system producing isotropic swelling base on the key properties such swelling rate, mechanical properties. The TVAAB5b gel compressed with strain rate of 0.0001 s^{-1} up to strain of 90 % at temperature of 110 °C was determined to be the most optimized gel system producing anisotropic swelling and the *DSA*, swelling rate, and time to reach equilibrium state of the gel were determined to be 22.0, 0.0019 min^{-1} , and 14.4, respectively. The anisotropic swelling behavior was explained by a thermodynamic cycle first proposed in this thesis.

CHAPTER I

INTRODUCTION

In this research, attempts to develop a hydrogel system predominantly for tissue expansion needed in reconstructive surgical applications have been performed. Tissue expansion has been often seen in human societies, for example, when a woman is pregnant the expansion of her abdominal wall or in tribal populations the expansion of the ears, lips or necks to enhance their beauty. Although the materials used to induce the tissue expansion are different, the tissue expansion is a common and important issue. In this study, the gels and hydrogels were prepared and their swelling properties were attempted to be controlled, which results in the control of tissue expansion for the use in specific surgery. The gels or hydrogels placed subcutaneously would expand by absorbing surrounding aqueous body fluids thereby exerting extensional forces on the surrounding skin that triggers regrowth of skin tissue if the expansion is slow enough not to induce necrosis of the tissue. To develop such hydrogel tissue expanders, an understanding of hydrogels and hydrogel tissue expanders as well as parameters to systematically control their swelling degree and rate is necessary. Additionally, the ability to control the swelling direction (anisotropy) of gels is another critical requirement for specific surgical applications such as the repair operations of cleft palates and syndactyly. Overall this research is involved in understanding polymeric systems for hydrogel expander applications and developing methodologies to systematically control the degree, rate, and direction of swelling in the hydrogel systems, while maintaining their mechanical properties. By manipulating molecular as well as macroscopic structures, these various properties can be controlled, which make it possible to derive hydrogels with predetermined properties.

Initially a description of what tissue expanders and specifically those based on hydrogel are, how they work in vivo, what properties induce skin expansion, and how they response to the living cells has been presented. In addition, the synthesis and characterizations of gels and hydrogels, what properties are important for the hydrogel tissue expander development, and what and how key factors affect critical properties are presented in Chapter II.

Based on prior work on hydrogels and hydrogel tissue expanders, a neutral hydrogel system was chosen with an ionic hydrogel system known to be biocompatible. In both systems, control over the network structure was undertaken, which changes mechanical and swelling properties of the hydrogel. The effect of key parameters such as the feed monomer ratio, initiator concentration and type, crosslinker concentration and type, UV intensity, ionizable moiety, and even swelling medium conditions such as pH and temperature on the properties of hydrogels has been investigated. The results of these studies are presented in Chapter IV and V. In these Chapters, the methods to improve the swelling ratio as well as the reason why the change in the variables affect swelling behavior such as equilibrium swelling ratio and swelling kinetics are also discussed.

Chapter VI describes the methodologies to control the swelling rate of several gel systems such as the gels encapsulated with different elastomeric films and with varying thicknesses of the films, the multilayers of alternating elastomer films and gels, the gel composite including silver nanoparticles, and the gels with hydrophobic moieties.

There are limited reports on the observation of the anisotropic swelling of gels or hydrogel films because it has not been widely studied. In this thesis work, two novel methodologies to obtain controlled anisotropic swelling of gels were investigated and the results are discussed in Chapter VII. One method is to control crosslinking density gradient in the gels through the use of a gradient photomask prepared in our lab. The other method is to subject the compression to make pre-formed gels using well controlled

compressive strain, strain rate and temperature to induce anisotropic swelling of compressed gels. The compressive stress induced anisotropic swelling is also explained by a thermodynamic cycle proposed in Chapter VII

Concluding remarks and suggested work that needs to be done for this research are mentioned in Chapter VIII. Appendix A discusses the development of photomasks used for UV-initiated free-radical polymerization, and Appendix B describes the positional self-diffusion coefficients of water in gradient hydrogels.

CHAPTER II

BACKGROUND

In this chapter, a review of tissue expanders and especially those made from hydrogel together with general discussion of hydrogels is provided. History of tissue expander, hydrogel tissue expander, their in-vivo and in-vitro swelling and biocompatibility are described. Definition, applications, synthesis methods, characterizations, swelling and mechanical properties and network structure characteristics of gels or hydrogels are reported as well as parameters affecting the properties and structure. Studies on anisotropic swelling of hydrogels are finally reported.

2.1. Tissue Expander

2.1.1. History of Tissue Expanders

Tissue expansion has been seen in the abdominal wall of a pregnant woman and neck growth of African women in a tribe. The first report of tissue expansion in medical use was presented in 1905 by Codvilla [1] in work related to extension of a femur. A material or device designed to induce such skin or tissue expansion for the purpose of reconstructive and plastic surgeries has been called tissue expander since then, Tissue expander has been used in the surgeries such as cleft palate repair [2, 3], breast reconstruction [4], anophtalmic socket repair [5] and so on. The first dedicated tissue expander was clinically used in 1957 by Neumann [6], who implanted a rubber balloon subcutaneously and inflated it with air from outside the body. The skin expansion was used for the reconstruction of an ear. Later silicone balloons were utilized by Radovan in 1979 [7] and later developed by Argenta [8]. These balloons used saline to inflate the

balloon via an injection port and were made in various shapes and sizes for different surgical requirements in different parts of the body. Inflatable balloon expanders are still the most widely used type in clinical tissue expansion. Figure 2.1 shows a schematic of a skin expander using an inflatable balloon with an injection port.

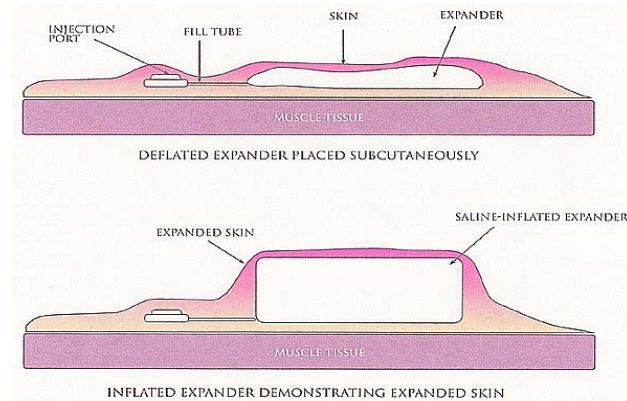


Figure 2.1. Schematic diagram of skin expander using an inflatable balloon. US Federal Government Public domain image. Source NIH (national institutes of health) (Reproduced from [9]).

In 1982 Austad and Rose [10] introduced a self inflating expander, which consisted of a permeable silicone membrane filled with a hypertonic saline solution. The use of hydrogels as tissue expanders in reconstructive surgery was first developed in 1992 by Downes *et al.* who exploited the osmotically driven expansion of a biocompatible poly(hydroxyethyl methacrylate) (HEMA) hydrogel [11]. Wiese [12] verified that hydrogels are efficient materials to induce the tissue expansion using vinyl-2-pyrrolidinone (VP)/ methyl methacrylate (MMA) copolymeric hydrogel and demonstrating their biocompatibility and swelling pressure, while Wiese criticized self inflating silicone expanders with two disadvantages. Firstly, expansion takes too long (8 ~ 14 weeks), and secondly, there will be the possibility of tissue necrosis induced by the

leakage of hypertonic solution from the balloon (see Figure 2.2). It was also reported by Wiese that the biocompatibility of VP/MMA hydrogel tissue expander was proved through in-vivo tests using several laboratory rats and usually swell and reach their equilibrium swelling state in 6-8 weeks by absorbing body fluids. A direct comparison between a conventional silicon balloon and a hydrogel expander with the same expanded volume was also undertaken by Wiese et al. [13]. Figure 2.3 shows silicon balloon expander and hydrogel expander.

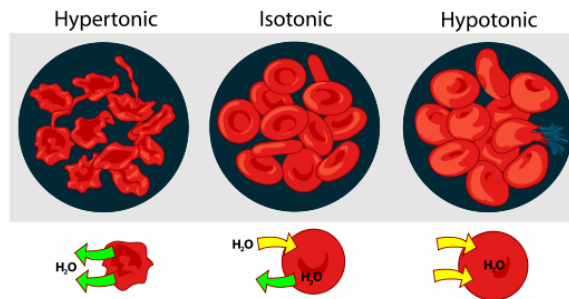


Figure 2.2. Effect of osmotic pressure, produced by a solution with different solute concentrations on the blood cells (Reproduced from [14]).



Figure 2.3. A conventional silicon balloon expander (left) and a hydrogel expander (right) with the same nominal final filling volume (scale in cm) (Reproduced from [13]).

Recently, Kobus [2] presented a preliminary report on cleft palate repair for 19 children aged from 2 to 3 years using the VP/MMA gels manufactured by OSMED (Ilmenau, Germany). Several VP/MMA gels were implanted under the mucoperiosteal layer of the hard palate in the first operation and 48 hours later a second operation was performed to repair cleft palate. Figure 2.4 shows the cleft palates before and after the two operations, as well as the hydrogels before and after the first operation.

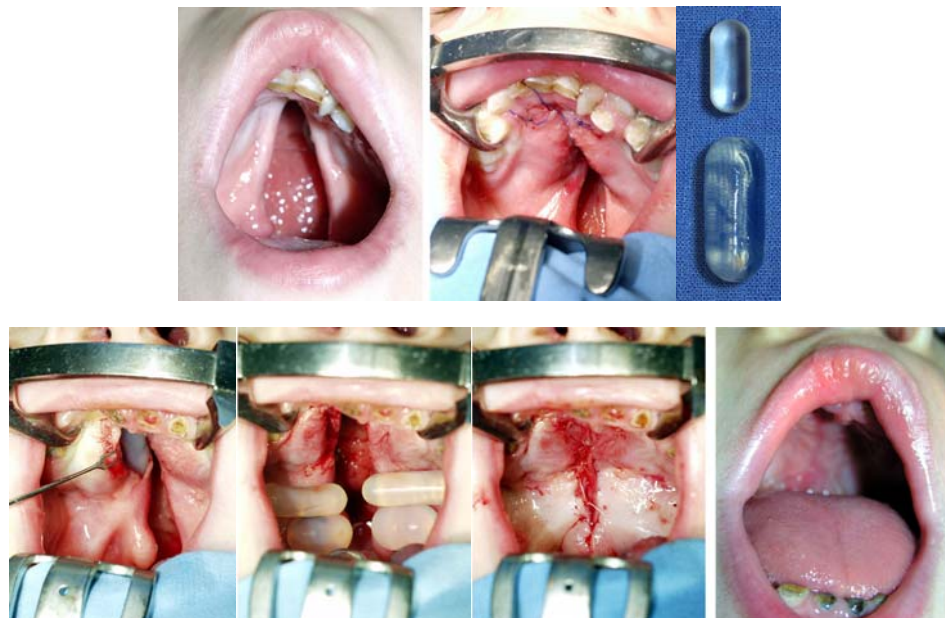


Figure 2.4. (Above, left) Unilateral incomplete cleft palate before treatment. (Above, center) Expanded mucoperiosteal tissue almost closing hard palate gap. (Above, right), Hydrogel expanders before and after swelling. (Below, left) Note exposed Expander after the expansion of 4 expanders. (Below, left center) Swelled cylinder-like expanders against the background of the palate. Immediate Result (Below, center right) and final outcome of palatoplasty without any relaxing incisions (Below, right) (Reproduced from [2])

In this work by Kobus, a very fast expansion time span was utilized which was criticized by Swan and coworkers [3] who emphasized the requirement for long in vivo swelling rates (more than 6 weeks), not only to avoid tissue necrosis, but also allow sufficient time for significant tissue growth (expansion) rather than stretching of the skin.

The slow swelling rate was also studied by Ronert and coworkers [4]. They used VP/MMA gels (OSMED, Germany) with 330 ml maximum swelling capacity and monitored the swelling behavior as a function of time of the hydrogels without a diffusive barrier envelope and compared this to a hydrogel covered with the silicone membrane with 0.2 to 0.5 mm thickness. The hydrogel without membrane showed relatively fast in vitro swelling compared to the hydrogel covered with the membrane. Time taken to reach 60 % of their respective maximum swelling ratios was achieved in 1 week for the uncoated gels and 2 weeks with the membrane. Ronert and coworkers also reported that hydrogel tissue expanders swell for 6 to 8 weeks in vivo and the slower swelling rate give more time for cells to recover to their isotonic swelling equilibrium state.

2.1.2. Polymers for Hydrogel Tissue Expanders

It has been known that poly(N-vinylpyrrolidone) (PVP) based copolymeric hydrogels induce high degrees of swelling in aqueous solution due to their hydrophilic functional groups. The PVP based copolymeric hydrogels [15, 16] are one of the most popular polymers used as biocompatible materials [17, 18]. PVP was the first synthetic polymer tested as a substitute for the artificial vitreous body of the eye [19]. Poly(methyl methacrylate) (PMMA) based copolymeric hydrogels [20, 21], which are known to be nontoxic and biocompatible, also shows a good mechanical strength for the tissue expander. When the VP/MMA hydrogels were implanted in the body, their volume was found to increase by approximately 250-300 % [12], which means volume swelling ratio

is in the range of 2.5 and 3.0. Later Wiese and his coworkers [13] replaced the CH₃ groups in the VP/MMA hydrogel chains with COOH groups, which produced higher swelling than VP/MMA hydrogels. This is because the carboxylic group can build up a higher osmotic pressure due to the dissociation of the COOH group into COO⁻ and H⁺. Although such attempts to use another material for tissue expansion, most hydrogels used clinically are still based on VP and MMA copolymers [2-4].

2.1.3. In Vitro/In-Vivo Swelling and Biocompatibility of Hydrogel Tissue Expanders

Measurements of in-vitro and in-vivo swelling of hydrogels have been also performed and compared by Wiese [12]. VP/MMA hydrogels were used and the importance of swelling pressure, P , which drives the swelling process, was determined. In the in-vitro swelling experiments, $P (= \pi - p = bc^a)$, where π is the osmotic pressure, p is the elastic contractibility of extended chains, b and a are constants, and c is the concentration) was monitored using a device as shown schematically in Figure 2.5[12]. The swelling ratio of the expander obtained was up to 22 in terms of volume. For in-vivo swelling of VP/MMA hydrogels, the gels were implanted in laboratory rats. After about 3 months, the expanders were removed for histology analysis and the increment in their volume was determined to be from 250 % to 300 % [12]. It was found that the expanded hydrogel was surrounded by fibrous capsules and there that was no inflammatory response, which indicated the expander is bio-benign.

Wiese and coworkers [13] presented the swelling properties and biocompatibility of modified VP/MMA hydrogels. They examined the effect of solvents and salt concentration on the swelling ratio and monitored the pressure using the device (Figure 2.5). They reported a sigmoidal shaped swelling pressure curve of the hydrogel expanders with time and explained that the linearly increasing region in the curve is

affected more by the pressure developed by the extension of chains in hydrogels during the swelling than by water diffusion.

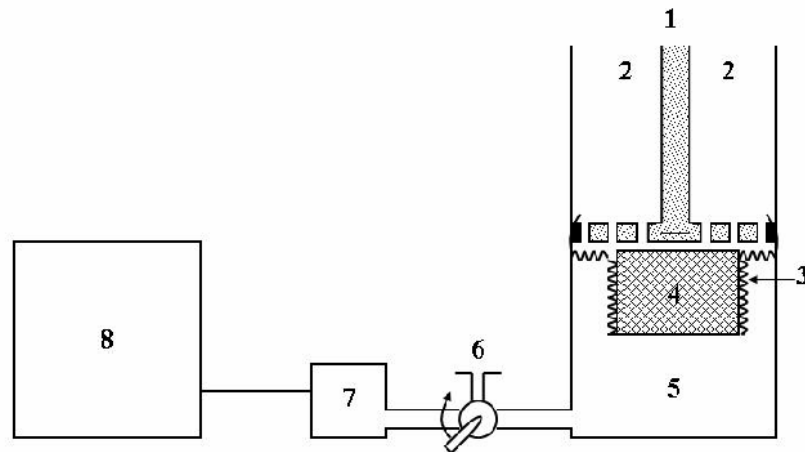


Figure 2.5. Schematic drawing of the pressure registration unit: (1) perforated piston with peripheral rubber sealing and lockable piston rod; (2) chamber with 0.9% NaCl-solution; (3) folded, waterproof membrane; (4) gel cylinder in expansion chamber; (5) measuring chamber; (6) triple way stopcock to evacuate the measuring chamber and approximate the membrane to the gel cylinder; (7) pressure transducer and (8) monitoring and recording system (Reproduced from [12]).

To assess biocompatibility, among many characterization methods, six different tests, which are cytotoxicity, cloning efficiency, mutagenicity, monocyte differentiation, mixed lymphocytes reaction (MLR), and foreign body reactions, were performed by Wiese and coworkers [12]. When testing for monocyte differentiation, the monocyte cells in the presence of hydrogels differentiated into normal macrophages and dendritic cells with expected morphology, indicating that the modified MA/VP hydrogel expander is biocompatible. The results of all six in-vitro tests proved the compatibility of the hydrogel expanders to the living tissues.

2.2. Hydrogels

2.2.1. Classification and Applications

Hydrogels are polymeric materials consisting of a three-dimensional network holding water within the mesh made by chemically or physically cross-linked polymer chains. Due to the network structure, they are able to swell but they do not dissolve in the aqueous solvents. Hydrogels have been classified in many different ways [17]. When the preparation method of hydrogel is considered, they are classified into four types: homopolymeric hydrogels, copolymeric hydrogels, multipolymeric hydrogels, and semi-interpenetrating polymeric hydrogels. When considering the ion content in the polymer chain, they are classified into neutral hydrogels and ionic hydrogels. The ionic hydrogels can be also categorized into anionic, cationic, and ampholytic hydrogels. The later have both positive and negative charges in the polymer chains and act as a base or as an acid depending on the characteristics of the surrounding environmental. Based on the chemical nature of the hydrogel, they are also classified into synthetic hydrogels, biological or biohybrid hydrogels. Biological hydrogels consist of natural polymers such as chitosan, collagen and alginate, and biohybrid hydrogels incorporate biologically active molecules in synthetic hydrogels [22]. Finally, classification depending on their physical structure is possibly giving chemical, physical, and topological hydrogels.

Hydrogels have frequently been used in various medical applications due to their excellent compatibility with living tissue and blood, their high oxygen permeability, and useful physical properties [23] as well as their ability to respond to their environment. Hydrogels were first developed by Wichterle and Lim in 1954 [24]. At that time, they used them as biomaterials. They synthesized copolymeric hydrogels of 2-hydroxyethyl methacrylate (HEMA) with ethylene dimethacrylate (EDMA) for clinical use as contact lens. Since hydrogels were initially used in biomaterials, they have been widely used in biomedical areas such as soft contact lenses [17, 25, 26], drug delivery systems [27-29],

artificial muscles [30, 31], biosensors [32, 33], wound dressings [34, 35], scaffolds [36, 37], and expanders [3, 12]. In addition, hydrogels have also been developed for the use in water filtration systems [38], soft robotic materials [39, 40], sensors [6], valves and switches [41, 42].

2.2.2. Synthesis

Synthesis of hydrogels is typically undertaken using chain polymerization mechanisms. Polymers can be prepared by solution polymerization with aqueous solvent but also by bulk polymerization without solvent. By definition, when the polymerization is preceded in an aqueous solvent (solution polymerization), hydrogels are obtained directly. When a bulk polymerization method is used for the synthesis, the final product is a gel since no solvent is involved for the system. In the latter case, the hydrogels are obtained after the gels have been swollen in an aqueous solvent.

In addition, hydrogels can be obtained not only by thermal polymerization but also by exposing a radiation. Thermal polymerization has been widely utilized to synthesize hydrogels [43, 44]. Several radiation types inducing γ -ray [15, 45] and electron beams (e-beams) [46, 47] and ultraviolet (UV) [15, 48, 49] have been used for the synthesis. Photo-polymerization requires a photosensitive initiator in order to produce a radical species through absorption of UV light of a certain wavelength.

Recently, hydrogels synthesized by photo-polymerization methods [15, 26, 27, 36, 37, 49-51] have been quite reported. In a photo-initiated reaction, a material irradiated by light absorbs light and becomes excited. The light absorption of a material, A , is determined by the empirical Lambert-Beer law ($A = \epsilon Cl$), where ϵ is the extinction coefficient, C is the concentration of a material, and l is the path length of light. The absorbance is defined by the equation, $A = \log_{10} (I_0/I_l)$ where I_0 is the light intensity of incident light and I_l is the light intensity after passing through the material. The

magnitude of the extinction coefficient depends on the type of chromophores in the material with its maximum absorbance occurring at a particular wavelength of the light [52]. The excited molecules dissociates into radicals, which initiate the radical chain polymerization. If the irradiated molecules are ionic, then the irradiation initiates ionic chain polymerization. For anionic polymerization to occur the monomer has to be electron withdrawing, and conversely electron donating for cationic polymerization. Photo-polymerization has several advantages over thermal polymerization: it occurs at ambient conditions, resulting in minimization of heating effects and no risk of living cell damage caused by high temperatures, polymerization times are relatively short and it can be used without solvent. Due to these advantages, this method has been used in not only synthesis of hydrogels but also many applications such as adhesives [53], dentistry [54, 55], painting, and cell encapsulation [51]. However, thermal polymerization is still explored due to simplicity and low cost.

2.2.3. Characterization of Gels

2.2.3.1. Gel Fraction, GF

When gels (or hydrogels) are obtained from the polymerization, the gel fraction (GF) of gels can be determined by soxhlet extraction. Non-reacted monomers and polymers, which did not participate in the gelation, are extracted by using a soxhlet extraction method [56, 57]. The gel fraction content (GF) is defined using the following relationship:

$$GF = \frac{W_f}{W_i} \quad (1)$$

where W_i and W_f are the weights of the gel before and after extraction, respectively. The gelation percent is $GF \times 100$.

2.2.3.2. Gel Composition and Chemical Structure

The chemical composition of the gels can be quantitatively determined using Fourier transform infrared (FTIR) [17, 20, 58] and attenuated total reflectance (ATR)-FTIR [59] spectroscopy, nuclear magnetic resonance (NMR) spectroscopy [20], and Raman spectroscopy [60].

2.2.3.3. Thermal Properties of gels

Thermal properties of gels have been characterized by differential scanning calorimetry (DSC) and thermogravimetric analysis (TGA). From DSC, the values of the glass transition temperature (T_g) for the gels can be obtained [61, 62] and their thermal stabilities determined using TGA. It is known that all T_g values observed for copolymeric gels depend on the copolymer composition. The effect of copolymer composition on T_g has been described using the Flory-Fox [28, 63] and the Gordon-Taylor equations [64, 65] shown in Equations (2) and (3), respectively.

$$T_g^{FF} = \frac{w_1}{T_{g,1}} + \frac{w_2}{T_{g,2}} \quad (2)$$

$$T_g^{GT} = \frac{w_1 T_{g,1} + k w_2 T_{g,2}}{w_1 + k w_2}, \quad k = \frac{\rho_1 T_{g,1}}{\rho_2 T_{g,2}} \quad (3)$$

where w_i , T_{gi} and ρ_i are the weight fractions, glass transition temperatures and densities of the two components ($i = 1$ and 2), respectively.

Malak and coworkers [65] reported that the T_g decreased with increasing the HEMA content for the VP/HEMA copolymer hydrogels. They also showed the composition dependence for their T_g which were also very well fitted to the Gordon-Taylor equation with k (the Gordon-Taylor constant) of 3. Al-Issa and coworkers [63] reported the T_g values VP/HEMA copolymers which were well fitted to the Flory-Fox

equation thus T_g of the copolymers could be predicted at all compositions. Geever and coworkers [62] also determined the T_g of VP/NIAAm gels using modulated DSC (MDSC) known to have relatively higher sensitivity and showed that the T_g values were 10 °C higher than that obtained by conventional DSC. With increasing NIAAm content in the gels, the T_g values decreased due to the relatively lower T_g of homopolymer of NIAAM than that of homopolymer of VP. Devine and Higginbotham [66] studied on VP/AA hydrogels physically crosslinked by photopolymerization and showed their T_g values decreased with increasing AA content in the gels.

Kwei reported that experimental T_g data can be fitted using the Kwei equation (Equation (4)) and The H-bonding interactions between constituent chain segments for copolymeric systems can be accounted for; where α and β are fitting parameters [67].

$$T_g^K = \frac{w_1 T_{g,1} + \alpha w_2 T_{g,2}}{w_1 + \alpha w_2} + \beta w_1 w_2 \quad (4)$$

Kuo *et al.* reported significantly higher T_g values than the mean of the pure components for low molecular weight PVP and PHEMA blends and diblock copolymers prepared by thermal polymerization and the higher values were explained with the H-bonding interactions between the hydroxyl-carbonyl groups [68].

2.2.3.4. Gel Swelling

The swelling behavior of the gels is typically observed by immersing the specimens of dried gels (or hydrogel containing a small content of water) into an aqueous solution at a predetermined temperature and monitoring their mass and volume change with time [44, 56, 69, 70]. The volume (q_v) and mass (q_m) swelling ratio are defined using the following equations:

$$q_m = \frac{m_s}{m_d} \quad \text{and} \quad q_v = \frac{V_s}{V_d} \quad (5)$$

where m_d is the mass of the dry gel, m_s is that of the swollen hydrogel at a time, V_d is the volume of the dried gel and of V_s is that of the swollen hydrogel at a specific time. In addition, the equilibrium swelling ratio in terms of volume and mass (q_{ve} and q_{me}) were also determined from the swelling behavior and diffusion characteristics of various hydrogels. The relationship between q_v and q_m is defined using the following equation [69]:

$$q_v = 1 + \frac{\rho_p}{\rho_s} (q_m - 1) \quad (6)$$

where ρ_p and ρ_s are the densities of the gel and the solvent (1 g/cm³ for water), respectively. Usually the hydrogel possessing more hydrophilic moiety in the chains show high q_v (or q_{ve}) and q_m (or q_{me}).

The swelling behavior of hydrogels can also be characterized from the point of view of the penetrant uptake behavior into crosslinked polymers. The penetrant diffusion into gels can be determined by analytical characteristics including a diffusion coefficient which is a variable in the mathematical equation for explaining swelling kinetics. The cooperative diffusion coefficient, D_c , can be evaluated from the data obtained from the swelling measurements and the self diffusion coefficient, D_s , from NMR measurements [71, 72]. Ray and his coworkers distinguished the D_s of water with temperature, diffusion coefficient of free water D_f and diffusion coefficient of bound water D_b associated with hydrogels [65, 72].

The swelling behavior and the diffusion of water into hydrogels can be also monitored by magnetic resonance imaging (MRI) [21]. The change not only in the swelling-induced volume or mass but also the transparency of hydrogels with time has

previously been reported [44, 62, 73]. Figure 2.6 shows MRI images of a poly(methyl acrylic acid) P(MAA) hydrogel swelling as a function of time at the pH of 7 after the gel had previously been soaked in aqueous buffer solution at the pH of 2.

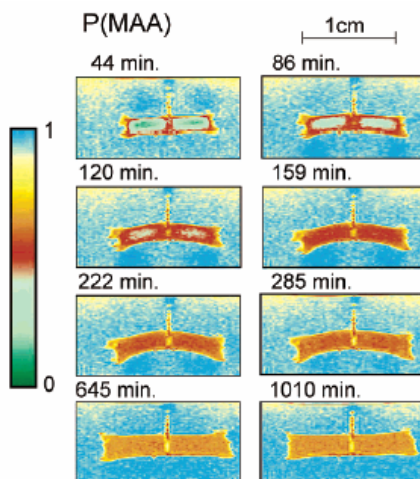


Figure 2.6. MRI images corresponding to the dynamic swelling isotherms of P(MAA) hydrogels in an aqueous solution at pH 7 and 25 °C. Prior to these measurements the gels had been soaked at pH 2 (Reproduced from [21]).

2.2.3.5. Mechanical Properties of Hydrogels

When hydrogels are used for a specific application, their structural integrity often needs to be maintained during their swelling. The elastic modulus, G and toughness of various hydrogels were evaluated by compressive stress and strain measurements using a dynamic mechanical analyzer (DMA) [74-77] or Instron micrometer [78]. David and coworkers [74] made an apparatus for the compression-stain measurement of PVP hydrogels crosslinked with various ethylene glycol dimethacrylate (EDMA) contents. They reported that the crosslinking density (ν_e) and mechanical properties of PVP

hydrogels increases with increasing content of the crosslinker (EDMA). Ravi and coworkers [77] studied the effect of water-ethanol composition effect on the mechanical properties. Malsanom and coworkers [78] studied the elastic properties of hydrogels synthesized from aqueous solutions of partially esterified hydroxypropylcellulose in addition to their swelling behavior and determined v_e and x values. They reported that the swelling ratio (q) decreased and v_e increased with increasing the degree of molar esterification. They also found that the gelation kinetics depends on the water-ethanol composition, which affects the properties of hydrogels. It is known that the toughness of hydrogels can be obtained from the stress and strain curve acquired from tensile test. Hiraguchi and his coworkers [76] synthesized clay nanocomposite PINPAm hydrogels and determined their mechanical properties. They showed that the composite hydrogels show very high toughness while hydrogels without clay particles has very low mechanical toughness and could extend up to strain of 900 % under the force of 6.2 N.

Atomic Force Microscopy (AFM) has also been used for determining the elastic modulus and surface morphology of hydrogels [79]. For determination of the mechanical properties of hydrogels, the bead of AFM tip should be large enough not to penetrate into hydrogel but rather deform it during the test [80].

2.2.3.6. Hydrogel Internal Morphology

Standard scanning electron microscopy (SEM) or environmental SEM (ESEM) has been used for observing the internal structure of hydrogels [81, 124, 140]. The use of SEM requires the hydrogels to be frozen and freeze-dried to remove the solvent without affecting the structure. Using ESEM, hydrogel specimens do not have to be dried to image them.

Guilherme and coworkers [81] observed the internal structure of for a sandwich-like IPN hydrogel of PNIPAAm in a PAAm network. Figures 2.7 (a) and (b) show SEM images of internal structure (internal layer (a) and external layer (b)) of the

IPN hydrogel. These authors reported that the internal layer of the PNIPAAm hydrogel, which shows LCST with the transition temperature at about 32 °C, shrank at the swelling temperature of 40 °C. While the external layers of the PAAm hydrogels swelled highly due to high hydrophilicity of PAAm. The collapsed structure of PNIPAAm inside the hydrogel contributed to improve the hydrogel strength.

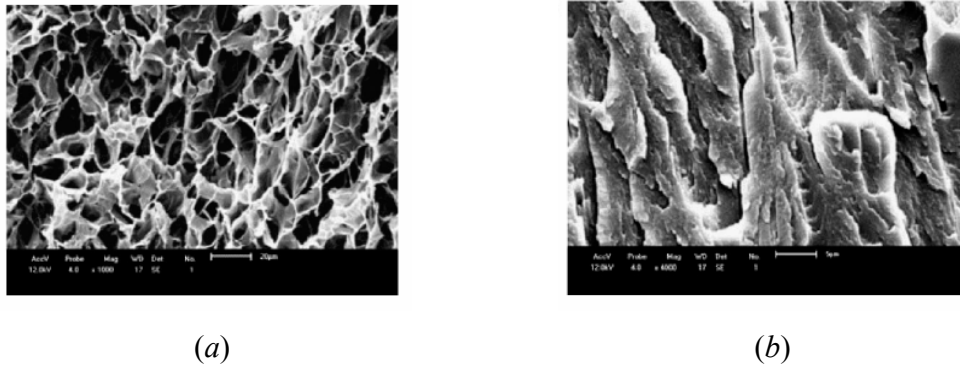


Figure 2.7. SEM images of sandwich-like IPN hydrogel having PNIPAAm inside PAAm networks. Micrographs of fractured hydrogel freeze-dried after swelling at 40 °C (a) external layer and (b) internal layer (Reproduced from [81]).

2.2.3.7. Biocompatibility of Hydrogel

When a host favorably responds to the implant material, the implant is considered to be biocompatible [82-85] so that when the material is implanted into the body, cells do not die but rather grow with subsequent rapid healing. When a host does not response to the implant and the material is considered to be biobenign. The hydrogel tissue expander should be at least biobenign.

To ascertain the biocompatibility of new materials before implantation, in vitro and/or in vivo tests are used. Usually an in-vitro cytotoxicity assay of the materials is performed as the first step for the verification of biocompatibility of the material and includes direct contact methods. In addition, the elution assay that is a quantitative method involves in counting the number of dead cells compared to living cells. Any toxic component from the materials hampers the metabolism and the functions of the cells and the synthesis of protein, and finally can induce cell death. Assays of cell adhesion, spreading and migration can also be used to determine the biocompatibility of the materials, as well as the protein production assay, which can be evaluated with calorimetry and fluorescent methods.

Ng and Swami [85] determined the biocompatibility of interpenetrating hydrogels of chitosan, VP, HEMA, N-hydroxymethyl maleimide (HMMI) using in-vitro tests. The cytotoxicity, proliferation and the viability of cells were investigated by MTT (3-(4,5-Dimethylthiazol-2-yl)-2,5-diphenyltetrazolium bromide, yellow tetrazolium salt) assay, a standard colorimetric assay, using human epidermal keratinocyte (HaCaT) cells. In this assay, MTT transformed into purple formazan crystals by the oxidation caused by the activation of an enzyme, which indicates the presence of living cells.

In addition, the inflammatory response to the implanted materials can be assayed using the cells such as neutrophils and macrophages. The in-vitro assay inflammatory response determines the adhesion, spreading, migration and death of cells, as well as cytokine release using some characterization methods such as radioactivity, spectrophotometry, ATP (Adenosine triphosphate) dependent luminometry, and immunohistochemistry [6, 84]. For the investigation of the in-vivo biobeneign properties, the materials are usually implanted in laboratory animals, where they remain for a few weeks. After the animals are euthanatized after a set period, the recovered implant material is treated using formalin and examined by conducting histomorphometry [84].

2.2.4. Swelling Behavior of Hydrogels

2.2.4.1. Thermodynamics of Hydrogel Swelling

As soon as a gel specimen is placed into water, an osmotic pressure of water inside and outside of the hydrogel is created and due to the water concentration gradient in the gel the water starts to diffuse into the gel spontaneously in order to reduce the Gibbs free energy of the system. Consequently, the hydrogel responds by swelling with time. The hydrogel approaches its equilibrium state when the driving force for the mixing between polymer species and solvent is balanced by the restoring force of the chains in the network due to the elasticity of polymer network.

The restoring force can be understood within the context of the elasticity of polymer network for a given load. The hydrogel is considered to display characteristic elastomer behavior as a function of force applied. At the molecular level, the deformation behavior of a polymer chain having a Gaussian chain distribution under constant load should be preceded by an understanding the elasticity of a polymer network because the behavior of one polymer chain between two crosslinking junctions in a polymer network can be considered to represent the behavior of a gel or hydrogel [86-88]. The probability distribution p of the end-to-end chain vector (r) is given by Equation (7). The restoring force (f) of a chain deformed due to constant applied load can be expressed in terms of the Helmholtz free energy A ($=E-TS$) and chain vectors as given by Equation (8).

$$p(\vec{r}_0) = \left(\frac{3}{2\pi Nb^2} \right)^{3/2} \exp\left(-\frac{3\vec{r}_0^2}{2Nb^2} \right) \quad (7)$$

$$f = \left(\frac{\partial A}{\partial r} \right)_{T,V} = \left(\frac{\partial E}{\partial r} \right)_{T,V} - T \left(\frac{\partial S}{\partial r} \right)_{T,V} \quad (8)$$

Here, N is the number of Kuhn segments of dimension, $b = \langle \vec{r}^2 \rangle^{1/2} / L$ (L is contour length of a chain), $\vec{r}_0(x_0, y_0, z_0)$ and $\vec{r}(x, y, z)$ are the end-to-end chain vectors before and after the deformation, S is entropy, E is internal energy, and T is the experimental temperature. S can be expressed by the number of conformations of a polymer chain (Ω), so that $S = k \ln \Omega$ (where k is a constant).

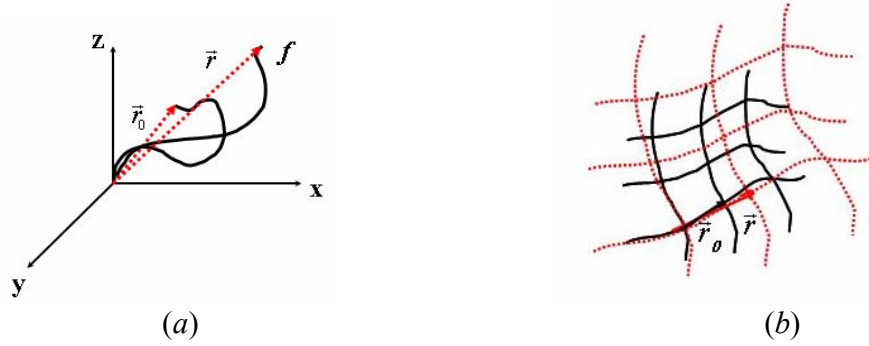


Figure 2.8. (a) the change of the end to end vector from \vec{r}_0 to \vec{r} of a polymer chain under a constant load, and (b) change in vector of a chain between two crosslinking junctions in a polymer network under the same condition as the applied to a polymer chain.

As indicated in Figure 2.8, an energy change occurs when a chain or network conformation changes due to an applied force. The entropy change ΔS can be determined by Equation (9).

$$\Delta S = -k_B \frac{3(r^2 - r_0^2)}{2Nb^2} = \frac{-3k \{x_0^2(\lambda_x - 1) + y_0^2(\lambda_y - 1) + z_0^2(\lambda_z - 1)\}}{2Nb^2} \quad (9)$$

Here, k_B is the Boltzmann constant, ν is the number of crosslinked strands per unit volume (V), and the x_0 , y_0 and z_0 are the components of \vec{r}_0 vector. For the deformation of a gel (see Figure 8(b)), the number of chains (n) in the gel should be considered, thus Equation (10) can be used to obtain the change of Helmholtz free energy for the deformation of the whole chains between two crosslinks in network ($\Delta\bar{A}_{el}$) shown in Equation (11).

$$\sum_{i=1}^n x_{0i}^2 = \sum_{i=1}^n y_{0i}^2 = \sum_{i=1}^n z_{0i}^2 = \frac{nNb^2}{3} \quad (10)$$

$$\Delta\bar{A}_{el} = -T\Delta\bar{S} = \frac{nk_B T}{2V} \{\lambda_x^2 + \lambda_y^2 + \lambda_z^2 - 3\} = \frac{\nu k_B T}{2} \{\lambda_x^2 + \lambda_y^2 + \lambda_z^2 - 3\} \quad (11)$$

When an isotropic deformation of polymer chain is considered for the gel swelling, all deformation ratios in x , y , and z direction are all same ($\lambda_x = \lambda_y = \lambda_z = \lambda$) and there is a simple relationship between λ and volume fraction of polymer at the equilibrium state of swelling, ν_{2e} (Equation (12)). Consequently $\Delta\bar{A}_{el}$ can be obtained in Equation (13) and (14) for the affine network model and phantom network model, respectively. Here the starting state of a gel is assumed as a dry state.

$$\lambda_x \lambda_y \lambda_z = \lambda^3 = V/V_0 = \nu_{2e}^{-1} \quad (12)$$

Assuming that the deformation of a chain in a gel follows the affine network model (the most established model of rubber elasticity proposed by Kuhn, each chain vector transforms linearly with macroscopic deformation), the deformation ratios of the polymer between networks in the x , y and z direction are simply λ_x , λ_y , and λ_z , respectively ($\lambda_x = x/x_0$, $\lambda_y = y/y_0$, and $\lambda_z = z/z_0$) [86] and the $\Delta\bar{A}_{el}$ for isotropic swelling of hydrogel is given by Equation (13). Here the functionality (ϕ) of the crosslink junctions

is considered since the hydrogel is not a perfect network and the logarithmic term is required for equilibrium swelling degree.

$$\Delta \bar{A}_{el} = \frac{3\nu k_B T}{2} \{\lambda^2 - 1\} - \frac{2\nu k_B T}{\phi} \ln \lambda^3 = \frac{3\nu k_B T}{2} \{v_{2e}^{-2/3} - 1\} - \frac{2\nu k_B T}{\phi} \ln v_{2e}^{-1} \quad (13)$$

When the deformation of a chain in a gel is consistent with a the phantom network model by James and Guth [89], the crosslinking junctions fluctuate without interfering by the neighboring chains and each chain vector transforms regardless of macroscopic deformation, , then the $\Delta \bar{A}_{el}$ for the isotropic swelling can be expressed by Equation (14)

$$\Delta \bar{A}_{el} = \frac{3\nu k_B T}{2} \left(1 - \frac{2}{\phi}\right) \{\lambda^2 - 1\} = \frac{3\nu k_B T}{2} \left(1 - \frac{2}{\phi}\right) \{v_{2e}^{-2/3} - 1\} \quad (14)$$

So far, only the change of free energy for the polymer deformation ($\Delta \bar{A}_{el}$) has been considered. However, for hydrogel swelling, not only $\Delta \bar{A}_{el}$ but also the change in the free energy of mixing ($\Delta \bar{A}_{mix}$) between the polymeric gel and solvent also contributes to the swelling. $\Delta \bar{A}_{mix}$ is defined as follows [86, 90].

$$\Delta \bar{A}_{mix} = kT(n_1 \ln v_1 + n_2 \ln v_2 + \chi n_1 v_2) \quad (15)$$

Here n_1 and n_2 are the mole fraction of polymer and solvent, respectively. The change of free energy for an isotropic swelling of a neutral hydrogel is given below.

$$\Delta \bar{A}_{swelling} = \Delta \bar{A}_{el} + \Delta \bar{A}_{mix} \quad (16)$$

The expression in terms of chemical potential contributed by mixing between polymer and solvent and by the elasticity of a polymer chain can be described as follows.

$$(\Delta \mu_1)_{swelling} = (\Delta \mu_1)_{mix} + (\Delta \mu_1)_{el} \quad (17)$$

At equilibrium, since the chemical potential of solvent for the system is zero (Equation 18), the relationships for the affine and phantom network model are obtained as shown in Equation (19) and (20), respectively.

$$\left[\frac{\partial (\Delta A_{swelling})}{\partial n_1} \right]_{n_2, T, V} = (\Delta \mu_1)_{swelling} = \mu_1 - \mu_1^0 = 0 \quad (18)$$

$$\ln(1 - v_{2e}) + v_{2e} + \chi v_{2e}^2 + \left(1 - \frac{2}{\phi}\right) v_e V \left\{ v_{2e}^{-1/3} - \frac{2}{\phi} v_{2e}^{-1} \right\} = 0 \quad (19)$$

$$\ln(1 - v_{2e}) + v_{2e} + \chi v_{2e}^2 + \left(1 - \frac{2}{\phi}\right) v_e V_1 v_2^{-1/3} = 0 \quad (20)$$

where μ_1 is the chemical potential of the solvent in the hydrogel, μ_1^0 is the chemical potential of the pure solvent, and $v_e (=v/(V \cdot N_{AV})$, V is the total volume of network) is the crosslink density. In addition, the Flory-Huggins parameter, χ and $v_e (= \rho / M_c$, ρ is the density and M_c is the molecular weight between crosslinks) and the M_c of hydrogels can also be determined from Equations (19) or (20) depending the model for analyzing a system.

When hydrogels contain ionic charges within the polymer network are swollen, the change of free energy for gel swelling has an additional term associated with the ionic free energy ($\Delta\bar{A}_{ion}$) and shows as follows:

$$\Delta\bar{A}_{swelling} = \Delta\bar{A}_{el} + \Delta\bar{A}_{mix} + \Delta\bar{A}_{ion} \quad (21)$$

The chemical potential terms for the ionic hydrogel system at the equilibrium are obtained from the derivative of each free energy terms, so that [86, 91].

$$\mu_1 - \mu_1^0 = 0 = (\Delta\mu_1)_{el} + (\Delta\mu_1)_{mix} + (\Delta\mu_1)_{ion} \quad (22)$$

$$(\Delta\mu_1^*)_{ion} - (\Delta\mu_1)_{ion} = (\Delta\mu_1)_{mix} + (\Delta\mu_1)_{el} \quad (23)$$

where $(\Delta\mu_1^*)_{ion}$ and $(\Delta\mu_1)_{ion}$ are the chemical potential difference of solvent outside and within the hydrogel, respectively. This difference between the ionic contribution on the chemical potential inside and outside the hydrogels is expressed as follows [86, 91].

$$\begin{aligned} (\Delta\mu_1^*)_{ion} - (\Delta\mu_1)_{ion} &= V_1 RT \left(\frac{i^2 c_2^2}{4I} \right) = V_1 RT \left(\frac{i^2}{4I} \left(\frac{v_2 \Phi}{\bar{v} M_0} \right)^2 \right) \\ &= V_1 RT \left(\frac{1}{4I} \left(\frac{K_a}{10^{-pH} + K_a} \right)^2 \left(\frac{v_2 \Phi}{\bar{v} M_0} \right)^2 \right) \end{aligned} \quad (24)$$

where V_1 is the molar volume of solvent, R is ideal gas constant, T is absolute temperature, i is the degree of ionization, c_2 is the mole concentration of ionizable polymer (v_2/v_u ; v_u is the molar volume of a repeat unit of ionizable polymer), I is the ionic strength of the solvent, v_2 is the polymer volume fraction, Φ is the weight fraction of

ionizable polymer in the gels, \bar{v} is the specific volume of polymer, and M_0 is the molecular weight of repeat unit. For hydrogels with monoprotic acid species, i is defined by acid ionization constant, K_a , and pH of the swelling medium.

In a phantom network model proposed by James and Guth [89] the polymer deformation gives the Equation (25) for $(\Delta\mu_1)_{el}$.

$$(\Delta\mu_1)_{el} = \frac{RT(1-2/\phi)V_1v_{2r}^{2/3}v_2^{1/3}}{\bar{v}M_c} \quad (25)$$

where, v_{2r} is the polymer volume fraction in the reference state (for the swelling of dry gel, $v_{2r}=1$) and ϕ is the number of branches originating from a crosslinking junction.

The complete expression for the swelling of hydrogels at the equilibrium state is finely given in Equation (26).

$$\ln(1-v_2) + v_2 + \chi v_2^2 + \frac{(1-2/\phi)V_1v_{2r}^{2/3}v_2^{1/3}}{\bar{v}M_c} = V_1 \left(\frac{1}{4I} \left(\frac{K_a}{10^{-pH} + K_a} \right)^2 \left(\frac{v_2\Phi}{\bar{v}M_0} \right)^2 \right) \quad (26)$$

Swelling behavior of hydrogels in aqueous solvent has analogies with polymer dissolution in a solvent [86]. The swelling behavior depends not only on the interactions between different segments within the polymer network chains but also interactions between the polymer chains and the surrounding solvent. Thus, the hydrophilicity (or hydrophobicity) of polymer chains plays an important role in the swelling behavior and equilibrium water content.

2.2.4.2. Kinetics of Hydrogel Swelling: Penetrant Diffusion in Hydrogels

Diffusion is a process of movement of molecules, heat, and momentum due to gradients in concentration, temperature, and velocity. The diffusion of penetrants such as

drug molecules or water molecules into or out of hydrogels induces the swelling of hydrogels and plays a very important role in many medical fields. When a gel is placed into the water, the water diffuses into the hydrogel via osmosis without dissolving the hydrogels because the hydrogel is crosslinked.

The type of mechanism of solvent diffusion into a polymer matrix as classified by Alfrey et al. [92] has been used for the characterization of the solvent diffusion into hydrogels. In their work, the penetration of solvent was categorized into three cases based on the relative rates of solvent penetration and polymer relaxation. Case I (or Fickian diffusion) occurs when the diffusion rate of solvent is significantly slower than that of polymer relaxation, Case II (or non-Fickian diffusion) occurs when the diffusion rate of solvent is much larger than that of the polymer chains, and Case III (or non-Fickian diffusion) occurs when the diffusion rate of solvent into a polymer matrix is comparable to that of the polymer chains. The time dependency for normalized solvent uptake is of the form, kt^n . The diffusion coefficient (D) of a solvent can be calculated [93] using the following equation.

$$\frac{W_t}{W_\infty} = kt^n = 4\left(\frac{Dt}{\pi l^2}\right)^n \quad (27)$$

where W_t and W_∞ are the weight of solvent uptake of hydrogel at time t and at equilibrium time t_∞ , respectively. The solvent uptake is normalized by the equilibrium solvent uptake. The variable k is the swelling rate constant which is related to the structure of the network, the variable n is the characteristic exponent which implies the type of transport mechanism (*i.e.* diffusion mode), and variable l is the film thickness. Prior to the calculation of D value for a penetrant through hydrogels, the k and n values are determined using a log-log plot for a normalized solvent uptake, *i.e.*

$\ln(W_t / W_\infty) = \ln k + n \cdot \ln t$. While the value of $n=0.5$ indicates Fickian diffusion, the n value ranging from 0.5 to 1.0 implies non-Fickian diffusion or anomalous diffusion mode.

Peppas et al. [69, 73, 94] reported that for the Fickian diffusion system the data taken from the initial 60 % of the penetrant uptake, which shows linearly increase with time, are analyzed using the Equation (27) to determine D and for the data taken from the last 40 % of the penetrant uptake, which are usually show exponentially increase with time, the value of D can be calculated by Equation (28) as follows [73]:

$$\frac{W_t}{W_\infty} = 1 - 8 / \pi^2 \left\{ \exp \left(- \frac{\pi^2 D t}{l^2} \right) \right\} \quad (28)$$

Factors such as crosslinking density, drug type, copolymer composition and polymer type [66, 133] which affect on swelling kinetics have also been investigated for certain hydrogel systems. Peppas and Brazel [73] reported that the mechanism of penetrant transport depends on the size of drug molecules and the size exclusion characteristics of the polymeric hydrogels.

2.2.4.3. Change in Transparency During Swelling

The change not only in the swelling-induced volume but also transparency of hydrogels with time has been previously been reported by several authors [44, 62, 73]. Geever [62] reported that the hydrogel initially became opaque and subsequently transparent as they approached their equilibrium swelling state. Brazel and Peppas [73] reported that solvent diffusion occurred in two steps. In the first step, only the edge of hydrogel became transparent and the core part remained opaque. In the second step, the core part also became transparent with anisotropic swelling. Chi and coworkers [44] also reported the appearance of opacity in tetrahydrofurfuryl methacrylate (THFMA)/HEMA

copolymer hydrogels during the swelling. They explained that when water diffused faster than polymer chain relaxation to equilibrate, the irregularity was made in pores in THFMA/HEMA hydrogels resulting in microheterogeneity. And they also mentioned that with swelling time, the microheterogeneity disappeared by the relaxation of chains in networks, which induces the transparency of fully swollen hydrogels. The same changes in transparency were observed for all gel compositions, which agree with the studies of Brazel and Peppas [73].

Extensive studies on spatial inhomogeneity in hydrogels (mostly charged hydrogels) [95-97] have been reported using scattering techniques such as dynamic light scattering (DLS), small-angle x-ray scattering (SAXS) or small angle neutron scattering (SANS). Shibayama observed large concentration inhomogeneity only at equilibrium swollen state of hydrogels due to the frozen topological structure in the gels [95].

2.2.5. Mechanical properties

The mechanical properties of hydrogels are dependent on their network structure and degree of swelling (q). Appropriate mechanical strength of hydrogels is need depending on their various applications. Specifically, for skin tissue expansion the moduli of hydrogels are supposed to be similar to those of human living tissues in the range between 0.1 kPa and 50 MPa [98, 99].

An understanding of the mechanical behaviors of hydrogels could be achieved based on the theory of the rubber elasticity and the statistical thermodynamic equation of state for the elasticity of polymer network as described in Section 2.2.4.

For the uniaxial deformation of a gel ($\lambda_x = \lambda$, $\lambda_y = \lambda_z = 1/\sqrt{\lambda}$), the $\Delta\bar{A}_{el}$ can be expressed with only λ as given in Equation (29) and the modulus (G) of the gel can be acquired from the slope of engineering stress (τ_{eng}) obtained by the second derivatives of $\Delta\bar{A}_{el}$ with respect to length as given in equation (30).

$$\Delta \bar{A}_{el} = \frac{\nu k_B T}{2} \{\lambda_x^2 + \lambda_y^2 + \lambda_z^2 - 3\} = \frac{3\nu k_B T}{2} \{\lambda^2 - 1\} \quad (29)$$

$$\begin{aligned} \left(\frac{\partial^2 \bar{A}_{el}}{\partial r^2} \right) &= \frac{\partial^2}{\partial r^2} \left\{ \frac{\nu k_B T}{2} \left(\lambda^2 + \frac{2}{\lambda} - 3 \right) \right\} = \tau_{eng} \\ &= \frac{\nu k_B T}{V} \{\lambda - \lambda^{-2}\} = \frac{N_{AV} \rho}{M_c} k_B T \{\lambda - \lambda^{-2}\} = \nu_e R T \{\lambda - \lambda^{-2}\} = G \{\lambda - \lambda^{-2}\} \end{aligned} \quad (30)$$

Where ν_e is the crosslinking density, N_{AV} is the Avogadro's number, R is the gas constant, and M_c is the molecular weight between crosslinks.

The engineering stress within at a dry unswollen gel under an uniaxially applied force is expressed by Equation (30), $\tau_{eng} = G\{\lambda - \lambda^{-2}\} = \nu_e R T \{\lambda - \lambda^{-2}\}$. For a swollen hydrogel, this equation above is modified to $\tau_{eng} = \nu_e R T \nu^{1/3} \{\lambda - \lambda^{-2}\}$. The curve of τ_{eng} versus λ using the theoretical equation is shown in Figure 2.9 as well as the typical experimental curve for τ_{eng} versus λ for the lightly crosslinked materials. For large deformation of hydrogels there is a significant deviation from the curve predicted by theoretical equation. The Mooney-Rivlin equation shown below is frequently used for fitting the high elongation data experimentally obtained for rubbers [91, 100].

$$\tau = 2 \left(C_1 + \frac{C_2}{\lambda} \right) \left(\lambda - \frac{1}{\lambda^2} \right) \quad (31)$$

For the swollen hydrogels, Equation (31) can be modified to give:

$$\tau = 2C_1 \nu_2^{1/3} \left(\lambda - \frac{1}{\lambda^2} \right) + 2C_2 \nu_2^{5/3} \left(\lambda - \frac{1}{\lambda^3} \right) \quad (32)$$

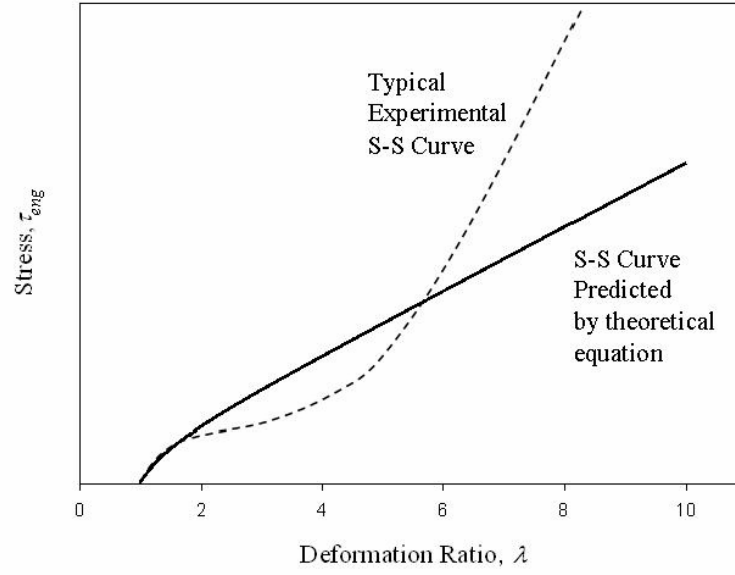


Figure 2.9. The curves of τ_{eng} versus λ obtained using the theoretical thermodynamic equation and by the deformation experiments in uniaxial direction for hydrogels.

The mechanical behavior of hydrogels is affected by the comonomer composition, crosslinking density, polymerization conditions, degree of swelling and the swelling medium, and is investigated by performing creep and stress relaxation test as well as dynamic test [101].

2.2.6. Network Structure Characteristics

The unique swelling behavior of hydrogels depends on their network structure characteristics. characteristics of network structure have been determined by a number of

researchers [43, 61, 89, 102] based on the equations developed by Flory and Rehner [61, 86] and the relationship introduced by Rubenstein and Colby [89].

Structural parameters such as the effective crosslinking density (ν_e), the molecular weight between crosslinking junctions (M_c), mesh size (ξ), and end-to-end distance in the unperturbed state ($\sqrt{\bar{r}_0^2}$) of the hydrogels are given by Equations (33) - (36).

$$G = \nu_e RT \nu_{2e}^{-1/3} = \nu_e RT q_{ev}^{1/3} \quad (33)$$

$$M_c = \rho / \nu_e \quad (34)$$

$$\xi = 0.071(\nu)^{-1/3} \sqrt{M_c} = q_v^{1/3} \sqrt{\bar{r}_0^2} \quad (35)$$

$$D_c = \frac{(k_B T)}{(6\pi\eta\xi)} \quad (36)$$

where $q_{ev} (=V_\infty/V_d)$, V_∞ and V_d are the volume of an equilibrium swollen hydrogel sample and the gel volume before swelling, respectively) is the equilibrium swelling ratio of gel, R is the gas constant, T is temperature, ρ is the density of the gel, k_B is Boltzmann's constant, and η is viscosity of the fluid.

When a hydrogel is fully swollen, the modulus can be expressed in the Equation (33) since its equilibrium swelling ratio in terms of volume (q_{ev}) can be used instead of the volume fraction of polymer at the equilibrium (ν_∞). The modulus (G) and q_{ev} are obtained via the mechanical and swelling measurements, respectively, from which ν_e and M_c can be calculated [43, 89] by using the Equations (33) and (34). The $\sqrt{\bar{r}_0^2}$ can be determined by scattering techniques such as small angle neutron scattering (SANS) [103] or small angle X-ray scattering (SAXS) [104]. In addition, the cooperative diffusion coefficient (D_c) can be obtained using Equation 36 [105] assuming that mesh size (ξ) is equal to the hydrodynamic correlation length (ξ_H) at the swelling equilibrium state [106],.

It is obvious that these structural parameters are related to the mechanical properties and swelling behavior [49, 57, 107-109].

The M_c of ionizable hydrogel can be determined using Equation (26). For the convenience, the expression is rearranged as shown below. M_c and χ values of the hydrogels are determined from the slope and exploration, respectively, of the plot of A as a function of B.

$$A = \chi + \frac{B}{M_c} \quad (37)$$

Where

$$A = \left(\frac{V_1}{4I} \left(\frac{K_a}{10^{-pH} + K_a} \right)^2 \left(\frac{v_2 \Phi}{\bar{v} M_0} \right)^2 \right) - \left(\frac{1}{v_2^2} \ln(1 - v_2) + \frac{1}{v_2} \right) \quad \text{and}$$

$$B = \left(\frac{(1 - 2 / \phi) V_1 v_{2r}^{2/3} v_2^{-5/3}}{\bar{v}} \right).$$

2.2.7. Parameters Affecting on Swelling and Network Structure

It has been shown that hydrogels possessing high v_e (or low M_c) usually show low q_e but high G , which indicates that the structure of the hydrogel determines the swelling and mechanical properties. These properties are affected by several factors such as the type of cross-linker, initiator or monomer [57, 70, 107-109, 110-112], feed monomer compositions [44, 70, 110], cross-linker concentrations [45, 57, 70, 107, 108, 110-112], initiator concentrations [107, 113, 114], photo-irradiation intensity [15, 45-49], hydrophobicity [115-117] and inclusions [40, 76, 118, 119]. All these factors can affect the structure of hydrogels and thus regulate their intrinsic properties such as swelling and mechanical properties.

In addition, environmental conditions experienced by the hydrogels such as the experimental temperature [57, 107, 120, 121], pH [22, 57, 107, 110, 122], penetrant (swelling agent or solvent) type [38, 123, 124], and applied electric field [125] or magnetic fields [31] affect their swelling behavior. In this section, reports on these parameters affecting the properties of hydrogels are described.

2.2.7.1. Control over the Structure of Hydrogels

2.2.7.1.1. Type and Composition of Feed Monomers

Muratore and coworkers [109] synthesized MMA/VP and MMA/HEMA copolymer hydrogels using γ -irradiation and investigated their swelling properties and structure characteristics. Equilibrium water content (EWC) and M_c of MMA/NVP copolymer hydrogels was much higher than that of MMA/HEMA copolymer hydrogels. The values of EWC and M_c for MMA/NVP and MMA/HEMA hydrogels increased with increasing VP content in MMA/NVP hydrogels and with decreasing HEMA content in MMA/HEMA hydrogels, respectively. Hill and coworkers [115] synthesized MMA/HEMA, BMA/HEMA, HEMA/cyclohexyl methacrylate (CHMA) hydrogels and compared their swelling kinetics. Water uptake at equilibrium, S_e , and diffusion coefficient, D were shown to be higher for MMA/HEMA hydrogel than BMA/HEMA and cyclohexyl methacrylate (CHMA)/HEMA hydrogels. They also reported that as BMA content increased in gels, S_e and D decreased (see Figure 2.10).

The swelling behavior of the VP/butyl acrylate (BA) copolymer hydrogels prepared using γ -irradiation was observed by Atta and Abdel-Azim [108]. They reported that as BA content increased, the q_e and M_c decreased but the ν_e and x increased.

Kim and his coworkers [39] prepared various AA/vinylsulfonic acid (VSA) copolymeric hydrogels with different feed monomer ratios and observed the swelling

behavior in 0.9 wt % aqueous NaCl solutions. The q_e obtained was determined to be in the range between 10 and 50 and increased with increasing VSA content in the hydrogels.

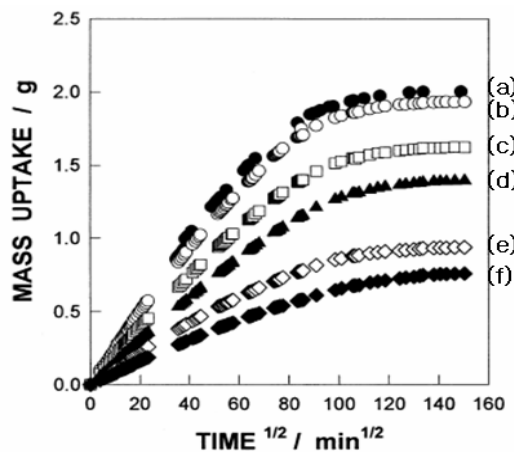


Figure 2.10. Water uptake measurements for BMA/HEMA copolymers of mole fraction of BMA (F_{BMA}): $F_{BMA} = 0.0$ (a); $F_{BMA} = 0.025$ (b); $F_{BMA} = 0.05$ (c), $F_{BMA} = 0.075$ (d); $F_{BMA} = 0.1$ (e); and $F_{BMA} = 0.15$ (f) (Reproduced from [115]).

2.2.7.1.2. Type and Concentration of Initiator

Hydrogels show smaller q_e with increasing initiator concentration (C_i) not only because more radicals induce more monomers propagating their polymerization [65] but also because the inhibition period is shortened at high C_i . However, there is also a possibility that q_e is small at high C_i due to free radical degradation or the higher chain termination rate.

Chung et al. [113] studied various dextran (Dex)/HEMA hydrogels prepared using various concentrations of potassium persulphate (KPS), initiator, and reported that the hydrogels showed smaller q_e with increasing C_i because more radicals induce more monomers propagating their polymerization. Polyacrylamide (PAAm) hydrogels have also been prepared using ammonium peroxydisulfate (APS), initiator, by Omidian and

Park [114]. They stated that the hydrogel showed lower q_e when higher C_i was used because the inhibition period is shortened at C_i .

Hosseinzadeh et al. [126] prepared kappa-carrageenan (κ C) based hydrogels using APS initiator and reported that there might be free radical degradation which can be occurred at the higher C_i .

Equilibrium swelling percent (q_e %) of methacrylamide (MAAm)/MAA (methacrylic acid) copolymer hydrogels was observed as a function of KPS concentration (see Figure 2.11) by Bajpai and Singh [107]. They reported that q_e % increased with increasing initiator concentration (C_i) due to relatively higher molecular weight polymeric chains, which was initiated by higher members of free radicals, and then it decreased with further increment in KPS concentration due to the higher chain termination rate.

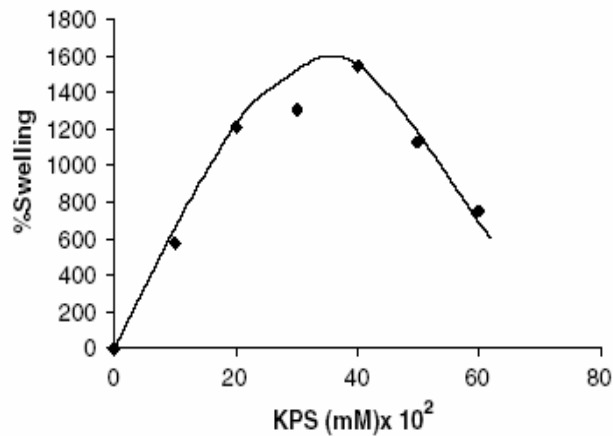


Figure 2.11. The swelling % of MAAm/MAA hydrogels as a function of initiator (KPS) concentration (Reproduced from [107]).

2.2.7.1.3. Type and Concentration of Crosslinker

It has been reported that as cross-linker concentration (C_c) decreases, the q_e and M_c of hydrogels increases [57, 107]. However, Ende and Peppas [110] did not observe

any effect of C_c on the swelling of hydrogels. They used acrylic acid (AA)/HEMA hydrogels crosslinked with ethylene glycol dimethacrylate (EGDMA) and showed that only a small portion of EPDMA participated in the synthesis of AA/HEMA hydrogels. The effect of functionality of crosslinker has also been reported, where it was found that the higher functional crosslinker produced higher values of q_e [108, 112].

Atta and Arndt [57] studied HEMA and VP copolymer hydrogels crosslinked in the presence of different concentrations of melamine trimethacrylamide (MMAm) and melamine triacrylamide (MAAm) as crosslinkers. MAAm was shown to be a better cross-linker for higher equilibrium swelling ratios (q_e) of VP/HEMA hydrogels with q_e decreasing with increasing concentration of both cross-linkers. Bajpai and Singh [107] studied the swelling behavior of various MAAm/MAA copolymeric hydrogels prepared with various concentration crosslinker of N,N-methylene bisacrylamide (BIS), and showed that as BIS concentration decreases, q_e and M_c increases.

Ende and Peppas [110] studied the swelling behavior and network structure characteristics of various AA/HEMA copolymer hydrogels crosslinked with various concentrations of ethylene glycol dimethacrylate (EGDMA), cross-linker, and reported that the q_e was not dependent of EGDMA concentration because only a small portion of EPDMA was incorporated in the synthesis of AA/HEMA hydrogels.

Atta and Abdel-Azim [108] observed the swelling behavior of the hydrogels synthesized using the hexafunctional crosslinker, 1,1,1-trimethylolpropane dimethacrylate (TPT), and the tetrafunctional crosslinker, N, N-methylene bisacrylamide (BIS). They found that the hydrogels crosslinked with TPT and smaller cross-linker concentration showed higher q_{me} or equilibrium water content (EWC). Xue and coworkers [112] prepared NIPAm/AA hydrogels crosslinked with the octafunctional crosslinker, glyoxal bis(diallylactal) (GLY) and the tetrafunctional crosslinker, BIS. They also found that the hydrogels crosslinked with GLY showed higher q_e at smaller concentrations.

2.2.7.1.4. Intensity of UV Irradiation

It has been shown that high photo-irradiation intensities for gel synthesis produce gels with high ν_e and low q_e [15, 45] as well as high G [49]. However, Henker and coworkers [46] reported that the radius of gyration (R_g) of PVP-PAA nanogels, prepared using electron-beam (e-beam) irradiation, initially increased and then decreased again with increasing e-beam dose due to the radical induced degradation of the chains.

It has been shown that higher photo-irradiation intensities for gel synthesis produces gels having an effective crosslinking density (ν_e), resulting in lower equilibrium swelling ratio (q_e). Kaplan and Guner [14] reported the ν_e in PVP gels varied with different γ irradiation doses and the use of higher doses produced higher ν_e and lower q_e values in the gel. Bhardwaj and coworkers [45] studied swelling kinetics of copolymer hydrogels of *p*-sodium styrene sulfonate (SSS) and vinyl benzyl trimethylammoniumchloride (VBT). They reported that the gel swelling kinetics was affected by the total dose of γ -irradiation as shown in Figure 2.12 and the hydrogels possessed higher ν_e and lower q_e when higher irradiation dose was used. Wong et al. [49] reported that higher UV exposure intensity produces PAAm hydrogels with higher moduli and ν_e , however they were not interested in the swelling of hydrogels affected by UV intensity.

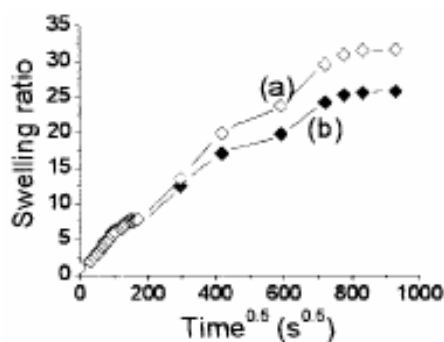


Figure 2.12. The swelling ratio of SSS-co-VBT gel vs. time for two total dose (a) 5 kGy and (b) 10 kGy (Reproduced from [45]).

Said and coworkers [47] synthesized carboxymethyl cellulose (CMC)/AAc using E-beam irradiation and investigated the effect of beam intensity on the swelling. They reported that the linkage between CMC and AAc inside the hydrogels increased with increasing beam dose. Henke and coworkers [46] studied PVP-PAA nanogels prepared using beam, and showed that the radius of gyration (R_g) of the nanogels with increasing the beam dose. Initially the R_g increased and then decreased with increasing beam dose due to the radical induced degradation of chains.

2.2.7.1.5. *Hydrophobicity*

Recently, the study on the introduction of hydrophobic parts in the hydrophilic hydrogel systems has been performed for drug delivery systems [115-117] in order to carry the drugs with hydrophobicity. Hydrogels possessing hydrophobic moieties in the chains show not only low q_e but also low D [110, 115, 117, 127].

Hill et al. [115] investigated the effect of hydrophobic moieties incorporated into the HEMA based copolymer hydrogels on their water uptake at equilibrium (S_e) and D and reported that S_e and D of BMA/HEMA and cyclohexyl methacrylate (CHMA)/HEMA hydrogels with more hydrophobic pendent groups showed lower S_e and D than MMA/HEMA hydrogels.

Vieira and coworkers [116] synthesized amphiphilic NIPAAm/PEG/dodecyl methacrylate (DOMA) hydrogels formed amphiphilic aggregates of 40-150 nm diameters, as determined by dynamic light scattering (DLS). This was explained by the hydrophobic moieties of DOMA aggregate in aqueous solutions with hydrophilic moieties of PEG on the surface of the aggregate, which induces nanogels with core-shell structure. Yu and Grainger [100] studied drug release from PNIPAAm gels incorporated with the hydrophobic alkyl acrylamide species, sodium acrylate (SA) as a comonomer. As SA content increased in the gel, a thermal phase transition temperature shifted to lower temperatures and decreased PNIPAAm gel swelling.

2.2.7.1.6. *Inclusions*

Composite hydrogels containing nano-size or micro-size particles can possess not only elastic properties due to the hydrogels but also specific properties induced by the inclusion type [40, 76, 118, 119].

Lee and Tsao [118] obtained a composite hydrogel by incorporating silver nanoparticles into an AA and poly(ethylene glycol) methyl ether acrylate (PEGMEA) solution and found that the q_e and D of AA/PEGMEA composite hydrogels were smaller than those of AA/PEGMEA hydrogels without the nanoparticles. However, the electrical conductivity and antibacterial activity were shown to be better than those of pure AA/PEGMEA hydrogels. Usually the composite hydrogels including nanoparticles show lower q_e .

However, for the NIPAAm/clay composite hydrogel systems developed Haraguchi and coworkers [76], high values of q_e , as well as extraordinary mechanical/optical properties of the hydrogels were obtained. They stated that although the system is a physical hydrogel, the clay particles act as a cross-linkers.

Dispenza and coworkers [119] reported both polyaniline (PANI)/PVP and PANI/PVA composite hydrogels. These composite hydrogels were obtained by in-situ γ -irradiation polymerization of aniline in the presence of PVP or PVA, which acted as a steric stabilizer. They also showed that PVP and PVA composite hydrogels dispersed with PANI particles of 30 nm diameter were very sensitive to pH, however, they did not show the swelling behavior of the composite hydrogels.

Ferrogels containing ferromagnetic particles is another type of composite hydrogels. Ramanujan and Lao [31] prepared a composite hydrogel possessing Fe_3O_4 particles dispersed in a PVA hydrogel matrix. They reported that the PVA/ Fe_3O_4 ferrogels were elongated and bent when a magnetic field was applied and the degree of elongation and deflection was dependent on the applied magnetic field strength.

2.2.7.2. External Conditions Hydrogels

2.2.7.2.1. Temperature of Swelling

Temperature responsive hydrogels have recently been applied in biomedical areas. Typically the temperature-sensitive hydrogels exhibit a low critical solution temperature (LCST). Below the critical temperature the hydrogels swell, and above it they shrink [25]. Poly(N-isopropylacrylamide) (PNIPAAm) hydrogel (LCST $\sim 35^\circ\text{C}$) is one of the most well known examples of temperature-sensitive hydrogels and has been used to investigate the volume phase transition induced by altering interaction between polymer molecules and solvent with temperature [4, 40, 76, 112, 121]. Takahashi and coworkers [121] reported that PNIPAAm hydrogels shows the drastic volume change and opaqueness around 35°C regardless of gel type as shown in Figure 2.13.

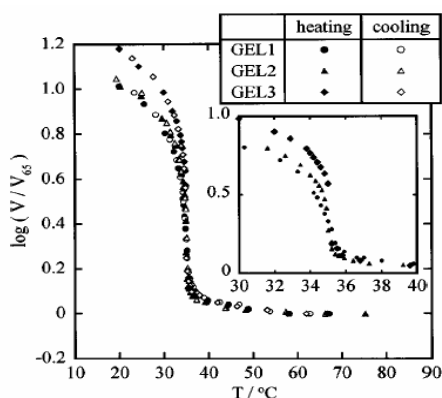


Figure 2.13. Temperature dependence of normalized volume V/V_{65} of PNIPAAm gel 1, 2, and 3 crosslinked with different monomer/cross-linker molar ratio of 20, 60, and 80, respectively. Here, V_{65} represents V of each gel at 65°C . The inset shows the enlargement around 35°C (Reproduced from [121]).

Sakellariou [128] showed LCST behavior in PVP hydrogels with a LCST is at around 140°C . This high LCST value of PVPs can be decreased by incorporating crosslinkers [57], although it was shown that their LCST values were all the same regardless of crosslinker concentrations [91, 103]. Atta and Arndt [57] used melamine

trimethacrylamide (MMAm) and melamine triacrylamide (MAAm) as crosslinkers and decreased the LCST of hydrogels to 30 - 45 °C. They also reported that the LCST of VP/HEMA hydrogels decreased with increasing HEMA content. The temperature dependence q_e of different NIPAAm/AA hydrogels crosslinked with different GLY concentrations was investigated by Xue and coworkers [112]. They showed the q_e of NIPAAm/AA hydrogels decreased with increasing temperature and their LCST values are around 27 °C regardless of GLY concentration, which agrees with the LCST values of PNIPAAm hydrogels obtained by Takahashi and coworkers [121].

2.2.7.2.2. pH

pH-sensitive hydrogels have a ionic network structure containing either acidic or basic groups on their chains which are sensitive to pH and ionic strength [25, 28, 45, 57, 110, 113]. These hydrogel sensors can be used to detect analytes and environmental changes around the sensor [22].

The pH-sensitive hydrogels have ionic network structures containing either acidic or basic groups in their network chain thus all ionic materials are sensitive to a pH and ionic strength [22, 25, 57, 110]. The effect of the pH of swelling medium on the swelling of PAA hydrogels crosslinked with 0.001 mol % of EGDMA was reported by Ende and Peppas [110] as well as higher swelling rates and q_e with decreasing pH.

Chung et al. [113] investigated the swelling behavior of Dextran/HEMA hydrogels at pH 5 - 7 and reported that the hydrogels showed higher q_e at higher pH. Atta and Arndt [57] studied the effect of pH on swelling behavior of VP/HEMA hydrogels crosslinked with MAAm investigated by and which showed that the q of VP/HEMA hydrogels stepwise increases from pH 2 up to pH 12 (Figure 2.14). They explained that the q of VP/HEMA gels drastically increased with increasing HEMA content at increasing pH from 4 to 7 because of the complete dissociation of the acid groups of MAAm above its dissociation constant, pK_a , and the q further increased with increasing

pH from 9.5 to 12 because of the hydrolysis of amide groups of VP or MAAM crosslinker.

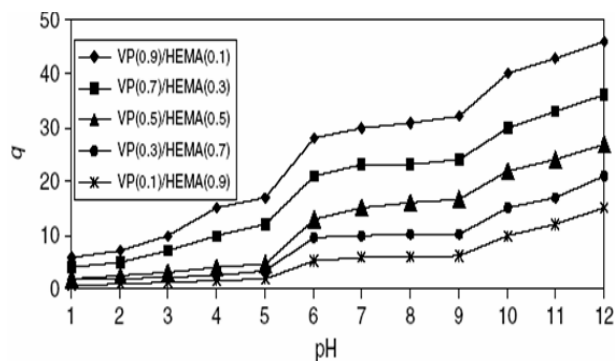


Figure 2.14. The q of VP/HEMA copolymers crosslinked with MAAM as a crosslinker as a function of pH in PB solutions at 25 °C (Reproduced from [57]).

The swelling of polyampholytic gels of *p*-sodium styrene sulfonate (SSS) and vinyl benzyl trimethylammoniumchloride (VBT), synthesized with various cross-linkers at different pHs, was observed by Bhardwaj and coworkers [45]. They reported that the q of the SSS/VBT gels increased from pH 1.0 up to pH 5.5 and decreased with increasing pH from 5.5 up to pH 9.0 as shown in Figure 2.15.

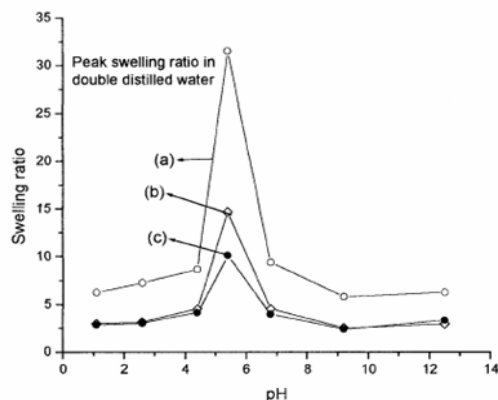


Figure 2.15. Effect of pH on swelling of SSS/VBT polyampholytic gels: (a) 10 mM, (b) 25 mM and (c) 50 mM concentration of BIS (Reproduced from [45]).

Bashir and his coworkers [28] developed a pH sensor using a silicone wafer microcantilever coated with PMAA and poly (ethylene glycol) dimethacrylate hydrogel as shown in Figure 2.16(a). When the pH is above the acid dissociation constant (pK_a) value of PMMA hydrogels, PMMA hydrogels became swollen, thus resulting in bending of the sensor as depicted in Figure 2.16(b). The sensitivity of the sensor was about $18.3 \mu\text{m}/\text{pH}$, which is sufficient for these sensors to be used in detecting an analytes and environmental condition around the sensor.

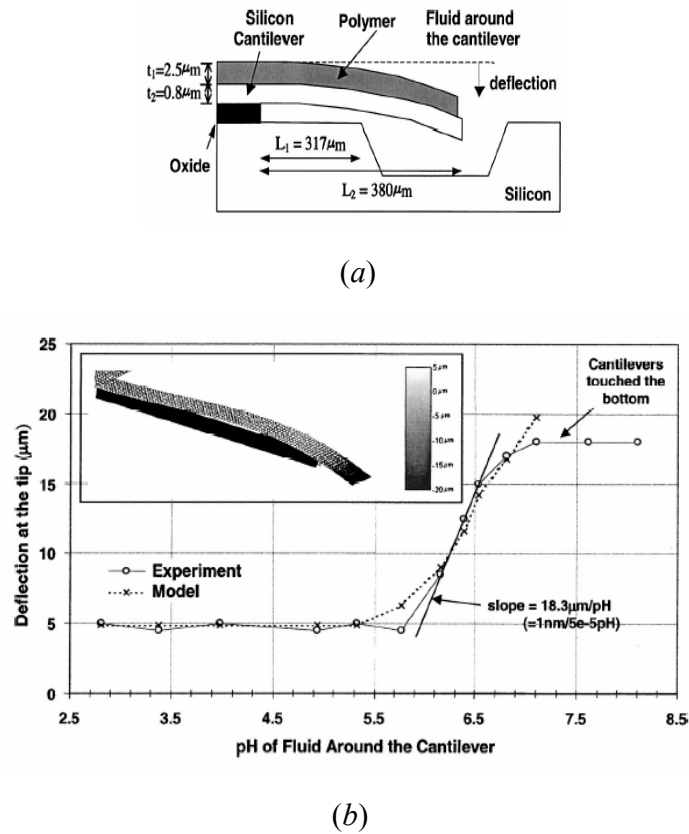


Figure 2.16. (a) Cross-sectional schematic of the cantilever/polymer structure and (b). Equilibrium cantilever deflection as a function of pH around the polymer. The solid line is experimental results. The dotted line is obtained with the cantilever and polymer modeled as a composite beam with no slip at the boundary. The inset shows three dimensional plot of the deflection of the cantilever/polymer at pH=7.0, obtained from the model (Reproduced from [28]).

2.2.7.2.3. Penetrant

Hoirra and Nizam [38] synthesized AAc/2-mercaptobenzimidazole (MBI) copolymer hydrogels using γ -irradiation for the use in the sorption of some divalent metal ions and investigated their swelling behavior in different solvent as well as their capacity for metal uptake. The swelling degree of AAc/MBI hydrogels in water and various organic solvents was obtained using the relationship:

$$swelling \ degree = \left(\frac{W_f - W_i}{W_f} \right) \quad (38)$$

where W_i and W_f are the initial and final weight of the hydrogels, respectively. As shown in the Table 1.1, it was observed that the AAc/MBI hydrogel show higher swelling degree in water and polar solvents than in non-polar solvents. The AAc/MBI hydrogels were also found to absorb toxic metals in water such as Hg^{2+} and Cd^{2+} .

Table 2.1. Swelling of AAc/MBI Hydrogel in various solvents [62].

Solvent	Swelling (%)
Water	190
Cyclohexane	20
Toluene	20
Benzene	25
Chloroform	30
Acetone	485
Methyl alcohol	670
Ethyl alcohol	775

Sun and Chu [124] studied the effect of solvent mixtures of dimethyl formamide (DMF) and water on the internal structure and swelling degree of the dextran-maleic acid (Dex-MA)/NIPAAm copolymer (NDF) hydrogels.

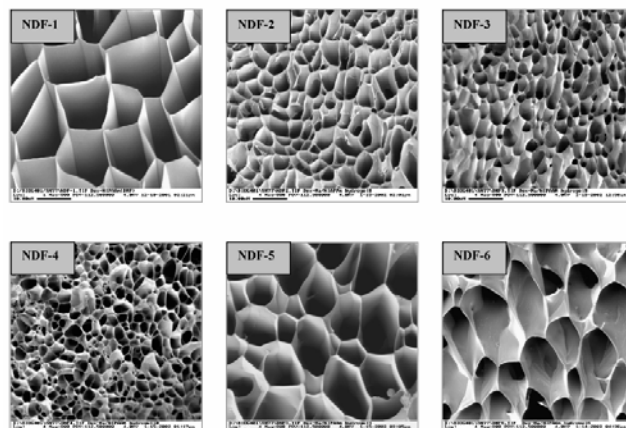


Figure 2.17. SEM images of equilibrated swollen NDF hydrogels (size of the bar is 10 μm) ($\times 800$). (NDF-1, 75 : 25 vol % DMF/distilled water; NDF-2, 62.5 : 37.5; NDF-3, 50 : 50; NDF-4, 37.5 : 62.5; NDF-5, 25 : 75; NDF-6, 12.5 : 87.5) (Reproduced from [124]).

Figure 2.17 shows SEM images of the freeze derided samples of swollen NDF 1-6 hydrogels immersed in different composition ratios of DMF and water. They observed the different composition ratios of water and DMF induced a three-dimensional porous network structure with different pore size from 2 to 22 μm and obtained swelling % (= swelling degree $\times 100$ %) of six various NDF hydrogels (Figure 2.18).

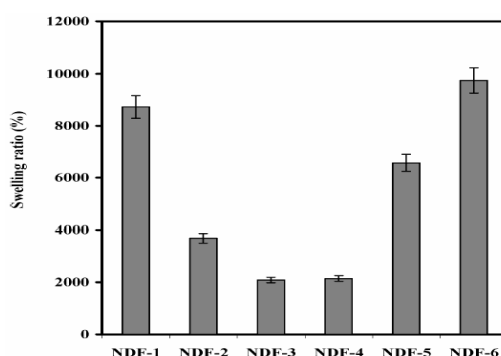


Figure 2.18. Equilibrium swelling ratios of NDF 1, 2, 3, 4, 5, and 6 hydrogels (Reproduced from [124])

2.2.7.2.4. *Applied Electric or Magnetic fields*

Several groups attempted to develop biomimic actuating hydrogel devices for use as artificial muscles [39, 40, 125], as well as soft actuators. For these applications, the hydrogels need to show a fast response to the applied electric or magnetic field. Consequently, charged hydrogels or hydrogels composites including electrically conductive particles or ferro-magnetic particles are appropriate candidates due to the fast change in their shape and volume under electric field and magnetic field, resulting in controlled shape and volume variation with the field.

Tanaka and coworkers [125] prepared the partially hydrolyzed PAAm hydrogels in water and acetone mixtures and investigated the hydrogel response to an applied electric field across the hydrogels. They showed that the volume of PAAm hydrogel continuously changed with applied field, where the degree of the volume change depended on the degree of ionization of acryl amide group ($-\text{CONH}_2$) in the PAAm hydrogels (see Figure 2.19).

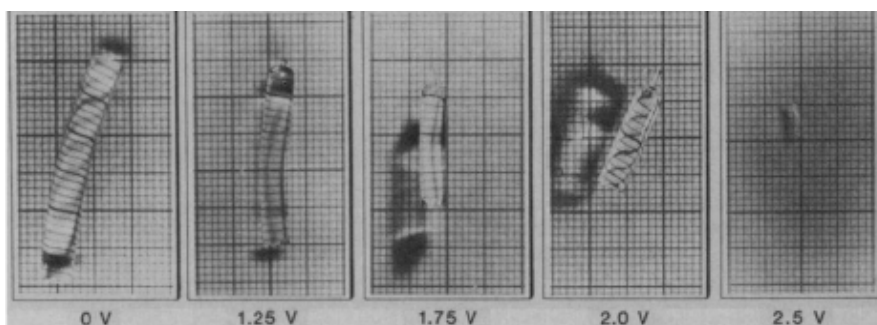


Figure 2.19. Photographic sequence showing how the volume of a 3-cm PAAm hydrogel immersed in 50 % acetone/water mixture diminishes with increasing applied electric field (0 ~2.5 V) (Reproduced from [125]).

Kim and coworkers [39] studied AA/vinylsulfonic acid (VSA) hydrogels as artificial muscles. The AA/VSA hydrogel contracted when an electric field (EF) was applied and the contraction percent $\{= (L_0 - L_1)/L_0 \times 100 \%$, where L_0 and L_1 is the initial and final lengths of the hydrogel, respectively} of the hydrogel decreased with increasing EF similar to the PAAm hydrogels prepared by Tanaka [125]. When the content of VSA increased, the contraction rate was found to be increase and the degree of contraction increased.

Ramanujan and Lao [40] synthesized a ferrogel with magnetic particles (Fe_3O_4) dispersed in PVA matrix and investigated its response to magnetic field (MF). Figure 2.20 shows the response of the PVA/ Fe_3O_4 ferrogel to magnetic field, where the ferrogel elongated when the magnetic field was applied and shrank when the MF is removed. With increasing Fe_3O_4 concentration, the threshold magnetic field, which is required to produce deflection of the ferrogel, decreased.

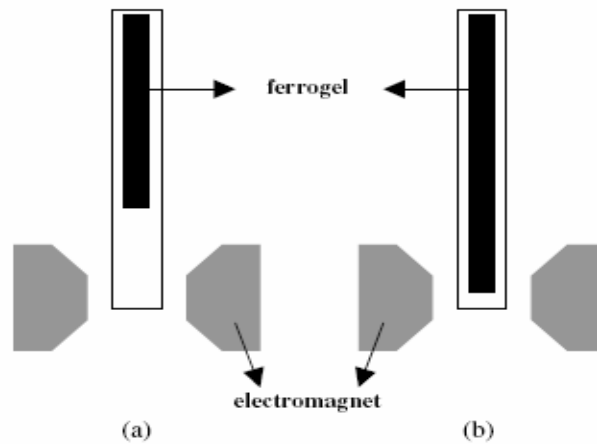


Figure 2.20. Elongation of a ferrogel under (a) no magnetic field and (b) maximal magnetic field at the lower end of the ferrogel (Reproduced from [40]).

2.3. Anisotropic Swelling of Hydrogels

It has been assumed that gels swell isotropically. In theories of gel swelling, the thermodynamics of the gel swelling is derived based on the assumption of isotropic swelling of gels and the structural parameters of gels are consequently predicted.

Li and Tanaka [129] explained the reason of isotropic swelling of gels by comparing the ink diffusion and gel swelling in water. Figure 2.21 shows schematically ink diffusion and gel swelling. The pure diffusion occurring in ink string placed in water produces the big change in the thickness of the string but the negligible change in its length. While in gel swelling, the changes in the length and thinness are similar. Li and Tanaka explain the reason of similar change in length and thickness is due to the nature of the modulus of gel to maintain its shape in order to minimize the shear energy, resulting in the isotropic swelling.

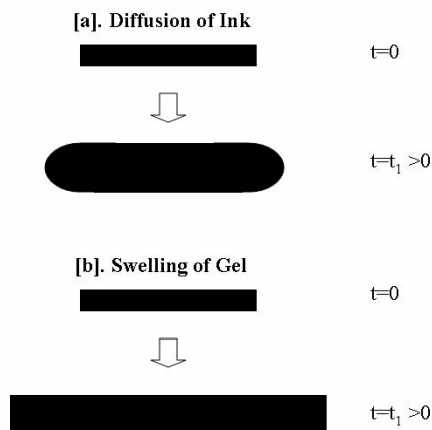


Figure 2.21. A schematic description of a diffusion process of ink molecules in (a) water and (b) the gel swelling process. For the former, the relative change of the length is negligible compared with that of the diameter. In the swelling of a long cylindrical gel, the relative change of the length and the diameter are the same (Redrawn from [129]).

There have been limited reports on the anisotropic swelling of some types of gels or hydrogels [73, 130, 131] unlike the assumption and reports of gel swelling.

Brazel and Peppas [73] described the dimensional changes of HEMA/MMA and PVA hydrogels showing anisotropic swelling. As shown in Figure 2.22, there are three stages to change the hydrogel state during gel swelling. At the first stage, only the edge part of glassy and dry gel swells, glassy core remains, and only big change in the thickness occurs. At the second stage, the thickness of the gel with disappearing glassy core decreases and length increases. This was explained to be due to polymer relaxation, resulting in transparency of the hydrogel. At the third stage, the thickness increases while maintaining the length of the hydrogel and become fully swollen state.

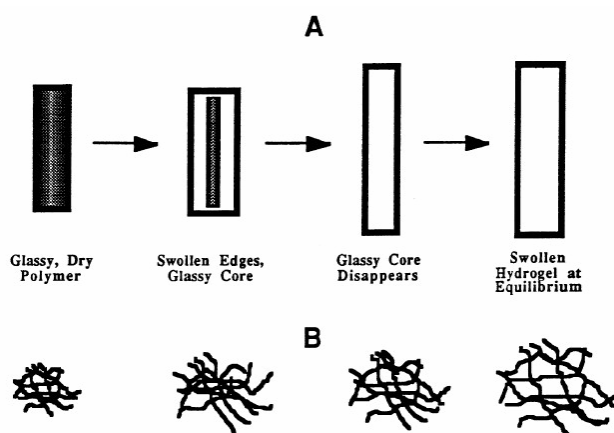


Figure 2.22. Depiction of polymer relaxation during water sorption into a slab geometry (A) and on the molecular level (B). Shaded area represents glassy polymer regions (Reproduced from [73]).

Edwards and coworkers [130] reported the anisotropic swelling of wet spun films of DNA showing 40 times expansion perpendicular to the molecular orientation and 1 or 2 times expansions parallel to chain orientation. The gel films showed the fast swelling

initially, and continued to swell for 18 hours, until it eventually dissolved in the swelling medium.

Boss and Stejskal [132] studied the hydrated vermiculite crystals (a clay possessing an ability to swell and shrink) with parallel silicate layers and observed about 100 times anisotropic expansion in thickness resulting from the water diffusion into the space between the parallel silicate layers from 100 to 1030 Å. In their study, pulsed magnetic-field gradient spin-echo NMR was used to investigate the diffusion of water. The anisotropy of sheared hydrogel composite of clay (LRD) and PEO was studied by small angle neutron scattering (SANS) [133].

The swelling of stearic acrylate (SA) and AA copolymeric gel films were investigated by He and coworkers [131]. The SA/AA gels were characterized using wide angle x-ray scattering (WAXS) and determined to be crystalline with an oriented SA. The gels also showed temperature-dependent anisotropic swelling behavior in water/ethanol mixtures with greater than 50 wt. % ethanol. This behavior results from an anisotropic crystalline structure remaining in swollen state, with equilibrium swelling ratios in the range between 1 and 2.1.

Tanaka and coworkers utilized electric fields (EF) to induce the swelling and deswelling of polyacrylamide (PAAm) gels possessing 20 % acrylic acid group converted from acrylamide groups [125]. It was shown that the shape of PAAm hydrogels changed above and below a critical EF strength and depended on the stress gradient along the EF lines in the gels inducing an anisotropic swelling of the hydrogel.

Harmon and coworkers [134, 135] reported the anisotropic swelling of UV-crosslinked N-isopropylacrylamide (NIPAAm), 2-(dimethylmaleimido)-N-ethyl-acrylamide (DMIAAm) and N, N-dimethyl acrylamide (DMAAm) terpolymeric gels and PNIAAm, DMIAAm, and acidic 3-acryloylamino-propionic acid (AAmPA) or basic N-(2-(dimethylamino)-ethyl)-acrylamide (DMAAAm) terpolymeric hydrogel films which were constrained. Anisotropic swelling behavior is sometimes seen in gel systems which

either under the stress or confined. The anisotropic swelling of NIPAAm based terpolymeric hydrogels was also explained using models for anisotropic gel swelling.

The models for anisotropic gel swelling were proposed by Tanaka and coworkers [136], Onuki [137], and Sekimoto and Kawasaki [138] as shown in Figure 2.23, which were based on either thin films coated on the substrate or volume instability of the gels at the phase transition resulting in buckling pattern.

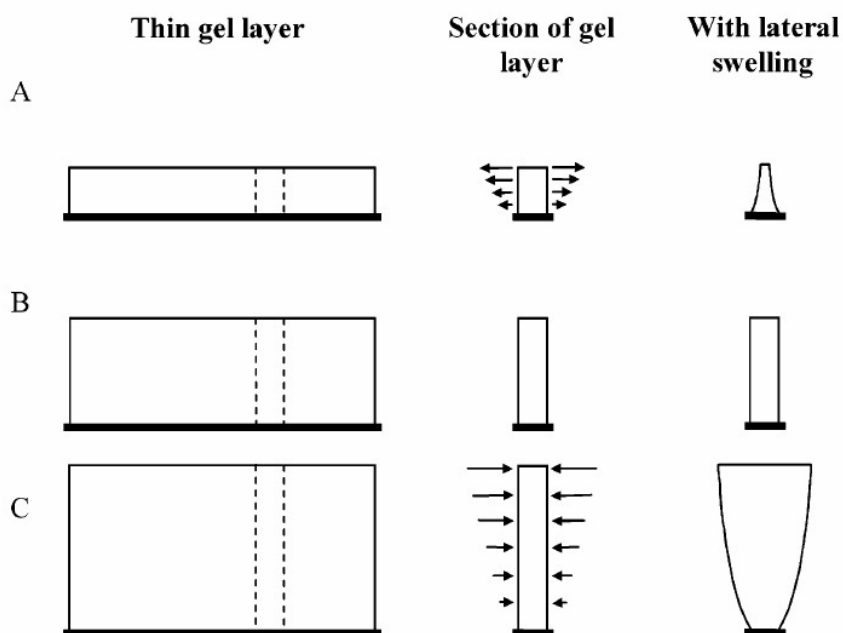


Figure 2.23. The hydrogel layer is cross-linked in some reference state (B), and the gel at the substrate remains in this reference state. The elastic energy of the network acts as compression when the gel layer is swollen (C) relative to the reference state and as elongation when the gel layer is collapsed (A) relative to the reference state. The compression or elongation increases monotonically and is greatest at the free surface of the gel. Our measurements are for infinitely wide films, but the exact shape of the gel with lateral swelling depends on both the film thickness and the aspect ratio of the gel layer (Reproduced from [134]).

Recently, Swan and co-workers [139] reported the anisotropic swelling from the gels compressed in the bulk state where expansion occur in the opposite direction to the compression direction and the ultimate expansion ratio was about 15 in only one direction. In their work, the compressed gels are shown to be not mechanically stable during not systematic compression process.

References

- [1]. Shan R. Baker, *Head & Neck*, “Fundamentals of Expanded Tissue”, pp. 327–333, 1991.
- [2]. K. F. Kobus, “Cleft palate repair with the use of osmotic expanders: a preliminary report” *J of Plastic, reconstructive & Aesthetic Surgery*, vol. 60, 414-421, 2007.
- [3]. Marc C. Swan, Tim E. E. Goodacre, Jan T. Czernuska and David G. Bucknall, “Cleft palate repair with the use of osmotic expanders: a response”, *J of Plastic, reconstructive & Aesthetic Surgery*, vol. 61, pp. 220-221, 2008.
- [4]. M. A. Ronert, H. Hofheinz, E. Manassa, H. Asgarouladi, and R. R. Olbrisch, “The Beginning of a New Era in Tissue Expansion: Self-Filling Osmotic Tissue Expander-Four-Year Clinical Experience”, *Plast. Reconstr. Surg.*, vol. 114(5), pp. 1025-1031, 2004.
- [5]. Arno Bacskulin, Martin Vogel, Karl Günter Wiese, Karsten Gundlach, Volker Hingst and Rudolf Guthoff, “New osmotically active hydrogel expander for enlargement of the contracted anophthalmic socket”, *Graefe’s Arch Clin Exp Ophthalmol*, vol. 238, pp. 24-27, 2000.
- [6]. Neumann C. G., “The expansion of an area of skin by progressive distention of a subcutaneous balloon” *Plast Reconstr Surg*, vol. 19, pp. 124-134, 1957.
- [7]. C. Radovan, “Development of adjacent flaps using a temporary expander”, *Plast Surg Forum*, vol. 2, pp. 62-71, 1979.
- [8]. L. C. Argenta, “Controlled tissue expansion in reconstructive surgery”, *Clin Plast Surg*, vol. 11, pp. 257-264, 1984.
- [9]. http://en.wikipedia.org/w/index.php?title=Image%3ATissue_expander_diagram.jpg, 2005.
- [10]. E. D. Austad and G. L. Rose, “A self-inflating tissue expander”, *Plast Reconstr Surg*, vol. 70, pp. 588-593, 1982.

- [11]. Richard Downes, Michael Lavin, and Richard Collin, “Hydrophilic Expanders for the Congenital Anophthalmic Socket”, *Advances in Ophthalmic Plastic and Reconstructive Surgery*, vol. 9, pp. 57-61, 1992,
- [12]. K. G. Wiese, “Osmotically induced tissue expansion with hydrogels: a new dimension in tissue expansion: A preliminary report”, *J of Craniomaxillofac Surg*, vol. 21, pp. 309-313, 1993.
- [13]. K. G. Wiese, D. E. H. Heinemann, D. Ostermeier, and J. H. Peters, “Biomaterial properties and biocompatibility in cell culture of a novel self-inflating hydrogel tissue expander”, *J. Biomed. Mater. Res.*, vol. 54 (2), pp. 179-188, 2001
- [14]. http://commons.wikimedia.org/wiki/Image:Osmotic_pressure_on_blood_cells_diagram.svg, 2007.
- [15]. H. Kaplan and A. Guner, “Characterization and Determination of Swelling and Diffusion Characteristics of Poly (N-vinyl-2-pyrrolidone) Hydrogels in Water”, *J. Appl. Polym. Sci.*, vol. 78, pp. 994-1000, 2000.
- [16]. L. C. Lopergolo, A. B. Lugao, and L. H. Catalani, “Direct UV photocrosslinking of poly (N-vinyl-2-pyrrolidone)(PVP) to produce hydrogels”, *Polymer*, 44, 6217-6222, 2003.
- [17]. Nicholas A. Peppas, *Hydrogels*, in *Biomaterials Science* 2nd ed., Academic Press, 2004.
- [18]. Fu-Jung Kao, Gurusamy Manivannan, and Samuel P. Sawan, “UV curable bioadhesives: copolymers of N-vinyl pyrrolidone” *J Biomed. Mater. Res. part A*, vol. 38, pp. 191-196, 1997.
- [19]. G. Scuderi, “Experimental vitreous transplantation: attempted partial replacement with homologous vitreous, heterologous liquor and polyvinylpyrrolidone solutions”, *Ann. Ophthalmol. Clin. Ocal.*, vol. 80, pp. 213-220, 1954.
- [20]. I. Calderara, R. Gougeon, L. Delmotte, V. Lemee, and D. J. Lounou, “NMR study of the structure and properties of poly(MMA-co-VP) crosslinked hydrogels”, *J. Polym. Sci.*, vol. 35, pp. 3619-3625, 1997.

- [21]. I. Quijada-Garrido, A. Prior-Cabanillas, L. Garrido, and J. M. Barrales-Rienda, "Swelling monitorization of poly [(N-isopropylacrylamide)-co-(methacrylic acid)] copolymers by magnetic resonance imaging", *Macromolecules*, vol. 38, pp. 7434-7442, 2005.
- [22]. N. A. Peppas, J. Z. Hilt, A. Khademhosseini, and R. Langer, "Hydrogels in biology and medicine: from molecular principles to bionanotechnology", *Advanced Materials*, vol.18, pp. 1345-1360, 2006.
- [23]. K. Dusek, "Responsive gels, volume transition I and II", *Adv. Polym. Sci.*, vol. 109 and 110, 1993.
- [24]. O. Wichterle and D. Lim, "Hydrophilic gels for biological use", *Nature*, vol. 185, pp. 177-182, 1960.
- [25]. B. D. Ratner and A. S. Hoffman, Synthetic Hydrogels for Biomedical Applications, in *Hydrogels for Medical and Related Applications* 2nd ed., 1976.
- [26]. Ioannis Tranoudis and Nathan Efron, "Water properties of soft contact lens material", *Contact Lens and Anterior Eye*, vol. 27, pp. 177-191, 2004.
- [27]. Sanxiu Lu and Kristi. S. Anseth, "Photopolymerization of multilaminated poly (HEMA) hydrogels for controlled release", *J. Control Release*, vol. 57, pp. 291-300, 1999.
- [28]. R. Bashir, J. Z. Hilt, O. Elibol, A. Gupta, and N. A. Peppas, "Micromechanical cantilever as an ultrasensitive pH microsensor", *Appl. Phys. Lett.*, vol. 81(16), pp. 3091-3093, 2002.
- [29]. R. Langer and N. A. Peppas, "Advances in biomaterials, drug delivery, and Bionanotechnology", *AIChE Journal*, vol. 49, pp. 2990-3006, 2003.
- [30]. Elizabeth A. Moschou, Marc J. Madou, Leonidas G. Bachas, Sylvia Daunert, "Voltage-switchable artificial muscles actuating at near neutral pH", *Sensors and Actuators B*, vol. 115, pp. 379-383, 2006.
- [31]. R. V. Ramanujan and L. L. Lao, "The mechanical behavior of smart magnet-hydrogel composites", *Smart Mater. Struct.*, vol. 15, pp. 952-956, 2006.

- [32]. J.P. Hervás Pérez, E. López-Cabarcos and B. López-Ruiz, “The application of methacrylate-based polymers to enzyme biosensors”, *Biomolecular Engineering*, vol. 23, pp. 233-245, 2006.
- [33]. Won-Gun Koh . Michael V. Pishko, “Fabrication of cell-containing hydrogel microstructures inside microfluidic devices that can be used as cell-based biosensors”, *Anal Bioanal Chem*, vol. 385, pp. 1389–1397, 2006.
- [34]. Haijun Yu, Xiaoyi Xu, Xuesi Chen, Jingquan Hao, and Xiabin Jing, “Medicated wound dressings based on poly (vinyl alcohol)/poly (N-vinyl pyrrolidone)/chitosan hydrogels”, *J. Appl. Polym. Sci.*, vol. 101, pp. 2453–2463, 2006.
- [35]. Matthew D. Phaneuf, Martin J. Bide, Susan L. Hannel, Michael J. Platek, Thomas S. Monahan, Mauricio A. Contreras, Tina M. Phaneuf, and Frank W. LoGerfo, *J. Biomed. Mater. Res. part A*, vol. 74A, pp. 666-676, 2005.
- [36]. Kytai T. Nguyen and Jennifer L. West, “Photopolymerizable hydrogels for tissue engineering applications”, *Biomaterials*, vol. 23, pp. 4307-4314, 2002.
- [37]. Jennie B. Leach, Kathryn A. Bivens, Charles W. Patrick, Jr., Christine E. Schmidt, “Photocrosslinked Hyaluronic Acid Hydrogels: Natural, Biodegradable Tissue Engineering Scaffolds”, *Biotech. And Bioeng.*, vol. 82(5), pp. 578-589, 2003.
- [38]. Horia M. M. Nizam El-Din, *Appl. Polym. Sci.*, “Radiation Synthesis and Application of a hydrogel Based on Acrylic acid and 2-Mercaptobenzimidazole”, vol.86, pp.1607-1614, 2002.
- [39]. Seon Jeong Kim, Han Il Kim, Sang Jun Park, In Young Kim, Sang Hoon Lee, Tae Soo Lee and Sun I Kim, “Behavior in electric fields of smart hydrogels with potential application as bio-inspired actuators”, *Smart Mater. Struct.*, vol.14, pp.511–514, 2005.
- [40]. R. V. Ramanujan and L. L. Lao, “The mechanical behavior of smart magnet-hydrogel composites”, *Smart Mater. Struct.*, vol. 15, pp. 952–956, 2006.
- [41]. E. Jakobs and Y. Hanein, “Micrometer scale gel patterns”, *Colloids and Surfaces A: Physicochem. Eng. Aspects*, vol. 290, pp. 33–40, 2006.

- [42]. David J. Beebe, Jeffrey S. Moore, Joseph M. Bauer, Qing Yu, Robin H. Liu, Chelladurai Devados and Byung-Ho Jo, "Functional hydrogel structures for autonomous flow control inside microfluidic channels", *Nature*, vol. 404, pp. 588–590, 2000.
- [43]. T. P. Davis and M. B. Huglin, "Effect of crosslinking on the properties of poly(2-hydroxyethyl methacrylate) hydrogels", *Angew. Makromol. Chem*, vol. 189, pp. 195-205, 1991.
- [44]. Phuong Ghi, David J. T. Hill, and Andrew K. Whittaker, "Water sorption by poly(tetrahydrofurfuryl methacrylate-co-2-hydroxyethyl methacrylate). I. A mass-uptake study", *J. Polym. Sci. Part B: Polymer Physics*, vol. 38, pp. 1939-1946, 2000.
- [45]. Y. K. Bhardwaj, V. Kumar, and S. Sabharwal, "Swelling behavior of radiation-polymerized polyampholytic two-component gels: dynamic and equilibrium swelling kinetics", *J. Appl. Polym. Sci*, vol. 8, pp. 730-742, 2003.
- [46]. A. Henke, S. Kadlubowski, P. Ulanski, J. M. Rosiak, and K. Arndt, "Radiation-induced cross-linking of polyvinylpyrrolidone-poly (acrylic acid) complexes", *Nucl. Instr. and Mech. in Phys. Res. B*, vol. 236, pp. 391-198, 2005.
- [47]. Hossam M. Said, Safaa G. Abd Alla and Abdel Wahab M. El-Naggar, "Synthesis and characterization of novel gels based on carboxymethyl cellulose/acrylic acid prepared by electron beam irradiation", *Reactive & Functional Polymers*, vol. 61, pp. 397-404, 2004.
- [48]. Ling Li and L. James Lee, "Photopolymerization of HEMA/DEGDMA hydrogels in solution", *Polymer*, vol. 46, pp. 11540-11547, 2005.
- [49]. J. Y. Wong, A. Velasco, P. Rajagopalan, and Q. Pham, "Directed movement of vascular smooth muscle cells on gradient-compliant hydrogels", *Langmuir*, vol. 19, pp. 1908-1913, 2003.
- [50]. Luke M. Geever, Declan M. Devine, Michael J.D. Nugent, James E. Kennedy, John G. Lyons and Clement L. Higginbotham, "Lower critical solution temperature control and swelling behaviour of physically crosslinked thermosensitive copolymers based on *N*-isopropylacrylamide", *European Polymer Journal*, vol. 42, pp. 69-80, 2006.
- [51]. John P. Fisher, David Dean, Paul S. Engel, and Antonios G. Mikos, "Photoinitiated polymerization of biomaterials", *Ann. Mater. Res.*, vol. 31, pp. 171-181, 2001.

- [52]. J. F. Rabek, *Mechanisms of Photophysical Processes and Photochemical Reactions in Polymers*, New York, Wiley & Sons, 1987.
- [53]. P. Dolez, M. Marek, and B. J. Love, "Photopolymerizable acrylic resin: Effect of curing time and temperature", *J. Appl. Polym. Sci.*, vol. 82, pp. 546-554, 2001.
- [54]. A. D. Neves, J. A. C. Discacciati, R. L. Orefice, and M. I. Yoshida, "Influence of the power density on the kinetics of photopolymerization and properties of dental composites", *J. Biomed. Mater. Res. Part B*, vol. 72, pp. 393-400, 2005.
- [55]. M. P. Patel and M. Braden, "Heterocyclic methacrylates for clinical applications. I. Mechanical properties", *Biomaterials*, vol. 12, pp. 645-648, 1991.
- [56]. M. Sen, N. Peker and O. Guven, "Radiation synthesis and characterization of N-vinyl-2-pyrrolidone/N-allylthiourea hydrogels and their use in the adsorption of invertase", *Die Angewandte Makromolekulare Chemie*, vol. 257, pp. 1-6, 1998.
- [57]. Ayman M. Atta and K-F Arndt, "Swelling behavior of pH-and temperature-sensitive copolymers containing 2-hydroxyethyl methacrylate and N-vinyl-2-pyrrolidone crosslinked with new crosslinkers", *Polym Int*, vol. 53, pp. 1870-1881, 2004.
- [58]. C. F. Huang, S. W. Kuo, F. J. Lin, C. F. Wang, C. J. Hung, and F. C. Chang, "Syntheses and specific interactions of poly (hydroxyethyl methacrylate-*b*-vinyl pyrrolidone) diblock copolymers and comparisons with their corresponding miscible blend systems", *Polymer*, vol. 47, pp. 7060-7069, 2006.
- [59]. I. Rehman, J. C. Knowles, W. Bonfield, "Analysis of in vitro reaction layers formed on Bioglass using thin-film X-ray diffraction and ATR-FTIR microspectroscopy" *Journal of biomedical materials research*, vol. 41, pp.162-166, 1998.
- [60]. S. K. Bajpai, "Swelling-deswelling behavior of poly(acrylamide-*co*-maleic acid) hydrogels", *J. Appl Polym Sci*, vol. 80, pp. 2782-2789, 2001.
- [61]. P. J. Flory and R. Rehner, "Statistical mechanics of crosslinked polymer networks. II. Swelling", *J. Chem. Phys.*, vol. 11, pp. 521-526, 1943.
- [62]. L. M. Geever, D. M. Devine, M.J.D. Nugent, J. E. Kennedy, J. G. Lyons, and C. L. Higginbotham, "The synthesis, characterisation, phase behaviour and swelling of

- temperature sensitive physically crosslinked poly (1-vinyl-2-pyrrolidinone)/poly (N-isopropylacrylamide) hydrogels”, *European Polymer Journal*, vol. 42, pp. 69-80, 2006.
- [63]. M. A. Al-Issa, T. P. Davis, M. B. Huglin and D. C. F. Yip, “Copolymerizations involving *N*-vinyl-2-pyrrolidone”, *Polymer*, vol. 26, pp. 1869 -1974, 1985.
- [64]. Ferdinand Rodriguez, Principles of Polymer Systems, 4th ed., Taylor & Francis: Washington DC; 1996.
- [65]. M. Malak, David J. T. Hill, and A. K. Whittaker, “Water sorption into poly [(2-hydroxyethyl methacrylate)-co-(1-vinyl-2-pyrrolidone)] at 310 K”, *Polym Int*, vol. 52, pp. 1740–1748, 2003.
- [66]. Declan M. Devine, Clement L. Higginbotham, “The synthesis of a physically crosslinked NVP based hydrogel”, *Polymer*, vol. 44, pp. 7851–7860, 2003.
- [67]. Kwei, T. K., “The effect of hydrogen bonding on the glass transition temperature of polymer mixtures”, *Journal of Polymer Science Part C-Polymer Letters*, vol. 22, pp. 307-313, 1984.
- [68]. Chih-Feng Huang, Shiao-Wei Kuo, Fang-Ju Lin, Chih-Feng Wang, Chen-Jui Hung and Feng-Chih Chang, “Syntheses and specific interactions of poly (hydroxyethyl methacrylate-*b*-vinyl pyrrolidone) diblock copolymers and comparisons with their corresponding miscible blend systems”, *Polymer*, vol. 47, pp. 7060-7069, 2006.
- [69]. P. L. Ritger and N. A. Peppas, “A simple equation for description of solute release. II: Fickian and anomalous release from swellable devices”, *J. Control. Release*, vol. 5, pp. 37-42, 1987.
- [70]. David J. T. Hill, M. C. H. Lim, and A. K. Whittaker, “Water diffusion in hydroxyethyl methacrylate (HEMA)-based hydrogels formed by γ -radiolysis”, *Polym. Int.*, vol. 48, pp. 1046-1052, 1999.
- [71]. Y. Yamane, I. Ando, F. L. Buchholz, A R. Reinhardt, and S. Schlick, “Detection of spatial inhomogeneity in poly (acrylic acid) gels by measuring time-dependent diffusion coefficients of a probe in NMR experiments: Effect of the degree of cross-linking and degree of swelling”, *Macromolecules*, vol. 37, pp. 9841-9849, 2004.

- [72]. S. S. Ray, P. R. Rajamohanan, M. V. Badiger, I. Devotta, S. Ganapathy, and R. A. Mashelkar, "Self-diffusion of water in thermoreversible gels near volume transition Model development and PFG NMR investigation", *Chemical Eng. Sci.*, vol. 53, pp. 869-877, 1998.
- [73]. C. S. Brazel and N. A. Peppas, "Dimensionless analysis of swelling of hydrophilic glassy polymers with subsequent drug release from relaxing structures", *Biomaterials*, vol. 20, pp. 721-732, 1999.
- [74]. T. P. Davis, M. B. Huglin and D. C. F. Yip, "Properties of poly (N-vinyl-2-pyrrolidone) hydrogels crosslinked with ethyleneglycol dimethacrylate", *Polymer*, vol. 29, pp. 701-706, 1988.
- [75]. S. A. Dubrovskii and G. V. Rakova, "Elastic and osmotic behavior and network imperfections of nonionic and weakly ionized acrylamide-based hydrogels", *Macromolecules*, vol. 40, pp. 7478-7486, 1997.
- [76]. K. Haraguchi, T. Takehisa, and S. Fan, "Effects of Clay Content on the Properties of Nanocomposite Hydrogels Composed of Poly (N-isopropylacrylamide) and Clay", *Macromolecules*, vol. 35, pp. 10162-10171, 2002.
- [77]. Nathan Ravi, Arpita Mitra, Paul Hamilton, and Ferenc Horkay, "Characterization of the network properties of poly(ethylene glycol)-acrylate hydrogels prepared by variations in the ethanol-water solvent composition during crosslinking copolymerization", *Journal of Polymer Science: Part B: Polymer Physics*, vol. 40, pp. 2677-2684, 2002.
- [78]. E. Marsano S, Gagliardi, F. Ghioni, and E. Bianchi, "Behaviour of gels based on (hydroxypropyl) cellulose methacrylate", *Polymer*, vol. 41 , pp. 7691-7698, 2000.
- [79]. S. H. Kim, A. Opdahl, C. Marmo, G. A. Somorjai, "AFM and SFG studies of pHEMA-based hydrogel contact lens surfaces in saline solution: adhesion, friction, and the presence of non-crosslinked polymer chains at the surface", *Biomaterials*, vol. 23, pp. 1657-1666, 2002.
- [80]. B. D. Ratner and V. V. Tsukuruk, *Scanning Probe Microscopy of Polymers*, ACS Symposium Series 694, American Chemical Society, 1998.
- [81]. Marcos R. Guilherme, Gilsinei M. Campese, Eduardo Radovanovic, Adley F. Rubira, Elias B. Tambourgi and Edvani C. Muniz, "Thermo-responsive sandwiched-

- like membranes of IPN-PNIPAAm/PAAm hydrogels”, *Journal of Membrane Science*, vol. 275, pp. 187–194, 2006.
- [82]. S. V. Bhat, *Biomaterials*, Narosa Publishing House, 2002.
- [83]. X. Wu, L. Black, G. Santacana-Laffitte, C. W. Patrick, Jr., “Preparation and assessment of glutaraldehyde-crosslinked collagen-chitosan hydrogels for adipose tissue engineering”, *J Biomed. Mater. Res. - Part A*, vol. 81, pp. 59-65, 2007.
- [84]. J. S. Terenoff and A. G. Mikos, *Biomaterials: The intersection of Biology and Materials Science*, Prentice Hall 1st ed., 2007.
- [85]. Loo-Teck Ng and Salesh Swami, “IPNs based on chitosan with NVP and NVP/HEMA synthesised through photoinitiator-free photopolymerisation technique for biomedical applications”, *Carbohydrate Polymers*, vol. 60, pp. 523-528, 2005.
- [86]. Paul J. Flory, *Principles of Polymer Chemistry*, Ithaca, NY: Cornell University Press, 1953.
- [87]. M. Doi, *Introduction to Polymer Physics*, Oxford Univ. Press, 1995.
- [88]. G. McCrum, C. P. Buckley, C. B. Bucknall, *Principal of Polymer Engineering*, Oxford Univ. Press, 1998.
- [89]. James E. Mark and Burak Erman, *Rubberlike Elasticity: A Molecular Primer*, John Wiley & Sons, Inc., 1988.
- [90]. M Rubinstein and R. H. Colby, *Polymer Physics*, Oxford Univ. Press Inc., New York, 2003.
- [91]. Lisa Barnnon-Peppas and Nikolaos A. Peppas, “Equilibrium swelling behavior of pH-Sensitive Hydrogels”, *Chemical Engineering Science*, vol. 46(3), pp. 715-722, 1991.
- [92]. T. J. Alfrey, E. F. Gurnee and W. G. Lloyd, “Diffusion in glassy polymers”, *Journal of Polymer Science*, vol.12, pp.249, 1966.
- [93]. J. Crank, *the Mathematical Diffusion* 2nd ed., Oxford Univ. Press, New York, 1975.

- [94]. C. S. Brazel and N. A. Peppas, "Mechanisms of solute and drug transport in relaxing, swellable, hydrophilic glassy polymers" *Polymer*, vol. 40, pp. 3393-3398, 1999.
- [95]. M. Shibayama, "Feature Article Spatial inhomogeneity and dynamic fluctuations of polymer gels", *Macromol. Chem. Phys.*, vol.199, pp. 1-30, 1998.
- [96]. I. Yazici, and O. Okay, "Spatial inhomogeneity in poly (acrylic acid) hydrogels", *Polymer*, vol. 46, pp. 2595-2602, 2005.
- [97]. H. Furukawa, K. Horie, R. Nozaki, and M. Okada, "Swelling-induced modulation of static and dynamic fluctuations in polymer gels observed by scanning microscope light scattering", *Physics Review E*, vol. 68, pp. 031406, 2003.
- [98]. J. A. Clark, J.C. Y. Cheng and K.S. Leung, "Mechanical properties of normal skin and hypertrophic scars", *Burns*, vol. 22(6), pp. 443-446, 1996.
- [99]. J. L. Leveque, P. Coruff, de Rigal, and P. Agache, "In vivo studies of the evolution of physical properties of the human skin with age", *International Journal of Dermatology*, vol. 23, pp. 322-329, 1984.
- [100]. L. H. Sperling, Introduction to Physical Polymer Science, New York: Wiley, 1986.
- [101]. Kristi S. Anseth, Christopher N. Bowman and Lisa Brannon-Peppas, "Mechanical properties of hydrogels and their experimental determination", *Biomaterials*, vol. 17, pp. 1647-1657, 1996.
- [102]. B. N. Preston and F. A. Meyer, "Physical behavior of gelatin gels: a simple model for connective tissue", *Biopolymers*, vol. 10, pp. 35-46, 1971.
- [103]. J. Tian, T. A. P. Seery, D. L. Ho, and R. A. Weiss, "Physically Cross-Linked Alkylacrylamide Hydrogels: A SANS Analysis of the Microstructure", *Macromolecules*, vol. 37, pp. 10001-10008, 2004.
- [104]. S. Mallam, F. Horkay, A. Hecht, and E. Geissler, "Scattering and swelling properties of inhomogeneous polyacrylamide gels", *Macromolecules*, vol. 22, pp. 3356-3361, 1989.

- [105]. F. Schosseler, F. Ilmain and S. J. Candau, "Structure and properties of partially neutralized poly (acrylic acid) gels", *Macromolecules*, vol. 24, pp. 225-234, 1991.
- [106]. P. G-. de Gennes, *Scaling Concept in Polymer Physics*, Cornell Univ. Press, Ithaca, New York, 1979.
- [107]. Sunil K. Bajpai and Surinderpal Singh, "Analysis of swelling behavior of poly (methacrylamide-co-methacrylic acid) hydrogels and effect of synthesis conditions on water uptake", *Reactive and Functional Polymer*, vol. 66, pp. 431-440, 2006.
- [108]. Aiman M. Atta and Abdel-Azim A. Abdel-Azim, "Effect of crosslinker functionality on swelling and network parameters of copolymeric hydrogels", *Polym. Adv. Technol.*, vol. 9, pp. 340-348, 1998.
- [109]. L. M. Muratore, K. Steinhoff and T. P. Davis, "Self-reinforcing hydrogels comprised of hydrophobic methyl methacrylate macromers copolymerised with either N-vinyl-2-pyrrolidone or 2-hydroxyethyl acrylate", *J. Mater. Chem.*, vol. 9, pp. 1687-1691, 1999.
- [110]. M. T. A. Ende and N. A. Peppas, "Transport of ionizable drugs and proteins in crosslinked poly(acrylic acid) and poly(acrylic acid-co-2 hydroxyethyl methacrylate)", *J. Appl. Polym. Sci.*, vol. 59, pp. 673-685, 1996.
- [111]. Tomas P. Davis and Malcolm B. Huglin, "Effect of crosslinking on the properties of poly(2-hydroxyethyl methacrylate) hydrogels" *Die Angewandte Makromolekulare Chemie*, vol. 189, pp. 195-205, 1991.
- [112]. W. Xue, S. Champ, M. B. Huglin, "Network and swelling parameters of chemically crosslinked thermoreversible hydrogels", *Polymer*, vol. 42, pp. 2247-2250, 2001.
- [113]. J. T. Chung, K.D.F. Vlugt-Wensink, W.E. Hennink, Z. Zhang, "Effect of polymerization conditions on the network properties of dex-HEMA microspheres and macro-hydrogels", *Int. J. Pharm*, vol. 288, pp. 51-61, 2005.
- [114]. Hossein Omidian and Kinam Park, "Experimental design for the synthesis of polyacrylamide superporous hydrogels", *Journal of Bioactive and Compatible Polymers*, vol. 17, pp. 433-450, 2002.

- [115]. D. J. T. Hill, N. G. Moss, P. J. Pomery, A. K. Whittaker, "Copolymer hydrogels of 2-hydroxyethyl methacrylate with n-butyl methacrylate and cyclohexyl methacrylate: synthesis, characterization and uptake of water", *Polymer*, vol. 41, pp. 1287-1296, 2000.
- [116]. N. A. B. Vieira, J. Ruggiero Neto, M. J. Tiera, "Synthesis, characterization and solution properties of amphiphilic N-isopropylacrylamide–poly (ethylene glycol)–dodecyl methacrylate thermosensitive polymers", *Colloids and Surfaces A: Physicochem. Eng. Aspects*, vol. 262, pp. 251-259, 2005.
- [117]. R. B. Greenwald, "PEG drugs: an overview", *J. Contr. Release*, vol. 74, pp. 159-171, 2001.
- [118]. W. F. Lee and K. T. Tsao, "Preparation and properties of nanocomposite hydrogels containing silver nanoparticles by ex situ polymerization", *J of Appl Polym Sci*, vol. 100, pp. 3653-3661, 2006.
- [119]. C. Dispenza, M. Leone, C. L. Presti, F. Librizzi, G. Spadaro, and V. Vetri, "Optical properties of biocompatible polyaniline nano-composites", *Journal of Non-Crystalline Solids*, vol. 352, pp. 3835–3840, 2006.
- [120]. Krisztina Laszlo, Katalin Kosik, and Erik Geissler, "Phase transition in poly (N-isopropylacrylamide) hydrogels induced by phenols", *Macromolecules*, vol. 37, pp. 10067-10072, 2004.
- [121]. K. Takahashi, T. Takigawa, and T. Masuda, "Swelling and deswelling kinetics of poly (N-isopropylacrylamide) gels", *J. Chemical Physics*, vol. 120(6), pp. 2972-2979, 2004.
- [122]. Horia M. Nizam El-Din, Safaa G. Abd Alla, and Abdel Wahab M. El-Naggar, "Swelling, Thermal and Mechanical Properties of Poly (vinyl alcohol)/Sodium Alginate Hydrogels Synthesized by Electron Beam Irradiation", *J. Macromolecular Sci., Part A*, vol. 44, pp. 47-54, 2007.
- [123]. Geoffrey M. Spinks, Chang K. Lee, Gordon G. Wallace, Sun I. Kim, and Seon Jeong Kim, "Swelling behavior of chitosan hydrogels in ionic liquid-water binary systems", *Langmuir*, vol. 22, pp. 9375-9379, 2006.

- [124]. S. Namkung and C. C. Chu, "Effect of solvent mixture on the properties of temperature-and pH-sensitive polysaccharide-based hydrogels", *J. Biomater. Sci. Polymer Edn*, vol. 17(5), pp. 519–546, 2006.
- [125]. T. Tanaka, I. Nishio, S-T. Sun, and S. Ueno-Nishio, "Collapse of Gels in an Electric Field", *Science*, vol. 218, pp. 467-469, 1982.
- [126]. H. Hosseinzadeh, A Pourjavadi, and G. R. Mahdavinia, "Modified carrageenan. 1. H-carragPAM, a novel biopolymer-based Superabsorbent Hydrogel", *Bioactive and Compatible Polymers*, vol. 20, pp. 475-490, 2005.
- [127]. H. Yu and D. W. Grainger," Modified release of hydrophilic, hydrophobic and peptide agents from ionized amphiphilic gel networks", *J. Contr. Release*, vol. 34, pp. 117-127, 1995.
- [128]. P. Sakellariou, "Theta temperature of poly (N-vinyl-pyrrolidone) in water", *Polymer*, vol. 33, pp. 1339-1342, 1992.
- [129]. Yong Li and Toyoichi Tanaka, "Kinetics of swelling and shrinking of gels", *J. Chem. phys.*, vol. 92 (2), pp. 1365-1371.
- [130]. G. S. Edwards, L. Genzel, W. L. Peticolas, and A. Rupprecht, " Measurements of a large anisotropy in the swelling of oriented DNA films in aqueous solution", *Biopolymers*, vol. 25, pp. 223-227, 1986.
- [131]. Xiaowei He, Atsushi Takahara, and Tisato Kajiyama, "Anisotropic swelling behavior of copolymer gel film with crystalline oriented side chains", *Polymer gels and Network*, vol. 5, pp. 429-438, 1997.
- [132]. B. D. Boss and A. D. E. O. Stejskal, "Restricted, anisotropic diffusion and anisotropic nuclear spin relaxation of protons in hydrated vermiculite crystals" *J. Coll. Interface Sci.*, vol. 26, pp. 271-278, 1968.
- [133]. Jun Li, Jun Jiang, Chunhwa Li, Min Y. Lin, Steve A. Schwarz, Miriam H. Rafailovich, Jonathan Sokolv, " Effect of temperature on shear-induced anisotropic structure in polymer clay hydrogels", *Macromol. Rapid Commun.*, vol. 27, pp. 1787-1791, 2006.

- [134]. M. E. Harmon, D. Kuckling, P. Pareek and C. W. Frank, "Photo-cross-linkable PNIPAAm copolymers. 4. Effects of copolymerization and cross-linking on the volume-phase transition in constrained hydrogel layers", *Langmuir*, vol. 19, pp. 10947-10956, 2003.
- [135]. Dirk Kuckling, Marianne E. Harmon and Curtis W. Frank, "Photo-cross-linkable PNIPAAm copolymers. 1. Synthesis and characterization of constrained temperature-responsive hydrogel layer", *Macromolecules*, vol. 35, pp. 6377-6383, 2002.
- [136]. Toyochi Tanaka, Shao-Tang Sun.; Yoshitsugu Hirokawa, Siji Katayama, John Kucera, Yoshiharu Hirose, and Takayuki Amiya, "Mechanical instability of gels at the phase transition", *Nature*, vol. 325, pp. 796-798, 1987.
- [137]. A. Onuki, "Volume-Phase Transition in Constrained Gels", *J. Phys. Soc. Jpn.* vol. 57, pp.1868-1871, 1988.
- [138]. Ken Sekimoto and Kyozi Kawasaki," Elastic instability of gels upon swelling" *J. phys. Soc. Jpn.*, vol. 56, pp. 2997-3000, 1987.
- [139]. M. Swan, D. G. Bucknall, T. Goodacre, J. Meakins and J. Czernuszka; *Soft Anisotropic Tissue Expander*; UK Patent 0600336.2; 2006.
- [140]. Agnes Safrany and Laszlo Wojnarovits, "Electron Beam Initiated Crosslinking in Poly(N-isopropylacrylamide) aqueous solution, *Radiation physics and Chemistry*, vol.69, pp. 289-293, 2004.

CHAPTER III

EXPERIMENTS

3.1. Preparation of Hydrogel Systems

3.1.1. Synthesis of VP/HEMA Gels

The VP/HEMA chemically crosslinked gels were synthesized by UV-initiated free radical photo-polymerization as well as thermal polymerization methods. Vinyl pyrrolidone (VP) and hydroxyethyl methacrylate (HEMA) were purified using vacuum-distillation before polymerization. For the UV-initiated free radical photo-polymerization, 2,2-dimethoxy-2-phenylacetophenone (Irgacure 651) was used as standard photoinitiator and N, N-methylene bisacrylamide (BIS) as standard cross-linker. Two more different cross-linkers, 1,1,2,2-tetraallyloxyethane (GLY) and diethylene glycol diacrylate (DEGDA) were also used to investigate the effect of functionality and the length of cross-linker molecule, respectively, on the swelling. Azo-isobutyronitrile (AIBN) was used as standard initiator for the thermal polymerizations but also used for photo-polymerization for the comparison between two polymerization methods. All chemicals were purchased from Aldrich Chem. Co and their chemical structures are shown in Figure 3.1.

For any specific gel, the correct ratio of these chemicals were poured into a sealed UV opaque vial and mixed at RT under continuous stirring for at least 12 hours before polymerization. Gels were prepared with variations in weight percentages of VP to HEMA (C_{VP}), the photoinitiator concentration (C_I) as well as cross-linker concentration (C_{CL}) and types. (see Tables 3.1 and 3.2 for details). After mixing, the reactant mixtures were degassed and purged with dry nitrogen gas was started in order to remove as much oxygen as possible which can act as a scavenger in the radical polymerization. The mixture was injected into a polymerization cell specially designed in this work (as shown in Figure 3.2 [1]) and then hermetically sealed under a N_2 atmosphere. The pregel

mixture was then irradiated for 2 hours with UV light from a Mercury arc lamp (with a wavelength range of 200-400 nm and a power of 200W). Photomasks consisting of carbon-printed PET films with varying UV transmittance were placed between the lamp and the cell window to modify the light intensity (I_{UV}) during the polymerization (Table 3.1). Details of photomasks are explained in Appendix A. The glass plate as well as the photomasks both reduce the total intensity transmitted to the gel, producing the UV intensities irradiated to the gel ranging from 7.5×10^{-3} to 2.65 mW/cm^2 . Considering the gelation point and gelation percent of gels, the gelation time was chosen to be 2 hours. The square sheets of gels with 1 mm thick with an area of 1 cm^2 were resulted from the gelation procedure. The uniformity of all the sample sizes meant that it was possible to make direct comparison between different gels in the swelling experiments.

Table 3.1. Conditions of UV initiated synthesis for VP/HEMA gels crosslinked with BIS

Gel code	VP:HEMA Feed Ratio (Wt. %)	Initiator Concentration (Wt. %)	Crosslinker Concentration (Wt. %)	UV Intensity Irradiated (mW/cm^2)	Photomask Type
UVHIB1	70: 30	0.80	0.20	0.2380	Mask3
UVHIB2	80: 20	0.80	0.20	0.2380	Mask3
UVHIB3	90: 10	0.80	0.20	0.2380	Mask3
UVHIB4	99: 01	0.80	0.20	0.2380	Mask3
UVHIB3a	90: 10	0.80	0.20	0.0075	Mask1
UVHIB3b	90: 10	0.80	0.20	0.0530	Mask2
UVHIB3c	90: 10	0.80	0.20	0.9200	Mask4
UVHIB3d	90: 10	0.80	0.20	1.6300	Mask5
UVHIB3e	90: 10	0.80	0.20	2.6500	Mask6
UVHIB3f	90: 10	0.80	0.20	Gradient	DGrad-Mask1
UVHIB3g	90: 10	0.50	0.20	0.2380	Mask3
UVHIB3h	90: 10	0.20	0.20	0.2380	Mask3
UVHIB3i	90: 10	0.80	0.40	0.2380	Mask3
UVHIB3j	90: 10	0.80	0.10	0.2380	Mask3
UVHIB3k	90: 10	0.80	0.05	0.2380	Mask3
UVHIB3l	90: 10	0.80	0.00	0.2380	Mask3

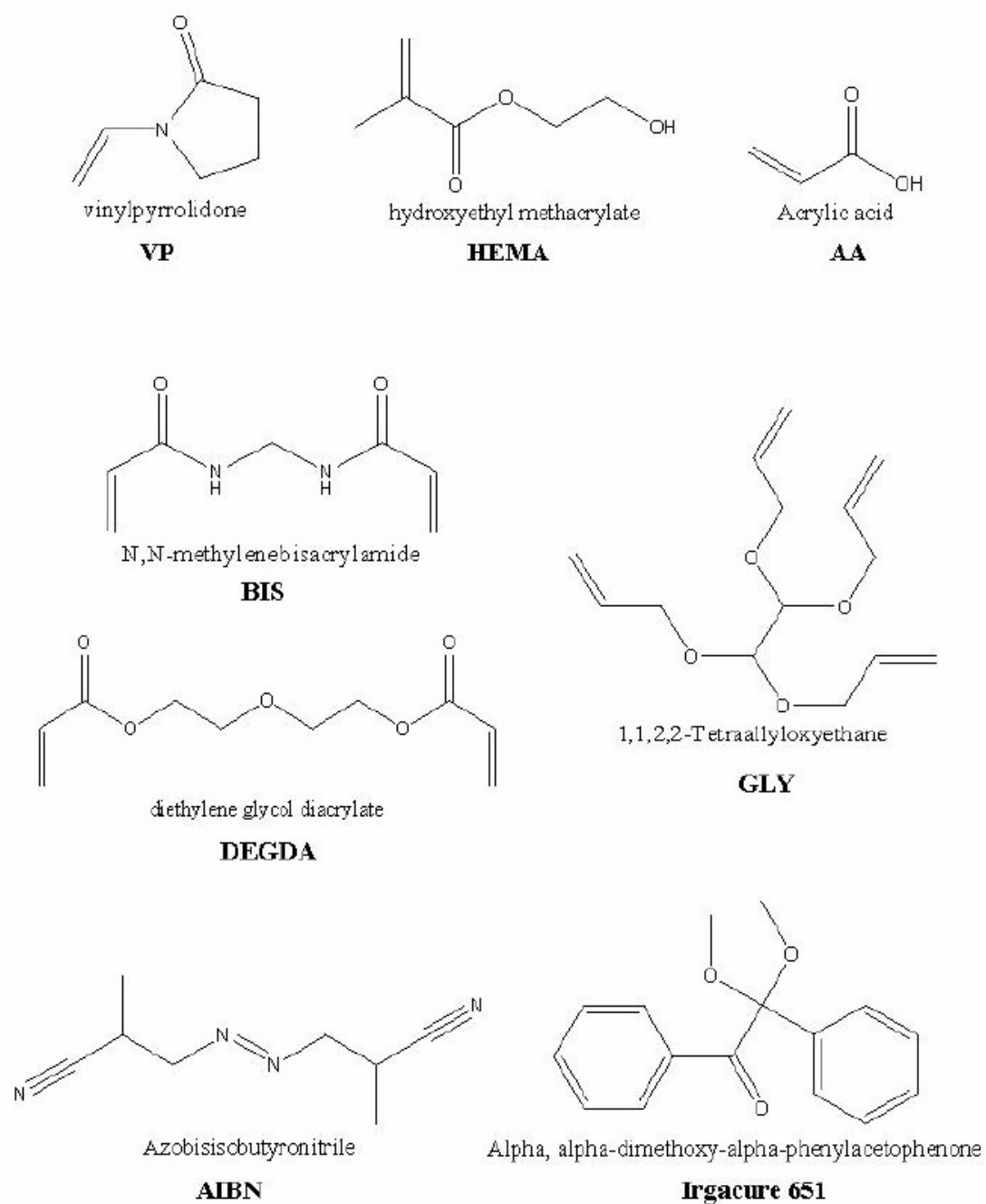


Figure 3.1. Chemical Structures of monomers of VP, HEMA, and AA, cross-linkers of BIS, DEGDA, and GLY, and initiators of AIBN and Irgacure 651.

Table 3.2. VP/HEMA gels UV initiated synthesized with various concentrations of GLY and DEGDA with feed VP:HEMA weigh ratio of 9:1, 0.8 wt. % Irgacure 651 and Mask3

Gel code	Crosslinker type	Crosslinker Concentration (Wt. %)
UVHIG3a	GLY	0.40
UVHIG3b	GLY	0.20
UVHIG3c	GLY	0.15
UVHIG3d	GLY	0.10
UVHID3a	DEGDA	0.40
UVHID3b	DEGDA	0.20
UVHID3c	DEGDA	0.10

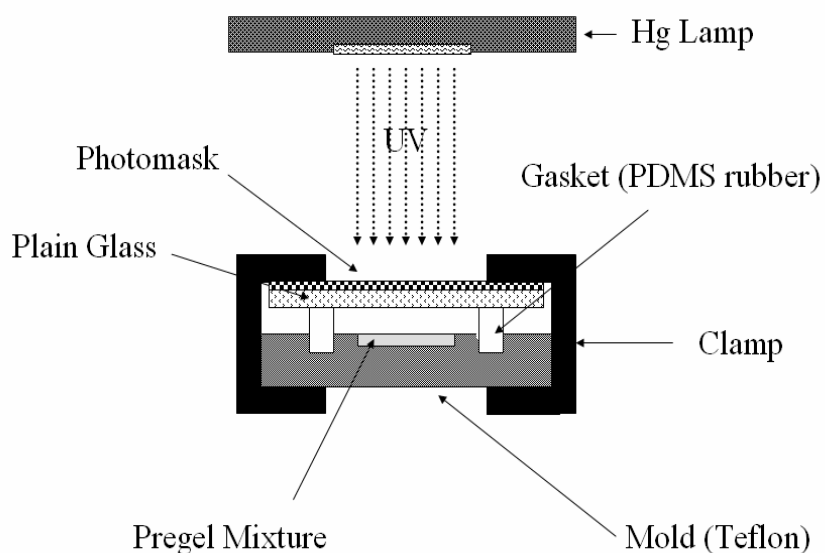


Figure 3.2. The schematic of an assembled device for UV-initiated polymerization

Various VP and HEMA gels thermally crosslinked with BIS using azo-isobutyronitrile (AIBN) initiator instead of the Irgacure 651 UV initiator were obtained at different feed ratios of VP and HEMA (see Table 3.3). In these gels 0.35 wt. % AIBN and 0.2 wt. % BIS were used in all cases. Each mixture was placed in a glass vial and then degassed using repeated freeze-thaw cycles (3 cycles). The sealed vial was subsequently placed into temperature controllable oil bath and the polymerization was carried out stepwise at 25 °C for 24 hours, followed by 24 hours at 35 °C, 4 days at 60 °C and finally 110 °C for 2 hours in an oil bath. The gels were removed from the glass tube, and the resulting cylindrical rod cut into discs and then dried under vacuum at 60 °C for at least 48 hours.

Table 3.3. Feed monomer ratio of VP/HEMA gels thermal synthesized with 0.35 wt. % AIBN and 0.2 wt. % BIS

Gel code	VP:HEMA
	Feed Ratio (Wt. %)
TVHAB1	70: 30
TVHAB2	80: 20
TVHAB3	90: 10
TVHAB4	99: 01

3.1.2. Synthesis of VP/AA Gels

3.1.2.1. Isotropic VP/AA Gel Systems

Vinyl pyrrolidone (VP) and acrylic acid (AA) and were purified using vacuum-distillation before polymerization. Mixtures of VP and AA with various weight ratios

(see Table 3.4) were UV-initiated polymerized with Mask 3, 0.8 wt. % Irgacure 651 photoinitiator and 0.2 wt. % BIS cross-linker using same polymerization procedures described for synthesizing VP/HEMA gels above.

All chemicals were purchased from Aldrich Chem. Co and their chemical structures are shown in Figure 3.1.

Table 3.4. Monomer feed ratio of VP/HEMA gels synthesized with various feed monomer ratio using 0.8 wt. % Irgacure 651, 0.2 wt. % BIS and Mask 3

Gel code	VP:AA Feed Ratio (Wt. %)
UVAIB1	100: 00
UVAIB2	90: 10
UVAIB3	80: 20
UVAIB4	70: 30
UVAIB5	60: 40
UVAIB6	50: 50
UVAIB7	40: 60
UVAIB8	30: 70
UVAIB9	20: 80
UVAIB10	90: 10
UVAIB11	00: 100

3.1.2.2. The Optimization of Gel Systems for Anisotropic Swelling Studies

The VP/AA copolymeric systems with 60wt% VP and 40 wt% AA feed composition (UVAIB5 gel) were chosen for anisotropic swelling studies. To acquire many numbers and bulky shape of VP/AA gel specimens for the swelling studies, the gels were synthesized using thermal polymerization.

To investigate the effect of C_C and crosslinker type on equilibrium swelling ratio (q_e) of UVAIB5 gels, the crosslinker concentration (C_C) of BIS was varied and BIS and DEGDA of 0.1 wt. % were used (see Table 3.5)

To optimize the initiator concentration (C_I) for the synthesis, the difference of C_I effect on the swelling behavior of two gel systems synthesized by UV-initiated polymerization and thermal polymerization was investigated. To compare the effect of AIBN and Irgacure 651 on the gel swelling, VP/AA gels prepared with both initiators with various concentrations prepared using UV initiated polymerization (Table 3.5). And using gels AIBN was used as an initiator since it is known that AIBN is also used for photopolymerization [2], VP/AA gels were synthesized using both polymerizations with various C_I as shown in Table 3.5. For the thermal polymerization, the synthesis was carried out at 25 °C for 24 hours, followed by 24 hours at 35 °C, 4 days at 60 °C and 110 °C for 1.5 hours. For the UV polymerization, Mask3 was used.

Table 3.5. Synthesis Conditions for VP/AA gels

Gel code	Polymerization (Polyn) Method	Initiator Type	Initiator Concentration (Wt. %)	Crosslinker Type	Crosslinker Concentration (Wt. %)
UVAIB5	UV Polyn	Irgacure 651	0.80	BIS	0.20
UVAIB5a	UV Polyn	Irgacure 651	0.80	BIS	0.10
UVAIB5b	UV Polyn	Irgacure 651	0.80	BIS	0.05
UVAID5a	UV Polyn	Irgacure 651	0.80	DEGDA	0.10
UVAAB5a	UV Polyn	AIBN	0.80	BIS	0.10
UVAAB5b	UV Polyn	AIBN	0.40	BIS	0.10
UVAAB5c	UV Polyn	AIBN	0.20	BIS	0.10
TVAAB5a	Thermal Polyn	AIBN	0.80	BIS	0.10
TVAAB5b	Thermal Polyn	AIBN	0.40	BIS	0.10
TVAAB5c	Thermal Polyn	AIBN	0.20	BIS	0.10

3.1.3. Synthesis of VP/*n*MA (*n* series methacrylate) Gels

Vinyl pyrrolidone (VP), methyl methacrylate (MMA), *n*-butyl methacrylate (BMA), *n*-octyl methacrylate (OMA) and *n*-dodecyl methacrylate (or *n*-lauryl methacrylate (LMA)) were purified using vacuum-distillation before polymerization. The VP/MMA, VP/BMA, VP/OMA, and VP/LMA copolymeric gels with the feed weight ratio of VP and *n*MA of 90:10 were prepared by UV-initiated free radical photopolymerization method using Irgacure 651 as the photoinitiator and BIS as the cross-linker in the synthesis conditions given in Table 3.6. These chemicals were purchased from Aldrich Chem. Co and their chemical structures are shown in Figure 3.3.

The UV-initiated and thermal polymerization procedures of the synthesis of VP/*n*MA gels are the same as those of VP/HEMA gels explained in section 3.1.1.

Table 3.6. VP/*n*MA gels photo-polymerized with 0.8 wt % Irgacure 651, 0.2 wt.% BIS, and Mask3

Gel Code	<i>n</i> in <i>n</i> MA	Number of Carbon (C) in <i>n</i>
UVMIB3	Methyl	1
UVBIB3	Butyl	4
UVOIB3	Octyl	8
UVLIB3	lauryl	12

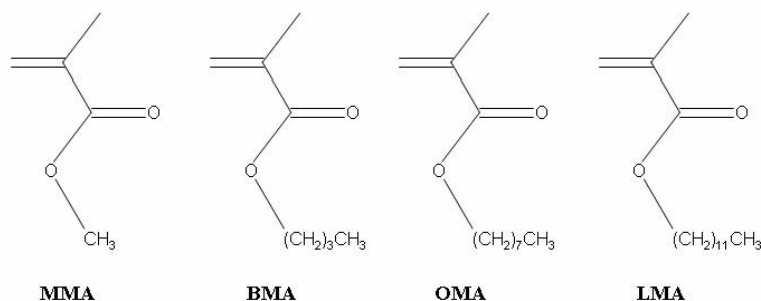


Figure 3.3. Chemical Structure of MMA, BMA, OMA, and LMA

3.1.4. Silver Nanoparticles-Gel Composite

Silver (Ag) nanoparticles were synthesized by the procedure suggested by Lee and Tsao [3]. 20 mL of 100 ppm ascorbic acid solution was added to 20 mL of 100 ppm aqueous AgNO_3 solution at room temperature, producing the silver nanoparticles of 200-300 nm size in aqueous solution (see Figure 3.4 (a)). The Ag-UVHIB 3 gel composites were synthesized using the method shown schematically in Figure 3.4 (b). In this method the Ag particle solution was mixed with the VHIB3 pregel and the mixture was schematically UV-initiated polymerized. The UVHIB3-Ag hydrogels obtained were fully swollen in distilled water and freeze-dried for 48 hours to remove all remaining water from the composite. The freeze-dried composite was cut into the required size, placed in the curing device, and swollen with the pregel mixture, and irradiated with UV, so that a semi-interpenetrating Ag-UVHIB 3 gel composite was obtained and its swelling behavior was compared with that of UVHIB 3 gel.

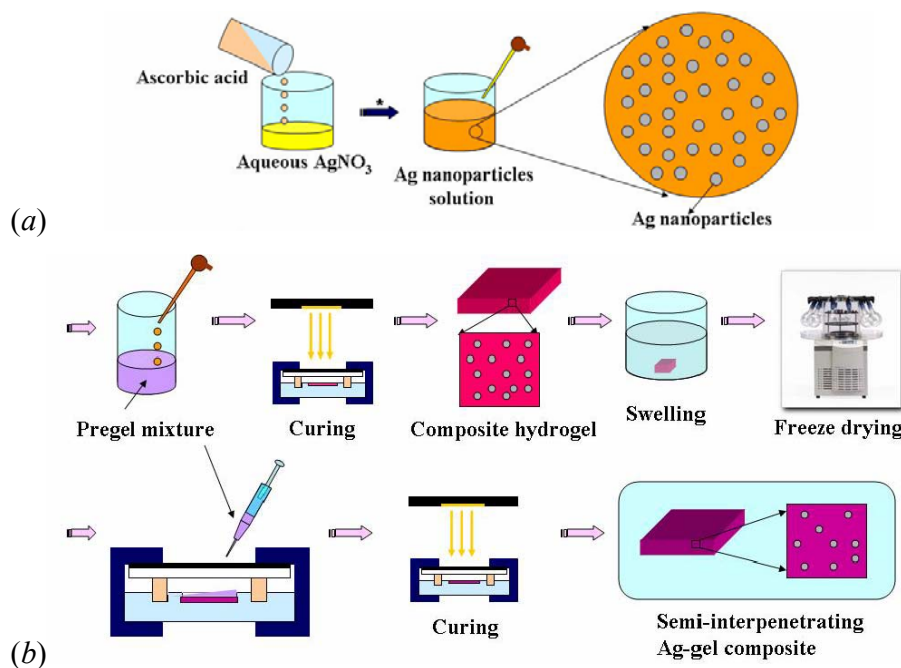


Figure 3.4. The synthesis of silver nanoparticles in aqueous solution (a) and the synthesis process of the silver nanoparticles-UVHIB 3 gel composite (b).

3.1.5. Encapsulation of Gels

The Polydimethylsiloxane (PDMS) elastomeric films with four different film thicknesses (d_e) were prepared using three different ratios of PDMS precursor and crosslinker (F_{PC}) at the room temperature for 2 hours and 110 °C for 12 hours (see Table 3.7). The stress at break (σ_b) and strain at break (ε_b) of the PDMS elastomers were measured at the strain rate ($\dot{\varepsilon}$) of 30 mm/min in a tensile test using an Instron. The elastic modulus (E) and toughness of the films were also determined. The PDMS elastomers were cut into rectangular shape with dimension 17 by 60 mm. The grips and a laser extensometer were used for the tensile test. PDMS Elastomer system producing the optimized toughness and ε_b was chosen for the use in encapsulating UVHIB3 gels.

Table 3.7. The conditions of preparing PDMS and PB elastomer films with various thickness

Elastomer Code	Ratio of PDMS Precursor and Crosslinker (F_{PC})	PB concentration in Solution with Toluene (wt. %)	Film Thickness, d_e (μm)
PDMS1a	10: 1.0	-	300
PDMS1b	10: 1.0	-	550
PDMS1c	10: 1.0	-	760
PDMS1d	10: 1.0	-	860
PDMS2a	10: 0.8	-	300
PDMS2b	10: 0.8	-	550
PDMS2c	10: 0.8	-	670
PDMS2d	10: 0.8	-	860
PDMS2e	10: 0.8	-	600
PDMS3a	10: 0.6	-	300
PDMS3b	10: 0.6	-	550
PDMS3c	10: 0.6	-	720
PDMS3d	10: 0.6	-	830
PB1a	-	1	300
PB2a	-	3	300
PB2b	-	3	275
PB2c	-	3	145
PB2d	-	3	75.0
PB2e	-	3	15.0

The UVHIB3 gels were also encapsulated by polybutadiene (PB) elastomer films with different film thickness (d_e) (see Table 3.7) by dip coating in a solution of 3 wt. % PB in toluene following by drying at 60 °C for 12 hours.

3.1.6. Multilayer of Gels and Elastomers (GE)_m

As shown in Figure 3.5, multilayers of gels and elastomers (GE)_m were prepared by alternating layers of UVHIB3 gel and PB elastomer. VP/HEMA gel layer was coated on to a silicone wafer and then was coated by a PB film using 5 wt% of PB solution in toluene. This process was repeated to build up alternating layers. For the UVHIB3 gel layer, the VHIB pregel mixture was coated on the silicone wafer and the UV was irradiated using Mask3 for the curing each gel layer under a N₂ atmosphere. The PB film layer solution-coated on the gel layer was dried at 60 °C for 12 hours. Slow cooling of each elastomer layer was required to avoid the occurrence of cracks in the gel layer. Two different (GE)_m were prepared for observing the swelling behavior and their parameters are detailed in Table 3.8.

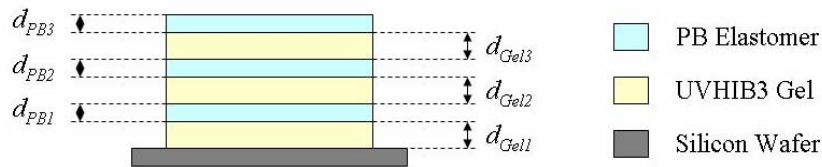


Figure 3.5. The schematic of a (GE)_m made of three layers of UVHIB 3 gel and PB elastomer membrane on the silicon wafer

Table 3.8. Thickness of UVHIB3 and PB rubber layers

Name	d_{Gel1} [μm]	d_{PB1} [μm]	d_{Gel2} [μm]	d_{PB2} [μm]	d_{Gel2} [μm]	d_{PB3} [μm]
(GE) _m 1	440	50	600	50	500	120
(GE) _m 2	400	100	350	60	640	150

3.1.7. Anisotropic Swelling Hydrogels

3.1.7.1. Morphologically Gradient-Induced Anisotropic Swelling Hydrogels

To induce anisotropic swelling, gels with architectural gradient (crosslinking density gradient) (DGrad-UVHIB3 gels) were prepared by UV-initiated polymerization using the device shown in Figure 2.2 using a discrete gradient photomask (DGrad-Mask1, see Appendix A). In this way, it is possible to locally control the UV irradiation intensity during the polymerization. It is expected that the network structure of the gels obtained using the patterned photomasks changes discretely which each section. The swelling behavior, elastic modulus, and network structure characteristic for each section of discrete gradient in the DGrad-UVHIB3 gels can be determined based on the results of analysis of UVHIB3, UVHIB3c, UVHIB3d, UVHIB3e hydrogels obtained by photomasks allowing different UV irradiation intensity (see Table 2 & Appendix A). The gradient in crosslinking density in DGrad-UVHIB3 caused anisotropic swelling, which was verified by stereo-optical microscopy.

Determination of the local self-diffusion coefficient (D_s) of water through DGrad3-UVHIB3 hydrogels was performed using diffusion MRI to verify the gradient morphology. DGrad3-UVHIB3 gels were prepared from a mask consisting of three distinct sections (DGrad-Mask2) shown in Figure A4 (see Appendix A).

3.1.7.2. Compressive Stress-Induced Anisotropic Swelling Hydrogels

Gel system showing optimized swelling behavior and mechanical properties was determined to be TVAAB5bgels prepared by thermal polymerization using feed weight ratio of VP and AA of 6:4, 0.1 wt. % BIS and 0.4 wt. % AIBN and was chosen for anisotropic swelling studies. The cylindrical rod shaped gels with a diameter of 8 mm, produced by the thermal polymerization, was cut into 5 mm slices and then dried under vacuum at 60 °C for at least 48 hours.

For inducing anisotropic swelling, the compressive force was applied to the TVAAB5b gel specimens using MTS Insight 2 uniaxial mechanical instrument with a thermal chamber and high load capacity (2000 N load) compression platens at various temperatures and loads. To avoid mechanical failure of the gels during the compression, the compression temperature (T_c), compression strain (ε_c), and compression strain rate ($\dot{\varepsilon}_c$) were controlled. The T_c was varied from 20 °C to 30 °C above and below the T_g of the TVAAB5b gel, i.e. in the range from 100 °C to 150 °C. The set ε_c values were 70 %, 80 %, 90 % and 95 %. The gel specimens were compressed with $\dot{\varepsilon}_c$ values of 0.0002 s⁻¹ to 0.01 s⁻¹. The compression processing conditions for preparing the compressed TVAAB5b gels is given in Table 3.9.

In the compression, each gel specimen was placed between the compression platens preheated at the set processing temperature and held at the temperature for annealing time of 1 hour to ensure uniform temperature distribution within the gel specimen. The annealing time to be used was roughly calculated using the lumped capacitance method for the sample considering heat conduction and radiation. The annealed gel was compressed up to the strain set point with set strain rate, held in compressed state, and then the compressed gel cooled down to room temperature.

The shape fixicity of the obtained specimens was determined using the following equation [4], providing the indication index of the shape memory properties of materials.

$$\text{Shape Fixicity} = \frac{\varepsilon_r}{\varepsilon_c} \times 100 \quad (38)$$

where the $\dot{\varepsilon}_c$ is compression strain which is set for the test and the ε_r is the resulting compressed strain which is obtained in the compressed gel.

Prior to the compression of gels strain recovery tests was performed by loading and unloading of the TVAAB5*b* to verify the occurrence of mechanical failure in the gels during the compression processing.

Table 3.9. The processing conditions of compression for the compressed TVAAB5*b* gels

Gel code	Compression Temperature, T_c (°C)	Compression Strain, γ_c (%)	Compression Strain Rate, $\dot{\gamma}_c$ (s ⁻¹)
TVAAB5 <i>b</i> _1	100	90	0.0010
TVAAB5 <i>b</i> _2	110	90	0.0010
TVAAB5 <i>b</i> _3	120	90	0.0010
TVAAB5 <i>b</i> _4	130	90	0.0010
TVAAB5 <i>b</i> _5	140	90	0.0010
TVAAB5 <i>b</i> _6	150	90	0.0010
TVAAB5 <i>b</i> _7	110	70	0.0010
TVAAB5 <i>b</i> _8	110	80	0.0010
TVAAB5 <i>b</i> _9	110	95	0.0010
TVAAB5 <i>b</i> _10	110	90	0.0002
TVAAB5 <i>b</i> _11	110	90	0.0001
TVAAB5 <i>b</i> _12	110	90	0.0100

3.2. Characterizations of Gels and Hydrogels

3.2.1. Gelation Point/Time and Percent

Gelation point was determined using UV spectrophotometer (Shimadzu UV-1601). During UV irradiation to the gel, UV absorbance spectra of pregel were collected with time up to the point where the UV absorbance spectra did not shifted. The point (or time) is considered as a gelation point (or gelation time). The gel percent was determined by soxhlet extraction of sol from the synthesized gel and using Equation (1), $GF = (W_f / W_i) \times 100$, where W_i and W_f are the weight of the polymerized gel after drying (W_f) and the weight of the dried gel after the washing steps (W_i), respectively.

3.2.2. Infrared Spectroscopy of Xerogels

The compositions of the gels obtained were quantitatively determined and the characteristic groups of the gels were qualitatively analyzed using Fourier Transform Infrared (FTIR) spectroscopy. Before the FTIR measurement, the gels were treated by repeated cycles of washing in ethanol and then distilled water followed by freeze-drying. After the final freeze-dried step the samples were cut and powdered, mixed with KBr, and then compressed using a standard IR disc press into a 0.22 mm thickness sample. The sample was analyzed using FTIR instrument (Bruker Vector 22), using a scanning resolution of 4 nm and a total of 32 scans per samples. Quantitative determination of the VP and HEMA content in the VP/HEMA xerogels were evaluate from the ratio of the peak areas of the two characteristic C=O stretching absorption peaks at 1660 and 1730 cm^{-1} for the VP and HEMA components, respectively [1, 5]. In addition, for the VP/AA xerogels the characteristic C=O peaks of AA and VP at 1730~1750 cm^{-1} and 1650 ~1680, respectively [1, 6, 7] were analyzed. Peak areas were determined by using commercially available software (PeakFitTM, Systat Inc).

3.2.3. Thermal properties of Xerogels

The freeze dried gel samples were placed in a vacuum oven for at least 48 hrs at 60 °C and 500 mmHg before the DSC and TGA measurements. The glass transition temperature (T_g) for various xerogels were obtained using a DSC (Seiko 220C DSC) at a heating/cooling rate of 10 °C/min, operating between 20 and 250 °C for VP/HEMA gels and 20 °C and 200 °C for VP/AA gels under a N₂ gas purge. The values of T_g reported were all obtained from the second heating cycle. The measured T_g values of gels were compared with the T_g values predicted based on the composition of gels using the Flory-Fox, Gordon-Taylor equations and Kwei equation, Equation (2) and Equation (3), and Equation (4), respectively.

Thermal stability of gels was evaluated by thermogravimetric analysis (TGA) (Seiko TG/DTA 320). The TGA measurements were carried out with a heating rate of 10 °C/min from 20 to 550 °C under a N₂ atmosphere.

3.2.4. Internal Structure of Xerogels and Gels.

The morphologies of equilibrium-swollen hydrogels were investigated by low voltage electron microscopy (LVEM5, Delong America Inc.). The gels were treated by repeated cycles of washing in ethanol and then distilled water, and then were frozen with liquid N₂ and cut with a sharp scalpel into smaller sized samples and freeze-dried for 48 hr. The freeze-dried samples were mounted onto a TEM grid (3 mm diameter), placed on an aluminum stud and sputter-coated with gold. Before imaging the specimens using LVEM5, they were dried at room temperature at very low vacuum.

The morphology of various TVAAB5*b* gel series compressed with different processing conditions was investigated using a Leica scanning electron microscope (SEM) with northern microtrace EDX spectrometer. The gel specimens were also sputter-coated with gold prior to the measurements.

3.2.5. Opacity in Heated Gels/Compressed Gels: Optical Microscopy

The gels synthesized by either thermal or photo-initiated polymerizations normally showed transparency. However when the gels were heated, their clarity changed from transparent to opaque. When the heated gel was compressed, transparency appeared in the middle of the compressed gel but still remain the opacity in the edge of the compressed gel. To determine the identity causing the clarity, gels without and with heat treatment as well as the compressed gels were analyzed by optical microscopy (OM).

3.2.6. Anisotropy of the compressed gels: Birefringence

To determine the expected anisotropy of molecular structure in the gel after compression processing, birefringence of TVAAB5b_2 gels were analyzed in polarized light at 0 and 90° angles between polarizer and analyzer using the configuration as shown schematically in Figure 2.6.

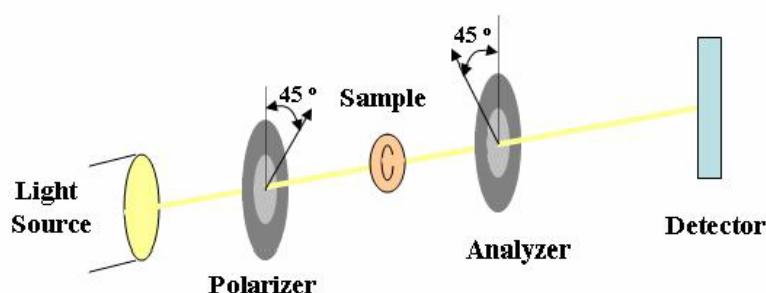


Figure 3.6. The schematic of experimental setup of polarized optical microscopy

3.2.7. Swelling Behavior of Gels

3.1.7.1. Swelling Ratio (q)

The gel specimens were dried in a vacuum oven at 500 mmHg and 60 °C for at least 48 hours prior to immersing into saline solution (sterile 0.5 wt% saline; Bausch And Lomb) at room temperature. Both the volume (monitored optically using a digital camera of the gel shape against a calibrated reference pattern) and the mass of the gels were measured at periodic intervals of time. To measure the mass, the hydrogels were taken out of the saline solution, and the surface water removed using filter paper before weighing. The solution was changed with fresh solution after each measurement. Using this procedure the volume ($q_v = V_s/V_i$) and mass ($q_m = m_s/m_i$) swelling ratios were determined where m_x and V_x are the mass and volume, respectively, of the dry gel at an initial time ($x=i$) and the hydrogel at a specific time ($x=s$) after swelling begins. Where volume swelling ratio is difficult to determine accurately due to the distortion of gel shape, it is also possible to determine this since q_v and q_m are related through the equation $q_v = 1 + \rho_p/\rho_{sol}(q_m - 1)$, where ρ_i are the densities of the gel ($i=p$) and solvent ($i=sol$), respectively. The volume ($q_{ev} = V_s/V_d$) and mass ($q_{em} = m_s/m_d$) equilibrium swelling ratios were obtained at infinite time when the hydrogels are fully swollen, where m_d and V_d are the mass and volume, respectively, of the dried sol-free gel.

For the ionizable hydrogel systems, VP/AA hydrogel systems, the pH of the swelling medium needed to be controlled during the swelling measurement since the swelling behavior of ionic hydrogels is sensitive to pH. To observe the composition-dependent swelling behavior, the pH was maintained at 7.4 by keep changing the swelling medium with fresh solution. This was chosen to mimic the pH commonly found in our bodies. To investigate the effect of pH on the equilibrium swelling ratio (q_e) of VP/AA Hydrogels (UVAIB gel series), the buffer solutions with pH 1.0 to pH 8.0 were

used. The pH of the swelling medium was often checked by a pH-meter (Leici/E-201-C, accuracy: 0.01). To observe the temperature effect on the q_e of VP/AA hydrogels, the q_e values of UVAIB3, UVAIB5, and UVAIB9 gels were measured at the temperature of 20.0 to 61.5 °C at a pH 7.4.

3.1.7.2. Swelling Rate

The diffusion coefficient (D) values for various hydrogel systems were determined using the following approaches. The initial rate of saline solution mass uptake in the initial gel swelling region (Figure 2.7), where mass swelling ratio increases linearly as a function of time, was analyzed using $w(t)/w_\infty = k t^n = 4(Dt/\pi l^2)^n$ (Equation (27)), where $w(t)$ and w_∞ are the weight of penetrant uptake by the hydrogel at time t and at equilibrium, respectively. The exponent n defines the diffusion mechanism and the constant $k = 4(D/\pi l^2)^n$ is defined by D and the thickness of the sample, l [8, 9].

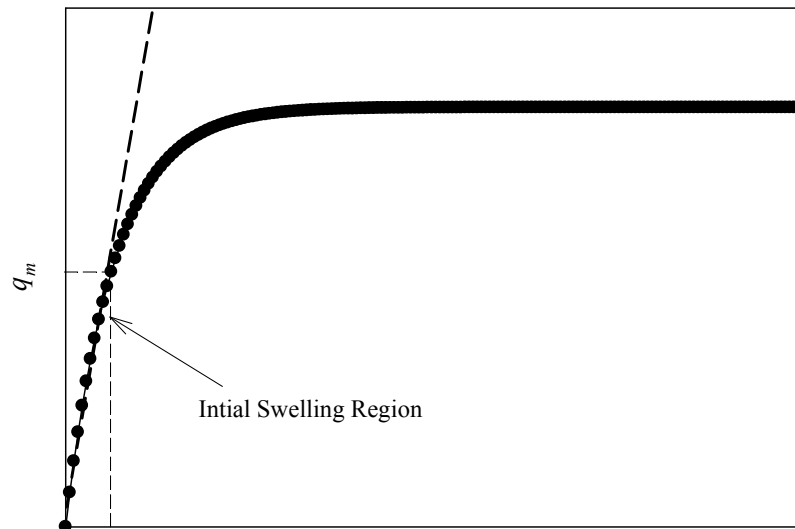


Figure 3.7. Mass swelling ratio (q_m) of gel as a function of time

The values of k and n were calculated from the slopes and intercepts of log-log plots of the penetrant uptake experimental data, *i.e.* $\log(w(t)/w_\infty)$ versus $\log t$ [10], allowing the value of D to be evaluated.

The initial swelling rate ($S_R = (q_{60\%} - 1)/t_{q_{60\%}}$, where $q_{60\%}$ is the 60 % swelling ratio of q_e) was determined from simply dividing the initial 60% increase in the q by the increment of time from zero to the time ($t_{60\%}$) at which q reach 60 % of q_e was also used in this work for convenience.

The time to reach maximum expansion of the system (t_{max}) was also used for analyzing the swelling kinetics of the hydrogel systems since it is an important factor for overall swelling kinetics.

3.2.8. Mechanical Properties of Hydrogels and Gels

The compressive modulus, G , of the hydrogels were obtained for the various hydrogels using a DMA (Mettler Toledo SDTA861e). The fully swollen hydrogels were tested in compression mode with an applied compression strain ranging between 0.01 % and 5.0% at 1 Hz measured at room temperature. The values of G reported were obtained from the linear region of the modulus-strain plot.

The mechanical properties of gels were determined by MTS Insight 2 uniaxial mechanical test machine attached with a thermal chamber and two platens with high load cell capacity (2000 N).

For the TVAAB5 series hydrogels, compression tests were carried out not only using DMA but also using the uniaxial instrument fitted with 10 N load cell to compare the modulus values determined by both techniques. The toughness for three TVAAB5 series hydrogels made with different AIBN concentrations were determined from the stress and strain curve obtained for each hydrogel.

3.2.9. Structural Characteristics, ν_e & M_c and Interaction Parameter, χ of Hydrogel

3.2.9.1. VP/HEMA hydrogels

The values of the effective cross-link density, ν_e and molecular weight between cross-links, M_c , of each hydrogel system were calculated from its modulus experimentally determined by DMA and equilibrium volume swelling ratio (q_{ve}) obtained by swelling measurements using Equations 33 and 34, $G = \nu_e RT q_{ve}^{1/3}$ and $M_c = \rho / \nu_e$, respectively, where R is ideal gas constant, T is absolute temperature of the system, ρ is the density of the (dry) gel and in the fully swollen (equilibrium) state [11, 12].

Once ν_e is calculated as mentioned above, the interaction parameter (χ) between polymer and swelling medium was also determined using Equation 22 for each system.

3.2.9.2. VP/AA hydrogels

The prediction of the swelling behaviour and network structure of hydrogels composing of monoprotic acid moieties was carried out using Equation (37), $A = \chi + B/M_c$

where
$$A = \left(\frac{V_1}{4I} \left(\frac{K_a}{10^{-pH} + K_a} \right)^2 \left(\frac{\nu_2 \Phi}{\bar{v} M_0} \right)^2 \right) - \left(\frac{1}{\nu_2^2} \ln(1 - \nu_2) + \frac{1}{\nu_2} \right) \quad \text{and}$$

$$B = \left(\frac{(1 - 2/\phi) V_1 \nu_{2r}^{2/3} \nu_2^{-5/3}}{\bar{v}} \right),$$
 which uses a the solvent and polymer mixing force

contribution developed by Flory-Huggins [13], elastic force contribution proposed by James and Guth for a phantom network [14], and ionic contribution by Brannon-Peppas and Peppas [15] on the chemical potential.

From the measurement of the q_{ve} values for the VP/AA hydrogels at different values of pH of the solution, the values of M_c and χ were determined from the determined from the slope and exploration, respectively, of the plot of A as a function of B.

The values of ν_e were determined using Equation (34).

References

- [1] J. Hannah Lee and David Bucknall, "Swelling Behaviour of Hydrogels Synthesized using Controlled UV-initiated Free Radical Polymerization", *Journal of Polymer Science B: Polymer Physics*, 46(14), 1450-1462, July 2008.
- [2]. Norman S. Allen (Ed.), *Photopolymerisation and Photoimaging Science and Technology*, Elsevier Applied Sci., 1989.
- [3] W. F. Lee and K. T. Tsao, "Preparation and properties of Nanocomposite Hydrogels Containing Silver Nanoparticles by Ex Situ Polymerization" *J of Appl Polym Sci* vol. 100, pp. 3653-3661, 2006.
- [4]. Jasmeet Kaursoin, Ashwini K. Agrawal, "Melt Spun Thermoresponsive Shape Memory Fibers based on Polyurethanes: Effect of Drawing and Heat-Setting on Fiber Morphology and Properties", *Journal of Applied Polymer Science*, vol. 103, pp. 2172-2182, 2007.
- [5]. F. Huang, S. W. Kuo, F. J. Lin, C. Wang, C. J. Hung, F. C. Chang, "Syntheses and specific interactions of poly (hydroxyethyl methacrylate-b-vinyl pyrrolidone) diblock copolymers and comparisons with their corresponding miscible blend systems", *Polymer*, vol. 47, pp. 7060-7069, 2006.
- [6]. H. M. Said, S. G. A. Abd Alla, and A. W. M. El-Naggar, "Structural Properties of-Irradiated Poly (vinyl alcohol)/Poly (ethylene glycol) Polymer Blends", *Reactive & Functional Polymers*, vol. 61, pp. 397-404, 2004.
- [7]. S. Jin, M. Liu, F. Shang, S. Chen and A. Niu, "Synthesis and characterization of pH-sensitivity semi-IPN hydrogel based on hydrogen bond between poly(N-vinylpyrrolidone) and poly(acrylic acid).", *Polymer*, vol. 47, pp. 1526-1532, 2006.
- [8]. J. Crank, *The Mathematics of Diffusion*; Oxford University Press: Oxford; 1975.
- [9]. A. Alfrey, E. F. Gurnee, and W. G. Lloyd, "Diffusion in glassy polymers", *Journal of Polymer Science*, vol. 12, pp. 249, 1966.

- [10]. Ritger, P. L and Peppas, N. A.,” A simple equation for description of solute release II. Fickian and anomalous release from swellable devices”, *J. Control. Release*, vol. 5 pp. 37-42, 1987.
- [11]. M. Rubinstein, R. H. Colby, *Polymer Physics*; Oxford University Press: New York; 2003.
- [12]. Tomas P. Davis and Malcolm B. Huglin, “Effect of crosslinking on the properties of poly(2-hydroxyethyl methacrylate) hydrogels” *Die Angewandte Makromolekulare Chemie*, vol. 189, pp. 195-205, 1991.
- [13]. Flory, P. J., *Principles of Polymer Chemistry*; Cornell University Press: New York; 1969.
- [14]. James E. Mark and B. Erman, *Rubberlike Elasticity: A Molecular Primer*, John Wiley and Sons, Inc, 1988.
- [15]. Lisa Barnnon-Peppas and Nikolas A. Peppas, “Equilibrium swelling behavior of pH-sensitive hydrogels”, *Chemical Engineering Science*, vol. 46(3), pp. 715-722, 1991.

CHAPTER IV

CONTROL OVER SWELLING DEGREE AND RATE OF NEUTRAL HYDROGEL OF VP/HEMA COPOLYMER

For the development of an optimized hydrogel system which has the potential for use in reconstructive surgical tissue expansion procedures and significantly improves upon current tissue expander materials, among the important macroscopic hydrogel properties needed to be considered the swelling degree (or swelling ratio) and rate is most significant. Hydrogels showing higher swelling ratios are beneficial for limiting the number of surgical procedures and consequently reducing the cost and risk of surgery. Sufficiently slow swelling rate of hydrogels are also important to avoid tissue necrosis and help tissue growth during the tissue expansion process. Since structural characteristics of hydrogels determine their swelling behavior and mechanical properties, analysis of structural characteristics is highly important.

In this chapter, the studies on the effect of key parameters such as monomer composition, initiator concentration, crosslinker type and concentration, and controlled ultraviolet (UV) irradiation intensity on swelling behavior of known as a biocompatible and neutral hydrogel system consisting of vinyl pyrrolidone (VP) and hydroxyethyl methacrylate (HEMA) copolymers. The structural characteristics of the hydrogels were analyzed as well as their mechanical stiffness.

It is known that poly(N-vinyl pyrrolidone) (PVP) based copolymeric hydrogels possessing very hydrophilic functional groups induce high degrees of swelling in aqueous solution. PVP was the first synthetic polymer tested as a substitute for the artificial vitreous body of the eye [1]. The VP based copolymeric hydrogels [2, 3] are one of the most popular systems used as biocompatible materials [4, 5]. Poly(methyl methacrylate) (PMMA) based copolymeric hydrogels [6, 7], which is both nontoxic and biocompatible,

is also a stable material for the tissue expansion. The use of N-vinyl pyrrolidone (VP)/methyl methacrylate (MMA) copolymeric hydrogels for tissue expansion has been reported [8-10].

2-hydroxyethyl methacrylate (HEMA) was chosen in stead of MMA because HEMA is more hydrophilic, and therefore should contribute to relatively higher degree of swelling of the hydrogels. It also capability to improve the mechanical strength of the hydrogel made of VP, whose hydrogel showed relatively poor mechanical strength. HEMA based hydrogels are known to be biocompatible and have been used in numerous biomedical applications [4, 11-14], and first reported by Downes and coworkers for the use of tissue expansion in reconstructive surgery [33].

Accordingly, VP/HEMA copolymeric hydrogels are considered to be a good candidate for the tissue expander. In this work, the VP/HEMA hydrogels were prepared by not only UV initiated polymerization [3, 16-19] but also thermal polymerization [20-22] and their properties were characterized and compared.

4.1. UV-Polymerized VP/HEMA Gels

4.1.1. Composition of Xerogels

Figure 4.1 shows the FTIR spectra for photo-polymerized VP/HEMA gels with various feed monomer ratios. The characteristic peaks observed at 1660 and 1730 cm^{-1} are associated with the stretching mode of the carbonyl groups ($\text{C}=\text{O}$) in the VP and HEMA components, respectively [17]. The shift in peak position of the carbonyl peak of VP to 1660 cm^{-1} from the expected value of 1680 cm^{-1} can be attributed to the hydrogen bonding interaction between the carbonyl group in the VP and the hydroxyl group in the HEMA [17].

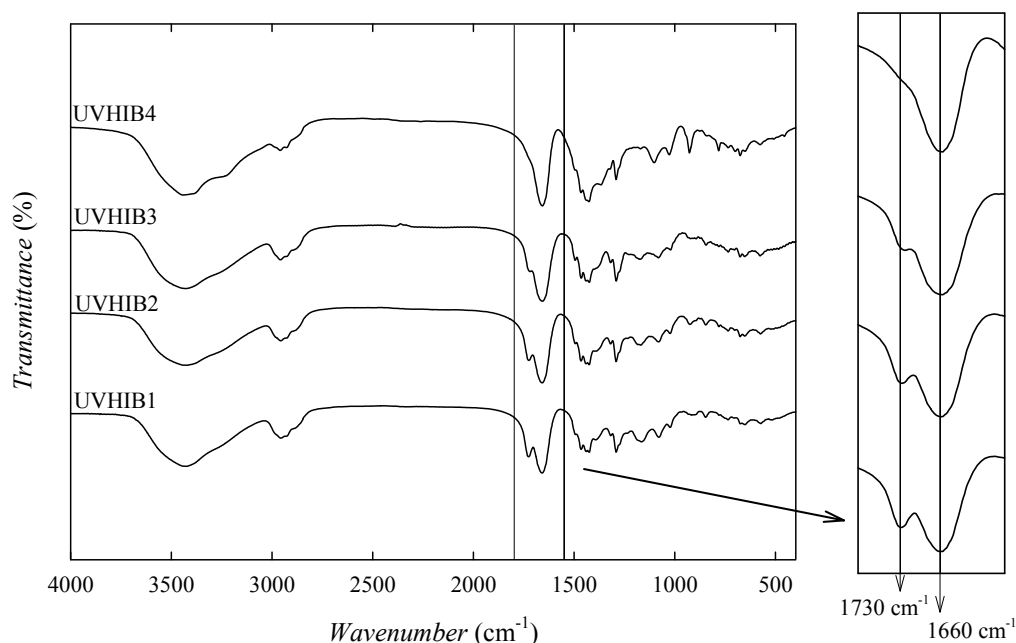


Figure 4.1. The IR spectra of VP:HEMA xerogels with various comonomer ratios (UVHIB1= 70:30, UVHIB2= 80:20, UVHIB3= 90:10, and UVHIB4= 99:01 of VP: HEMA).

Deconvolution of the FTIR data using peak fitting procedures gave the ratios of VP and HEMA content in the various gels from the relative peak area ratios, as reported in Table 3.1. The measured final composition ratio of the gels all differ from the initial monomer feed composition, because of the different reactivity ratios of VP and HEMA ($r_{VP} : 0.02 \sim 0.10$ and $r_{HEMA} : 2.97 \sim 3.40$) [20]. This difference in reactivity has been shown to cause HEMA to polymerize faster than VP in thermal and solution polymerization of these monomers [21]. During network formation in radical polymerizations the diffusivity of the radicals depends on the reaction time (or conversion), and consequently length of the growing chain [23], due to the reduction of radical mobility caused by the increasing viscosity of the mixture. Consequently with increasing reaction time there will be a greater tendency of the radicals to propagate with their nearest monomer neighbors

regardless of whether it is VP or HEMA. In this study, bulk polymerization is utilized where the effects of diffusion in controlling the reaction are significantly more pronounced compared to solution polymerization. Consequently, although HEMA monomers polymerize faster than VP, only relatively short sequences of HEMA are expected along the network chains, a situation which might be different from solution polymerization where the sequences can be more block-like as explained.

Table 4.1. Composition Ratios of VP and HEMA units in photo-polymerized VP/HEMA gels.

Gel Code	VP:HEMA composition ratios	Gelation (%)
UVHIB1	57 : 43	68.2 ± 2.71
UVHIB2	65 : 35	65.4 ± 1.52
UVHIB3	73 : 27	61.8 ± 2.18
UVHIB3 _c	72 : 29	63.7 ± 1.91
UVHIB3 _d	73 : 27	64.8 ± 0.82
UVHIB3 _e	71 : 29	62.8 ± 1.14
UVHIB3 _g	71 : 29	62.1 ± 2.51
UVHIB3 _h	72 : 28	62.5 ± 0.73
UVHIB4	89 : 11	12.4 ± 5.91

Although a large variation exists between the initial monomer feed ratio and the composition ratios of VP and HEMA units in the VP/HEMA gels for the gel prepared with various monomer feed ratios, the final composition is independent of I_{UV} or C_I within experimental error as shown in Table 4.1 and Figures 4.2 (a) and (b). It is thought because that the small variations in I_{UV} or C_I used in this work were not sufficient to produce significant variation in the gel composition.

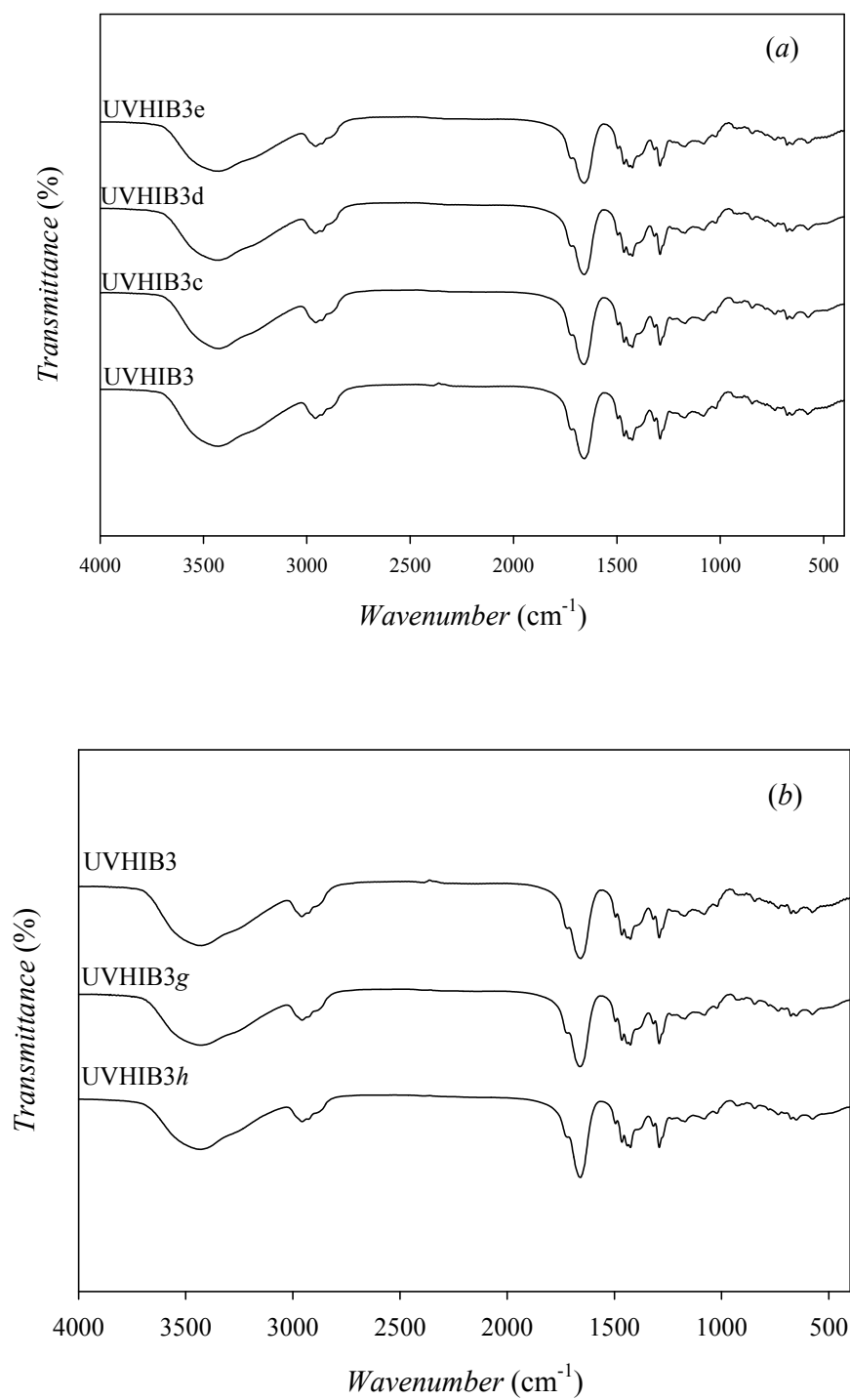


Figure 4.2 . The IR spectra of VP/HEMA xerogels with various I_{UV} (UVHIB3= 0.238, UVHIB3c=0.92, UVHIB3d=1.63, and UVHIB3e=2.65 mW/cm²) (a) and with different C_I (UVHIB3 =0.8, UVHIB3g =0.5, UVHIB3h = 0.2 wt %) (b).

4.1.2. Gelation of Xerogels

The gelation point (or time) of a pre-gel mixture during UV-initiated polymerization was evaluated using UV spectroscopy in addition to gelation percentage determination. Figure 4.3 shows the UV spectra of a VP/HEMA pregel mixture with 7:3 feed ratio of VP and HEMA as a function of reaction time. It can be seen that the absorbance (A) of the gel peak at a wavenumber of ~ 320 nm increases with time (up to 90 min). However, given that $A = -\log_{10}(T)$ where T is the transmittance, values of $A \geq 2.5$ are well beyond the accuracy of experimental determination due to the near zero transmittance at this value of A . Therefore above times of ~ 30 mins it is not possible to follow the extent of reaction by observation of this peak intensity. However, at a wavenumber of 380 nm (where A remains below 2), the UV intensity spectra increases with time and becomes approximately constant after 70 mins. Given these results it was assumed that after 90 mins UV irradiation complete gelation will be obtained. To confirm this gelation point the gelation percentage values of UVHIB1 gels prepared were determined with increasing UV irradiation time (Figure 4.4). They were found to increase slightly from 50 % to 70 % with increasing UV irradiation time up to 2 hours.

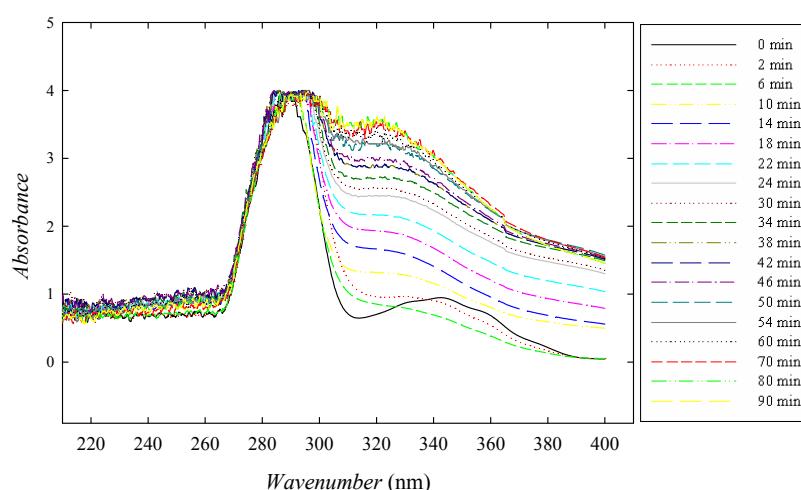


Figure 4.3. UV Spectra of UVHIB1 pregel mixture during its polymerization at certain time interval

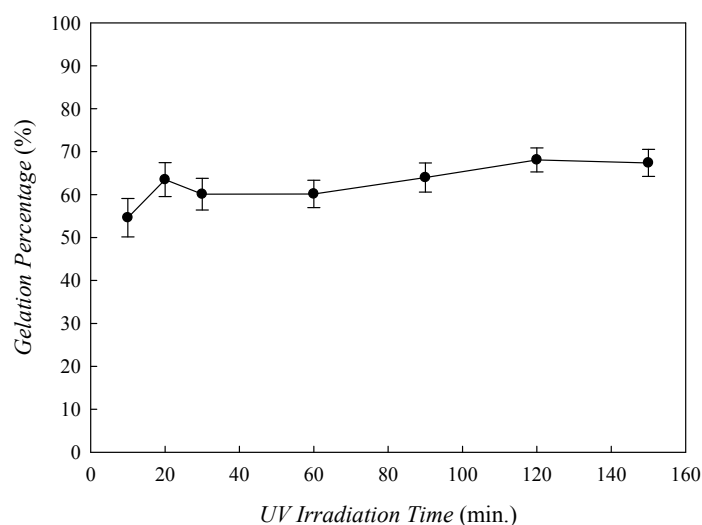


Figure 4.4. Gelation Percent of UVHIB1 gels irradiated by UV for different exposure times

Although the shift of the absorbance spectra with time was clear, with time only slight increase in gelation percent was obtained. This might be because during gels were dried after UV irradiation for the synthesis, polymerization proceeds in the gels. The UVHIB1 gels showed highest gelation percent among the UVHIB gel series. In this study 120 min (or 2 hours) was used for the UV irradiation time since the gelation time produce the gels having highest gelation percent. Most VP/HEMA hydrogel systems achieved 50 % ~ 70 % gelation percents except gels synthesized with a feed ratio of 99 wt. % VP (UVHIB4) showing high swelling and low mechanical integrity, resulting in broken debris. For the given in Table 4.1, UV-initiated polymerization can be seen to be an inefficient compared to thermal polymerization, leaving large amount of unreacted monomers, oligomers and polymer chains which are not crosslinked. The gelation percent values obtained in this work is consistent with those obtained by Li and coworkers who showed gel conversion rising from only 34 % at 0.25 mW/cm² UV intensity to approximately 70 % for light intensities of greater than 4.9 mW/cm², for HEMA gels crosslinked with DEGDMA or TEGDMA [16].

4.1.3. Thermal Analysis

Only a single T_g is observed for all the thermal and UV-initiated gels prepared, indicating that VP and HEMA segments in the gels are miscible at all volume fractions. The observed T_g values are however, strongly dependent on composition as shown in Figure 4.5 (a) where the T_g of the gel increases approximately linearly with VP content (C_{VP}). These values of T_g for the UV-initiated polymerized gels are compared to those obtained for thermal-initiated polymerized gels. The relationship between T_g and composition for copolymeric systems can be predicted using the Gordon-Taylor (G-T) equation (Equation (3), Chapter 2). The T_g and density values of thermally polymerised pure PVP and PHEMA are 186 °C and 1.25 g/cm³ and 118 °C and 1.1 g/cm³, respectively. There is a clear difference between the measured T_g values and those predicted from the G-T equation (see Figure 4.5 (a)). The discrepancy is most probably associated with the existence of H-bonding between the VP and HEMA segments as observed through IR measurements that the shift in peak position of the carbonyl peak of VP from 1680 to 1660 due to H-bonding. These H-bonding interactions between constituent chain segments are accounted for in the Kwei equation (Equation (4), Chapter 2) [24]. Best fits to the T_g data for the thermally-initiated gels were obtained when $\alpha = 1$ and $\beta = 50$, whilst for the UV-initiated gels the best fit is achieved when $\alpha = 14$ and $\beta = 30$ (see Figure 4.5 (a) (ii) and (iii)). The value of β corresponds to the strength of the H-bonding in the system and reflects the balance between self- and inter-segmental association for the H-bonding. The thermally polymerized gels have a larger value of β indicating stronger H-bonding interactions between the VP and HEMA segments in the system. Huang *et al.* also reported significantly higher T_g values than the mean of the pure components for low molecular weight PVP and PHEMA blends and diblock copolymers prepared by thermal polymerization and explained those higher values to be due to the H-bonding interactions between the hydroxyl-carbonyl groups [17]. However, in VP/HEMA gels the H-bonding

between VP and HEMA segments will be dissociated during swelling because the water molecules will form H-bonding with segments in the network chains. By comparison, a smaller value of β observed for the UV-initiated polymerized gels indicates there is less extensive H-bonding in these gels, which is associated with a more open network structure and therefore larger distances between VP and HEMA segments. Such a network structure might be caused by incomplete network formation associated with fast termination or the chain decomposition during the UV-initiated gelation process, and ultimately a larger numbers of chain ends in the gel. An additional influence on reducing the T_g is the higher content of HEMA moieties in the gel network obtained due to the fast polymerization induced by UV irradiation. For the gels with a feed composition of VP:HEMA 90:10 T_g is seen to decrease approximately linearly with I_{UV} (see Figure 4.5 (b)), but is independent of C_I (see Figure 4.5 (c)), and all the values are lower than the predicted values estimated from the Gordon-Taylor equation. The reduction in T_g with increasing I_{UV} is not associated with changes in composition since these gels all contain approximately the same values of VP:HEMA ratio. The effect is thought to be associated with changes in the network structure, namely, a larger numbers of chain ends obtained as I_{UV} increases, which therefore produce reduction in T_g .

All the gel specimens show similar TGA behavior with an approximate 10 % weight loss over the temperature range from approximately 50 °C to 130 °C, followed by an additional 80% weight loss between 390 and 450 °C as shown in Figure 37. PVP is known to be thermally stable and degrades in a single step at about 400 °C [25], which is clearly observed in the current gels. The low temperature weight loss at 50-130 °C can be attributed partially to loss of residual water and unreacted monomer. However, since the samples are carefully dried under vacuum some of this weight loss must be associated with degradation of the HEMA segments or possibly the VP fragments which are now directly bonded to HEMA segments and therefore are not as thermally stable as it would

be in a PVP homopolymer or network. With increasing HEMA content in the feed composition the amount of weight loss between 50-130 °C decreases (see Figure 4.6 (a)).

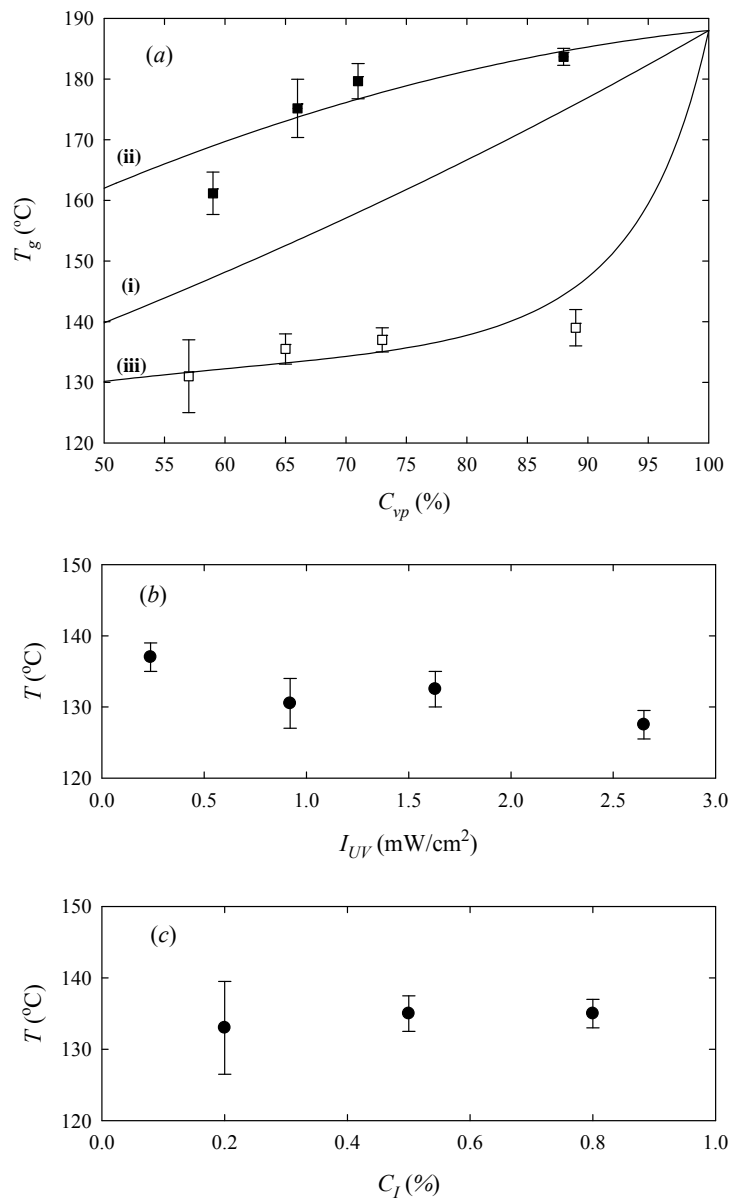


Figure 4.5. The effect of (a) VP content in the gels obtained by UV (□) and thermal (■) polymerization, (b) UV light intensity and (c) initiator concentration on the T_g of VP/HEMA gels. Predicted values for T_g are plotted in (a) using the Gordon-Taylor equation (i), as well as the Kwei equation, when (ii) $\alpha = 1$ and $\beta = 50$ and (iii) $\alpha = 14$ and $\beta = 30$.

In addition, the onset temperature of the second degradation step also decreases, which indicates a reduction in the thermal stability associated with the difference in HEMA composition in the gels. Neither UV light intensity (I_{UV}) nor initiator concentration (C_I) has any significant effect on the thermal stability of VP/HEMA gels, indicating that the thermal stability is dominated purely by the amount of HEMA in the system and its effect on the VP stability as shown in Figure 4.6 (b) and (c).

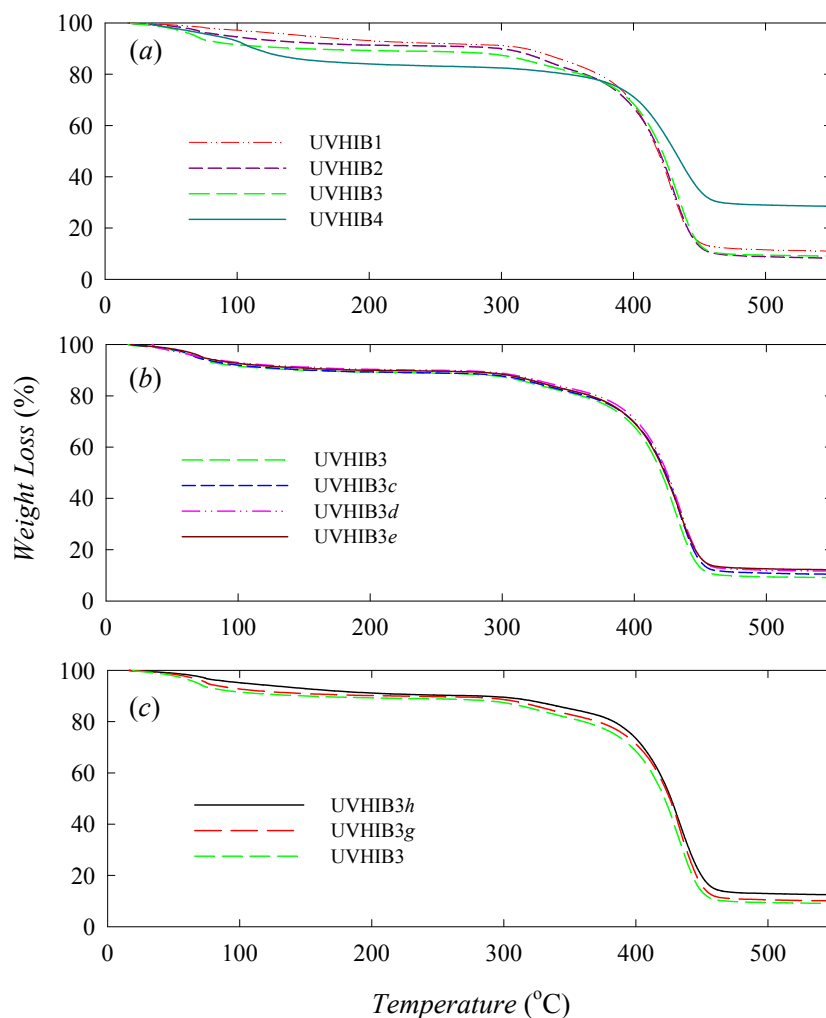


Figure 4.6. TGA diagrams of UVHIB gels synthesized with various (a) feed monomer ratios (b) UV irradiation intensities, and (c) initiator concentrations.

4.1.4. Color Changes in Gels

The yellowish color found in all UVHIB gels synthesized the UV-initiated curing was observed. Discoloration from colorless to yellowish color was occurred during the curing. This yellowish color was disappeared again after 48 hours. It has been reported that the photoyellowing emergence is due to the tendency of photoinitiators to photoyellow the materials or acrylate-related color change [26]. In this study we have used the Irgacure 651 (benzyl dimethyl ketal) as a photoinitiator and this has been reported to have a quite high tendency to photoyellow due to the side reaction such as recombination of two radical components with aromatic group which is formed by the decomposition of photoinitiator under UV. Although the acrylate-based material will show the yellowish phenomenon, it seems that the HEMA is not the one causing the yellow color because it has been reported that mostly aromatic based acrylate will induce the discoloration due to the production of quinone type structure (quinoid). Decker and coworkers has presented that aromatic polyurethane acrylate has much higher yellow index than aliphatic polyurethane acrylate gel [27]. Consequently, it could be thought that the cause of the discoloration of gel is due to the quinoid obtained from the Irgacure 651 during UV radiation process. In addition, the disappearance of the yellow color of gel after some time was also similar result to the study on the photobleaching the yellow color in the presence of O₂. [28]

4.1.5. Swelling Kinetics of Gels

All the UV polymerized VP/HEMA gels studied show similar swelling behavior with an initial rapid swelling phase at short times (0-70 minutes) before the penetrant uptake slows at intermediate times (70-300 minutes) and eventually the hydrogels become fully swollen and an asymptotic (equilibrium) swelling ratio (q_e) is reached in

about 300-400 minutes (t_{\max}). A representative set of swelling curves with time are shown in Figure 4.7 for 90:10 VP/HEMA gels polymerized with various UV intensities

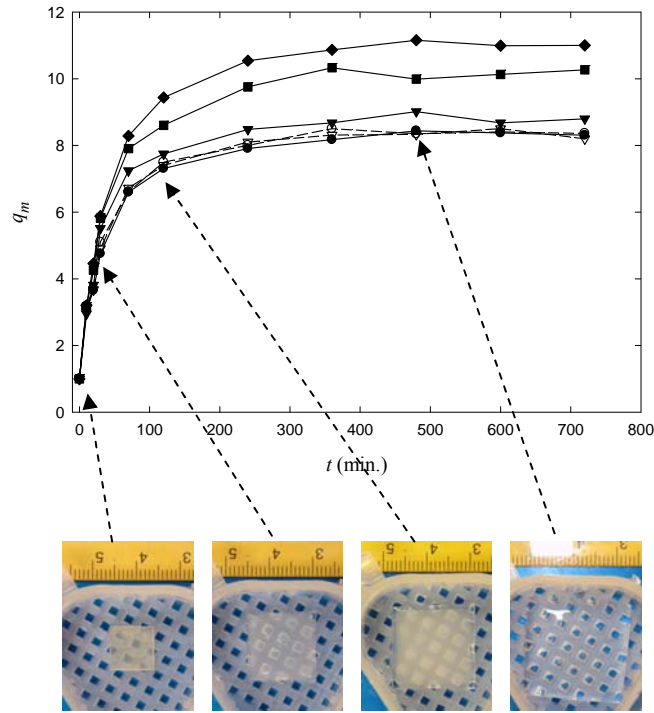


Figure 4.7. Swelling behavior of various UVHIB3 gels polymerized using different photomasks (UV intensities); (∇) mask1, (\circ) mask2, (\bullet) mask3, (\blacktriangledown) mask4, (\blacksquare) mask5 and (\blacklozenge) mask6 (Each q_m point is the averaged one of three measured values). Pictures are VH 3 hydrogels taken at 0, 40, 120 and 480 min during the swelling measurement.

Although the gels were initially transparent, they become slightly opaque during the preliminary swelling phase, caused by the development of micro-heterogeneities in the hydrogel [29]. However, as the hydrogels approach equilibrium swelling they return to full transparency, once the micro-heterogeneities have been eliminated. The same changes in transparency are observed for all gel compositions and agree with studies with Brazel and Peppas [30]. Extensive studies on spatial inhomogeneity in hydrogels (mostly

charged hydrogels) [31-33] have been reported using scattering techniques such as dynamic light scattering (DLS), small-angle x-ray scattering (SAXS) or small angle neutron scattering (SANS). Shibayama represented large concentration inhomogeneity appears only at equilibrium swollen state of hydrogels due to the frozen topological structure in the gels [31]. Although the VP/HEMA gels obtained by UV irradiation in this work were all transparent in the fully swollen state, the hydrogels also showed a transient opaque state during the swelling. This mechanism for this opacity is unknown at the moment but could be investigated using scattering methods in future work.

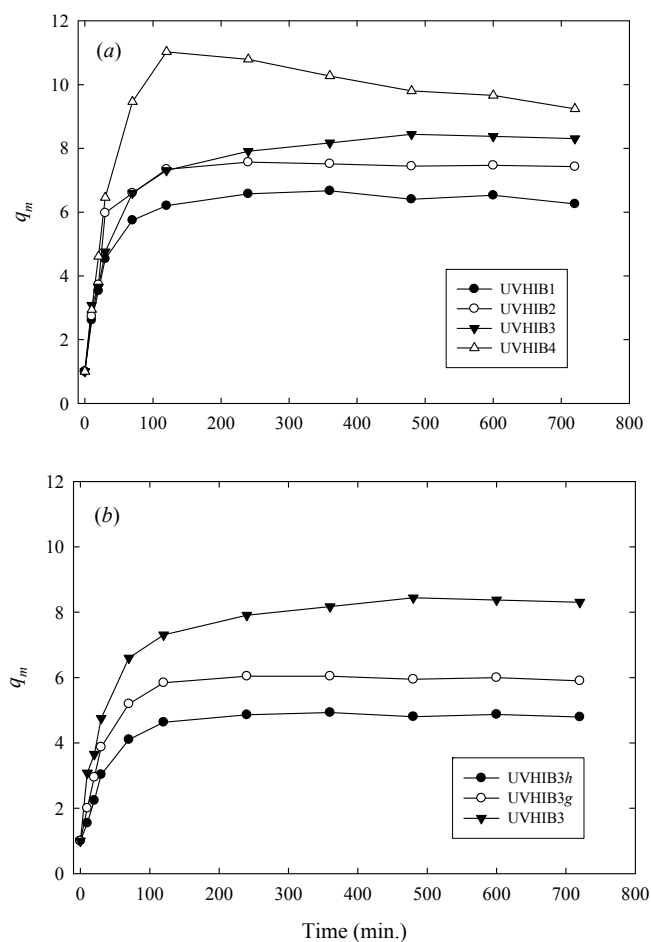


Figure 4.8. Swelling behavior of various (a) UVHIB gels polymerized with different feed monomer ratios and (b) UVHIB3 gels synthesized with different C_{FS} (Each q_m point is the averaged one of three measured values).

Similar swelling behavior is also observed for gels with varying feed monomer ratio and concentrations of initiator and crosslinker. The only exception to this behavior is observed for UVHIB4 hydrogels which initially swell for approximately the first 120 minutes giving a maximum value of $q_m = 11$, and then subsequently q_m decreases and finally asymptotes to give a value of $q_m = 9$ as shown in Figure 4.8 (a). This behavior is most probably associated with loss of mechanical integrity as seen by the significant reduction in modulus for the fully swollen UVHIB4 hydrogel ($G = 3.5 \pm 0.5$ kPa, see Figure 4.10). This reduction in modulus readily is most probably due to a partial disintegration of the hydrogel in its highly swollen state caused by the prolonged immersion in saline solution enabling the weakly cross-linked material. This could be exacerbated by increased stress within the hydrogel caused by rapid uptake of the penetrant without sufficient time for the polymer chains to relax, leading to crack formation and crazing [30]. It is thought that among the VP/HEMA gels synthesized with different compositions, the 90:10 VP:HEMA feed composition hydrogel has the best overall properties for use as a tissue expander, since it develops a large swelling ratio yet maintains sufficient mechanical integrity. Accordingly, this composition was used for studying the effect of initiator concentration, crosslinker concentration and type and UV intensity on the characteristics of the gel and hydrogels. Figures 4.8 (b) shows that with decreasing initiator concentration (C_I) for synthesizing gels, swelling rate was slightly slower and equilibrium swelling ratio was also smaller.

The swelling rate of the VP/HEMA gel system was expressed by the diffusion coefficient (D) of the penetrant (saline) in this work. The D and diffusion exponent n for each VP/HEMA gel was calculated from the initial linear portion of the swelling curves, taken only from the initial 60% increase in mass swelling ratio. As shown in Figure 4.9 (a), the value of D increases as C_{VP} increases. This behavior is expected since when the fraction of more hydrophilic material increases the passage of saline through the gel is increasingly promoted and consequently diffusion increases.

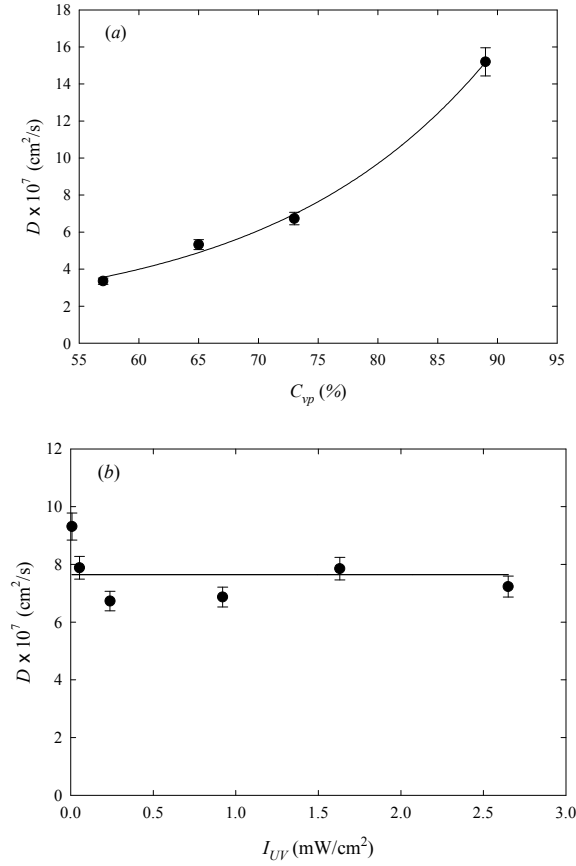


Figure 4.9. Effect of (a) VP content in VP/HEMA gel and (b) UV intensity on penetrant diffusion coefficient (D).

For the 90:10 VP:HEMA feed monomer ratio hydrogels prepared with different initiator concentrations (C_I), there is a marginal increase in D with increasing C_I , from $(6.06 \pm 0.31) \times 10^{-7}$ cm²/s at $C_I = 0.2$ wt% to $(6.73 \pm 0.34) \times 10^{-7}$ cm²/s at $C_I = 0.8$ wt%, which is probably due to an increase in M_c . However, due to the extremely small fraction of Irgacure 651 initiator incorporated into the network the increase in D observed is small compared to experimental error and further investigations are therefore required to evaluate this behavior further. With increasing cross-linker concentration (C_C), the D value decreases as expected, since the higher C_C will increase effective cross-linking density (ν_e) in the gels which will prohibit solvent from penetrating through the gel network. For the 90:10 VP:HEMA feed composition gels, the value of D appears to be

essentially independent of I_{UV} as shown in Figure 4.9 (b) . However, as discussed below increasing I_{UV} has limited effect on the value of v_e . Although the variation in D with increasing I_{UV} is rather weak, an effect is observed in the internal structure of gels, and in particular the number of chain ends in the system.

Determination of the exponent n allows the type of penetrant transport mechanism in the gel systems to be evaluated. As a function of C_{VP} the values of n are all essentially larger than 0.5 indicating that the saline solution diffusion mechanism is anomalous [53] *i.e.* non-Fickian or (Case III diffusion). This is associated with a comparable relaxation rate of polymer chains in the hydrogel compared to the diffusion velocity of the water which is coupled with the higher hydrophilicity of VP component [2]. The value of n equal to 0.76 ± 0.08 is a maximum for a C_{VP} of 99 wt% and decreases to a minimum of 0.54 ± 0.06 when $C_{VP} = 70$ wt%, indicating a change of mechanism from being anomalous (non-Fickian) to Fickian ($n=0.5$ [34]) with increasing HEMA content. These results are consistent with observation of Fickian diffusion mechanisms reported for HEMA based copolymeric hydrogels [29, 35, 36], and non-Fickian diffusion observed for VP based copolymeric hydrogels [37]. Given that the diffusion mechanism is dominated by the VP to HEMA ratio it is not surprising that the value of n for the 90:10 VP:HEMA gels was found to be independent of I_{UV} with a mean value of 0.59 ± 0.06 .

4.1.6. Characteristics of VH/HEMA hydrogels

4.1.6.1. Effect of Feed Ratio of VP and HEMA

As discussed above, the network structure can be elucidated through measurements of q_{ve} (or q_{me}) and G , from which the values of the effective cross-link density (v_e) and average molecular weight between cross-links (M_c) can be determined. The value of q_{ve} for the various gels was seen to increase with increasing C_{VP} (see Figure

4.10 (a)). This behavior is mainly due to the increase in the water mass uptake caused by the increase of the highly hydrophilic VP moieties present in the gel. With a larger water uptake the increase in q_{ve} is accompanied by a corresponding decrease in modulus, simply due to the increased volume of water uptake within the polymer network (Figure 4.10 (a)). As shown in Figure 4.10 (b), the calculated values of ν_e and M_c respectively decrease and increase, with increasing C_{VP} content.

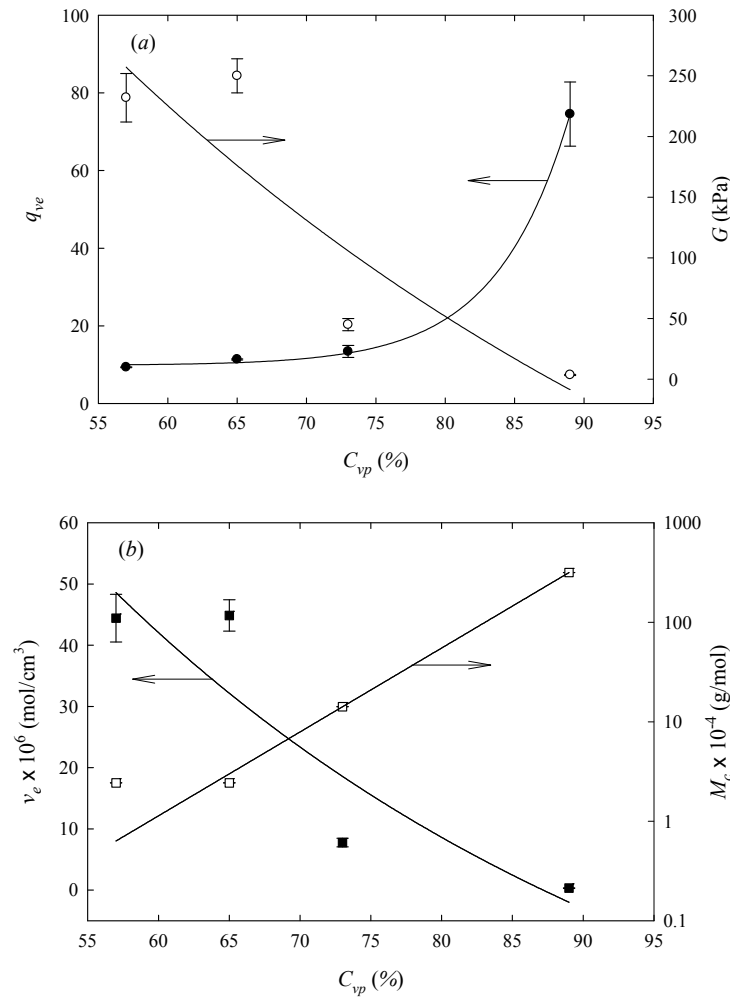


Figure 4.10. Effect of VP content (C_{VP}) in VP/HEMA gels on (a) measured equilibrium volume swelling ratio (q_{ve}) and compression modulus (G) and (b) calculated effective cross-link density (ν_e) and average molecular weight between cross-links (M_c).

4.1.6.2. Effect of Initiator Concentration (C_I)

For a fixed VP feed composition of 90:10 VP:HEMA, the gels synthesized using varying initiator concentrations show an increasing q_{ve} and a decreasing G with increasing C_I as shown in Figure 4.12. This behavior is anomalous and is the exact opposite behavior to that expected when compared to many thermally-initiated free-radical polymerized gels [38, 39] for which most studies on the effect of initiator on the swelling of hydrogel have been performed. In thermally induced free-radical polymerized gels, a higher concentration of initiator would be expected to produce increased numbers of propagating sites leading to shorter chain lengths, as well as increased cross-links per unit volume. Consequently, with increasing initiator concentration a gel with higher values of effective cross-link density (*i.e.* low M_c values) and smaller values of swelling ratios would be expected. Clearly the mechanism of gel formation observed in the current UV-initiated gels differs from that induced by thermal-initiated free-radical polymerization. In all free-radical polymerizations, the propagation rate of radicals follows a first order kinetics with respect to their concentration, whilst their termination rate follows second order kinetics. Consequently, an increase of initiator concentration will induce faster radical termination rates [40]. Compared to thermally initiated polymerization, it is known that UV initiated reactions have faster overall reaction rates, resulting in an increase in the termination rates [16]. Consequently, with increasing free-radicals associated with increased UV initiator the possibility exists for more radicals being able to induce a greater number of premature chain termination steps in the network resulting in a number of uncross-linked chains. Some of these will not be covalently bonded into the network and are subsequently washed out, but a number are partially incorporated at only one end and are therefore form dangling chains. These results are consistent with the reduced T_g values which indicate an increased excluded volume in these systems [41].

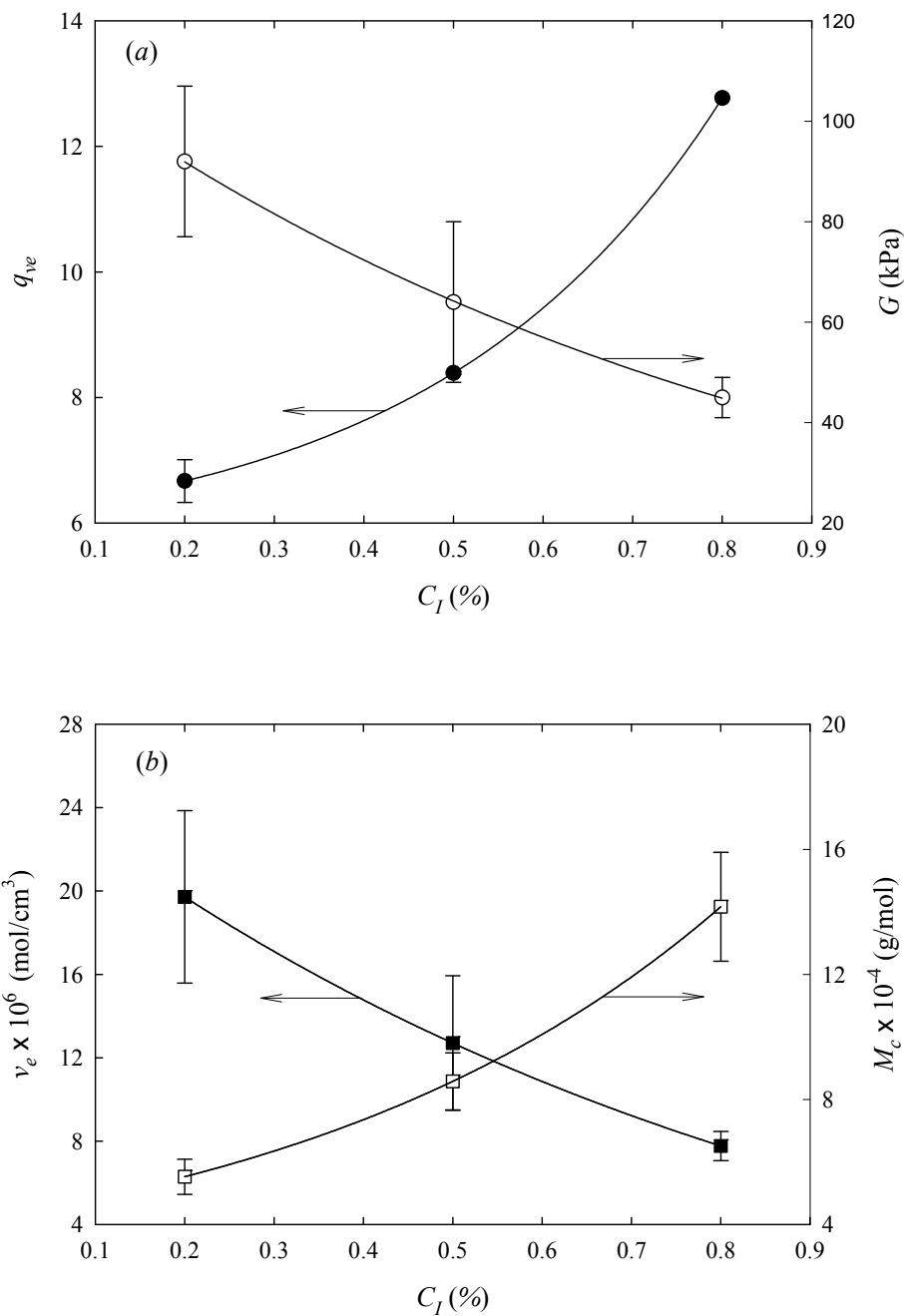


Figure 4.11. Effect of initiator concentration (C_I) on (a) measured equilibrium volume swelling ratio (q_{ve}) and compression modulus (G) and (b) calculated effective cross-link density (v_e) and average molecular weight between cross-links (M_c) of VP/HEMA hydrogels.

4.1.6.3. Effect of UV Irradiation Intensity (I_{UV})

The effect of UV intensity during polymerization on the characteristic parameters of the hydrogels is shown in Figure 4.12. Contrary to expectations, the values of the equilibrium volume swelling ratio (q_{ve}) of the hydrogels are seen to increase and the modulus (G) decreases with increasing I_{UV} . This result is similar to the behavior observed for both electron induced gelation [42, 43] and also UV-initiated solution polymerization of PHEMA gels [16]. It is however, the exact opposite expansion behavior to that observed for hydrogels synthesized by gamma-radiation [2, 19] where an increase of γ -radiation produced higher cross-linking densities and consequently lower values of q_{ve} of the swollen gels. Wong *et al.* [44] have also showed that increased exposure to higher UV intensities produces polyacrylamide hydrogels with higher moduli which would result in a reduction of the observed swelling ratio. The q_{ve} and G dependence on I_{UV} for the UV-initiated PHEMA gels synthesized by Li *et al.* using solution polymerization is associated with gels containing increased polymer cyclization in the resulting gels as a result of the presence of the water and high light intensities in the reaction [16]. In the current bulk polymerized gels, it is believed that the observed q_{ve} and G dependence on I_{UV} results from a completely different mechanism compared to that of solution polymerized gels. This behavior is associated with the oxidative decomposition of the gel which could occur during UV-irradiation due to increased UV intensity or exposure time used in the current polymerization. This would lead to an increasing number of dangling chains and increases in M_c with increasing exposure time. Alternatively high rates of gelation could also cause higher numbers of dangling chain ends in the gel network structure, similar to the results observed for higher initiator concentrations. During UV-initiated polymerization the UV intensity has been shown to affect the polymerization rate as a function of the time during gelation [16]. In this case, for higher UV intensities higher reaction rates occur at the beginning of the

polymerization reaction so that 80% conversion occurs after the first few minutes, before reaction rates decrease with increasing time of reaction.

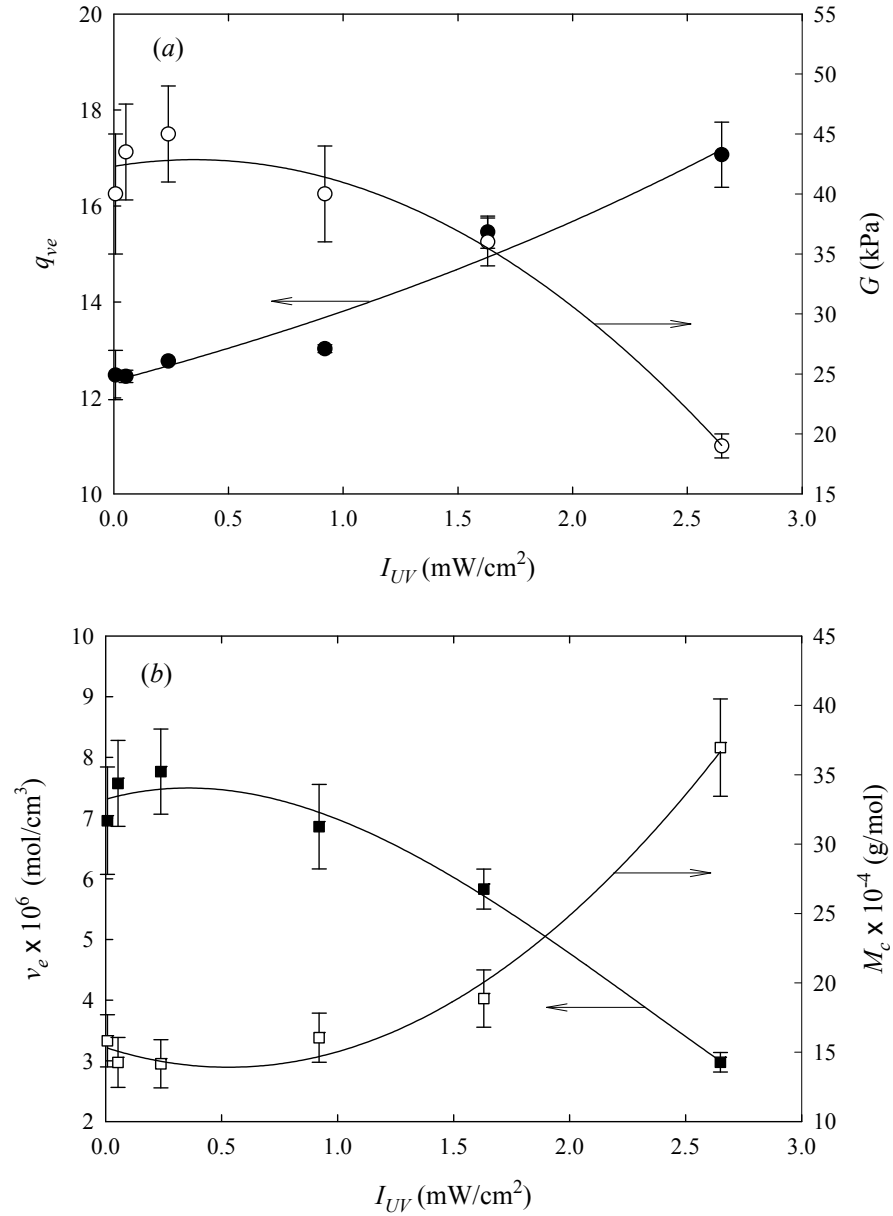


Figure 4.12. Effect of UV intensity (I_{UV}) on (a) measured equilibrium volume swelling ratio (q_{ve}) and compression modulus (G) and (b) calculated effective cross-link density (ν_e) and average molecular weight between cross-links (M_c) of VP/HEMA hydrogels.

4.1.6.4. Molecular Network Structure of UVHIB Hydrogels

Whether chain scission or premature termination of the growing chains occurs at higher UV intensity, the end result is a network structure with increasing numbers of dangling chain ends and larger M_c (or lower ν_e), which show unexpectedly high values of swelling ratio (q_{ve}) and smaller values of G . Possible schematic structures of the hydrogels under different I_{UV} and C_I conditions are shown in Figure 4.13. The proposed structure also accounts for the observed anomalous behavior of increasing q_{ve} with increasing C_I . In this case increased dangling ends could result with increasing C_I due to the possibility of rapid chain termination occurring during polymerization, meaning only one end of the chain to be incorporated into the 3D network of the gel.

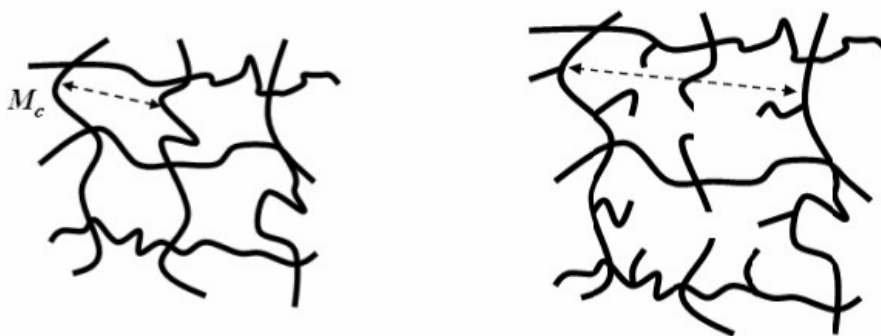


Figure 4.13. Schematic network structure at fully swollen state of hydrogels prepared at (a) lower and (b) higher UV intensity/initiator concentration. The average molecular weight between two cross-links making a complete mesh (M_c) increases (as shown by the arrows) with increasing UV intensity/initiator concentration.

4.1.6.5. Effect of Crosslinker Concentration (C_C) and Type

It was found that the characteristics of VP/HEMA gels were affected by not only the crosslinker concentration (C_C) but also crosslinker types. Besides N, N-methylene bisacrylamide (BIS), 1,1,2,2-tetraallyloxyethane (GLY) and diethylene glycol diacrylate (DEGDA) were also used for studying the effect of functionality and the length of crosslinker molecule, respectively, on the swelling of the gels synthesized with three different crosslinkers possessing various C_C .

Figures 4.14 (a) and (b) shows the equilibrium volume swelling ratio (q_{ve}) and modulus (G), respectively, of the UV-polymerized VP/HEMA gels synthesized at different crosslinker concentrations for BIS, DEGDA and GLY crosslinkers. Regardless of crosslinker type, the gels crosslinked with the higher C_C produced lower q_{ve} and higher G as expected. It is probably because the higher C_C induces higher degree of crosslinking directly affecting swelling ratio. As shown in Figure 4.14, the UVHIG3 gels synthesized with GLY produced the highest q_{ve} (lowest G) values and UVHIB3*i*-UVHIB3*l* gels obtained with BIS produced the lowest q_{ve} (highest G) values among all gels when the same C_C was used. The UVHIG3 gels consequently have the lowest v_e (highest M_c) and the UVHIB3*i*-UVHIB3*l* gels the highest v_e (lowest M_c) values among the gels, as shown in Figures 4.15 (a) and (b). These results also confirmed that the gels synthesized with decreasing C_C produce the gels with higher q_{ve} and smaller G due to the effect of decreasing crosslink density (increasing in the M_c values) in gels. It was found that the empirical relationship between q_{ve} and C_C is as follows and fits the q_{ve} values in Figure 4.15 (a).

$$q_{ve} = a_1 + \frac{a_2}{C_C} + \frac{a_3}{C_C^2} \quad (40)$$

The coefficients a_1 , a_2 , and a_3 were specific for each given crosslinker. The values of the coefficients determined for BIS, DEGDA and GLY are listed in the Table 4.2.

The BIS crosslinker is tetrafunctional, which means that it has capability to crosslinks to 4 molecules, and GLY has octafunctionality. Contrary to expectations, it was observed in the current work that the increment in the crosslinker functionality did not increase ν_e thereby decrease equilibrium swelling ratio (q_e) but rather increased q_e and decreased ν_e . The reason is thought to involve both the steric hindrance effect of GLY compared to BIS as well as the reduced compatibility between the monomers and GLY, which induces lower ν_e . Both these factors could lower the efficiency of crosslinking in the gel network. These results agreed well with those of the study by Xue and coworkers [46] that thermally polymerized N-isopropylacrylamide (NIPA)/acrylic acid (AA) copolymeric hydrogels crosslinked GLY and BIS were prepared and compared the resulting lower critical swelling temperature (T_c) and equilibrium swelling ratio (q_e). The NIPA/AA gels crosslinked with GLY possessed the higher q_e and lower T_c although no effect of C_C of GLY on the T_c was observed unlike the gels with BIS. Huglin and coworkers [47] also studied thermally polymerized hydrogels of NIPA and AA, with methacrylic acid (MMA) or 2-methyl-2-acrylamido-propanesulfonic acid (AMPS) as a comonomer prepared with various concentrations of BIS and reported that higher concentration of BIS produced the gels showing smaller q_e and no effect of C_C of BIS on the T_c . The VP/HEMA gel systems used in this thesis do not show any T_c , thus the effect of C_C and type of a crosslinker on the T_c of the gels has not been verified. Atta *et al.* [48] presented the effect of crosslinker functionality on characteristics of vinyl pyrrolidone (VP)/butyl acrylate (BA) hydrogels polymerized by ^{60}Co gamma irradiation. These results showed that the gels crosslinked with hexafunctional crosslinker trimethylolpropane trimethacrylate (TPT) yield higher q_e than the gels crosslinked with BIS. They explained that q_e values are inversely proportional to the reactivity of the crosslinker with monomers for hydrogel systems.

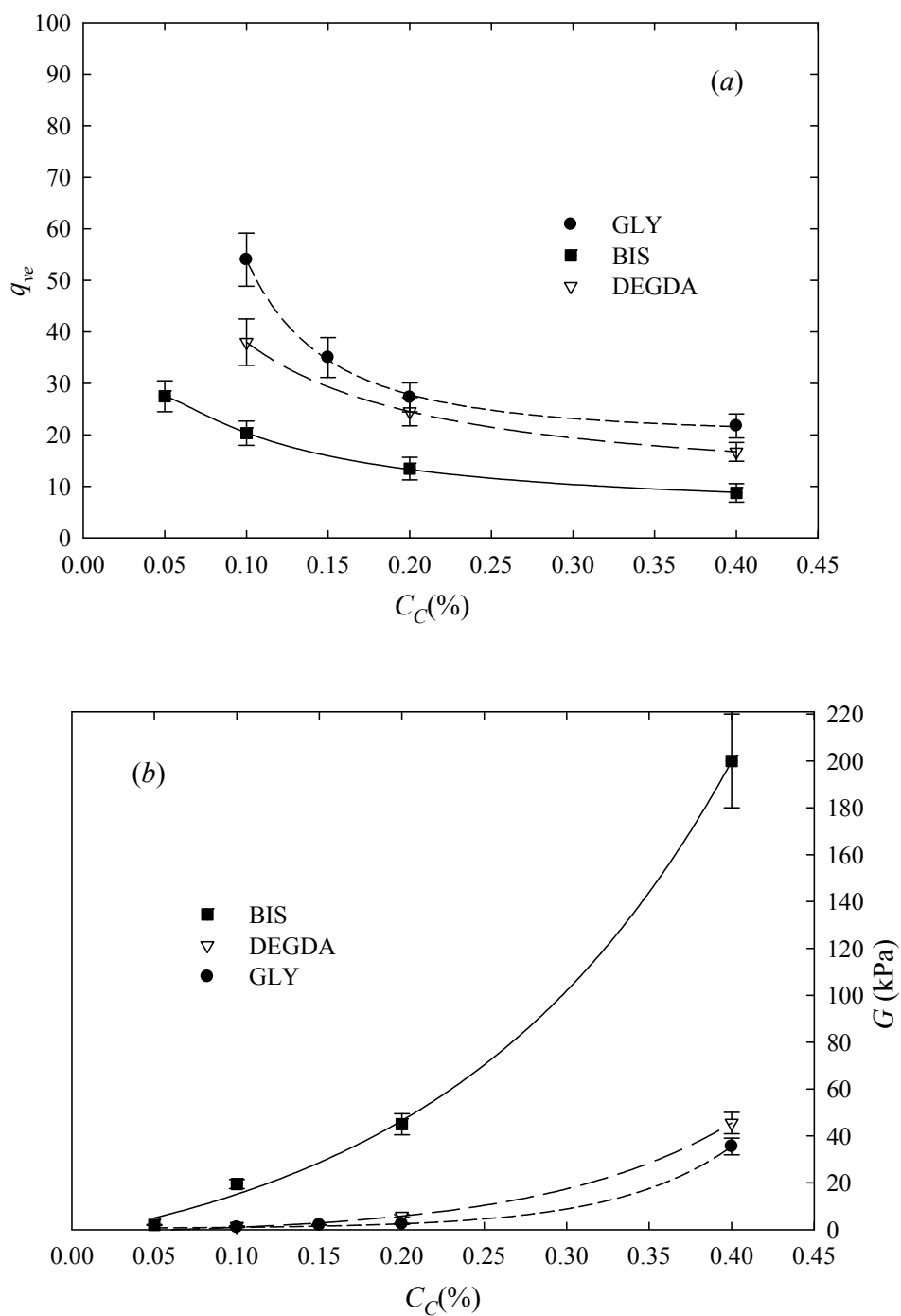


Figure 4.14. (a) q_{ve} and G of the UV-polymerized VP/HEMA gels synthesized with various crosslinkers (BIS, DEGDA and GLY) at different crosslinker concentrations.

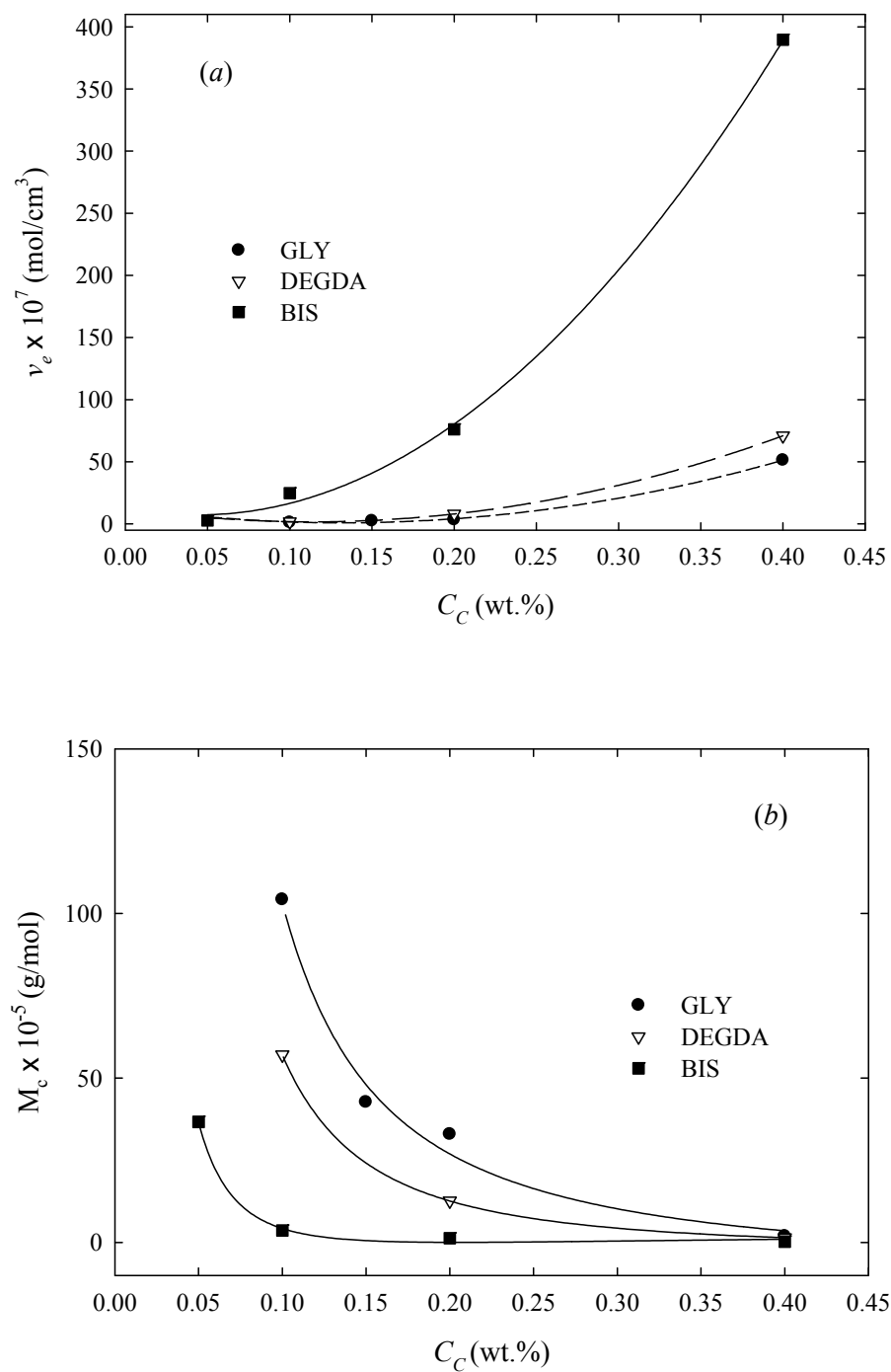


Figure 4.15. (a) v_e and M_c of the UV-polymerized VP/HEMA gels synthesized with various crosslinkers (BIS, DEGDA and GLY) at different crosslinker concentrations.

Table 4.2. The fitting coefficients a_1 , a_2 , and a_3 for BIS, DEGDA and GLY

Coefficient Crosslinker Type	a_1	a_2	a_3	r^2
BIS	3.77 ± 0.33	2.14 ± 0.07	-0.05 ± 0.00	0.999
DEGDA	8.20 ± 0.00	3.54 ± 0.00	-0.06 ± 0.00	1.000
GLY	20.0 ± 1.19	-0.28 ± 0.27	0.37 ± 0.01	0.999

Gels crosslinked with DEGDA possessing longer molecular structure produced higher q_e and lower v_e than those with BIS. This is either due to steric effect and the compatibility (or reactivity) of the crosslinker with the monomers. Kasgöz and coworkers [49] who reported that long and flexible polyethyleglycol (400) diacrylate (PEG(400)DA) crosslinker has been used for preparing acrylamide (AAm) and maleic acid (MA) copolymeric gels instead of BIS and the use of PEG(400)DA resulted in the higher q_e due to the long structure.

It was found that the initial swelling rate (R_s) values of all VP/HEMA gels seemed to be unaffected by the concentration and type of crosslinker and were all about 0.1 min^{-1} , meaning the increment of 0.1 mass swelling ratio per min. The diffusion coefficient (D) values were determined to be randomly in the range between $2.0 \times 10^{-7} \text{ cm}^2/\text{s}$ and $9.0 \times 10^{-7} \text{ cm}^2/\text{s}$ and independent of concentration and type of crosslinker and the values. It is thought that the lack of systemic variation results from the small amount

of crosslinker used for making gel diffusion behavior insensitive to crosslinker types and concentrations.

The χ values calculated for the VP/HEMA gels crosslinked with the three different crosslinkers BIS, DEGDMA and GLY are plotted as a function of crosslinker concentration and shown in Figure 4.16 (a). Due to the small weight percent of crosslinker was used for each gel system, the difference between the different systems for χ values is small, and all values are near 0.5 and efficiently independent of crosslinker concentration. But the values are influenced by crosslinker type. Overall the χ values obtained for the gels crosslinked with BIS are generally the highest (0.514 ± 0.005) and the gels with GLY the lowest (0.506 ± 0.008), with 0.508 ± 0.006 χ values for gels with DEGDMA. This behavior can be understood that GLY possessing smallest χ value contributes to make the gels relatively more miscible with swelling medium, while BIS possessing largest value contributes to make the gels less miscible with swelling medium. The deviation of χ for crosslinkers with different C_C is less than 1%, which indicates that the χ values are not affected by the crosslinker amount used for preparing gels.

Although theoretically χ value does not depend on the volume fraction (v_2) of polymer in solution system [50], it has been shown that χ values increased linearly with increasing v_2 for a number of systems as given by empirical relationship; $\chi = A_1 + A_2 v_2$, where A_1 and A_2 are specific coefficients for each given system [50-52]. For fully swollen hydrogel systems, the v_2 is equal to the inverse of equilibrium swelling ratio (q_{ve}) so the relationship between χ and q_{ve} can be expressed as follows; $\chi = B_1 + B_2/q_{ve}$, where B_1 and B_2 are specific coefficients for each given system. Using this relationship, the χ values for gel systems crosslinked with different crosslinkers are fitted as shown in Figure 4.16 (b). The χ values are attempted to be fitted by the relationship and the values of B_1 , B_2 and r^2 determined are listed in Table 4.3. The χ values obtained shows

approximately constant over the range of q_{ve} measured and does not well follow the relationship with q_{ve} ($r^2 \sim 0.2-0.32$).

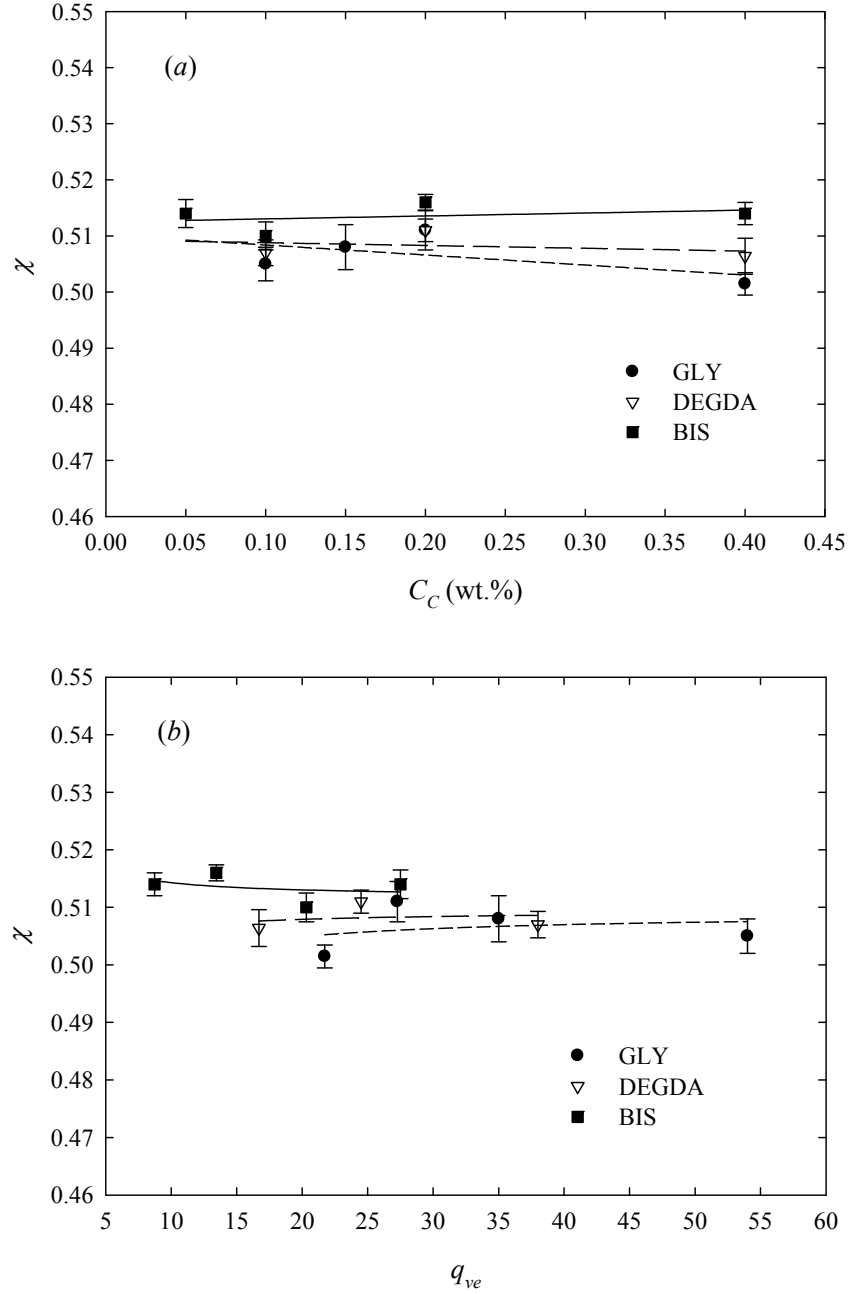


Figure 4.16. The χ of the UV-polymerized VP/HEMA gels synthesized as a function of (a) C_C and (b) q_{ve} for three different crosslinkers (BIS, DEGDA and GLY).

Table 4.3. The fitting coefficients, B_1 and B_2 for BIS, DEGDA and GLY

Crosslinker Type	Coefficient			
		B_1	B_2	r^2
BIS		0.51 ± 0.00	0.03 ± 0.05	0.32
DEGDA		0.51 ± 0.01	-0.08 ± 0.24	0.24
GLY		0.51 ± 0.01	-0.03 ± 0.25	0.20

The compatibility among the components for the hydrogel systems (two monomers (VP and HEMA), crosslinker, and water) was analyzed by Hansen solubility parameters [53, 54] and correlated with the equilibrium swelling ratio (q_{ve}) of VP/HEMA hydrogels. This is based on the assumption that the molecules bonded by similar type of forces are more compatible with each other. In other words molecules with similar Hansen solubility parameters are expected to be more compatible.

Cohesive energy (E_{coh} , J/mol) of many liquids or amorphous polymers have 3 contributions to the total energy: 1) dispersive energy (E_d , non-polar bonds), 2) polar energy (E_p , permanent dipole-permanent dipole bonds), and 3) hydrogen bonding energy (E_h , hydrogen bonds). The total solubility parameter (δ_t , $J^{1/2}/cm^{3/2}$) can be described using three Hansen solubility parameters as follows; $\delta_t^2 = \delta_d^2 + \delta_p^2 + \delta_H^2$ where δ_d is the solubility parameter for dispersion forces, δ_p is the solubility parameter for polar forces, δ_h is the solubility parameter for hydrogen bonding forces. The Hansen solubility parameters for VP, HEMA, BIS, GLY, DEGDA, and water were predicted by the group contributions using the following equations (method of Hoftyzer and Krevelen) and determined values are listed in Table 4.4.

$$\delta_d = \frac{\sum F_{di}}{V}, \delta_p = \frac{\sqrt{\sum F_{pi}^2}}{V}, \text{ and } \delta_h = \sqrt{\frac{\sum E_{hi}}{V}} \quad (41)$$

where F ($=\sqrt{E_{coh} \cdot V}$, $\text{J}^{1/2} \cdot \text{cm}^{3/2}/\text{mol}$) is the molar attraction constant, F_{di} is the molar attraction constant for dispersion forces per structural group, F_{pi} the molar attraction constant for polar forces per structural group, and V is the molar volume (cm^3/mol).

Table 4.4. Hansen solubility parameters for VP, HEMA, BIS, GLY, DEGDA, and water

Components	δ_t ($\text{J}^{1/2}/\text{cm}^{3/2}$)	δ_d ($\text{J}^{1/2}/\text{cm}^{3/2}$)	δ_p ($\text{J}^{1/2}/\text{cm}^{3/2}$)	δ_h ($\text{J}^{1/2}/\text{cm}^{3/2}$)
VP	28.3	22.4	14.4	9.53
HEMA	23.6	18.8	4.62	13.6
BIS	23.9	19.9	9.47	9.25
DEGDA	20.8	17.6	9.19	8.51
GLY	19.9	18.1	3.59	7.34
Water	46.2	19.5	25	33.5

The Hansen solubility parameters determined for VP are very similar to the values published in the literature [55], indicating the validity of this procedure of predicting these parameters. Since the feed monomer ratio of gel system used in this study was 90:10 VP:HEMA, it is thought that the interaction or bond between a crosslinker and VP predominates. As like a smaller difference between δ_t values of the crosslinker and monomer ($|\delta_t^{VP} - \delta_t^{CX}| \sim \text{small}$) for more miscibility between crosslinker and monomer a smaller difference between each Hansen solubility parameter component of the crosslinker and VP ($|\delta_d^{VP} - \delta_d^{CX}|$, $|\delta_p^{VP} - \delta_p^{CX}|$, and $|\delta_h^{VP} - \delta_h^{CX}| \sim \text{small}$) is expected for the case more miscible between crosslinker and VP. The differences between the Hansen

solubility parameter components of VP and crosslinkers are listed in Table 4.5. It is thought that when HEMA content increases, the difference between each Hansen solubility parameter component of the crosslinker and HEMA needs to be considered. As seen in the table 4.5, the differences between each δ component values of VP and BIS are the smallest, which correlates with smallest q_{ve} values of the VP/HEMA gels crosslinked with BIS over crosslinker concentration among the gels with GLY and DEGDA associated with a higher degree of crosslinking in the network caused by better compatible with BIS. Compared DEGDA with GLY, $|\delta_d^{VP} - \delta_d^{CX}|$ is slightly higher for the use of DEGDA which is unexpected. However $|\delta_p^{VP} - \delta_p^{CX}|$ and $|\delta_h^{VP} - \delta_h^{CX}|$ values are almost two times smaller for DEGDA. This agrees well with the higher q_{ve} of the VP/HEMA gels crosslinked with DEGDA than that with GLY. Using these approximations it becomes clear why the VP/HEMA gels crosslinked GLY have lower crosslinking density and smaller equilibrium swelling ratio despite the higher functionality of GLY.

Table 4.5. Difference between each Hansen solubility parameters of VP and crosslinker

System	$ \delta_t^{VP} - \delta_t^{CX} $ (J ^{1/2} /cm ^{3/2})	$ \delta_d^{VP} - \delta_d^{CX} $ (J ^{1/2} /cm ^{3/2})	$ \delta_p^{VP} - \delta_p^{CX} $ (J ^{1/2} /cm ^{3/2})	$ \delta_h^{VP} - \delta_h^{CX} $ (J ^{1/2} /cm ^{3/2})
VP-BIS	4.40	2.50	4.93	0.28
VP-DEGDA	7.50	4.80	5.21	1.02
VP-GLY	8.40	4.30	10.8	2.19

Clearly the difference between each Hansen solubility parameter components for the crosslinker and monomers used for the gel synthesis can qualitatively indicate relative degrees of crosslinking and hence swelling ratio of the various gel systems.

4.2. Thermal Polymerized VP/HEMA Gels

4.2.1. The Gelation and Composition of Gel

Figure 4.17 shows the FTIR Spectra of the VP/HEMA copolymeric gels thermally synthesized with various feed monomer ratios. The peaks observed at 1660 cm^{-1} and 1730 cm^{-1} are C=O stretching absorption peaks of the VP and HEMA components, respectively, as described in section 4.1.1. As HEMA content in the gels increases, the area of the C=O peak at 1730 cm^{-1} decreases. The quantitative determination of monomer unit compositions in xerogels was carried out by deconvoluting two peaks. From the ratio of the areas of the two characteristic peaks, the ratio of VP and HEMA units in the xerogels was obtained for the gels prepared with various feed monomer ratios. The compositions of VP and HEMA in the gels determined from this analysis are given in Table 4.6.

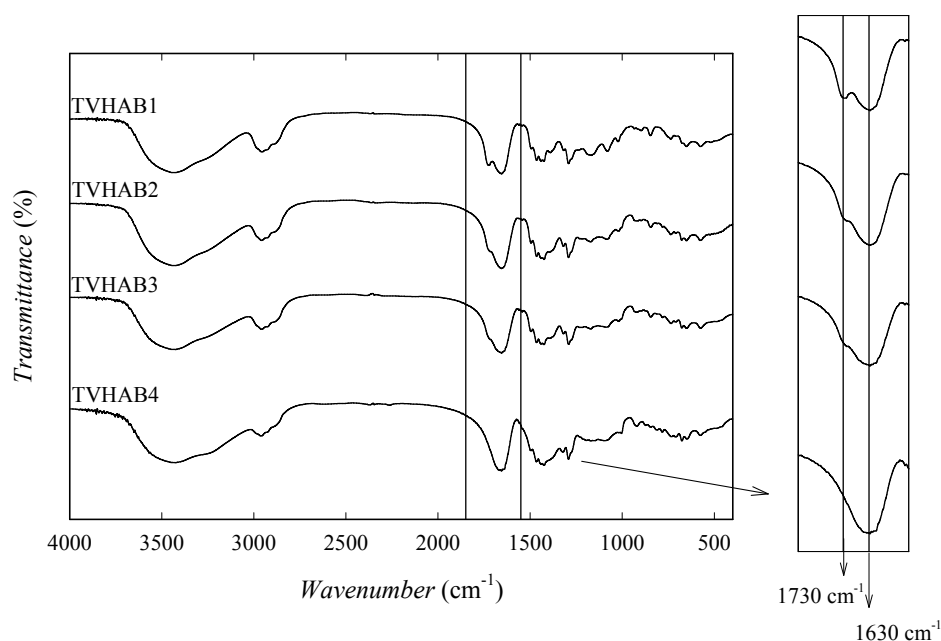


Figure 4.17. The IR spectra of VP:HEMA xerogels thermally synthesized with various comonomer ratios (TVHAB1= 70:30, TVHAB2= 80:20, TVHAB3= 90:10, and TVHAB4= 99:01 of VP: HEMA).

Table 4.6. Characteristics of for VP/HEMA gels thermally synthesized

Gel code	VP:HEMA Feed Ratio	VP:HEMA Composition Ratios	Gel % (%)
TVHAB1	70:30	63.8 : 36.2	93.0 ± 3.9
TVHAB2	80:20	67.9 : 32.1	85.2 ± 4.2
TVHAB3	90:10	71.5 : 28.5	83.6 ± 4.6
TVHAB4	99:01	91.8 : 8.02	56.8 ± 6.1

Compared with the photo-polymerized VP/HEMA (UVHIB) gels, the thermally polymerized VP/HEMA (TVHAB) gels have higher gelation percent for gels prepared with equivalent feed monomer ratios. This is thought to be due to the longer reaction times and milder conditions used for the thermal polymerization. Polymerization kinetics is affected by polymerization types (thermal or photo-initiated reaction). As VP wt. % in the feed composition increased for TVHAB gels, the gelation percent decreased as observed for the UVHIB gels (see Table 4.1), although the decrease in the gelation percent of TVHAB gels (see Table 4.6) is more noticeable. The TVHAB4 gels containing the highest content of VP relatively more hydrophilic have the smallest gelation percent of all the gels studied. More hydrophilic moieties absorb solution more and produce higher swelling degree accompanied with poor mechanical integrity and broken debris. Consequently, the sol percent of TVHAB4 could be overestimated due to the broken hydrogel fragments. Similar results were also obtained in photo-polymerized gels with 99 wt. % VP as feed composition for the same reasons

4.2.2. Glass Transition Temperature, T_g

The effect of gel composition on the T_g of TVHAB gels was investigated and attempted to be fitted using the Flory-Fox, Gordon-Taylor, and Kwei equations (Equation (2), (3) and (4), respectively). The Kwei Equation well fitted the T_g data, indicating H-

bonding interactions between constituent chain segments. Comparison with the values of T_g for photo-polymerized gels is explained in section 4.1.3.

4.2.3. Morphology

The morphologies of equilibrium-swollen TVHAB hydrogels were investigated by low voltage electron microscopy (LVEM). Figure 4.18 shows the LVEM images of swollen hydrogels with 4 different compositions, taken in two different positions in the gel to demonstrate the spatial variation. Although it is shown that the TVHAB4 hydrogels containing the highest VP content show surface roughness and tortuosity compared to others, there is generally no clear structural difference between the other hydrogels and even position-dependent morphology is shown for hydrogels. This might be because of sample preparation. However, due to this lack of clear microstructural distinction and the absence of scattering data, the structural characteristics were based solely analyzed using the structural parameters (v_e and M_c) calculated from swelling and mechanical measurements, thermal data and FTIR spectra in the rest of work.

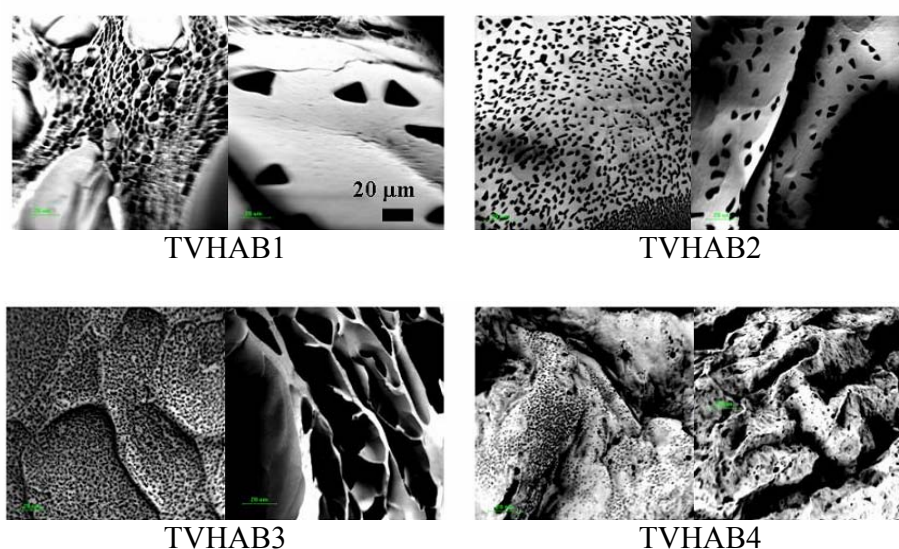


Figure 4.18. LVEM images of VP/HEMA copolymeric hydrogels with various compositions of monomer units (See Table 4).

4.2.4. Swelling Studies

The swelling behavior of VP/HEMA copolymeric gels thermally synthesized with various feed monomer ratios and the diffusion characteristics of swelling medium into the gels were characterized. The mass swelling ratio (q_m) of the TVHAB gels were observed as a function of time as shown in Figure 4.19. It is clearly seen that the equilibrium mass swelling ratio (q_{me}) of TVHAB4 was much higher than that of the other gels. The change in the diameter of a TVHAB3 hydrogel disk during the swelling was observed and taken as pictures at 0, 200, 400, and 600 minutes. The diameter of hydrogel disks increased with time as shown in the pictures

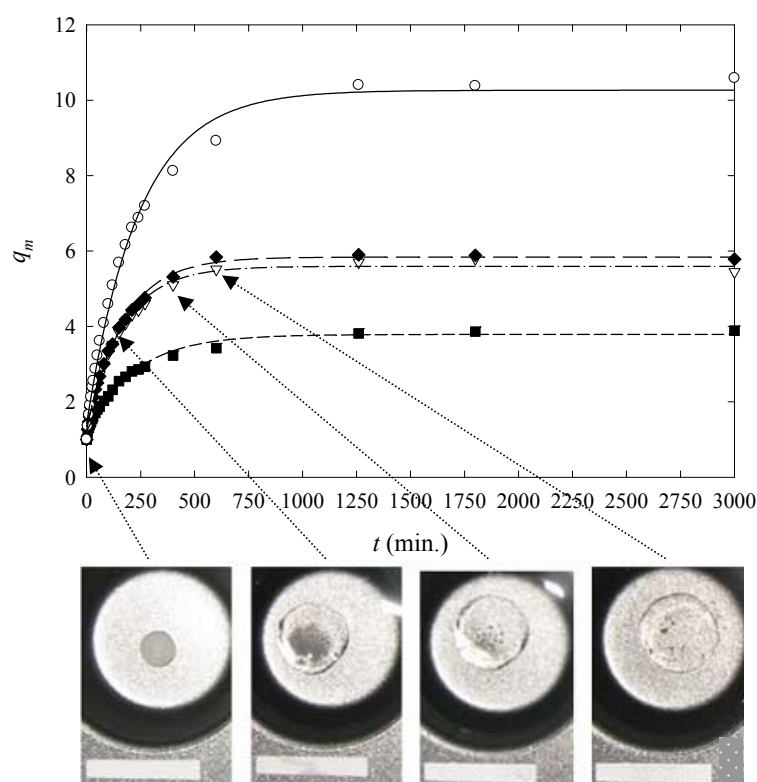


Figure 4.19. Swelling behavior of thermally polymerized VP/HEMA gels with various compositions; (■) TBHAB1, (▽)TBHAB2, (◆) TBHAB3, and (○) TBHAB4 gels (Each q_m point is the averaged one of three measured values). Pictures are TBHAB3 hydrogels taken at 0, 200, 400, and 600 min during the swelling measurement (The size of white bar: 2.54 cm).

It was found that the relationship between q_m of the gels obtained by both thermal and UV-initiated polymerization (see the section 4.1.5) and t in this study is as follows;

$$q_m = a_1 + a_2 \times (1 - \exp(a_3 \cdot t)) \quad (42)$$

The coefficients a_1 , a_2 , and a_3 in this empirical equation are specific for a given hydrogel system. Although for investigation of gel swelling with time, many researchers have used the Equations (27) and (28) from which D and diffusion mode of penetrant, the mass swelling ratio values with time well fitted with Equation (42) for all gel systems used in this work.

It has been widely reported that the swelling of hydrogels regardless of the gel synthesis method (thermal and UV-initiated polymerizations) is generally isotropic. In our study the initial swelling of the gels synthesized by thermal and UV-initiated polymerization showed anisotropy forming bell shape, which makes it difficult to directly quantify the swelling ratio purely from the observation of dimensional change of hydrogels. For this reason the swelling behavior of hydrogels was quantified by the mass swelling ratio (q_m) determined from the mass change of the hydrogels during swelling in this study. The equilibrium mass swelling ratios (q_{me}) were then converted into equilibrium volume swelling ratios (q_{ve}) using the equation, $q_v = 1 + \rho_p / \rho_{sol} (q_m - 1)$, where ρ_i are the densities of the gel ($i=p$) and solvent ($i=sol$), respectively, for analyzing the structural characteristics.

For TVHAB1, TVHAB2 and TVHAB3 gels, the swelling increases rapidly in the beginning at short times (0-100 minutes) and slows at intermediate times (100-600 minutes) reaching an equilibrium state around 600 minutes (t_{max}) as shown in Figure 4.19. By comparison, TVHAB4 gels initially swell faster in the first 300 minutes but only reach an equilibrium state about 1000 minutes (t_{max}). These t_{max} values (600 minutes or

1000 minutes) of TVHAB hydrogels are approximately twice as long as those observed for UVHIB hydrogels (300-400 minutes).

The initial swelling ratio (R_s) of TVHAB gels are in the range of 0.011 min^{-1} to 0.029 min^{-1} compared to the values in the range of 0.126 min^{-1} to 0.182 min^{-1} for UVHIB gels, which is shown in Figure 4.20. The UVHIB gels initially swell much faster (6~10 times) than TVHAB gels, which might be because the thickness of TVHAB gel specimens is 5 times larger than that of UVHAB gels.

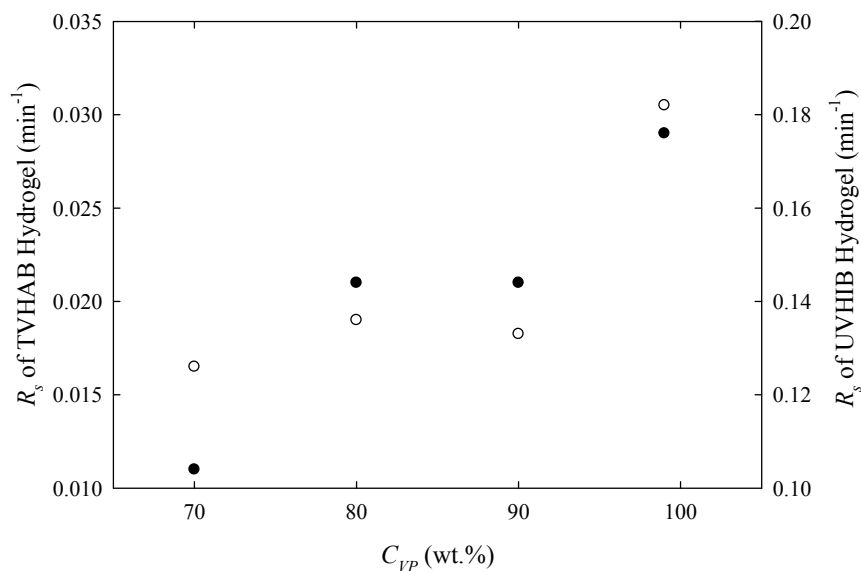


Figure 4.20. Initial Swelling rate (R_s) of thermally polymerized VP/HEMA (TVHAB) gels (●) and photo-polymerized VP/HEMA (UVHIB) gels (○) as a function of VP feed weight %.

Diffusion behavior of saline solution into TVHAB gels was also analyzed. Figure 4.21 shows the diffusion coefficient D increased from 4.36×10^{-7} to $13.7 \times 10^{-7} \text{ cm}^2/\text{s}$ with increasing C_{vp} . This increase is not only due to the VP content but also is understood to

be due to different internal structures forming during the swelling depending on their respective compositions.

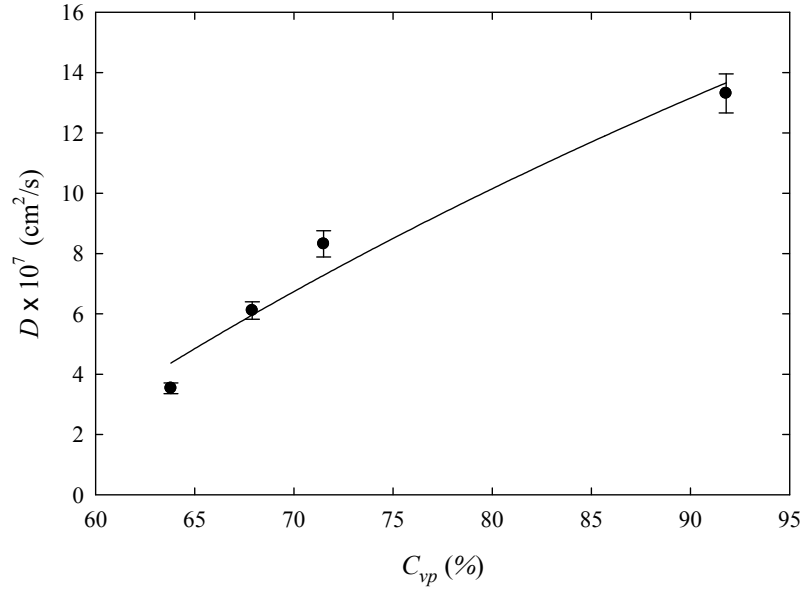


Figure 4.21. Penetrant diffusion coefficient (D) as a function of VP content in thermally synthesized VP/HEMA gels

The TVHAB4 gels was found to have the largest diffusion exponent (n) of 0.89 ± 0.06 . The minimum value of $n = 0.57 \pm 0.05$ was obtained for TVHAB1 gels. The values of n decreased with increasing HEMA content in gels as seen in the photo-polymerized gels. The values of n for all TVHAB hydrogels are between 0.5 and 1, which indicates non-Fickian diffusion (or Diffusion Case III) [34]. The reason of this non-Fickian diffusion is associated with the higher amount of VP as discussed in 4.1.5), which is in good agreement with the behavior of the hydrogels of VP and acrylamide [56].

From a practical point of view of developing a gel system for the use as tissue expanders, the initial swelling rate (R_s) expressed as a function of swelling ratio (q) and the time to reach maximum expansion of the system (t_{max}) are more convenient parameters to quantify the system.

4.3. Conclusions

A number of VP/HEMA gels were synthesized using UV-initiated free radical polymerization where UV irradiation intensity, feed ratio of two monomers, concentration of initiator, and concentration and type of crosslinker have been systematically varied. These gels were also compared to the VP/HEMA gels synthesized by thermal polymerization methods. It was shown that the feed composition (comonomer ratio, initiator concentration and cross-linker concentration and type) as well as the UV irradiation intensity have significant effects on the swelling behavior, elastic modulus, and gel network structure of the hydrogels.

The q_{ve} and D values of photo-polymerized VP/HEMA gels were a little higher than those of thermally polymerized gels that possessed the higher gelation percent and T_g . The crosslinking network structure for the photo-polymerized gels was found to have a lower crosslinking density and hence higher swelling ratio compared to thermally polymerized gels. However, it was found that increasing VP content of the VP/HEMA gels produced gels with higher q_{ve} and the diffusion mechanism changes from Fickian at low VP content to anomalous at high VP content regardless of the polymerization method.

For a fixed 90:10 VP:HEMA feed monomer ratio, the unexpected swelling characteristics of the UV-initiated polymerized gels obtained was observed with an increase in both initiator concentration (C_I) as well as UV intensity (I_{UV}) used for the photo-polymerization. Increase in both these parameters produces an increase in swelling ratio and consequently a decrease in the measured modulus, which indicates a decrease in effective crosslink density and an increase in molecular weight between crosslinks. This behavior is the opposite to that observed in thermally or γ -radiation initiated polymerizations of hydrogels where increases in either initiator concentrations or radiation intensities produce hydrogels with a decreasing swelling ratios and increasing moduli. These results were explained by proposing a model for the gel network with a

3D cross-linked network which also contains dangling chain ends. It is thought that these dangling chains either result from chain scission caused by high UV dosage or exposure time, or from chain termination without becoming cross-linked into a network due to high polymerization rates induced by UV irradiation or high initiator concentration. From our data it is not possible to evaluate which of these mechanisms is the most likely cause of the dangling ends. However, as a result a reduction of effective cross-link density and increase in average molecular weight between cross-links is observed for higher UV intensities and initiator concentrations. In addition, the increased number of dangling chain ends in the proposed network structure can also be supported by the reduction in measured T_g compared with predicted values based on the Gordon-Taylor equation due to the increased free-volume associated with the increase in chain ends.

For a fixed 90:10 VP: HEMA feed monomer ratio the effect of concentration and type (BIS, GLY with higher functionality, and DEGDA with longer molecular structure) of crosslinker, the characteristics of hydrogels prepared by UV initiated polymerization were observed. It was found that for all 3 types of crosslinker the swelling ratios (or molecular weight between crosslinks) increased and the modulus (or crosslinking density) decreased with decreasing amount of crosslinker. The GLY crosslinker produced gels possessing the highest swelling ratio and lowest mechanical stiffness, with the BIS crosslinked gels yielding the smallest swelling ratio and highest mechanical stiffness. The reason for this behavior is thought to be associated with steric hindrance effects and/or compatibility between the monomers and crosslinker. The compatibility between the monomers and crosslinkers was determined by Hansen solubility parameters for the dispersion, polar, and hydrogen bond forces. In addition, the compatibility between gels crosslinked with different crosslinkers and saline solution was also analyzed by interaction parameter (χ) to study the effect of the types of crosslinkers. It was found that the χ values obtained for the gels crosslinked with BIS were generally the highest and the gels with GLY the lowest, which indicates that the gels crosslinked with GLY are

more miscible with the swelling medium. The difference between each Hansen solubility parameter components of between VP and BIS was the smallest, which indicates that the difference between each Hansen solubility parameter components of the crosslinker and monomers ($|\delta_d^{Mo} - \delta_d^{CX}|$, $|\delta_p^{Mo} - \delta_p^{CX}|$, and $|\delta_h^{Mo} - \delta_h^{CX}|$) can qualitatively determine relative degree of crosslinking degree and swelling ratio compared among hydrogel systems.

References

- [1]. G. Scuderi, “Ricerche Sperimentali sul Trapianto del Vitreo (Tentativi Sostotuzione Parziale con Vitreo Omologo, con Liguor Eterologo, con Soluzione di Polivinilpirrilidone), *Ann. Ophthalmol. Clin. Oncol.*, vol. 80, pp. 213-220, 1954.
- [2]. H. Kaplan and A. Guner, “Characterization and determination of swelling and diffusion characteristics and poly(Nvinyl-2-pyrrolidone) and poly(N-vinyl-2-pyrrolidone)/K₂S₂O₈ hydrogels in water., *J. Appl. Polym. Sci.*, vol. 78, pp. 994-1000, 2000.
- [3]. L. C. Lopergolo, A. B. Lugao, and L. H. Catalani, “Direct UV photocrosslinking of poly (N-vinyl-2-pyrrolidone)(PVP) to produce hydrogels”, *Polymer*, vol. 44, pp. 6217-6222, 2003.
- [4]. Nicholas A. Pappas, *Hydrogels*, in *Biomaterials Science* 2nd ed., Academic Press, 2004.
- [5]. Fu-Jing Kao, Gurusamy Manivannan, Samuel P. Sawan, “UV curable bioadhesives: Copolymers of *N*-vinyl pyrrolidone” *J Biomed. Mater. Res. part A*, vol. 38, pp. 191-196, 1997.
- [6]. I. Calderara, R. Gougeon, L. Delmotte, V. Lee, and D. J. Loughnou, *J. Polym. Sci.* vol. 35, pp. 3619-3625, 1997.
- [7]. I. Quijada-Garrido, A. Prior-Cabanillas, L. Garrido, and J. M. Barrales-Rienda, “Swelling monitorization of Poly [(N-isopropylacrylamide)-co-(methacrylic acid)] Copolymers by Magnetic Resonance Imaging”, *Macromolecules*, vol. 38, pp. 7434-7442, 2005.
- [8]. K. G. Wiese, D. E. H. Heinemann, D. Ostermeier, and J. H. Peters, “Biomaterial properties and biocompatibility in cell culture of a novel self-inflating hydrogel tissue expander”, *J. Biomed. Mater. Res.*, vol. 54 (2), pp. 179-188, 2001.
- [9]. K. G. Weise, “Osmotically induced tissue expansion with hydrogels: a new dimension in tissue expansion? A preliminary report” *J of Craniomaxillofac Surg*, vol. 21, pp. 309-313, 1993.

- [10]. A. Bacsuklin, M. Vogel, K. G. Wiese, K. Gundlach, V. Hingst, and R. Guthoff, "New osmotically active hydrogel expander for enlargement of the contracted anophthalmic socket", *Graefe's Arch Clin Exp Ophthalmol*, vol. 238, pp. 24-27, 2000.
- [11]. Sanxiu Lu and Kristi. S. Anseth, "Photopolymerization of multilaminated poly (HEMA) hydrogels for controlled release", *J. Control Release*, vol. 57, pp. 291-300, 1999.
- [12]. O. Wichterle and D. Lim, "Hydrophilic gels for biological use", *Nature*, vol. 185, pp. 177-182, 1960.
- [13]. Loo-TecK Ng and Satesh Swami, "IPNs based on chitosan with NVP and NVP/HEMA synthesised through photoinitiator-free photopolymerisation technique for biomedical applications", *Carbohydrate Polymers*, vol. 60, pp. 523-528, 2005.
- [14]. Gavin Hoch, Anuj Chauhan, and C. J. Radke, "Permeability and diffusivity for water transport through hydrogel membranes" *J. Membrane Sci.*, vol. 214, pp.199-209, 2003.
- [15]. R. Downes, M. Lavin, and R. Collin, "Hydrophilic expanders for the congenital anophthalmic socket", *Advances in Ophthalmic Plastic and Reconstructive Surgery* vol. 9, pp. 57-61, 1992.
- [16]. L. Li and L. J. Lee, "Photopolymerization of HEMA/DEGDMA hydrogels in solution", *Polymer*, vol. 46, pp. 11540-11547, 2005.
- [17]. C. F. Huang, S. W. Kuo, F. J. Lin, C. Wang, C. J. Hung, F. C. Chang, "Syntheses and specific interactions of poly (hydroxyethyl methacrylate-b-vinyl pyrrolidone) diblock copolymers and comparisons with their corresponding miscible blend systems", *Polymer*, vol. 47, pp. 7060-7069, 2006.
- [18]. P. Dolez, M. Marek, and B. J. Love," Photopolymerizable acrylic resin: Effect of curing time and temperature" *J. Appl. Polym. Sci.*, vol. 82, pp. 546-554, 2001.
- [19]. Bhardwaj, Y. K.; Kumar, V.; Sabharwal, S., "Swelling behavior of radiation-polymerized polyampholytic two-component gels: dynamic and equilibrium swelling kinetics", *J. Appl. Polym. Sci.*, vol. 88, pp. 730-742, 2003.

- [20]. M. A. Al-Issa, T. P. Davis, M. B. Huglin and D. C. F. Yip, "Copolymerizations involving *N*-vinyl-2-pyrrolidone", *Polymer*, vol. 26, pp.1869 -1974, 1985.
- [21]. M. M. Faragalla, D. J. T. Hill, and A. K. Whittaker, "The copolymerization of *N*-vinyl-2-pyrrolidone with 2-hydroxyethyl methacrylate", *Polymer Bulletin*, vol. 47, pp. 421-427, 2002.
- [22]. B. Ahmad, S. Bashir, S. Nisa, and M. B. Huglin, " Chemically crosslinked *N*-vinyl-s-pyrrolidone/2-hydroxyethyl methacrylate (VP/HEMA) copolymer for the controlled Release of cyclic oligopeptide", *Turk J. Chem*, vol. 28, pp. 279-285, 2004.
- [23]. K. Dusek, "Diffusion control in the kinetics of cross-linking" *Polymer Gels and Networks*, vol. 4, pp. 384-404, 1996.
- [24]. T. K. Kwei, "The effect of hydrogen bonding on the glass transition temperature of polymer mixtures", *Journal of Polymer Science Part C-Polymer Letters*, vol. 22, pp. 307-313, 1984.
- [25]. Y. A. Aggour, "Characterization and evaluation of copolymers of end-allenoxypolyoxyethylene macromonomers and *N*-vinyl-2-pyrrolidone", *Eur. Polym. J.*, vol. 35, pp. 1173-1178, 1999.
- [26]. Norman S. Allen, Photopolymerization and Photoimaging Science and Technology, Elsevier Science Publishing Co., Inc, New York, 1989.
- [27]. C. Decker, K. Moussa and T. Bendaikha, "Photodegradation of UV-cured coatings II. polyurethane-acrylate networks," *J. Polym. Sci., Polym. Chem.*, vol. 29, pp. 739-747, 1991.
- [28]. C. Decker and T. Bendaikha, "Photodegradation of UV cured coatings. I: Epoxy-acrylate networks", *J. Radiat. Curing*, vol. 11(2), pp. 6-13, 1984.
- [29]. P. Ghi, D. J. T. Hill, and A. K. Whittaker, "Water Sorption by Poly (tetrahydrofurfuryl methacrylate-co-2-hydroxyethyl methacrylate). I. A Mass-Uptake Study", *J. Polym. Sci., Part B: Polym. Phys*, vol. 38, pp. 1939-1946, 2000.
- [30]. C. S. Brazel and N. A. Peppas, "Dimensionless analysis of swelling of hydrophilic glassy polymers with subsequent drug release from relaxing structures", *Biomaterials*, vol. 20, pp. 721-732, 1999.

- [31]. M. Shibayama, "Feature Article Spatial inhomogeneity and dynamic fluctuations of polymer gels", *Macromol. Chem. Phys.*, vol.199, pp.1-30, 1998.
- [32]. H. Furukawa, K. Horie, R. Nozaki, and M. Okada, "Swelling-induced modulation of static and dynamic fluctuations in polymer gels observed by scanning microscope light scattering", *Physics Review E*, vol. 68, pp. 031406, 2003.
- [33]. I. Yazici, and O. Okay, "Spatial inhomogeneity in poly (acrylic acid) hydrogels", *Polymer*, vol. 46, pp. 2595-2602, 2005.
- [34]. A. Alfrey, E. F. Gurnee, and W. G. Lloyd, "Diffusion in glassy polymers", *Journal of Polymer Science*, vol. 12, pp. 249, 1966.
- [35]. M. T. A. Ende and N. A. Peppas, "Transport of ionizable drugs and proteins in crosslinked poly(acrylic acid) and poly(acrylic acid-co-2 hydroxyethyl methacrylate)", *J. Appl. Polym. Sci.*, vol. 59, pp. 673-685, 1996.
- [36]. D. J. T. Hill, M. C. H. Lim, and A. K. Whittaker, "Water diffusion in hydroxyethyl methacrylate (HEMA)-based hydrogels formed by g-radiolysis", *Polym. Int.*, vol. 48, pp. 1046-1052, 1999.
- [37]. M. Sen, N. Pekel, and O. Guven, "Radiation synthesis and characterization of N-vinyl-2-pyrrolidone/N-allylthiourea hydrogels and their use in the adsorption of invertase", *Angew. Makromol. Chem.*, vol. 257, pp. 1-6. 1998.
- [38]. J. T. Chung, K. D. F. Vlugt-Wensink, W. E. Hennink, and Z. Zhang, "Effect of polymerization conditions on the network properties of dex-HEMA microspheres and macro-hydrogels", *Int. J. Pharm.*, vol. 288, pp. 51-61, 2005.
- [39]. H. Omidian, and K. Park, "Experimental design for the synthesis of polyacrylamide superporous hydrogels", *Journal of Bioactive and Compatible Polymers*, vol. 17, pp. 433-450, 2002.
- [40]. Ferdinand Rodriguez, Principles of Polymer Systems, 4th ed., Taylor & Francis: Washington DC; 1996.
- [41]. R. Gaylord, "Entanglement and excluded volume effects in rubber elasticity", *J. Polym. Eng. Sci.*, vol. 19, pp. 263- 266, 1979.

- [42]. A. Henke, S. Kadlubowski, P. Ulanski, J. M. Rosiak and K. F. Arndt, "Radiation-induced cross-linking of polyvinylpyrrolidone-poly (acrylic acid) complexes", *Nucl. Instrum. Methods Phys. Res., Sect. B*, vol. 236, pp. 391-398, 2005.
- [43]. H. M. Said, S. G. A. Abd Alla, and A. W. M. El-Naggar, "Structural properties of-irradiated poly (vinyl alcohol)/poly (ethylene glycol) polymer blends", *Reactive & Functional Polymers*, vol. 61, pp. 397-404, 2004.
- [44]. J. Y. Wong, A. Velasco, P. Rajagopalan, Q. Pham, Q, "Directed movement of vascular smooth muscle cells on gradient-compliant hydrogels", *Langmuir*, vol. 19, pp. 1908-1913, 2003.
- [45]. J. Hannah Lee and David G. Bucknall, "Swelling behaviour of hydrogels synthesized using controlled UV-initiated free radical polymerization", *Journal of Polymer Science B: Polymer Physics*, vol. 46(14), pp. 1450-1462, 2008.
- [46]. Wei Xue, Simon Champ, Malcolm B. Huglin, "New superabsorbent thermoreversible hydrogels" *Polymer*, vol. 42, pp. 2247-2250, 2001.
- [47]. Malcolm B. Huglin, Yan Liu, and Jose L. Velada, "Thermoreversible swelling behaviour of hydrogels based on N-isopropylacrylamide with acidic comonomers", *Polymer*, vol. 38, pp. 5785-5791, 1997.
- [48]. Aiman M. Atta and Abdel-Azim A. Abdel-Azim, "Effect of crosslinker functionality on swelling and network parameters of copolymeric hydrogels", *Polym. Adv. Technol.*, vol. 9, pp. 340-348, 1998.
- [49]. Hasine Kasgöz, Ismail Aydin, and Ahmet Kasgöz, "The effect of PEG(400)DA crosslinking agent on swelling behaviour of acrylamide-maleic acid hydrogels", *Polymer Bulletin*, vol. 54, pp. 387-397, 2005.
- [50]. Flory, P. J., in *Principles of Polymer Chemistry*; Cornell University Press: New York; 1969.
- [51]. M. Nagy, "A comparative and systematic thermodynamic study of aqueous solutions and hydrogels of homo- and copolymer of poly(vinyl alcohol)", *Phy. Chem. Chem. Phys.*, vol. 2, pp. 2613-2622, 2000.

- [52]. Nitin S. Patil, Jonathan S. Dordick and David G. Rethwisch, “Macroporous poly(sucrose acrylate) hydrogel for controlled release of macromolecules”, *Biomaterials*, vol 17, pp. 2343-2350, 1996.

- [53]. D. W. Van Krevelen, *Properties of Polymers: Their Correlation with Chemical Structure; Their numerical Estimation and Prediction from Additive group Contributions*, Elsevier, 1990.

- [54]. Charles M Hansen, “Aspects of solubility, surfaces and diffusion in polymers”, *Press in organic Coating*, vol. 51, pp. 55-66, 2004.

- [55]. J. Brandrup and E. H. Immergut, *Polymer Handbook*, Wiley, New York, 1989.

- [56]. Tomas P. Davis and Malcolm B. Huglin, “Effect of crosslinking on the properties of poly(2-hydroxyethyl methacrylate) hydrogels” *Die Angewandte Makromolekulare Chemie* , vol. 189, pp. 195-205, 1991.

CHAPTER V

CONTROL OVER SWELLING DEGREE AND RATE OF IONIC HYDROGEL OF VP/AA COPOLYMER

Control over swelling behavior of neutral hydrogel of VP/HEMA has been investigated to find desirable swelling degree and rate for the use of tissue expansion. In order to significantly improve the swelling ratio of VP based hydrogels, instead of HEMA the ionic moiety acrylic acid (AA) was introduced in the molecular chains of hydrogels. It has been shown that hydrogels composed of AA units have shown that with increasing AA content higher equilibrium swelling ratios (q_e) are produced due to higher osmotic pressures induced by the dissociation of carboxyl groups in the AA moieties into carboxylate anions and hydrogen ions during the swelling [1-3]. This behavior is also seen in other polymer electrolytes in dilute solution [4]. VP/AA hydrogel systems have studied for pharmaceutical applications, especially drug delivery [5-7] due to their biocompatibility.

The VP and AA copolymeric gels were synthesized with varying VP and AA feed ratio, initiator type and concentration, crosslinker type and concentration as well as polymerization method in order to find the hydrogel system with optimized properties such as swelling degree and rate and mechanical properties.

5.1. Comparison of swelling behavior of VP/HEMA gels and VP/AA gels

The swelling behavior of VP/AA gels (UVHIB gels) and VP/HEMA gels (UVAIB gels) in saline solution was compared to verify the benefit to introduce AA moieties in gel network for acquiring larger swelling capacity. Figure 5.1 shows the swelling behavior of UVHIB (UVHIB 3) gels and UVAIB (UVAIB 2) gels synthesized

with 90:10 feed monomer ratio of VP:HEMA and VP:AA, respectively. The UVHIB 3 gels swell to a great extent and were found to have slow rate. The equilibrium volume swelling ratio (q_{ve}) of the UVHIB 3 and UVAIB 2 hydrogels determined to be 13.4 and 40.6, respectively. The diffusion coefficient (D) values for UVHIB 3 and UVAIB 2 are $7.67 \times 10^{-7} \text{ cm}^2/\text{s}$ and $3.57 \times 10^{-7} \text{ cm}^2/\text{s}$, respectively. The initial swelling rate (R_s) values are 0.133 min^{-1} and 0.034 min^{-1} for UVHIB 3 and UVAIB 2, respectively. Since VP/AA copolymeric hydrogels have not only higher q_{ve} but also slower D and R_s compared to VP/HEMA gels, they therefore possess more desirable properties for the use of tissue expansion as we discussed in chapter 2.

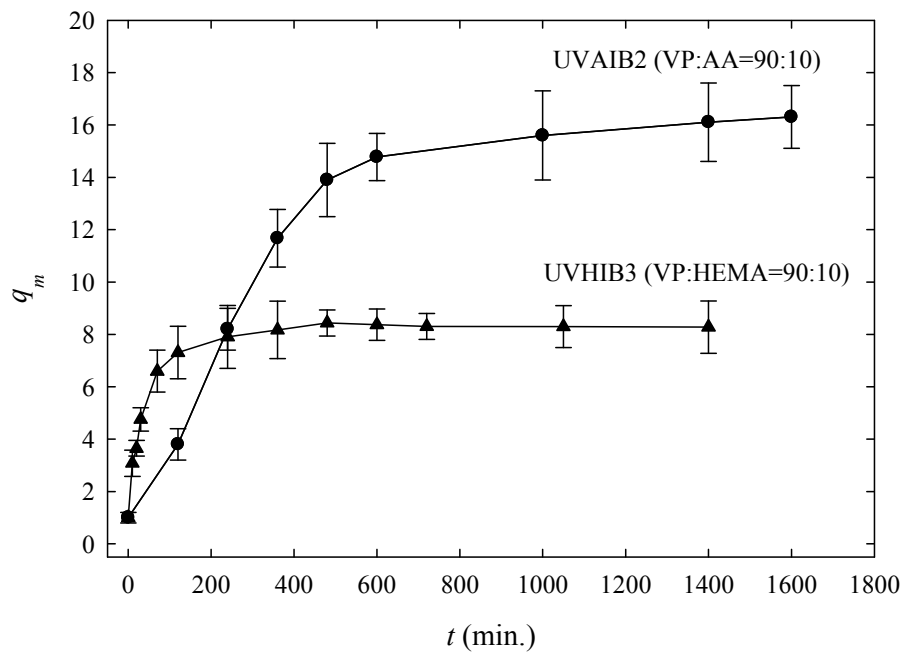


Figure 5.1. The mass swelling ratio (q_m) of VP/AA gels and VP/HEMA gels prepared with VP:HEMA and VP:AA of 90:10, respectively

5.2. UV-Polymerized VP/AA Gels with Various Ratios of Monomers

5.2.1. Swelling Behavior

Hydrogels composed of AA units have shown that with increasing AA content in the gels the hydrogels have higher q_e [1-3], it was accordingly expected that the VP/AA hydrogel prepared with higher AA content will swell more. Various photo-polymerized VP/AA (UVAIB) gels were synthesized with increasing feed AA weight (C_{AA}) (see Table 3.4 for their synthesis conditions) to obtain the hydrogel system showing higher swelling degree and its synthesis condition. From the results of VP/HEMA hydrogels, it was noticed that the thermodynamic and kinetic swelling behavior of gels are dependent on their feed ratio of comonomer.

Figure 5.2 shows the composition-dependent q_{ve} of UVAIB hydrogels fully swollen at 7.34 pH and room temperature. The q_{ve} values of the UVAIB gels are

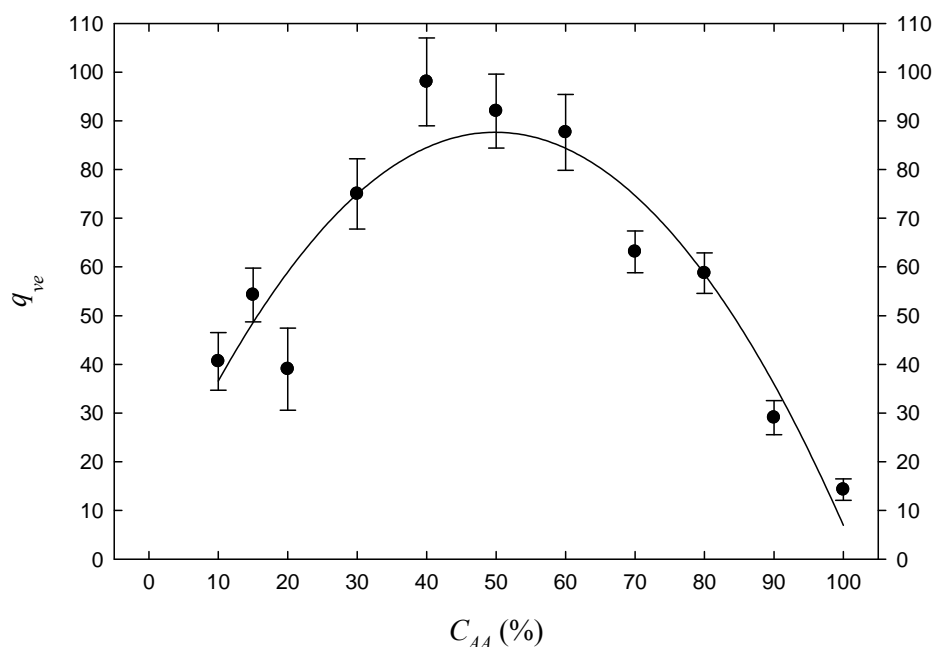


Figure 5.2. The equilibrium volume swelling ratio (q_{ve}) of VP/AA hydrogels as a function of the feed weight % of AA (C_{AA})

expressed as a function of feed weight % of AA (C_{AA}). The maximum q_{ve} is shown around 40~50 wt. % of C_{AA} . Instead of an increase in q_{ve} with C_{AA} as anticipated the data could be fitted with relationship, $q_{ve} = a_1 + a_2 C_{AA} + a_3 C_{AA}^2$ where the coefficients a_1 , a_2 , and a_3 are specific for a given hydrogel system. The values of a_1 , a_2 , and a_3 for the VP/AA hydrogels were determined to be 7.72, 3.21, and -0.03, respectively, with R-square $r^2=0.94$. With increasing C_{AA} , the q_{ve} increases up to 108 at $C_{AA} = 40$ wt. % and subsequently decreases to 12 at $C_{AA} = 99$ wt. %. This anomalous swelling behavior of photo-polymerized VP/AA gel systems showing a distinct maximum value of q_e at 40~50 wt. % of C_{AA} disagrees with the expected q_e values as a function of C_{AA} based on a conventional gel model (refer to the equation (37)). Possible explanations for these results are discussed below.

Figure 5.3 shows the mass swelling ratio (q_m) values of the UVAIB gels with time. All gels initially swell rapidly and slowly reach an equilibrium state via an intermediate state. As seen for the VP/HEMA hydrogels, time dependent q_m values of various VP/AA hydrogels were well fitted using the empirical relationship with high r-square values (~ 0.99) for all gels, $q_m = a_1 + a_2 \times (1 - \exp(-a_3 \cdot t))$ where the coefficients a_1 , a_2 , and a_3 are specific for a given system. The values of a_1 , a_2 , and a_3 for the VP/AA hydrogels prepared with increasing C_{AA} were determined, which are listed in Table 5.1.

It is shown that the UVAIB5 gel produces highest degree of swelling, which is unexpected result and discussed using q_{ve} later in this section. It should be noticed that the t_{max} for the UVAIB gels was dependent on the C_{AA} with values varying from 1100 (18.3 hours) minutes to 2800 minutes (46.7 hours) (Table 5.2). These t_{max} values for the UVAIB gels are much longer than those of VP/HEMA gels synthesized by thermal polymerization (TVHAB gels) (300-400 minutes) and that of VP/HEMA gels synthesized by UV-initiated polymerization (UVHIB gels) (600-1000 minutes). The t_{max} values of UVAIB hydrogels linearly increases with the corresponding q_{ve} values (Figure 5.2)

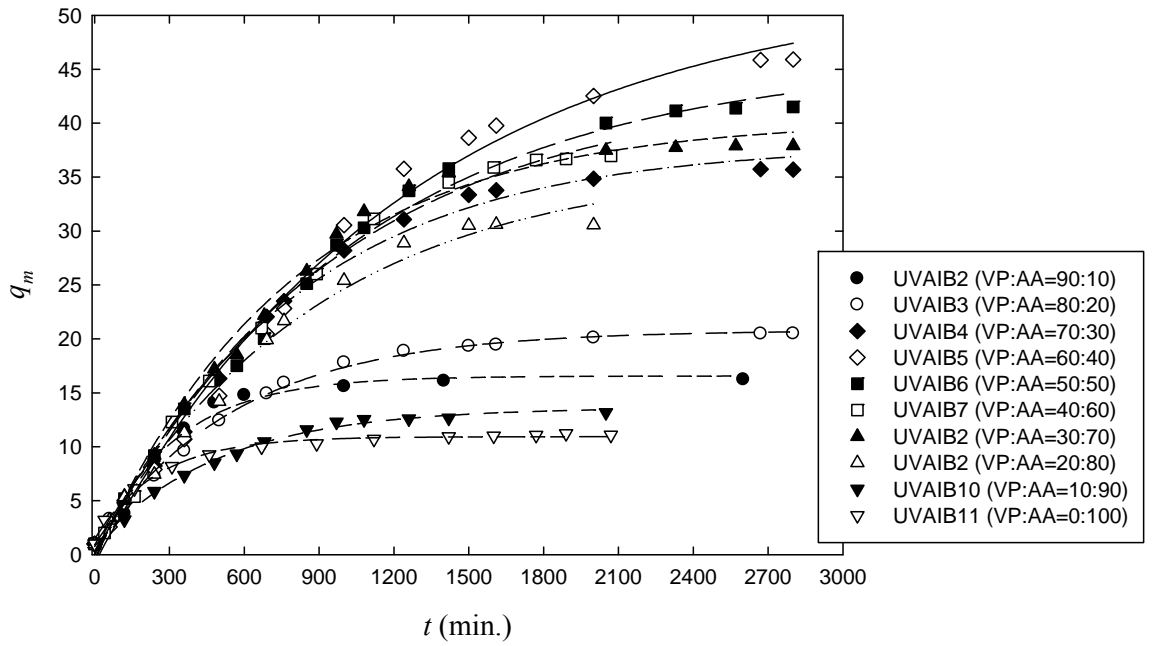


Figure 5.3. The mass swelling ratio (q_m) with time for fully swollen VP/AA hydrogels prepared with different AA feed content (C_{AA}).

Table 5.1. The fitting coefficients a_1 , a_2 , and a_3 and r-square for UVAIB hydrogels prepared with various C_{AA}

Coefficient C_{AA} (wt. %)	Coefficient			
	a_1	a_2	a_3	r^2
10	0.088	16.47	0.003	0.98
20	0.905	19.89	0.002	0.99
30	-0.400	38.42	0.001	0.99
40	-0.790	53.80	0.001	0.99
50	-0.044	46.00	0.001	0.99
60	0.029	43.04	0.001	0.99
70	-0.612	40.92	0.001	0.99
80	0.295	35.99	0.001	0.99
90	0.753	12.88	0.002	0.99
100	1.404	9.538	0.004	0.99

Table 5.2. The R_s and t_{\max} of UVAIB hydrogels prepared with various C_{AA}

C_{AA} (wt. %)	R_s (min^{-1})	t_{\max} (hour)
10	0.0298	16.67
20	0.0234	25.00
30	0.0306	33.33
40	0.0288	46.67
50	0.0292	42.83
60	0.0288	31.50
70	0.0305	34.16
80	0.0275	26.83
90	0.0157	17.97
100	0.0179	11.17

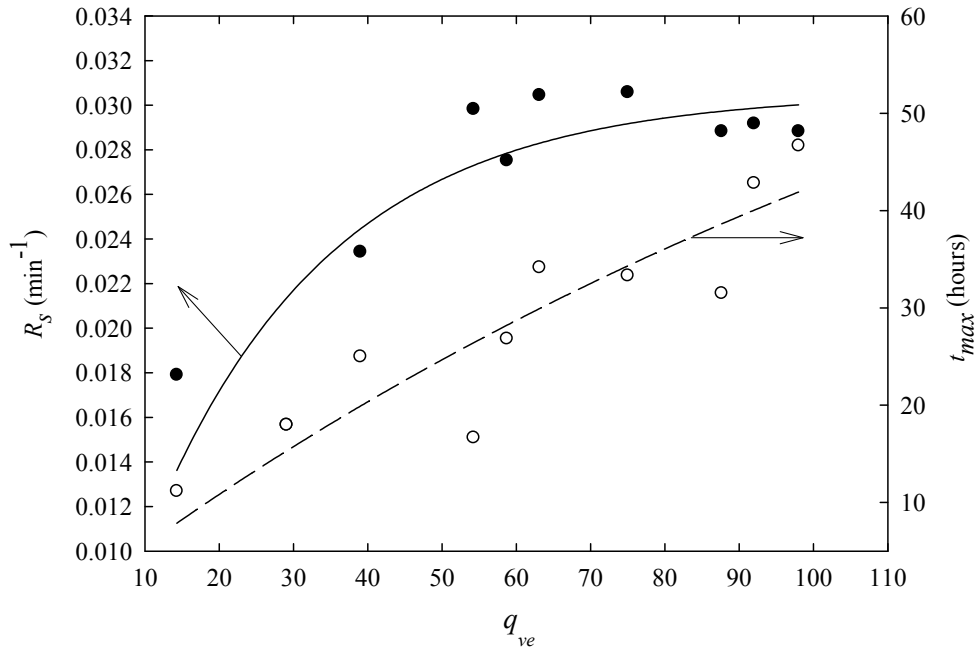


Figure 5.4. The R_s and t_{\max} of UVAIB gels as a function of q_{ve} .

The initial swelling rate (R_s) values of the UVAIB gels varied randomly with C_{AA} and are in the ranges from 0.016 min^{-1} to 0.031 min^{-1} . It was expected that R_s should increase with increasing C_{AA} , so the observed results may be due to the anomalous swelling behavior affected by monomer feed composition. However there is a strong dependence of R_s on q_{ve} (see Figure 5.4) with R_s increasing with increasing q_{ve} . The R_s values (0.016 min^{-1} - 0.031 min^{-1}) of a UVAIB gels are similar to those of TVHAB gels and slower than those of UVHIB gels.

The diffusion characteristics of a penetrant diffusing the VP/AA hydrogels were also characterized. Figure 5.5 shows the diffusion coefficient (D) of saline solution as a function of C_{AA} . With increasing C_{AA} , the values of D also decrease and then increase at above C_{AA} of 50 wt. %. The gels synthesized with 40 or 50 wt% of C_{AA} (UVAIB5 and UVAIB 6) which produce the higher swelling ratio (q) have the lowest values of D . This is opposite not only to the trends of R_s for the UVAIB gels but also to the expected result based on that UVAIB5 and UVAIB 6 gels which longer molecular weights between crosslinks (M_c) (see the sections 4.1.5 and 4.1.6). In such gels, penetrant diffuses faster into the gel networks with larger M_c (larger mesh size). It is thought that this unexpected behavior of D might be associated with intermolecular hydrogen bonding interactions between AA unit and VP. In the initial stage of swelling, the H-bonding interactions in the gel state is higher for the systems prepared with a stoichiometry of VP and AA close to 1:1. These interactions might hinder the diffusion of penetrant, resulting in smaller D . Although the initial diffusion of saline solution into VP/AA gels prepared with a stoichiometry of VP and AA close to 1:1 is the smallest, overall they swell faster, which suggests that the interaction between the AA and VP is broken down faster by absorbing aqueous solvent with time.

The diffusion exponent (n) of the various UVAIB hydrogels are all in the range from 0.77 to 1.17, which indicates the diffusion of saline solution into the UVAIB gels all

follows non-Fickian diffusion (or diffusion case III) [13]. This diffusion behavior is probably because of the ionic units of AA and the highly hydrophilic units of VP.

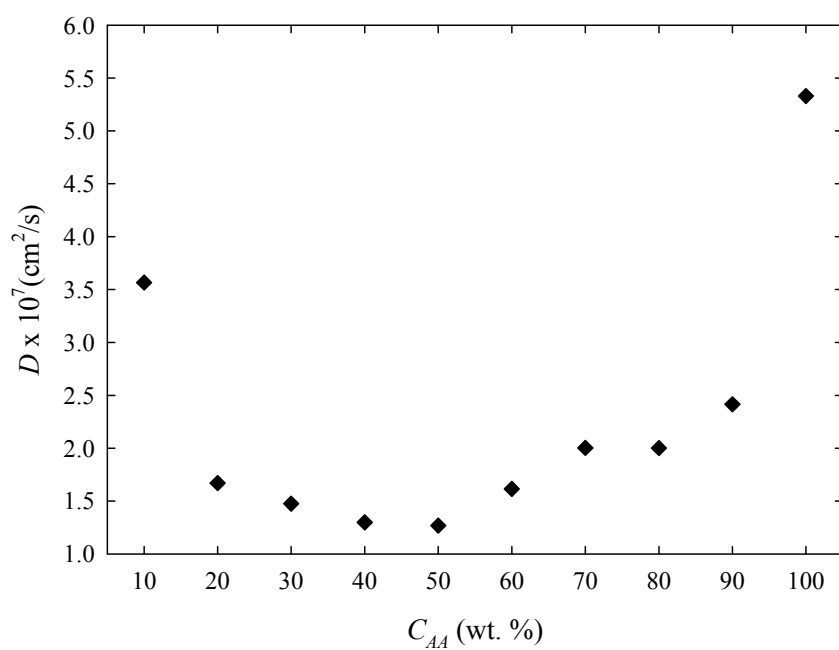


Figure 5.5. The D of saline solution diffusing into UVAIB hydrogels as a function of C_{AA}

5.2.2. Mechanical Stiffness of VP/AA Hydrogels

Figure 5.6 depicts the compressive modulus (G) of the VP/AA fully swollen hydrogels as a function of C_{AA} . With increasing C_{AA} , G decreases to 8.67 ± 5.12 kPa at $C_{AA} = 40$ wt. % and then drastically increases from $C_{AA} = 70$ wt. % up to 240 ± 47.2 kPa at $C_{AA} = 90$ wt. %. The value of G of UVAIB2 and UVAIB11 (synthesized with C_{AA} 10 wt. % and 100 wt. %, respectively) are smaller than expected and probably associated with phase separation within the hydrogels, as confirmed by the development of turbidity. As expected, the hydrogel system possessing higher q_{ve} (*cf* Figure 5.2) has smaller G .

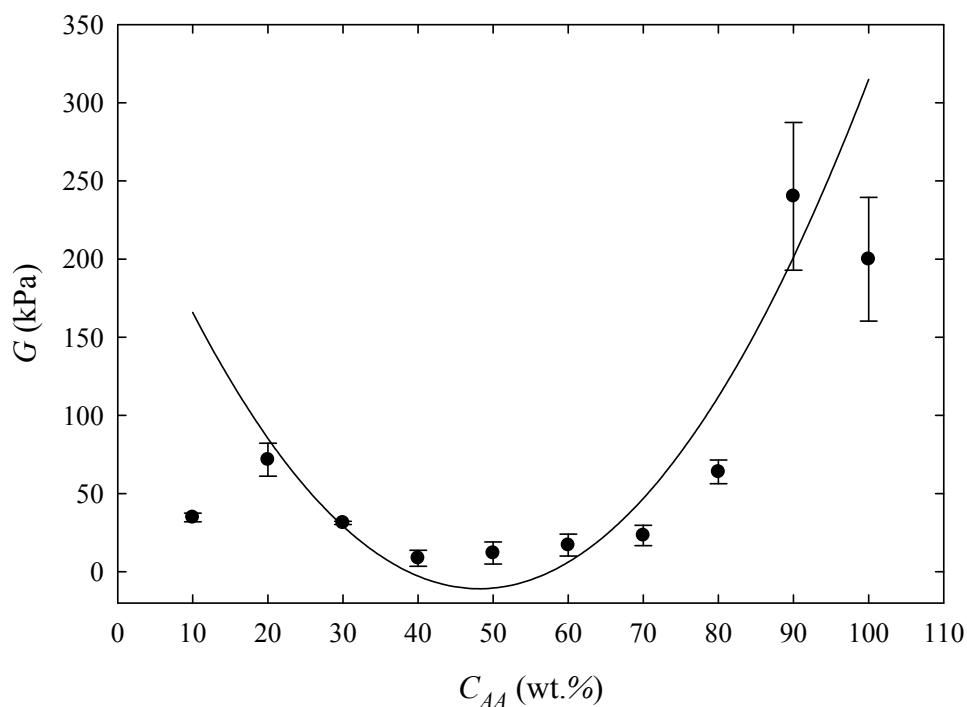


Figure 5.6. The G of fully swollen VP/AA hydrogels prepared with different C_{AA} (Two deviated values were not used for fitting the modulus values).

5.2.3. pH-Dependent Swelling Behavior

The equilibrium volume swelling ratio (q_{ev}) of the photo-polymerized VP/AA (UVAIB) gels was determined at various pH of the swelling medium in order to investigate whether or not different hydrogel systems have different transition point in pH. The experiments were carried out with buffer solutions of pH 1, 2, 4, 6, and 8 at an ionic strength of 1×10^{-4} mol/cm³ and at room temperature.

Figure 5.7 shows the q_{ve} of hydrogels determined at different pHs for 8 different hydrogels obtained with various feed weight ratio of VP:AA. The q_{ve} of various ionic VP/AA hydrogels was sensitive to not only VP:AA feed weight ratios but also pH of swelling medium. The reason for the pH-sensitivity is clearly directly related to ionic AA units in the hydrogels.

For all the hydrogel systems, the q_{ve} does not change below pH of 2 but increase rapidly from pH of 2 to pH of 6. The mid-point (transition point) of this increases at around pH of 4 and also makes the onset point of turbidity in the hydrogels. These observations agree well with known reports that volume of a pH-sensitive material abruptly changes around the pH corresponding to their dissociation constant (pK_a) [8]. The pK_a of AA is 4.25 [9]. It is seen that the transition point is independent of the amount of ionic units (C_{AA}) and it was confirmed that C_{AA} -dependent anomalous swelling is not due to the transition point since all hydrogels show a volume transition at similar pH ($pH \approx 4$). The increment in the q_{ve} is more drastic for the hydrogel system possessing higher q_{ve} . From pH of 6 to pH 8, the q_{ve} does not change again because of the completion of dissociation of AA groups at around pH 6. Caykara and Kantoglu [8] studied the pH-dependent swelling behavior of copolymeric hydrogels of N-vinyl-2-pyrrolidone (VP) and crotonic acid (CrA) and also reported the swelling ratio suddenly increased around pH corresponding pK_a 4.69, which is the pK_a of CrA and reached a maximum swelling ratio between a pH of 5 and 6.

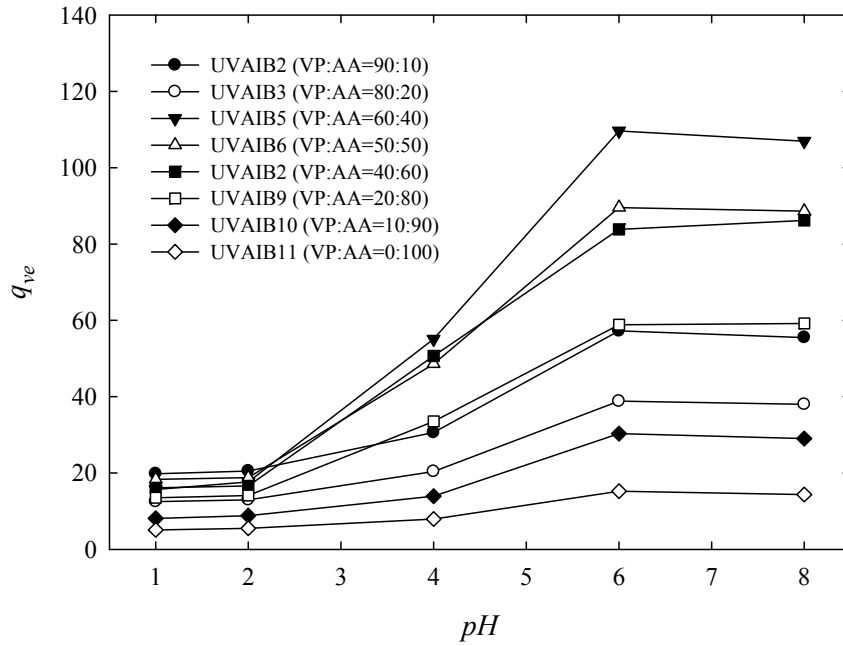


Figure 5.7. The equilibrium volume swelling ratio (q_{ve}) of VP/AA hydrogels determined at different pH for 8 different hydrogels obtained with various feed weight ratio of VP:AA.

5.2.4. Structure Parameters, M_c & v_e and Interaction Parameter, χ

The M_c and χ values for UVAIB hydrogels were determined using equation (39). The relevant parameters used for the calculations are as follows; ionic strength, $I=0.1$ M, molar volume solvent, $V_l = 18$ g/cm³, the number of branches originating from crosslinking agent, $\phi = 4$, dissociation constant of AA, $pK_a = 4.25$, specific volume of dry polymer, \bar{v} , which is in the range between 72 to 111 cm³/mol and dependent of their composition. As shown in Figure 5.8, the M_c values show a maximum at $C_{AA} = 40$ wt. % and are in the range between 1×10^4 and 5×10^5 mol/cm³. The v_e values show a corresponding minimum at 40~60 wt. % of C_{AA} and are in the range between 5×10^{-6} and 6×10^{-5} mol/cm³.

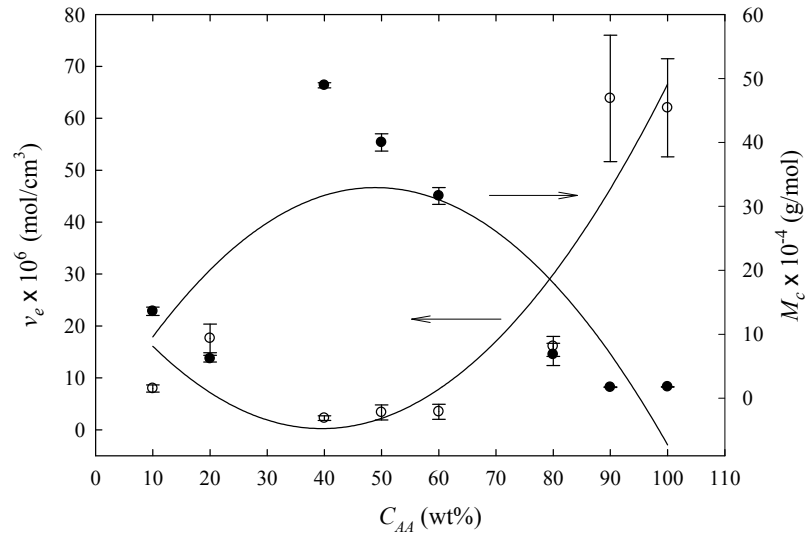


Figure 5.8. The molecular weight between crosslinks (M_c) and crosslink density (v_e) of UVAIB hydrogels prepared with different feed weight % of AA (C_{AA}).

The calculated values of interaction parameter between UVAIB hydrogel and swelling medium (χ) between 0.48 and 0.51 are shown as a function of C_{AA} in Figure 5.9 (a). The values of χ below 0.5 indicate a higher osmotic pressure build up in the system and more miscible between polymer and swelling medium, which agrees with a higher swelling in that region (see Figure 5.2). The reported values of χ for PVP hydrogels and PAA hydrogels are 0.49 ~ 0.5 and 0.45 ~ 0.5, respectively. [10, 11]. The determined values of χ for VP/AA hydrogels in this study are in the ranges of the reported values.

It has been reported that the χ values increases linearly with v_2 as given relationship; $\chi = A + Bv_2$ [4]. For fully swollen hydrogel systems, the v_2 is equal to the inverse of equilibrium swelling ratio (q_{ve}) so the relationship between χ and q_{ve} can be expressed as follows; $\chi = B_1 + B_2/q_{ve}$, where B_1 and B_2 are specific coefficients for each given system. Figure 5.9(b) shows the values of χ for UVAIB hydrogels as a function of

q_{ve} and was fitted with the relationship shown above. The determined B_1 and B_2 values for the UVAIB hydrogels are 0.50 ± 0.01 and 1.56 ± 0.48 , respectively, with r-square $r^2=0.82$. The smaller χ value is related with higher miscibility between UVAIB polymer and swelling medium, resulting in higher q_{ve} (Figure 5.9(b)).

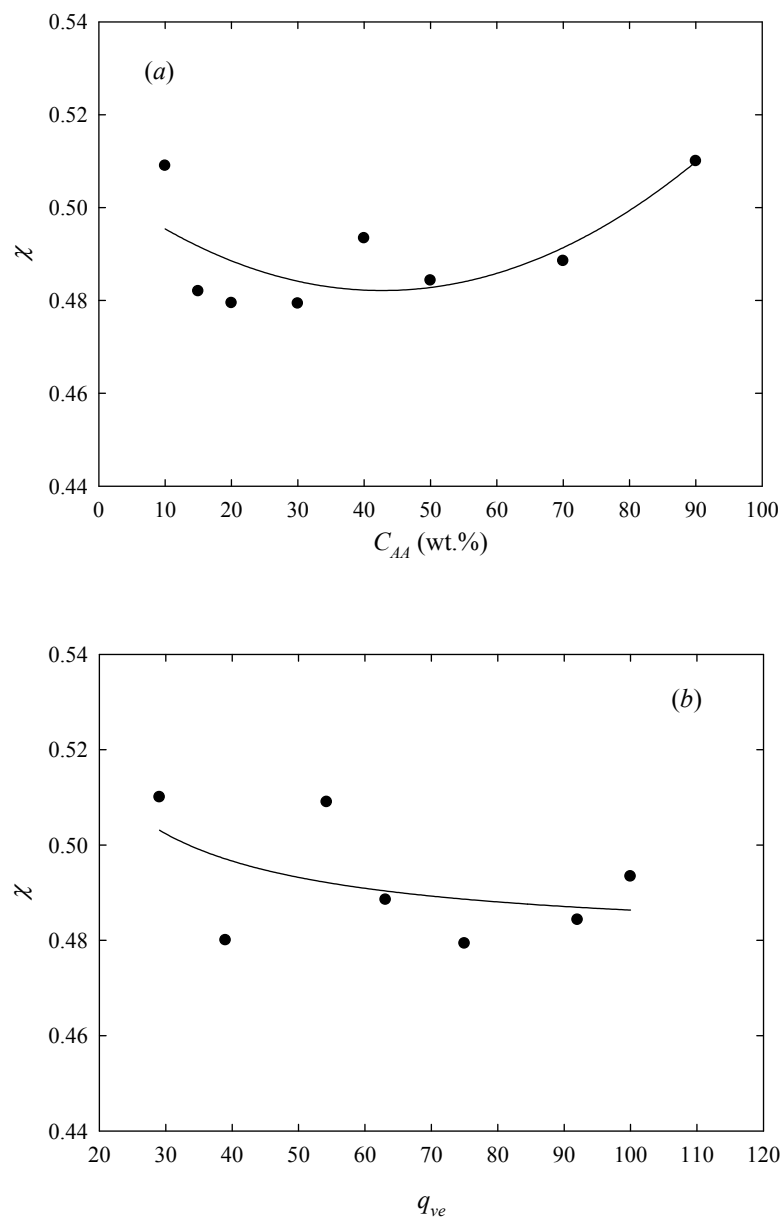


Figure 5.9. The χ of the UVAIB hydrogels as a function of (a) C_{AA} and (b) q_{ve}

5.2.5. Temperature-Dependent Swelling Behavior

The effect of temperature on the q_{ve} values of three different UVAIB hydrogels (UVAIB3, UVAIB5 and UVAIB9 having VP:AA feed weight ratio 80:20, 60:40, and 20:80, respectively) was investigated to check the existence of their critical volume transition temperatures (T_c) which might be the reason of the anomalous composition-dependence swelling behavior. The one assumption about the anomalous swelling behavior is that each hydrogel prepared with a different VP:AA feed weight ratio might have a different T_c , and correspondingly unexpected q_{ve} measured at room temperature.

As shown in Figure 5.10, the UVAIB5 hydrogels show higher q_{ve} over the entire temperature range than the UVAIB3 and UVAIB9 hydrogels. The q_{ve} values of fully

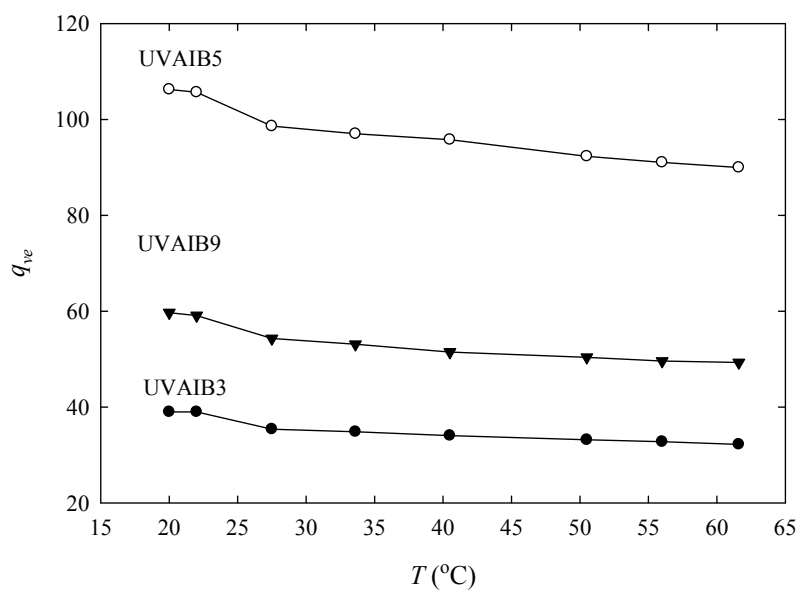


Figure 5.10. The equilibrium volume swelling ratio (q_{ve}) of fully swollen three VP/AA hydrogels prepared with different AA feed content (C_{AA}) with temperatures.

swollen UVAIB hydrogels gradually decrease from 109 to 90 with increasing temperature from 20 to 62 °C, which indicates that the volume is decreased since $v_2=1/q_{ve}$ for fully swollen hydrogels. Clearly in these UVAIB hydrogel systems, T_c was not observed unlike the PNIPAMM [12] which displays a drastic volume phase transition (LCST) induced by altering interaction between polymer molecules and solvent around critical temperature. Consequently, it is thought that the anomalous swelling behavior observed for the UVAIB hydrogels prepared with various feed ration of VP and AA is not affected by the temperature-dependent swelling behavior of UVAIB hydrogels.

5.2.6. Gelation Percent of VP/AA Xerogels

Figure 5.11 shows the gelation percent of the various UVAIB xerogels. As seen in the figure, the gels synthesized with of 40~60 wt. % C_{AA} show the lowest values of the gelation percent. This behavior is consistent with that observed for G as a function of C_{AA} (see Figure 5.6) and overturned curve of q_{ve} as function of C_{AA} (see Figure 5.2). For this reason, it is thought that the gelation percent of UVAIB gels also affects or involved with the q_{ve} and M_c of UVAIB gels. The reason for the observed gelation percent with C_{AA} might be related to the intermolecular hydrogen bonds between carbonyl groups (C=O) on the VP unit and carboxylic acid groups on the AA unit. Thus when the stoichiometry of VP and AA is close to 1:1, the greatest degree of intermolecular interaction is expected to be produced. Since the molar mass of VP and AA is 111 g/mol and 72 g/mol, respectively, to obtain the stoichiometry of VP and AA close to 1:1 the weight ratio between VP and AA should be about 40:60, a value where the largest q_{ve} was observed. It is thought that a lower gelation percent might be caused by the reduced probability to make crosslinking junctions because of the stronger H-bonding interaction between VP and AA, resulting in larger M_c (or larger q_{ve}).

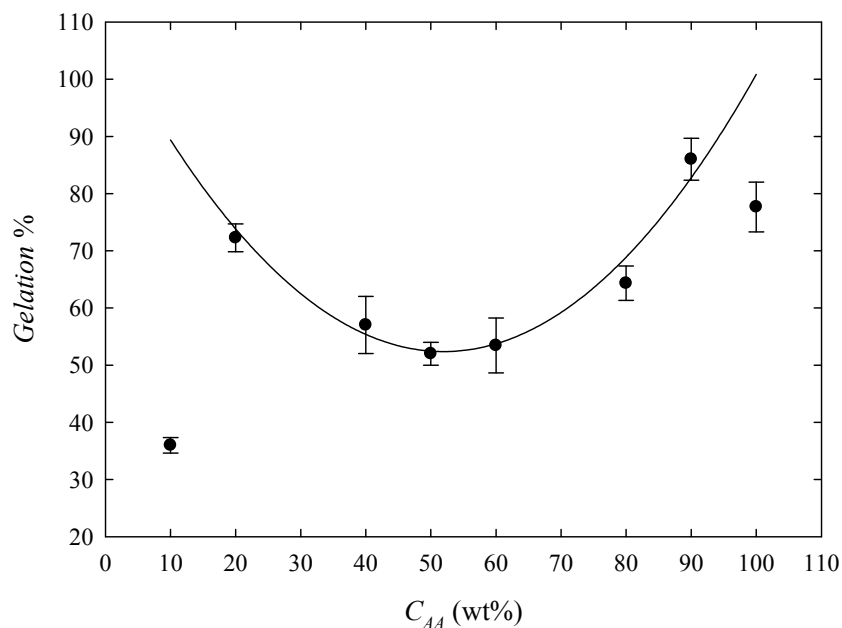


Figure 5.11. The gelation percent of UVAIB gels synthesized with different C_{AA} by UV-initiated polymerization.

5.2.7. Glass Transition Temperature, T_g

It was found that all of the UVAIB xerogels prepared with various C_{AA} have a single observed T_g , which means VP and AA segments in the gels are miscible at all the VP:AA feed ratios or too small sequence blocks of VP or AA units to be distinguishable to detect. The T_g values are dependent of the feed ratio of VP and AA as shown in Figure 5.12. The T_g values of PVP and PAA xerogel are 186 °C and 109 °C, respectively. The measured T_g values of various UVAIB xerogels were attempted to be fitted with the Flory-Huggins, Gordon-Taylor and Kwei equations (*rf* Chapter 3). As shown in the Figure, the data are well fitted with the Kwei equation (where $\alpha = 1$ and $\beta = 50$), which indicates that there is significant H-bonding interaction occurring in the system. At the

composition range having stoichiometry of VP:AA of 1:1 (at 40, 50, and 60 of C_{AA}), only the Kwei equation can fit the data which indicates that in these compositions stronger H-bonding interaction is involved. This is also agreed with the published reports that the complex structure in the PVP/PAA hydrogels is due to the H-bonding interaction [3, 14]. These results seem to support the results of D depending on the C_{AA} , (see Figure 5.5). The stronger H-bonding interaction between VP and AA units exists in the gel state would hinder the diffusion of swelling medium into the network. This relationship between T_g and D for C_{AA} used for preparing the VP/AA gels can be associated with gelation percent with C_{AA} . It is thought that the H-bonding interaction between VP and AA in pregel mixture already existed prior to the polymerization hinder the reaction with crosslinker, resulting in low gelation percent but high M_c .

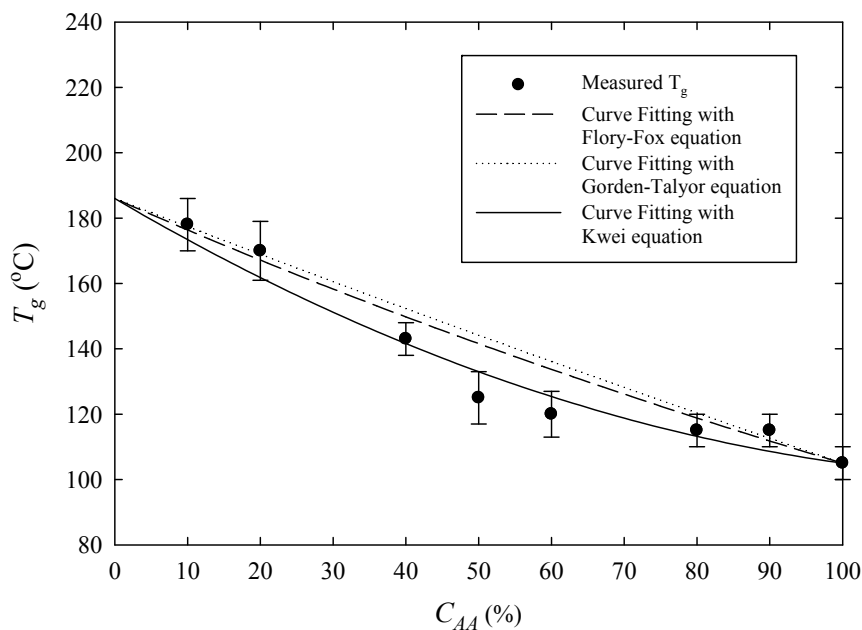


Figure 5.12. The measured values of glass transition temperature (●) of UVAIB xerogels prepared with different C_{AA} and predicted values for T_g are plotted using the Flory-Fox equation (---), the Gordon-Taylor equation (.....), as well as the Kwei equation (—, $\alpha = 1$ and $\beta = 50$).

5.2.8. IR Spectroscopy of VP/AA Xerogels

The chemical structure of VP/AA gels was characterized by analyzing their FTIR spectra. Figure 5.13 shows the FTIR spectra of VP/AA xerogels prepared with 90:10, 60:40, 10:90 and 100:0 feed ratio of VP:AA (UVAIB2, UVAIB5, UVAIB10, and UVAIB11, respectively). The characteristic peaks at 1665 cm^{-1} and 1730 cm^{-1} observed for UVAIB2 are related with the stretching mode of the carbonyl groups ($\text{C}=\text{O}$) in the VP and AA components in the gels, respectively [3, 14, 15, 16]. The intermolecular interaction between carboxylic acid groups (COOH) in AA units is assigned to the peak of 1712 cm^{-1} and when the COOH groups complex with the $\text{C}=\text{O}$ groups in the VP units, the COOH peak shifts from the 1712 cm^{-1} to 1730 cm^{-1} [17]. For UVAIB11 xerogel, PAA homopolymeric xerogel the peak at 1710 cm^{-1} and with increasing AA weight % the area (or height) of the peak at 1730 cm^{-1} gets increased, which indicates intermolecular interaction between COOH groups. In addition, with increasing AA from 10 to 90 wt. %, the peak at 1665 cm^{-1} shifts to 1635 cm^{-1} , which agrees with result for the intercalation between AA and VP units causing shift the peak of $\text{C}=\text{O}$ in VP from 1665 to $1635\sim 1640\text{ cm}^{-1}$ [18]. These results obviously indicate the interaction between VP and AA, which is consistent with the T_g and D results. However, the absorption peak at 1635 cm^{-1} for UVAIB11 xerogel is considered to be due to asymmetric stretching of COO in AA [19], which is discussed in detail below. The strong peaks at 3449 cm^{-1} shown in the spectra of UVAIB5, UVAIB10, and UVAIB11 are considered to be the H-bonded stretching of O-H groups in AA [15, 16, 19]. The peak shown at 1570 cm^{-1} for UVAIB11 shown in Figures 5.13 and 5.14 is considered to be attributed to the electron delocalized COO groups in AA units [20], which might be an indication of the acid anhydride groups produced during the melt polymerization of pregel consisting of the higher AA content used in this study. Anhydride formation of poly(acrylic acid) occurs due to thermal instability caused by the high temperature used in thermal and melt polymerization [21]. However, Kottle and McGaugh [22] reported that the anhydride group is formed from the intra- and inter-

molecular reaction between carboxylic acid groups (COOH) in AA units at the temperature range between 25 °C and 150 °C. Consequently, it is thought that even at room temperature anhydride formation in these gels may be occurred and also the anhydride groups between COOH groups since VP/AA gels might forms due to the use of UV initiated and melt polymerization (no solvent used). To verify the formation of anhydride groups in the UVAIB11, UVAIB11 xerogels was hydrolyzed for 2 hours in water of 120 °C since acid anhydride groups can be dissociated into COOH groups in water and under higher temperature. The FTIR spectra of PAA xerogels synthesized by

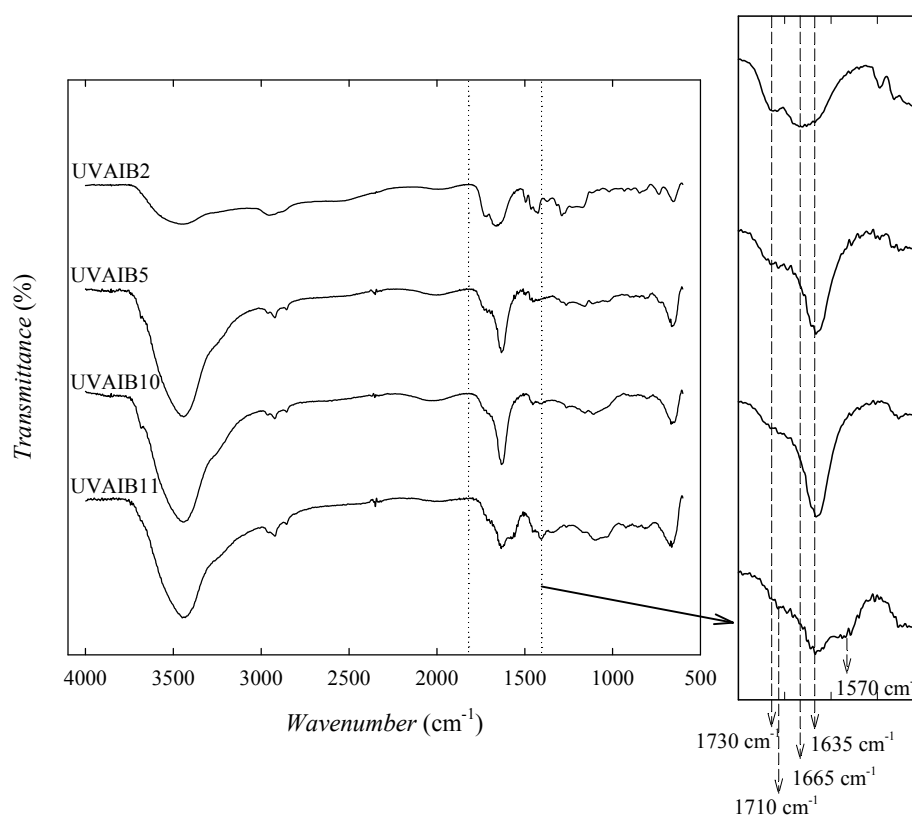


Figure 5.13. The IR Spectra of UVAIB2 (90:10 feed ratio of VP:AA), UVAIB5 (60:40), UVAIB10 (10:90), UVAIB11 (0:100) xerogels

UV-initiated polymerization (UVAIB11) before and after the hydrolysis are compared as shown in Figure 5.14. After the hydrolysis the peak shown at 1570 cm^{-1} disappeared, which indicates the existence of anhydride group in UVAIB11 gel (PAA gels). In the spectra of UVHIB10 gel (see Figure 5.13) the peak at 1570 cm^{-1} is not seen although this gel prepared with higher AA content, which might be because the amount of the anhydride groups is too small to be detected.

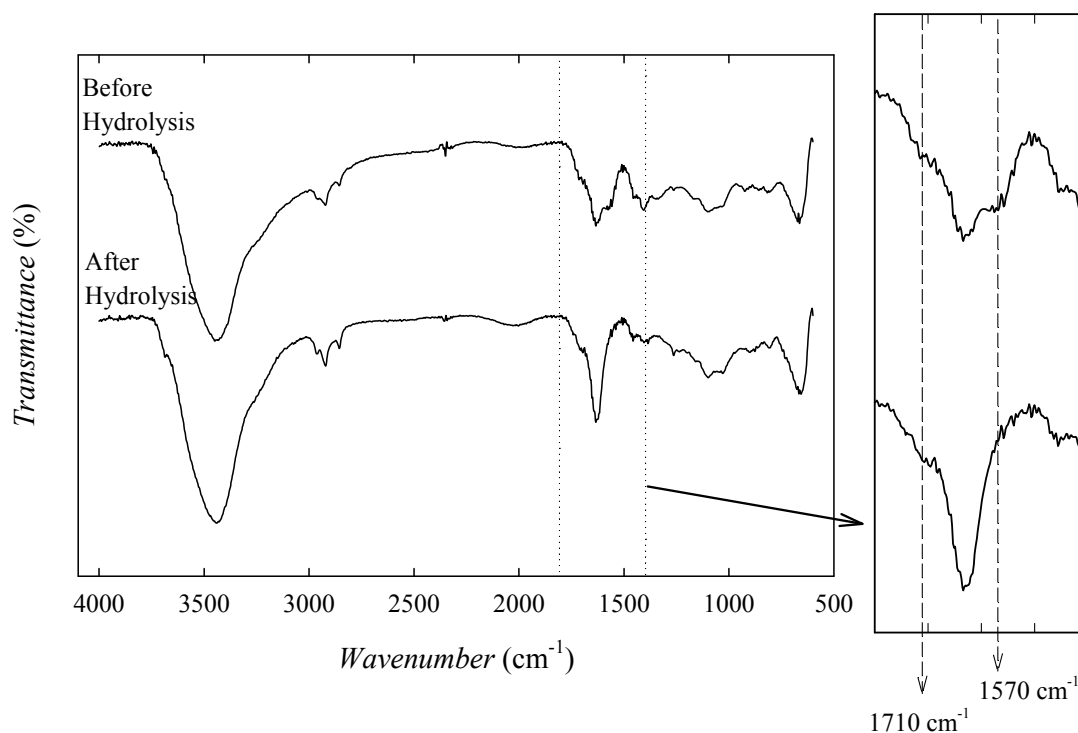


Figure 5.14. The IR Spectra of the UVAIB11 xerogel (0:100 feed ratio of VP:AA) before and after the hydrolysis preformed at $100\text{ }^{\circ}\text{C}$ for 2 hours

5.2.9. Possible Explanations of Anomalous Composition-Dependent Swelling Behavior

The VP/AA gel systems UV-initiated polymerized with various feed weight ratio of VP and AA show anomalous composition-dependent swelling behavior that the maximum q_{ve} was shown in the gels prepared with 40~50 wt. % of feed AA weight. Based in the results of swelling studies, the determination of gelation percents and glass transition temperatures and identifying the molecular structure, the unexpected swelling behavior attempts to describe with two possible explanations.

The H-bonding interactions between VP and AA monomers in the pregel mixture might hinder the gelation during the polymerization, resulting in the lowest gelation % for the gel system obtained with the stoichiometry between two VP and AA components close to 1:1. The H-bonding interactions between VP and AA units might make nice assemble-like structure which can boost the polymerization but not gelation because less chance to meet the crosslinkers around them because of the transient molecular arrangement, resulting in higher molecular weight between crosslinks (M_c) accompanied with lower crosslinking density (v_e), consequently higher q_{ve} .

In addition, the formation of the acid anhydride groups for the gel systems occurs above 40~50 wt. % of C_{AA} during the gelation (see Figure 5.15(b)). During the swelling at room temperature, the structure is expected to be stable, which does not contribute to the increase of osmotic pressure of the hydrogels. With increasing C_{AA} above 40~50 wt. % an increase in anhydride group formation is expected, which results in a higher v_e and smaller M_c , resulting in smaller q_{ve} . For the VP/AA gels prepared with less than C_{AA} 40~50 wt. % where no formation of anhydride groups occurs, increasing C_{AA} causes q_{ve} to increase due to the increase osmotic pressure caused by the dissociation of more COOH groups into COO⁻ and H⁺ as shown in Figure5.15(a).

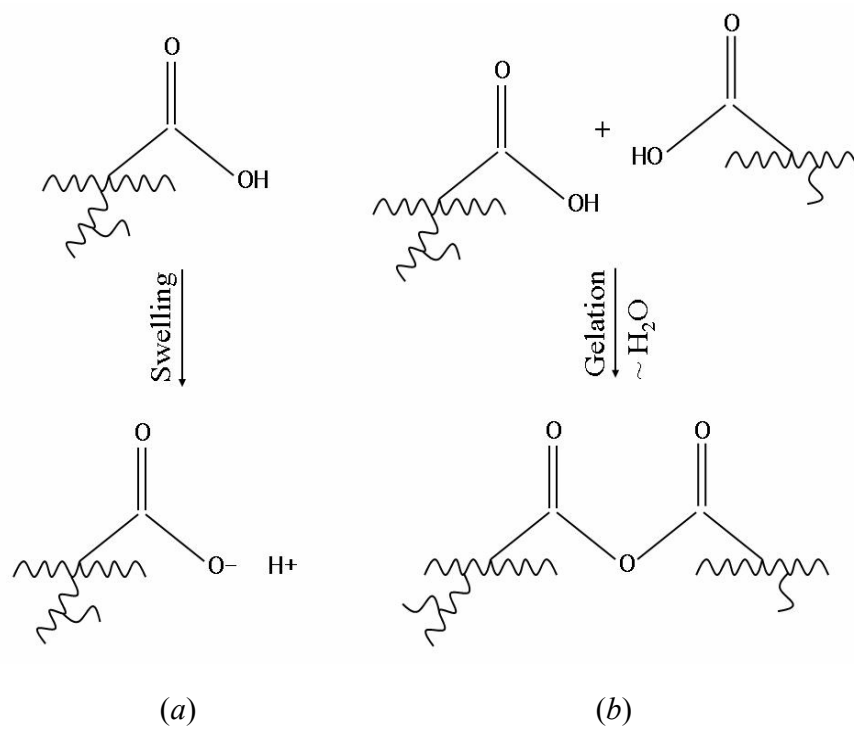


Figure 5.15 A schematic of (a) the molecular structures of the VP/AA gel synthesized with lower C_{AA} (less than 40~50 wt. %) and of the gel after the swelling, and (b) the formation of anhydride group during the synthesis of the gel with higher C_{AA} (higher than 40~50 wt. %) in their network (For easy understanding, only COOH groups are denoted on the chains).

5.3. Effect of Crosslinker Concentration (C_C) and Type on VP/AA hydrogels

From the results of VP/AA gels photo-polymerized with various VP and AA feed weight ratio, it was found out that the VP/AA gels prepared with VP:AA feed weight ratio of 40:60 showed the maximum swelling degree and reasonable mechanical integrity. Thus, the VP/AA gels were utilized for further study.

According to the results of the effect of C_C and crosslinker type on the VP/HEMA hydrogels (see Section 4.1.6.5), it was found that lower concentration of crosslinker produces higher swelling gels and DEGDA gives higher gel swelling ratio (q) than BIS. Here, the effect of the feed concentration and type of crosslinker on the swelling of VP/AA was also investigate to obtain the synthesis condition for the gels having the highest swelling and appropriate mechanical integrity. Figure 5.16 shows the mass swelling ratio (q_m) with swelling time for the VP/AA gels synthesized with varying weight percent of BIS and 0.1 wt. % of DEGDA. The gels synthesized with 0.05 wt. %

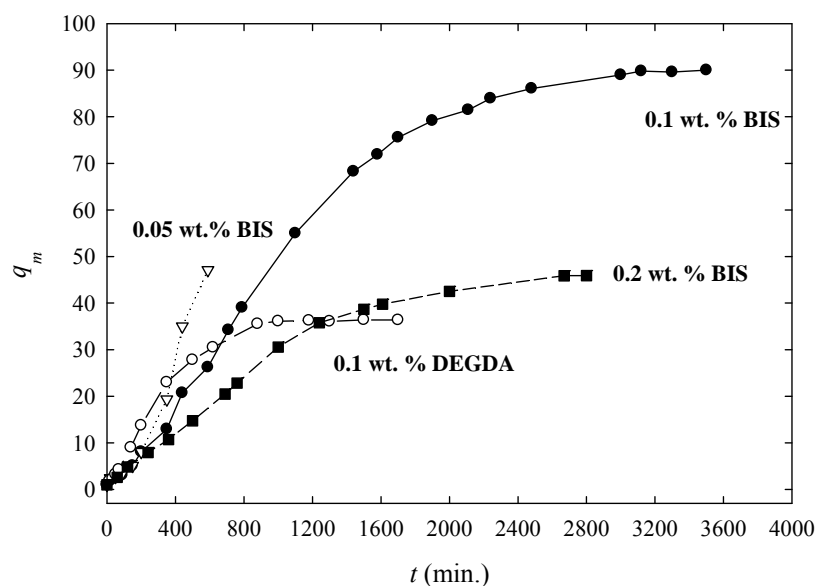


Figure 5.16. The mass swelling ratio of the VP/AA gels synthesized with BIS of 0.05, 0.1, and 0.2 wt. % and DEGDA of 0.1 wt. % as a function of time

(UVAIB5b gels) became mechanically unstable after the q_m reached 46 so the q_m was not able to be monitored. As expected, the gels prepared with lower concentrations of BIS initially swell faster and takes longer time to reach an equilibrium state, but also swell to the higher degree. The values of R_s , t_{max} , q_{ve} and G for the photo-polymerized gels are listed in the Table 5.3. The UVAIB5a gels (prepared with 0.1 wt. % of BIS) produce higher q_{ve} and t_{max} compared with UVAIB5 gels (prepared with 0.2 wt. % of BIS) and UVAID5a gels (prepared with 0.1 wt. % of DEGDA).

Table 5.3. Characteristics of for VP/AA gels photo-polymerized with 0.1 and 0.2 wt. % BIS and 0.1 wt. % DEGDA

Gel code	q_{ve}	G (kPa)	R_s (min ⁻¹)	t_{max} (min./hr./days)
UVAIB5	98.0 ± 9.02	8.68 ± 5.12	0.029	2800/46.7/1.94
UVAIB5a	170 ± 11.1	4.34 ± 1.27	0.047	3120/50.0/2.08
UVAID5a	36.4 ± 2.45	1.61 ± 1.02	0.069	1180/19.7/0.82

It is noticeable that DEGDA produced higher q_{ve} for the VP/HEMA gels than BIS but lower q_{ve} for the VP/AA gels than BIS even if it swells faster in the beginning as expected. This is attempted to explain below by the Hansen solubility parameters discussed in Section 4.1.6.5. It is suggested in the section that the difference between each Hansen solubility parameter component of the crosslinker and monomers used for synthesis can qualitatively indicates relative degree of crosslinking and swelling ratio. The Hansen solubility parameters for VP, AA, BIS, and DEGDA predicted by the group contributions using the method of Hoftyzer and Krevelen are listed in Table 5.4. And the difference between each Hansen solubility parameter of VP and crosslinkers (BIS or

DEGDA) and that of and AA and crosslinkers are listed in Table 5.5. The values of the solubility difference between BIS and the monomer are the smallest which means the greatest amount of compatibility, resulting in higher crosslinking degree (lower q_{ve}). However, comparing polar components of the difference in the solubility parameter of AA and crosslinker $|\delta_p^{AA} - \delta_p^{CX}|$, the value for DEGDA is smaller than for BIS. It is thought that this might be responsible for the higher crosslinking degree of VP/AA gels crosslinked with DEGDA and smaller q_{ve} as shown in the Figure 5.16.

Table 5.4. Hansen solubility parameters for VP, AA, BIS, and DEGDA

Components	δ_t (J ^{1/2} /cm ^{3/2})	δ_d (J ^{1/2} /cm ^{3/2})	δ_p (J ^{1/2} /cm ^{3/2})	δ_h (J ^{1/2} /cm ^{3/2})
VP	28.3	22.4	14.4	9.53
AA	26.1	20.9	7.78	13.6
BIS	23.9	19.9	9.47	9.25
DEGDA	20.8	17.6	9.19	8.51

Table 5.5. Difference between each Hansen solubility parameter of VP and crosslinker (BIS and DEGDA) and AA and crosslinker (BIS and DEGDA)

System	$ \delta_t^{Mo} - \delta_t^{CX} $ (J ^{1/2} /cm ^{3/2})	$ \delta_d^{Mo} - \delta_d^{CX} $ (J ^{1/2} /cm ^{3/2})	$ \delta_p^{Mo} - \delta_p^{CX} $ (J ^{1/2} /cm ^{3/2})	$ \delta_h^{Mo} - \delta_h^{CX} $ (J ^{1/2} /cm ^{3/2})
VP-BIS	4.40	2.50	4.93	0.28
VP-DEGDA	7.50	4.80	5.21	1.02
AA-BIS	2.20	1.00	1.69	4.35
AA-DEGDA	5.30	3.30	1.41	5.09

5.4. Final Optimization of the VP/AA Gel System for Anisotropic Swelling: Effect of C_I on the Swelling of the Gels by UV-initiated and Thermal Polymerizations

Of the system studied the VP/AA gel system synthesized with the VP:AA feed weight ratio of 40:60, the 0.8 wt. % Irgacure 651 and 0.1 wt. % BIS by UV-initiated polymerization (UVAIB5a) is the most desirable properties such as the highest swelling degree as well as slower swelling rate and reasonable mechanical stiffness. However, the size of the gels photo-polymerized was not found to be to the post-processing of the a gel for anisotropic swelling studies, therefore thermal polymerization for preparing VP/AA gels is using while keeping the VP and AA feed weight ratio of 60:40 and 0.1 wt. % crosslinker since as it was found from the previous work that the swelling behavior depending on the monomer composition and on the crosslinker concentration show the same trend regardless of polymerization method. However, the swelling behavior depending on the initiator concentration can be different depending on the polymerization method (either thermal or UV polymerization) as mentioned in section 4.1. Consequently, the effect initiator concentration and type on the swelling behavior of the VP/AA gels for photo- and thermal polymerizations was investigated and compared to obtain the gel system with desirable properties

The same type of an initiator, azo-bis-isobutyronitrile (AIBN), was used for exact comparison of polymerization method. Prior to this work, the swelling behavior of the VP/AA gels UV-initiated polymerized with either 0.8 wt. % Irgacure 651 or 0.8 wt. % AIBN (UVAIB5a and UVAAB5a gels, respectively) was compared since Irgacure 651 has been used for swelling studies for UV-cured gels but thermally cured gels needed to be prepared for the studies of direct comparison between polymerization methods. As illustrated in Figure 5.17, the UVAAB5a gels produce the larger q_{ve} (~1.5 times higher than that of UVAIB5a) and R_s (~2.3 times faster than that of UVAIB5a) and take longer time to reach maximum swollen state ($t_{max} = 7110$ min. (4.94 days), ~2.5 times longer than that of UVAIB5a),

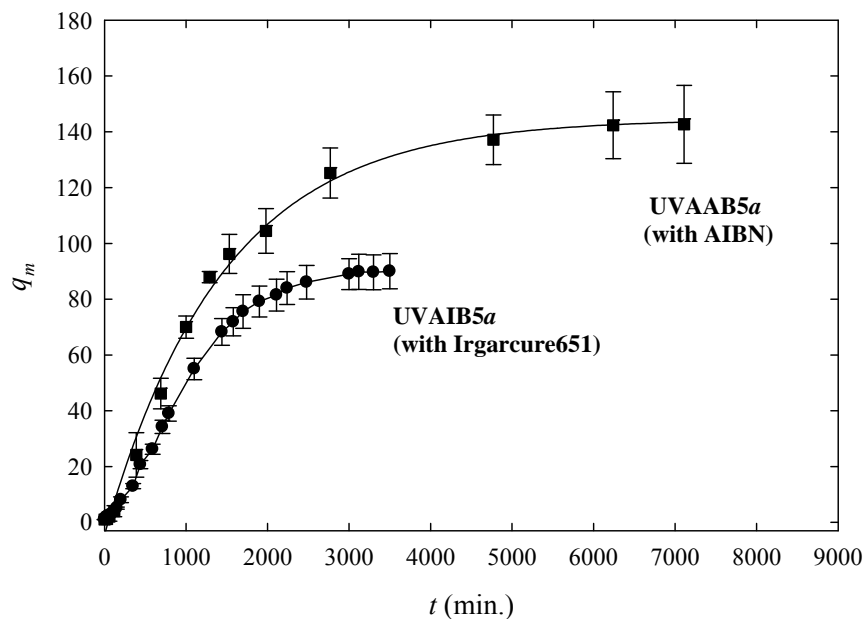


Figure 5.17. The mass swelling ratio (q_m) of the VP/AA gels synthesized with AIBN and Irgarcure 651 of 0.8 wt. % as a function of time

With various concentration of AIBN, the VP/AA gels were prepared by photo- and thermal polymerizations. As shown in Figure 5.18, overall the gels synthesized by UV irradiation swell to a higher degree and faster. Photo-polymerized VP/AA (UVAAB) gels synthesized by smaller C_I swell less and slower, resulting in the smaller q_{ve} (see Figure 5.19) as well as lower R_s and shorter t_{max} (see Figures 5.20 (a) and (b)). This is the opposite behavior to the well known tendency observed in the gel systems prepared by thermally-initiated free-radical polymerization [23, 24]. This is explained more in detail in Section 4.1.6.2, with the lower crosslinking density (v_e) (or the higher molecular weight between crosslinks (M_c)) caused by a gel network structure with dangling chains that is obtained in the UV-initiated polymerization inducing fast reaction kinetics [25]. In the thermal polymerization, with increasing C_I , the M_c decreases, resulting in smaller q_{ve} .

As shown in Figure 5.18, thermally polymerized gels (TVAABV gels) swell to higher and faster with decreasing C_I , which is the opposite result to the case of the photo-polymerized gels. The reason is explained in Section 4.1.6.2. Moreover, TVAABV gels takes much longer times to reach to the maximum swelling than that of photo-polymerized gels.

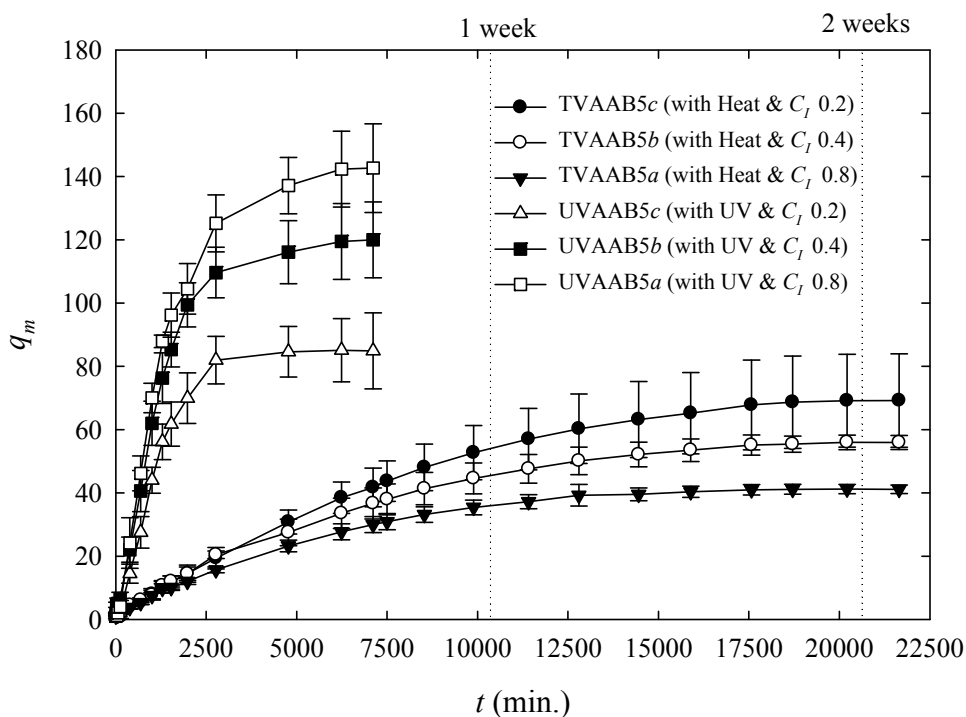


Figure 5.18. The mass swelling ratio (q_m) of the VP/AA gels synthesized with various weight % of initiator (AIBN) by UV-initiated (UV) and thermal (Heat) polymerizations.

Figure 5.19 compares q_{ve} values obtained from photo-polymerized VP/AA (UVAAB) gels and the thermal polymerized (TVAAB) gels synthesized with 0.2, 0.4, and 0.8 wt. % of AIBN. The q_{ve} values of all UVAAB gels are higher than TVAAB gels. With decreasing C_I from 0.8 wt. % to 0.2 wt. %, the q_{ve} values of UVAAB gels increase from 140 ± 19 to 240 ± 23.3 , respectively, and those of TVAAB gels increase from 67.4 ± 8.21 to 113 ± 24.2 , respectively.

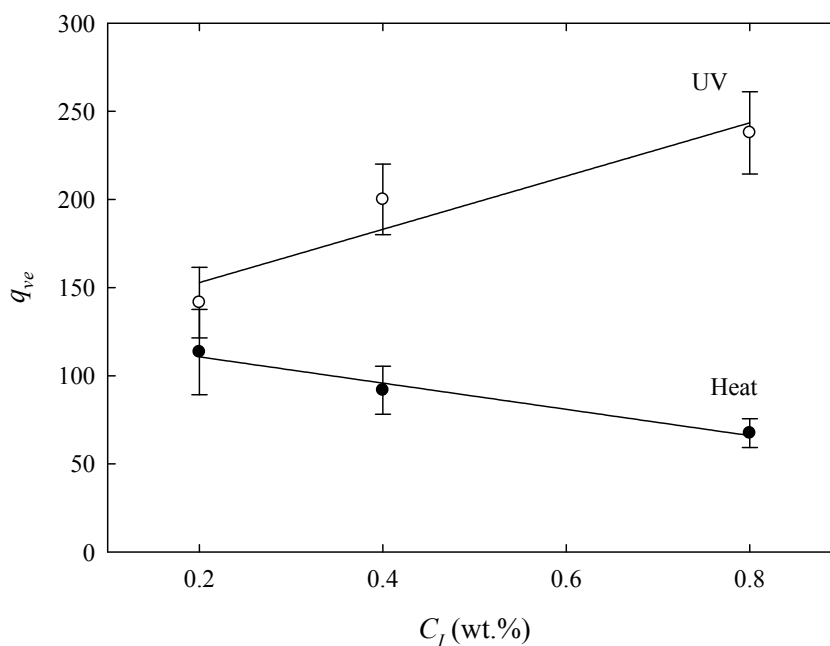


Figure 5.19. The q_{ve} of VP/AA gels UV-initiated (UV) and thermally (Heat) polymerized with initiator concentration of 0.2, 0.4, and 0.8 weight %.

Figures 5.20 (a) and (b) illustrate the R_s and t_{max} values, respectively, of the photo-polymerized VP/AA (UVAAB) gels and thermal polymerized (TVAAB) gels synthesized with the AIBN feed weight of 0.2, 0.4, and 0.8 wt. %. With decreasing C_I

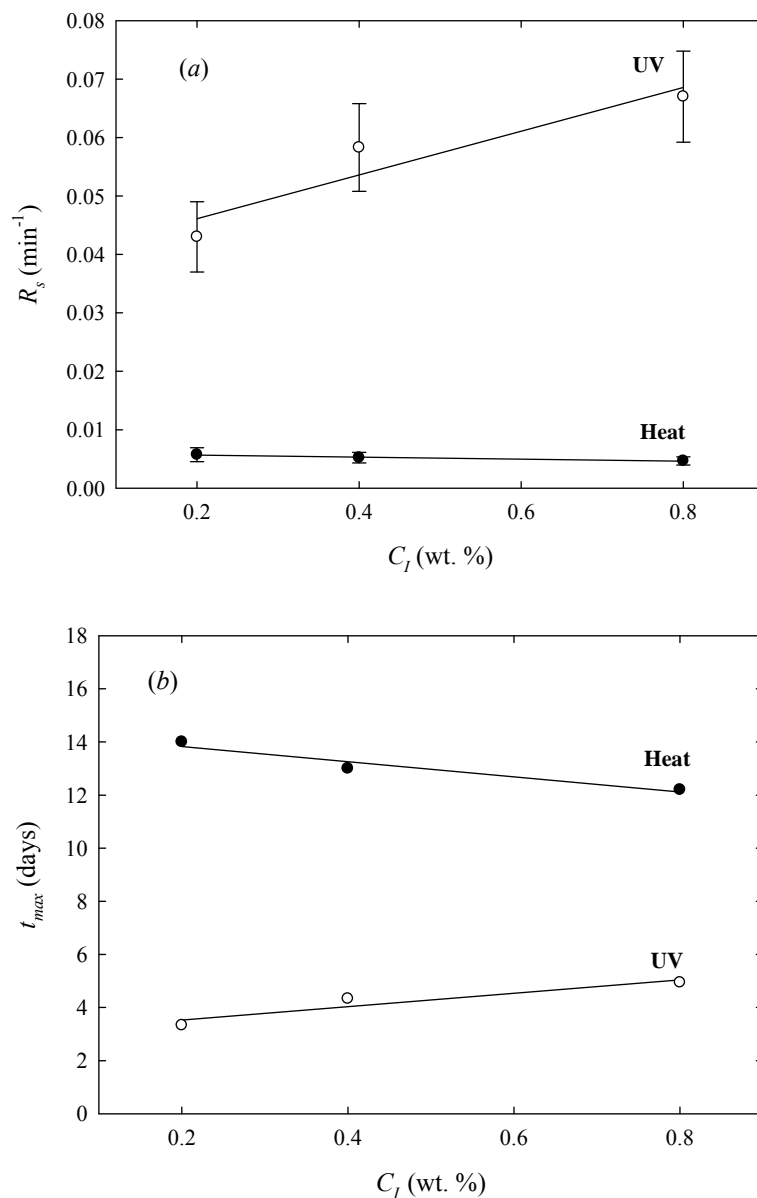


Figure 5.20. The (a) R_s and (b) t_{max} of VP/AA gels UV-initiated (UV) and thermally (Heat) polymerized with initiator concentration of 0.2, 0.4, and 0.8 weight %.

from 0.8 wt % to 0.2 wt. %, the R_s values of UVAAB gels decrease from $0.067 \pm 0.008 \text{ min}^{-1}$ to $0.043 \pm 0.006 \text{ min}^{-1}$, respectively and those of TVAAB gels slightly increase from $0.0047 \pm 0.0007 \text{ min}^{-1}$, to $0.0057 \pm 0.0012 \text{ min}^{-1}$, respectively. The R_s values of UVAAB gels are 8~14 times higher than those of TVAAB gels, which is considered to be due to the lower crosslinking density of UVAAB gels. With decreasing C_I from 0.8 wt % to 0.2 wt. %, the t_{max} values of UVAAB gels decrease from 4.94 days to 3.33 days, respectively, and those of TVAAB gels increase from 12.2 days to 14 days, respectively.

Although, it seems that all three TVAAB gels have quite high q_{ve} and long t_{max} , among these gels only the one system having optimal properties was selected by determining mechanical properties such as toughness and stiffness for the anisotropic swelling studies. As shown in Figure 5.21, the TVAAB gel producing highest swelling (TVAAB5c, $q_{ve} \sim 113$) has the smaller G ($\sim 3.5 \text{ kPa}$) but highest toughness ($\sim 110 \text{ J/m}^3$). By comparison, the TVAAB gel producing lowest swelling (TVAAB5a, $q_{ve} \sim 67$) has the

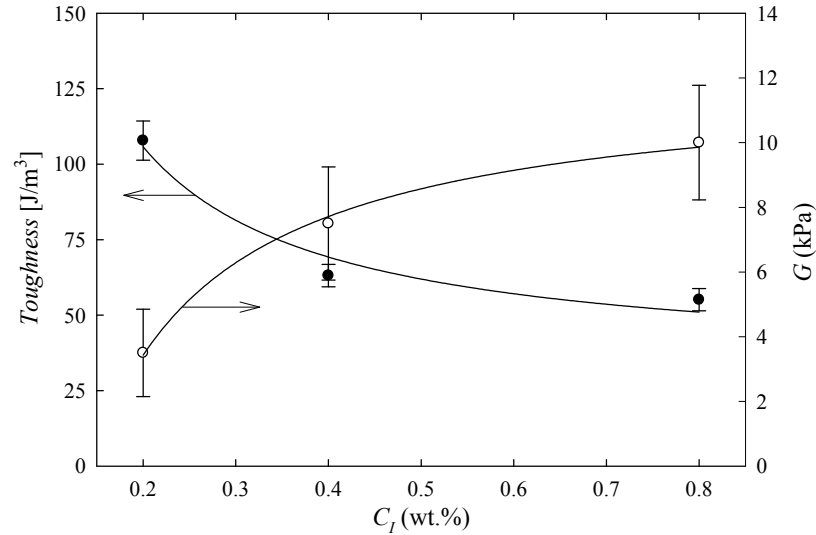


Figure 5.21. Toughness and Modulus of TVAAB gels thermally polymerized with initiator concentration of 0.2, 0.4, and 0.8 weight %.

smaller G (~ 10 kPa) but highest toughness (~ 55 J/m³). It is obvious that the gel with highest G as well as highest toughness is desirable for the use of tissue expansion. For these reasons, the TVAAB5b gel system is determined to be the best in both properties.

The TVAAB5b gel system was therefore utilized for the anisotropic swelling studies for the development of anisotropic swelling hydrogel having a potential for the use for tissue expansion. The synthesis conditions determined and the characteristic properties measured or calculated of TVAAB5b gels are listed in Table 5.6.

Table 5.6. The synthesis conditions and characteristic properties of the optimized gel system, TVAAB5b gel

Gel Code	Synthesis Conditions	
TVAAB5b	Synthesis Method	Thermal Induced Free Radical Polymerization With Solvent
	VP:AA feed weight (molar) ratio	40:60 (1:1)
	Initiator Type	AIBN
	C_I (wt. %)	0.4
	Crosslinker Type	BIS
	C_C (wt. %)	0.1
	Measured Characteristic Properties	
	q_{ve}	91.7 ± 13.6
	G (kPa)	7.50 ± 1.75
	Toughness (J/m ³)	65.0 ± 3.71
	R_s (min ⁻¹)	0.0052 ± 0.0009
	t_{max} (days)	13.0 ± 0.40
	Gel ρ (g/cm ³)	1.21 ± 0.01
	T_g (°C)	130
	Calculated Characteristic Properties	
	v_e (mol/cm ³)	6.71×10^{-7}
	M_c (g/mol)	1.80×10^6
	D (cm ² /s)	1.85×10^{-7}
	n	0.77 ± 0.02
	χ	0.496 ± 0.011

5.5. Conclusion

For various VP/AA copolymeric hydrogels synthesized with increasing AA weight ratio from 10 wt. % to 100 wt. % by UV-initiated polymerization, anomalous swelling behavior was found. Contrary to expectations based on published data and theory that with increasing AA weight percent the equilibrium volume swelling ratio increases, VP/AA hydrogels showed a distinct maximum q_{ve} with a corresponding minimum in G values for C_{AA} of 40-60 wt. %. It is thought that the anomalous monomer composition-dependent swelling behavior might be caused because of the H-bonding interaction between VP and AA monomers which ultimately at the stoichiometry of VP:AA of 1:1 result in the higher M_c via the polymerization like the “zipper effect”. From analysis of chemical molecular structure by FTIR spectroscopy, the existence of anhydride groups formed in the gels synthesized with AA weight ratio above approximately 40~60 wt. % could be partially responsible for the anomalous composition-dependent swelling behavior. The existence of anhydride group formed in the bulk polymerization might induce higher crosslinking density, which could lead to the low degree of swelling.

As observed for VP/HEMA hydrogels, the VP/AA gels prepared with lower crosslinker concentrations showed higher degree of swelling. However, the VP/AA gels crosslinked with BIS showed higher degree of swelling than the gels crosslinked with DEGDA. By considering the Hansen solubility parameters, it is thought that this might be caused by stronger polar forces between AA and DEGDA, which is considered to have higher crosslinking density and lower degree of swelling compared with those between AA and BIS. In this study, the VP/AA gels crosslinked with 0.1 wt. % BIS showed highest swelling degree and appropriate mechanical stiffness. It was shown that the photo-polymerized VP/AA gels prepared using AIBN initiator showed higher degree

of swelling and longer time to reach an equilibrium state (t_{max}) than the gels prepared with Irgacure 651 (UV-sensitive photoinitiator).

A study of the effect of the concentration (0.2, 0.4 and 0.8 wt. %) of AIBN initiator on the swelling behavior of the gels synthesized by both UV-initiated and thermal polymerization was carried out. Thermally polymerized VP/AA gels show somewhat lower degree of swelling than the UV-polymerized, however they still have quite higher degree of swelling ($q_{ve} = 67-113$) than that of hydrogel system presently commercially used for the tissue expansions (q_{ve} of VP/MMA = 10-25). Moreover, the thermally polymerized gels initially swell quite slowly and have longer t_{max} , about 12 -15 days. Based on the report [26] the determined values of t_{max} for the *in vivo* studies are between 1.3 and 1.6 slower than that *in vitro*. Accordingly, it is expected that the t_{max} of VP/AA gels for the *in vivo* studies can be between 15.6 days and 24 days, which is at the moment not the exact time range for the use of tissue expansion to avoid tissue death (6~8 weeks). However, this work is on the right tack but needs more work.

As seen in the study of the effect of initiator concentration on the swelling of VP/HEMA gels, it was confirmed that the photo-polymerized gels prepared with higher initiator concentration exhibit a higher degree of swelling, which might be due to lower crosslinking density caused by more dangling chains in the gel network. In addition, the thermal polymerized gels prepared with higher initiator concentration show lower degree of swelling due to longer molecular weights between crosslinks, as expected from the published literatures. Although the thermally polymerized gels prepared with lower initiator concentration (0.2 wt. %) show higher swelling, when the toughness and modulus were considered, the thermally polymerized gels prepared with 0.4 wt. % initiator were finally determined to be the system with optimal properties. Therefore, the VP/AA prepared with VP and AA weight ratio of 60:40, 0.1 wt. % BIS crosslinker and 0.4 wt. % AIBN initiator by thermally polymerization was utilized for the anisotropy swelling studies discussed in Chapter 7.

References

- [1]. Fredric L. Buchholtz and Nicholas A. Peppas, Superabsorbent polymers: science and technology, *American Chemical Society*, Washington, DC, 1994.
- [2]. Ying Zhao, Juan Kang, and Tianwei Tan, "Salt-, pH-and temperature-responsive semi-interpenetrating polymer network hydrogel based on poly (aspartic acid) and poly (acrylic acid)", *Polymer*, vol. 47, pp. 7702-7710, 2006.
- [3]. Safaa G. Abd Alla, Horia M. Nizam El-Din, Abdel Wahab M. El-Naggar, "Structure and swelling-release behaviour of poly (vinyl pyrrolidone)(PVP) and acrylic acid (AAc) copolymer hydrogels prepared by gamma irradiation", *European Polymer Journal*, vol. 43, pp. 2987-2998, 2007.
- [4]. Flory, P. J., in Principles of Polymer Chemistry; Cornell University Press: New York; 1969.
- [5]. Declan M. Devine, Sinead M. Devery, John G. Lyons, Luke M. Geever, James E. Kennedy and Clement L. Higginbotham, "The synthesis, characterisation, phase behaviour and swelling of temperature sensitive physically crosslinked poly (1-vinyl-2-pyrrolidinone)/poly (N-isopropylacrylamide) hydrogels", *European Polymer Journal*, vol. 42, pp. 69-80, 2006.
- [6]. Sanjeeb Kumar Sahoo, Tapas K. De, P. K. Ghosh, and Amarnath Maitra, "pH-and thermo-sensitive hydrogel nanoparticles", *Journal of Colloid and Interface Science*, vol. 206, pp. 361-368, 1998.
- [7]. Eugen Barbu, Indrajeetsinh Sarvaiya, Keith L Green, Thomas G Nevell, John Tsibouklis, "Vinylpyrrolidone-co-(meth) acrylic Acid Inserts for Ocular Drug Delivery: Synthesis and Evaluation", *J. Biomed Mater Res*, vol. 74A, pp. 598-606, 2005.
- [8]. Turcer Cayjara and Ömer Kantoğlu, "Thermal behavior and network structure of poly(N-vinyl-2-pyrrolidone-crotonic Acid) hydrogels prepared by radiation-induced polymerization", *Polym. Adv. Technol.*, vol. 15, pp. 134-139, 2004.
- [9]. M. Sen and O. Güven, "Prediction of swelling behaviour of hydrogels containing diprotic acid moieties", *Polymer*, vol. 39(5), pp. 1165-1172, 1998.

- [10]. James E. Mark and B. Erman, Rubberlike Elasticity: A Molecular Primer, John Wiley and Sons, Inc, 1988.
- [11]. Ferenc Horkay, Ichiji Tasaki, and Peter J. Basser, "Osmotic Swelling of Polyacrylate Hydrogels in Physiological Salt Solutions, *Biomacromolecules*, vol.1, pp.84-90, 2000.
- [12]. K. Takahashi, T. Takigawa, and T. Masuda, "Swelling and deswelling kinetics of poly (N-isopropylacrylamide) gels", *J. Chemical Physics*, vol. 120(6), pp. 2972-2979, 2004.
- [13]. T. J. Alfrey, E. F. Gurnee and W. G. Lloyd, "Diffusion in glassy polymers", *Journal of Polymer Science*, vol. 12, pp. 249, 1966.
- [14]. Artur Henke, Slawomir Kalubowski, Piotr Ulanski, Janusz M Rosiak, and Karl-Friedrich Arndt, " Radiation-Induced Crosslinking of Polyvinylpyrrolidone-Poly(acrylic acid) Complex", *Nuclear Instruments and Methods in Physics Research B*, vol. 236, pp. 391-398, 2005.
- [15]. Nicolas Gatica, Natali Fernandez, Alejandra Opazo, and Deodato Radic, "Synthesis and Characterization of Functionalized vinyl Copolymers I. Structure-Monomer Reactivity Relationship in Copolymer Containing N-vinyl-2-pyrrolidone Moieties" *J. Chil. Chem. Soc.*, vol. 50, pp. 581-585, 2005.
- [16]. Shuping Jin Mingzhu Liu, Fen Zhang, Silan Chen, and Aizhen Niu, " Synthesis and Characterization of pH-sensitivity semi-IPN Hydrogel Based on Hydrogen bond between Poly(N-vinyl pyrrolidone) and Poly(acrylic acid)", *Polymer*, vol. 47, pp. 1526-1532, 2006.
- [17]. Myung-Kwan Chun, Chong-Su Cho, Hoo-Kyun Choi , "Mucoadhesive drug carrier based on interpolymers complex of poly(vinyl pyrrolidone) and poly(acrylic acid) prepared by template polymerization", *Journal of Controlled Release*, vol. 81, pp. 327-334, 2002.
- [18]. Declan M. Devine and Clement L. Higginbotham, "Synthesis and characterisation of chemically crosslinked N-vinyl pyrrolidone based hydrogels", *European Polymer Journal*, vol. 41, pp. 1272-1279, 2005.
- [19]. S. K. Bajpai and Seema Dubey, "In vitro dissolution studies for release of vitamin B₁₂ from poly(N-vinyl-2-pyrrolidone-co-acrylic acid) hydrogels", *Reactive &*

Functional Polymers, vol. 62 pp. 93–104, 2005.

- [20]. Hsin-Cheng Chiu, Yi-Fong Lin, and Yuan-Hung Hsu, “Effects of acrylic acid on preparation and swelling properties of pH-sensitive dextran hydrogels”, *Biomaterials*, vol. 23, pp.1103–1112, 2003.
- [21]. H. Blanco-Fuente, S. Anguiano-Igea, F. J. Otero-Espinar and J. Blanco-Mendez, “Kinetics of anhydride formation in xerogels of poly(acrylic acid)”, *Biomaterials*, vol. 17, pp.1667-1675, 1996.
- [22]. S. Kottle and M. C. McGaugh, “The thermal degradation of poly(acrylic acid)”, *Polymer Letter*, vol. 5, pp. 817-820, 1967.
- [23]. J. T. Chung, K. D. F. Vlugt-Wensink, W. E. Hennink, and Z. Zhang, “Effect of polymerization conditions on the network properties of dex-HEMA microspheres and macro-hydrogels”, *Int. J. Pharm.*, vol. 288, pp.51-61, 2005.
- [24]. H. Omidian and K. Park, “Experimental design for the synthesis of polyacrylamide superporous hydrogels”, *Journal of Bioactive and Compatible Polymers*, vol.17, pp. 433-450, 2002.
- [25]. J. Hannah Lee and David G. Bucknall, “Swelling behaviour of hydrogels synthesized using controlled UV-initiated free radical polymerization”, *Journal of Polymer Science B: Polymer Physics*, vol. 46(14), pp. 1450-1462, 2008.
- [26]. Marc Sawn, Anisotropic Self-inflating Tissue Expanders in Reconstructive Plastic Surgery, DPhil thesis, Trinity College of University of Oxford for the degree, submitted 2008.

CHAPTER VI

CONTROL OVER SWELLING RATE OF OTHER GEL SYSTEMS

It was found that the incorporation of ionic AA moieties instead of HEMA units into VP based network reduced the swelling rate of gels. In this chapter, other attempts to control and slow down the swelling rate of hydrogel are discussed using the VP/HEMA hydrogel system. Many studies of the swelling rate have focused on increasing swelling or deswelling rates, namely fast stimuli-sensitive response, for applications such as drug delivery systems, actuators or sensors [1, 2, 3]. Superporous hydrogel systems are a representative example [4, 5], which has very large and fast swelling behavior and is used in many drug delivery systems. However, not many studies on reduced swelling have been reported. For tissue expansion, materials the swelling rate must be slow enough to avoid interfering in cell liability and growth. The target time to reach fully swollen state for tissue expansion is around 4 week sand 8 weeks in-vivo. The optimized hydrogels (Chapter 5) in this study talk about 2 weeks to reach an equilibrium state. Consequently, methods to control or reduce the swelling rate have been investigated. In this chapter the gels comprising hydrophobic moieties, gel composites with the silver nanoparticles, the gels encapsulated with elastomer films, and finally the multilayers of alternating elastomer films and polymeric gels are discussed.

6.1. VP Based Gels with Hydrophobic Species

Hydrogels are the materials composed of hydrophilic species to absorb a aqueous media. However, recently the inclusion of hydrophobic moieties in hydrogel systems, resulting in the amphiphilic hydrogels, has been investigated [6-9] because the hydrophobic moieties can interact or dissolve hydrophobic or amphiphilic drugs. It has

been reported that PEG based polymers with hydrophobic moieties or biopolymers with hydrophobic moieties also can attach with hydrophobic drugs [10, 11], thus the hydrogels can be used as drug carriers.

Hill and coworkers [8] studied the effect of hydrophobic moieties in hydroxyethyl methacrylate (HEMA) copolymeric hydrogels on their swelling behavior and showed that hydrogels of methyl methacrylate (MMA) and HEMA have higher equilibrium swelling ratios and diffusion coefficient (D) values than hydrogels of butyl methacrylate (BMA) and HEMA or hydrogel of cyclohexyl methacrylate (CHMA) and HEMA.

The swelling behavior of amphiphilic terpolymeric hydrogels of N-isopropylacrylamide (NIPAAm), PEG and dodecyl methacrylate (DOMA) was studied by Viera and coworkers [10]. The system displayed a LCST caused by the NIPAAm units. The values of the critical temperature can be varied by both the composition between NIPAAm and DOMA and the self-aggregation occurred due to the hydrophobic DOMA units.

In this study, the effect of hydrophobicity on their swelling behavior, mechanical stiffness and structure characteristics of photo-polymerized the N-vinylpyrrolidone (VP) based hydrogels was investigated. Specifically, their swelling rate was characterized and compared by determining the swelling rate (R_s) and time to reach to fully swollen state (t_{max}). The hydrophilicity of VP based hydrogels was varied by copolymerizing with various methacrylates with different alkyl group lengths. The feed weight ratio of VP and methacrylate, concentration of Irgacure 651 initiator and concentration of BIS crosslinker in all systems were held constant is 90:10, 0.8 wt. %, and 0.2 wt. %, respectively. The various methacrylate used in this work were methyl methacrylate (MMA), butyl methacrylate (BMA), octyl methacrylate (OMA) and lauryl methacrylate (LMA).

6.1.1. Swelling Studies

The swelling behavior with time of the four copolymer gels composed of VP and the various MA and the UVHIB3 gel are shown in Figure 6.1. The synthesis conditions for four VP/MA gels and the chemical structure of various methacrylates are shown in Table 3.6 and Figure 3.3 (see Section 3.1.3). The degree of swelling of the UVMIB3 gels is higher than other VP/MA gels, which is probably due to relatively more hydrophilic properties of MMA. However, the UVMIB3 gels with MMA swell more than UVHIB3

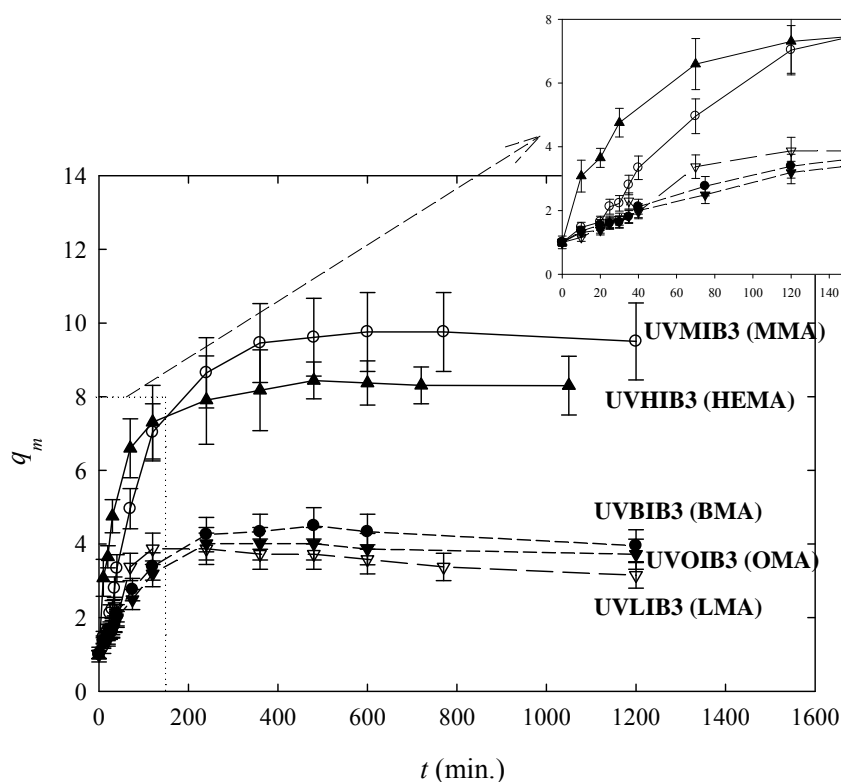


Figure 6.1. The mass swelling ratio (q_m) of UVMIB3, UVBIB3, UVOIB3, UVLIB3, and UVHIB3 as a function of swelling time (the inserted figure shows the enlarged initial swelling behavior of the gels up to the swelling time 150 min.).

gels with HEMA, which is unexpected since HEMA is more hydrophilic than MMA. This needs to be studied more. The q_{ve} of the four different VP/MA gels are shown in Figure 6.2 as a function of the number of carbon (C) in the alkyl group of each methacrylate incorporated in the corresponding gel. The q_{ve} values geometrically decrease with increasing C with the following relationship: $q_{ve} = a_1 + a_2 / C + a_3 / C^2$, where the coefficients a_1 , a_2 , and a_3 can be determined for the number of C . The determined coefficient values of a_1 , a_2 , and a_3 are 4.24 ± 0.82 , 4.58 ± 5.98 , and 6.01 ± 5.28 , respectively.

As expected, compared to the UVHIB3 gels, the VP/MA (UVHIB3) gels swell more slowly (see Figure 6.1). Overall the VP/MA gels initially swell fast in the at short times (0-100 minutes) and reaches the fully swollen state between 120 minutes and 600 minutes depending on the system.

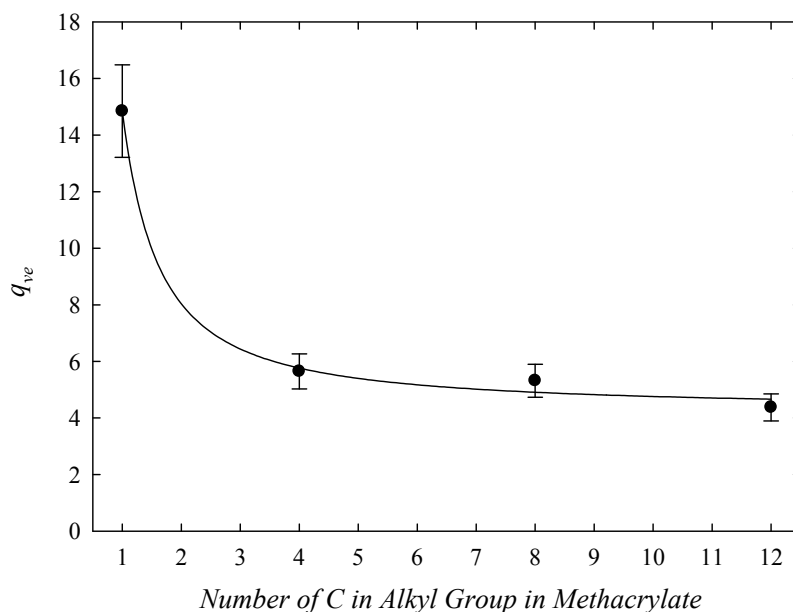


Figure 6.2. The q_{ve} and G of VP/MA hydrogels as a function of the number of carbon (C) in the alkyl group of each methacrylate.

Figure 6.3 shows the R_s and t_{max} of the various VP/MA gels. The UVMIB3 gels yield the fastest R_s ($\sim 0.057 \text{ min}^{-1}$) (which is even faster than that of UVHIB3 gels ($\sim 0.038 \text{ min}^{-1}$)), and the longest t_{max} (~ 600 minutes, 10 hours), while UVLIB3 gels yield the slowest R_s ($\sim 0.024 \text{ min}^{-1}$) and the shortest t_{max} (~ 120 minutes, 2 hours).

Clearly the hydrogels with more hydrophobicity have smaller values of R_s and t_{max} as well as smaller values of q_{ve} . More hydrophobic comonomer units are expected to obstruct more the initial diffusion of aqueous medium into the hydrogels due to less compatibility with the aqueous medium, resulting in smaller R_s . The weaker interaction

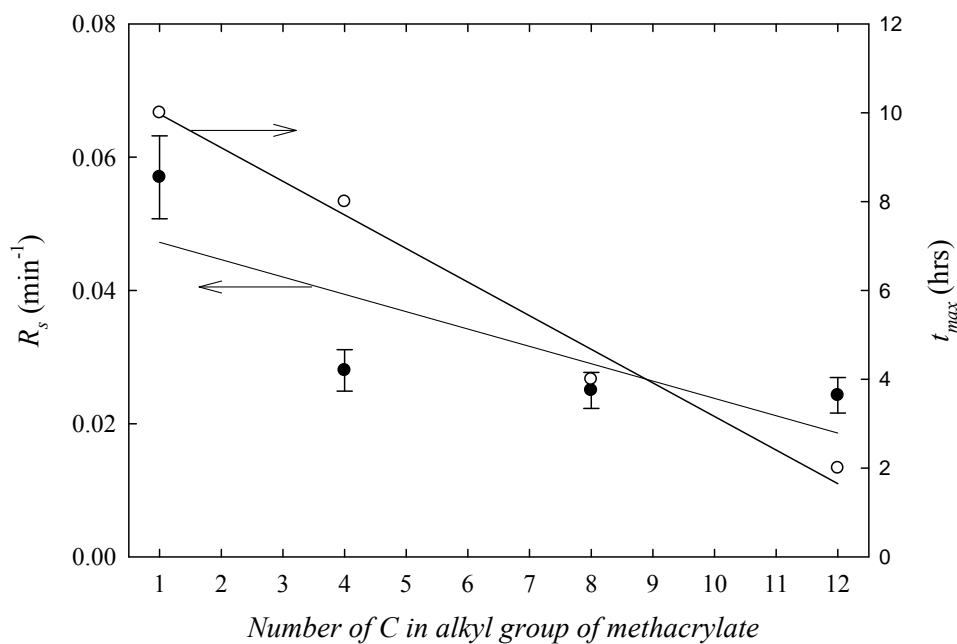


Figure 6.3. The R_s (●) and t_{max} (○) of VP/MA hydrogels as a function of the number of carbon (C) in the alkyl group of each methacrylate.

between aqueous medium and polymer in the equilibrium state results in smaller q_{ve} and larger χ values (see Figure 6.4). A polymer solution system with higher χ value has reduced interactions between the polymer and the solvent and increased polymer-polymer interactions [12, 13]. The UVLIB3 hydrogels with LMA possesses the highest χ values calculated using Equation (22), and the lowest q_{ve} values. In this case the longer alkyl groups (more hydrophobic molecules) interact and aggregate more, which induce more phase separation and consequently greater opacity. The aggregation also causes an increase in crosslinking density and accordingly a reduction in the degree of swelling.

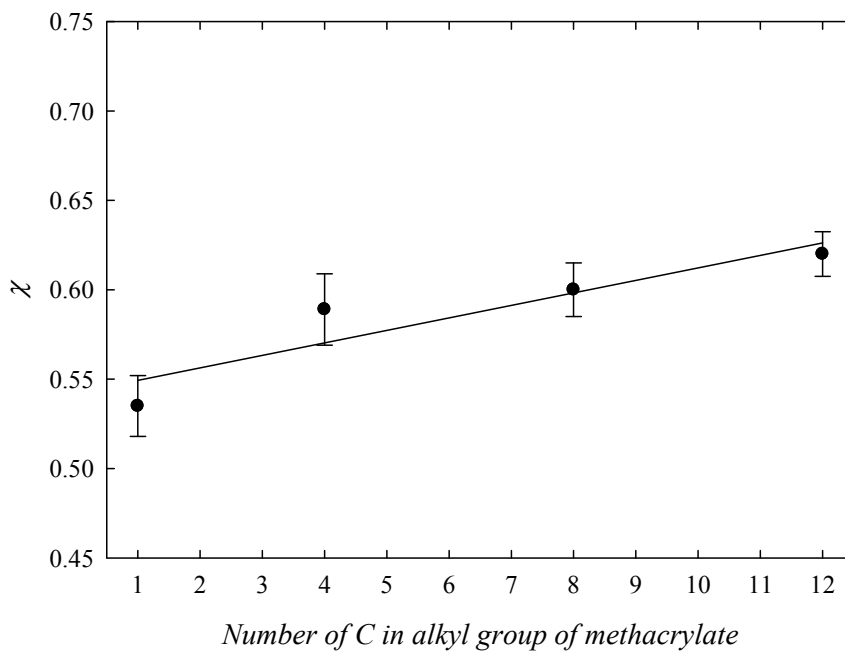


Figure 6.4. The of VP/MA hydrogels as a function of the number of carbon (C) in the alkyl group of each methacrylate

6.1.2. Mechanical Stiffness and Structural Parameters (M_c and ν_e)

Figure 6.5 depicts the G values of the four different VP/MA copolymer hydrogels as a function of the number of alkyl carbons (C). The G values increase linearly with increasing number of carbon because the hydrogels with longer alkyl groups absorb less water due to increased aggregation regions within hydrophobic alkyl groups. These aggregated parts act as reinforcement for the hydrogels. The UVLIB3 hydrogels with the largest number of carbons in the alkyl group have the highest G of 760 kPa, while UVMIB3 hydrogels with the lowest number of carbons have the smallest G of 75 kPa. These values of G are larger than that for the UVHIB3 hydrogels (19 kPa), which is thought to be caused by the aggregation of hydrophobic species causing reinforcement.

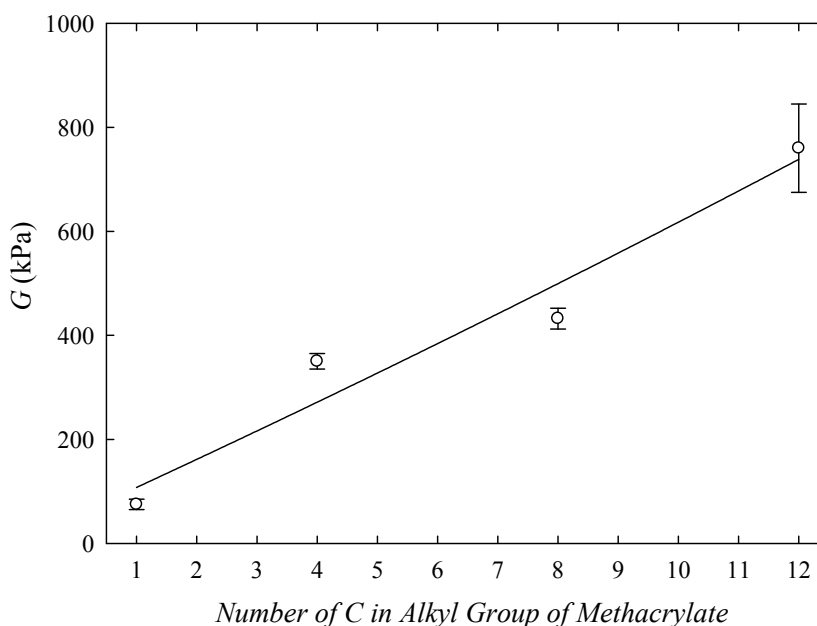


Figure 6.5. The G of VP/MA hydrogels as a function of the number of carbon (C) in the alkyl group of each methacrylate

Based on the measured values of q_{ve} and G , the molecular weight between crosslinks (M_c) and crosslinking density (v_e) of the VP/MA hydrogels were calculated using the Equations (33) and (34), as shown in Figure 6.6. As expected, the M_c decreases with the number of alkyl carbons (C) and the v_e increases roughly linearly with increasing the number of C . The UVLIB3 hydrogels show the shorter M_c (~ 5000 g/mol) and the highest v_e ($\sim 2.07 \times 10^{-4}$ mol/cm³). These results are consistent with the increased aggregation of the longer hydrophobic parts. The UVMIB3 hydrogels having the longest M_c (~ 75000 g/mol) and highest v_e ($\sim 1.43 \times 10^{-5}$ mol/cm³) leads to the largest q_{ve} values

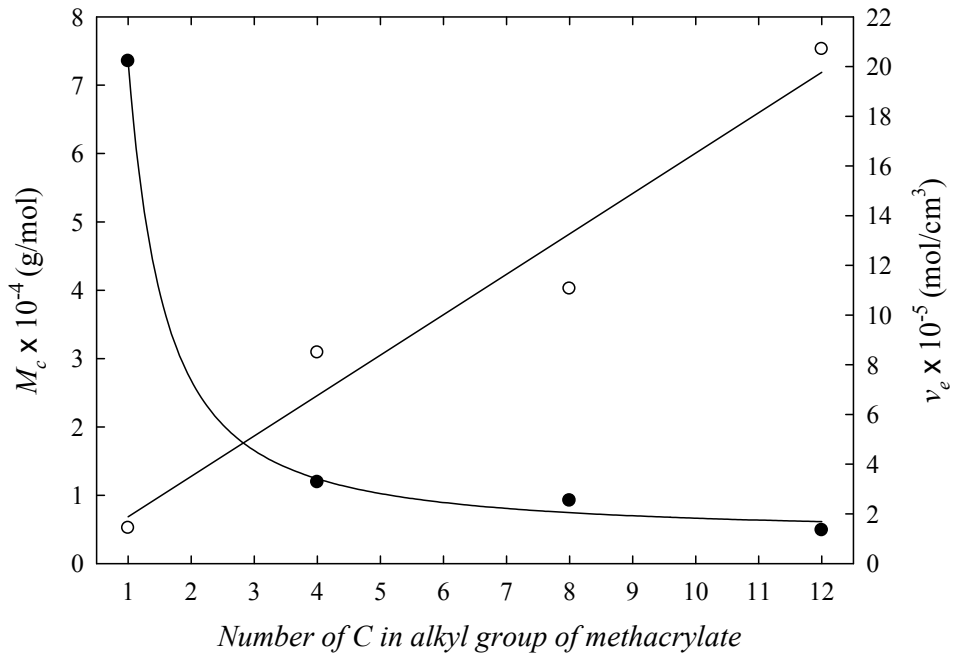


Figure 6.6. The M_c (●) and v_e (○) of VP/MA hydrogels as a function of the number of carbon (C) in the alkyl group of each methacrylate.

6.2. VP/HEMA Gel Composites with Silver Nanoparticles

Recently, the hydrogel composites with nanoparticles have been studied because of the properties improvement. Nanoparticles most typically used have been silver, clay, and silica. Hydrogel composites of poly(N-isopropylacrylamide) (PNIPA) and clay [14] showed improved properties such as transparency, mechanical strength and toughness, improved swelling ratio, increased deswelling rate, in addition to modification of critical temperature at which the various properties changes. The clays are behaved to act as multifunctional crosslinkers and with increasing clay concentration the deswelling rates become shorter. Studies on composites of polyvinylformamide (PVFA) and polyvinylamine (PVAm) hydrogels with silica particles were carried out using small angle neutron scattering (SANS) by Meyer and coworkers [15]. They found that the correlation length of the PVAm/silica hydrogel composite in water is much larger than that of PVFA/silica hydrogel composites, which explains why the PVAm/silica hydrogel composites have higher swelling capacities. The silver particles are known to have a good anti-microbial activity [16-18], and have therefore been used for instance in the formulation of dental resin composites and in coatings of medical devices. Lee and Tsao [18] prepared composite hydrogels of poly(acrylic acid-co-poly(ethylene glycol) methyl ether acrylate) and 250-300 nm silver nanoparticles. The inclusion of the silver nanoparticles affects the swelling rate and mechanical strength but the degree of swelling was not influenced by the inclusion. In addition, the composite hydrogels showed high electrical conductivity and *E-coli* inactivation.

6.2.1. Preparation and Swelling Studies

The gel composites with silver particles was synthesized by mixing ascorbic acid solution with an aqueous AgNO₃ (see section 3.1.4 (refer to [18])) and prepared by two

steps of UV-curing procedure which was used to obtain the gels without water. After the first UV-cure, the hydrogel composites included water. Following this step, hydrogel composites were freeze-dried to effectively remove water. The freeze-dried gel composites were mixed with the VP/AA pregel mixture and then UV-cured for the second procedure. The semi-interpenetrating Ag-UVAIB3 gel composites with silver particles of approximately 0.2 wt. % were obtained. The swelling behavior with time of the Ag-UVAIB3 gel composites was compared with that of the UVHIB3 gels, the results of which are shown in Figure 6.7. The Ag-UVAIB3 gel composites swell slower than

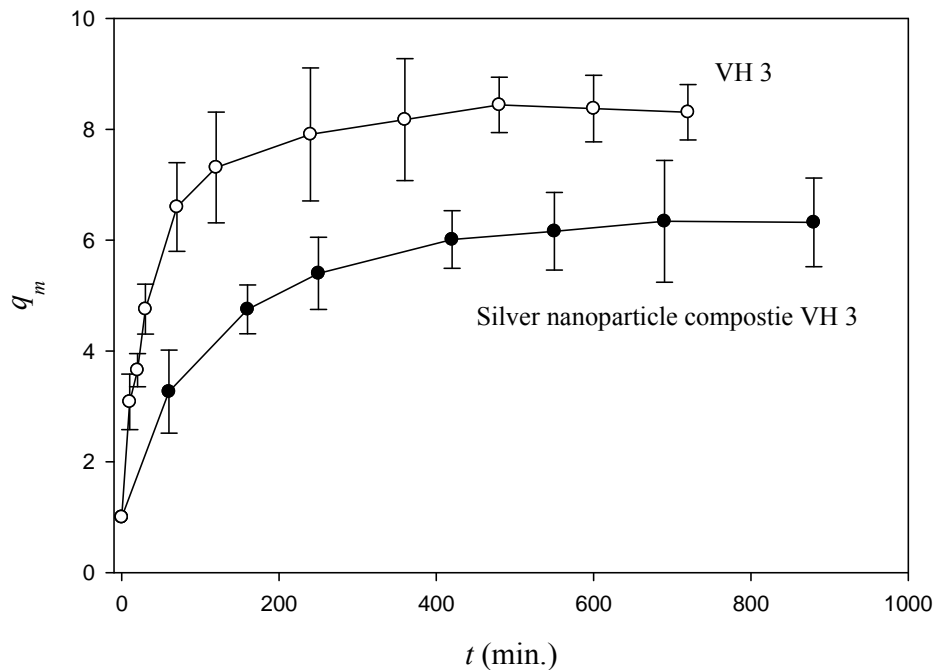


Figure 6.7. Mass swelling ratio (q_m) of the semi-interpenetrating Ag-UVAIB3 gel composites and UVHIB3 gels as a function of time.

UVHIB3 gels in initial swelling phase (0-70 minutes) and reach the equilibrium state in about 700-900 minutes (t_{max}) with smaller degree of swelling than the UVHIB3 gels. As shown in Figure 6.8, the R_s values (0.038 min^{-1}) of Ag-UVAIB3 gel composites are 3 times slower than that of UVHIB3 gels (0.133 min^{-1}) and the t_{max} values (690 minutes (11.5 hours)) of Ag-UVAIB3 gel composites are twice as long as those for the UVHIB3 gels (360 minutes (6 hours)). The slow swelling rates produced by Ag-UVAIB3 gel composites, agree well with the studies of Lee and Tsao [18] on composite hydrogels of poly(acrylic acid-co-poly(ethylene glycol) methyl ether acrylate) and 250-300 nm silver nanoparticles. The silver nanoparticles may be acting as crosslinkers or the particles might block the pores, resulting in the slower diffusion rate. However, unlike the result presented by Lee and Tsao, the degree of swelling shown by Ag-UVAIB3 gel composites including the silver nanoparticles is smaller than the gel without silver nanoparticles, an unfavorable characteristic for a candidate material to use as a tissue expander.

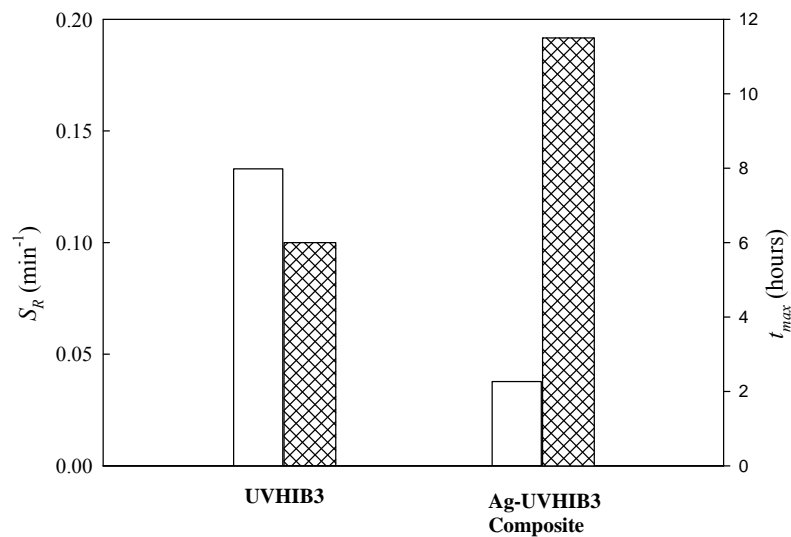


Figure 6.8. The R_s (□) and t_{max} (▤) of both semi-interpenetrating Ag-UVAIB3 gel composites and UVHIB3 gels

6.3. VP/HEMA Gels Encapsulated by Elastomer Films

The encapsulation of a hydrogel has been studied as one of the methods to control drug, gene or cell delivery or release. [2, 6, 19]. Peppas and coworkers [2] studied that for the hydrogels used for scaffolds for tissue engineering encapsulated by semipermeable membranes are able to control the selective diffusion of nutrients or growth factors as well as protect allergenic or xenogenic cells from the immune system. Peppas and Litger [20] reported swelling behavior of membrane coated hydrogels is controlled by non-Fickian diffusion, resulting in long term release of drugs. Beak and coworkers [4] demonstrated control over swelling rate of acrylic acid and acryl amide copolymeric superporous hydrogels by coating with an amphiphilic block copolymer poly(ethylene glycon-b-tetramethylene oxide) (PEGTMO) film. Depending on the concentration of PEFTMO solution, the swelling rate was bale to be varied.

In this study, swelling rate was investigated for gel systems encapsulated with elastomeric films. The VP/HEMA gels were coated with the polydimethylsiloxane (PDMS) elastomeric films. These films were optimized by measuring the mechanical properties for different ratios of PDMS precursor and crosslinker and various film thicknesses. The gels were also encapsulated with by polybutadiene (PB) elastomeric films with different thickness and the effect of the film thickness.

6.3.1. Elastomeric Films to Encapsulate Gels

To optimize the preparation condition for obtaining PDMS film with the most desirable mechanical properties to coat the gels, the mechanical properties of PDMS elastomer films was investigated. The stress of the PDMS elastomer films with four different film thicknesses (d_e) and with three different ratios of PDMS and crosslinker (F_{PC}) was measured as a function of stain. The conditions used in preparing PDMS films are listed in the Table 3.7 in the section 3.1.5. The stress at break (σ_b), strain at break

($\varepsilon_b = \Delta d_e / d_e$), elastic modulus (E), and toughness of the films were determined for the various films (Table 6.1). Each value reported is the average of three determined for each film. The σ_b and E values of PDMS1 films and PDMS2 films are similar and higher than those of PDMS3 films with the F_{PC} of 10:0.6. Although ε_b values of PDMS3 films with smaller film thickness are higher, those of PDMS2 films are reasonable, except when the film is 300 μm thick. The variation of ε_b and toughness with film thickness are in Figures 6.9 (a) and (b). It is shown that the PDMS2 films have higher toughness over the entire range of d_e . Reasonable ε_b values for the films of 550 and 760 μm thickness (PDMS2b and PDMS2c, respectively) are observed. It was also found that the toughness increases with decreasing d_e of the film and the films of PDMS2a and PDMS2b have higher toughness than PDMS2c and PDMS2d films. Compared with PDMS2a films, the PDMS2b films have higher ε_b . It is believed that PDMS2b films, which have an F_{PC} of 10:0.8 and d_e of 550 μm , are the most desirable for enduring the expansion of gel encapsulated by the film.

Table 6.1. Mechanical Properties of PDMS Elastomer Films

Elastomer Code	Stress at Break (MPa)	Strain at Break	Modulus (MPa)	Toughness $\times 10^{-6}$ (J/m ³)
PDMS1a	1.40	1.32	1.06	0.92
PDMS1b	1.47	1.15	1.28	0.85
PDMS1c	1.03	1.04	0.99	0.54
PDMS1d	1.02	0.83	1.23	0.42
PDMS2a	1.55	1.23	1.26	0.95
PDMS2b	1.26	1.44	0.88	0.91
PDMS2c	1.05	1.34	0.78	0.70
PDMS2d	1.02	1.25	0.82	0.64
PDMS3a	0.68	2.00	0.34	0.68
PDMS3b	0.55	1.89	0.29	0.52
PDMS3c	0.44	1.42	0.31	0.31
PDMS3d	0.31	1.12	0.28	0.17

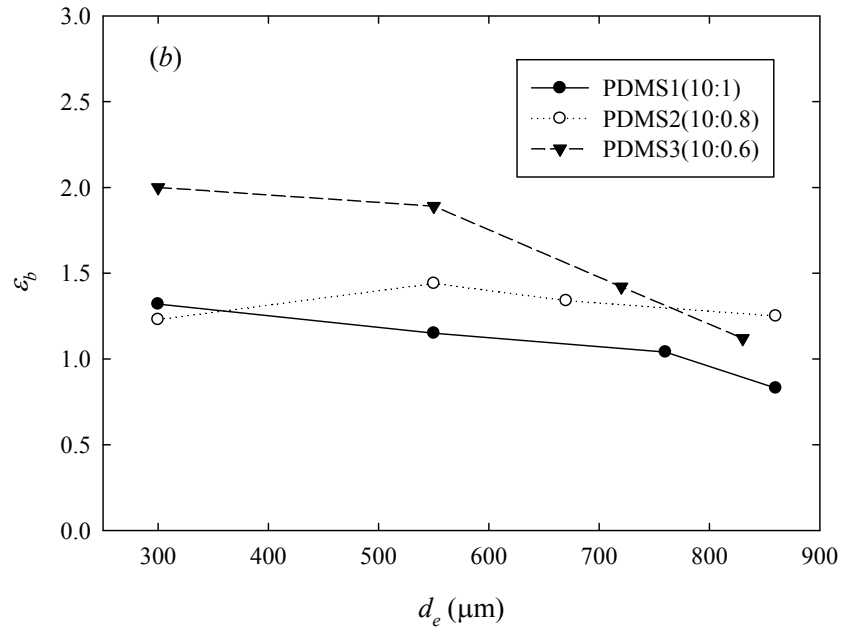
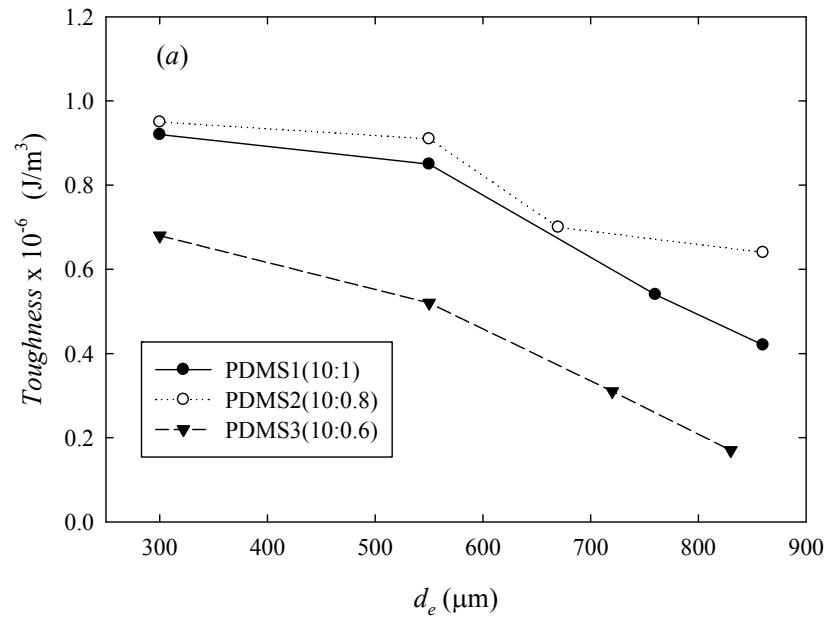


Figure 6.9. The (a) *toughness* and (b) ϵ_b of PDMS films as a function of film thickness for three different F_{PC} used for making films

The VP/HEMA gels were coated by polybutadiene (PB) elastomer with different d_e by varying the number of coating process and PB solution concentration. The reported values of σ_b , ε_b , and toughness of PB elastomer are ~ 2 MPa, 0.5 and $\sim 0.5 \times 10^6$ J/m², respectively [21]. When a solution of PB in toluene used for coating the gels was fixed, the increased number of coating process produces thicker d_e of the film encapsulating the gels. The PB solution with 3 wt. % was accordingly used for encapsulating gels to decrease the number of coating process compared with the PB solution with 1 wt. %

6.3.2. Swelling Studies

Figure 6.10 shows the swelling behavior as a function of swelling time of the UVHIB3 gels encapsulated by a PDMS film 600 μm thick as well as various PB

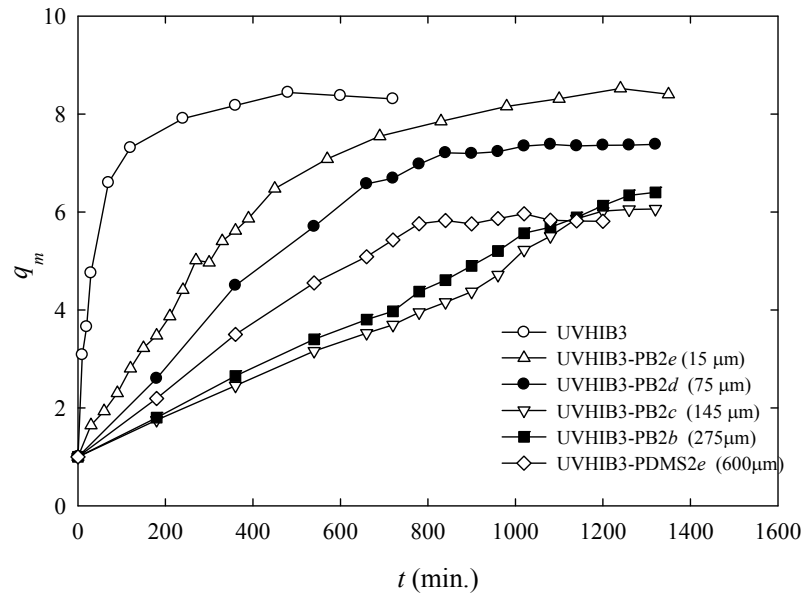


Figure 6.10. Mass swelling ratio (q_m) of the UVAIB3 gels encapsulated with different PB films with different d_e values or PDMS2e of 600 μm film thickness (Legend denotes the gels and the elastomer film type and the film thickness).

elastomer films with d_e values of 15 μm , 75 μm , 145 μm and 275 μm . Gels encapsulated with PB film 300 μm thick disintegrated after 1200 min, thus further studies of PB1a and PB2a could not be performed. However, their initial mass swelling ratio (q_m) increase before the PB film disintegrated like that of PB2b gel system with PB 275 μm thick. Although the swelling behavior of PB2b and PB2c are similar, the swelling of the gels encapsulated with thicker film are depressed more. However, the UVHIB3 gels coated by PB2e film 15 μm thick swell slowly and as much as the UVHIB3 gel without coating. Clearly, it can be thought that when very thin encapsulation films are used, the gels swell slower than the gel without a barrier film but their swelling degree can be maintained. This result is well agreed with studies on the swelling behavior of AA/AM SPHs coated with poly(ethylene glycon-b-tetramethylene oxide) (PEGTMO) [4].

The swelling rate was evaluated from the initial swelling rate (R_s) and the time to achieve the fully swollen state (t_{max}). The gel coated with PDMS film approaches the saturation point quicker than the gels coated with PB films and the PDMS2b film was found to be mechanically less stable than PB film (See Figure 6.10).

The values of R_s and t_{max} of the VP/HEMA gels coated with various PB films with different film thicknesses are shown in Figure 6.11. It is shown that with increasing d_e , the R_s increases with the following hyperbola relationship: $R_s = a_1 + (a_2 \cdot d_e / (a_3 + d_e))$ and t_{max} decreases with the following rational equation: $t_{max} = ((b_1 + b_2 \cdot d_e) / (1 + b_3 \cdot d_e))$, where the coefficients a_1 , a_2 , a_3 , b_1 , b_2 , and b_3 might be specific under a given gel system and for the UVHIB3 gels. The values of a_1 , a_2 , and a_3 fitting R_s values the values are 6.02 ± 2.45 , 14.6 ± 2.99 and 0.004 ± 0.005 with r square $r^2=0.96$ and the values b_1 , b_2 , and b_3 fitting t_{max} values are 0.04 ± 0.00 , 0.76 ± 0.62 and 174 ± 84.0 with r square $r^2=0.99$.

The R_s of the UVAIB3 gels coated with PB2e films only 15 μm thick is about 3 times slower than those of the UVAIB3 gels without coating. Similarly, t_{max} is roughly 3 times longer for the coated gel system. By encapsulating the gels with sufficiently thin

elastomeric films, the swelling rate is able to be controlled while maintaining the degree of swelling.

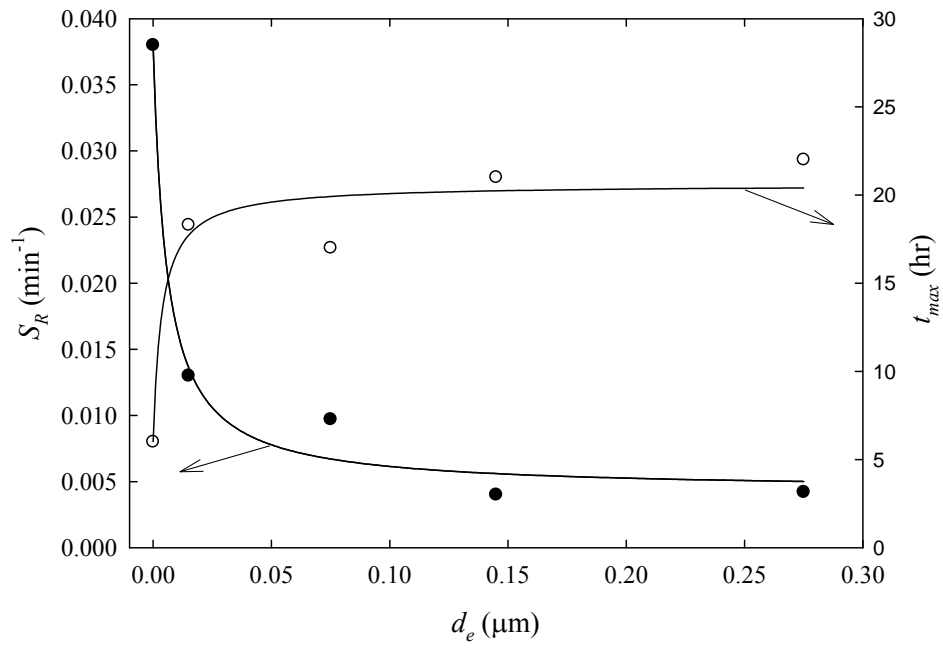


Figure 6.11 The R_s (●) and t_{max} (○) of the UVAIB3 gels encapsulated with different PB films with different d_e values

6.4. Multilayer of Elastomer and Hydrogels

Studies on multilayer of alternating gel and elastomer films ((GE)_m) were carried out in order to evaluate their efficiency in controlling the swelling rate of hydrogels and to satisfy medical requirements.

Many studies on the multilayer systems composed of polyelectrolytes prepared via the interaction between opposite charges in the alternating polyelectrolyte layers [22, 23]. However, few studies on the (GE)_m systems have rarely been reported.

6.4.1. Preparation and Swelling Studies

As shown in Figure 3.5 and Table 3.8 of Section 3.1.6, (GE)_m systems were prepared by alternating layers of UVHIB3 gel and PB elastomer with micron thickness. When the (GE)_m was prepared, the gel layers sometimes formed cracks, which might be due to the difference in the thermal expansion coefficient of VP/HEMA gel and PB rubber that occurred during heating and cooling times used for making PB layers. Thus careful slow cooling was adapted for the preparation the (GE)_m systems.

The swelling behavior of the two different (GE)_m systems was observed and compared with that of the UVHIB3 gel. Unlike the other swelling measurements, the diffusion of a saline solution was in one dimension as shown in Figure 6.12, using a PB elastomer gasket for the (GE)_m systems. The saline solution was added to a top layer with the area of 10 mm × 10mm. The top layer composed of the PB rubber film, which acts as a barrier controlling the diffusion of saline solution.

Mass degree of swelling (q_m) of two (GE)_{ms} (see Table 9) of alternating UVHIB3 gel and PB elastomer film layers as a function of swelling time are plotted in Figure 6.13 and compared to that for UVHIB3 gel. The q_m values of UVHIB3 gel were recalculated since the area involved in the diffusion is 2.4 times larger than that of (GE)_{ms}. The swelling rate of both (GE)_{ms} was significantly slower than that of UVHIB3 gel.

With 1-dimensional R_s values for (GE)_m1 and (GE)_m2 systems are $1.12 \times 10^{-4} \text{ min}^{-1}$ and $0.512 \times 10^{-4} \text{ min}^{-1}$, respectively. The R_s of the UVHIB3 gel is 0.021 min^{-1} and 200 ~ 400 times larger than those of (GE)_ms. It is also seen that the R_s of the (GE)_m2, whose the first layer PB membrane is 100 μm thick, is about two time smaller than (GE)_m1 whose the first layer PB film 50 μm thick. The 1-dimensional R_s values of the multilayer decreases proportional to the top PB rubber layer thickness and the R_s values are directly affected by the top layer thickness in this work. Although the (GE)_m2 with thicker top rubber layer initially shows slow swelling behavior, around at 10 days the q_m of GE-MULTI 2 almost approaches the q_m of (GE)_m1. The multilayer systems of alternating gels and elastomer films are very effective in decreasing the swelling rate, however, they largely depress the degree of swelling

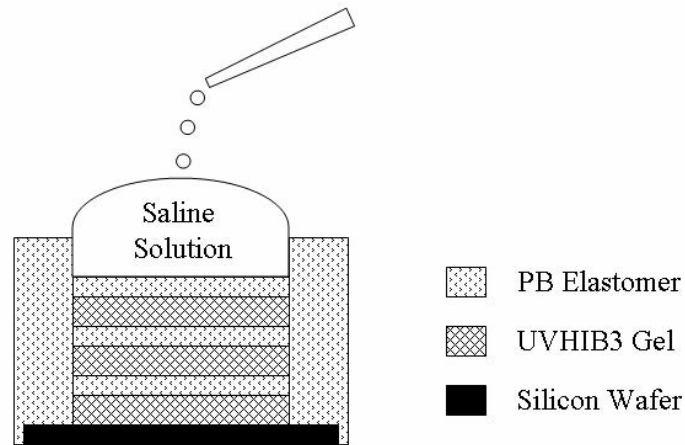


Figure 6.12. The schematic of a swelling measurement setup for a (GE)_m made of UVHIB3 gel and PB rubber layers

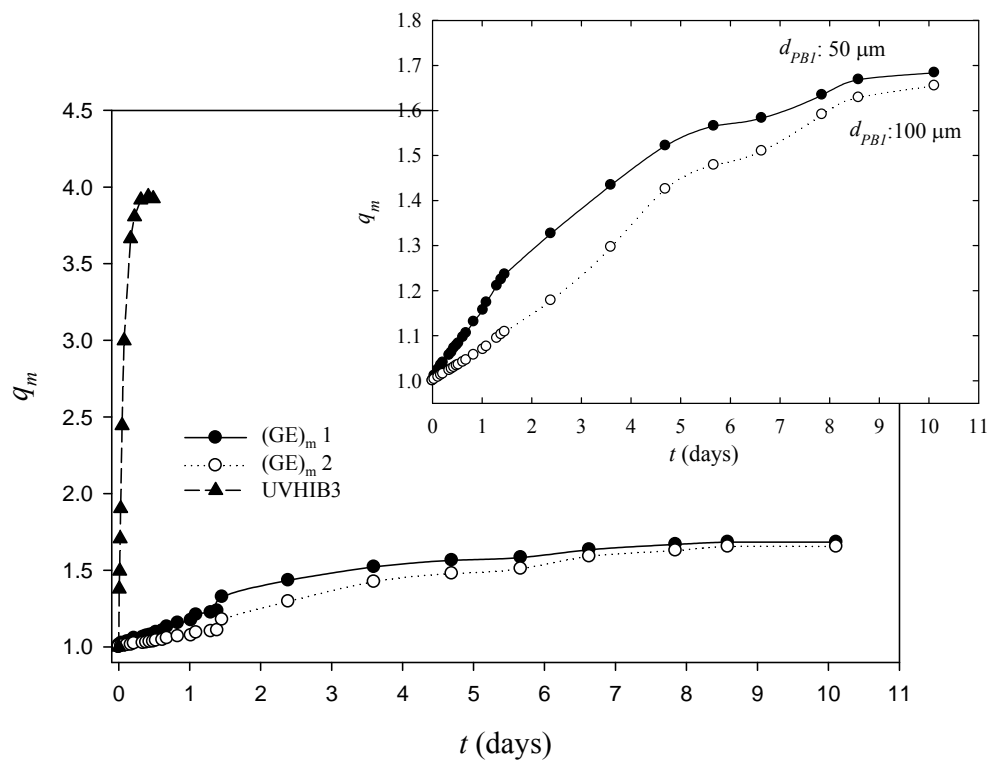


Figure 6.13. The q_m of two $(GE)_m$ s as a function of time (The diffusion rate of a saline solution of $(GE)_m 1$ and $(GE)_m 2$ is $2.49 \times 10^{-3} \text{ mgH}_2\text{O}/\text{cm}^2 \cdot \text{sec}$ and $6.34 \times 10^{-4} \text{ mgH}_2\text{O}/\text{cm}^2 \cdot \text{sec}$, respectively).

6.5. Conclusions

Methods to control or slow the swelling rate of gels were studied by investigating the effect of the microstructure changes by including hydrophobic moieties or silver nanoparticles in the gels. In addition, the effect of macrostructure changes by encapsulating the gels or by making multilayers of altering gels and elastomer films were also investigated.

Various vinylpyrrolidone (VP) based copolymeric gels were UV-polymerized by introducing various methacrylates (MA) and the effect of the number of carbon in the alkyl group of methacrylate on the swelling behavior, modulus, and structural parameters of various gels was investigated. By increasing the number of alkyl carbons in the methacrylate, the VP/MA gels have smaller equilibrium volume swelling ratios (q_{ve}), larger interaction parameters between polymer and solvent (χ), higher crosslinking densities (v_e), lower average molecular weight between crosslinks (M_c), slower initial swelling rates (R_s) and shorter time to reach to fully swollen state (t_{max}), and higher mechanical stiffness (G). The longer alkyl groups (more hydrophobic molecules) interact and aggregate more, resulting in an increase of crosslinking in the hydrogels. The inclusion of hydrophobic moieties in hydrogels is effective in reducing swelling rate, however is not effective in maintaining the equilibrium swelling ratio and lengthening the time to reach an equilibrium state. This indicates that the inclusion of hydrophobic moieties is not desirable for the use in tissue expander.

Semi-penetrating VP/HEMA gel composites with silver nanoparticles were prepared by a novel process to investigate the effect of the particulate inclusions on the swelling behavior of the composites. The q_{ve} and R_s of the VP/HEMA gel composite are smaller than those of the VP/HEMA gel without silver particles, however the t_{max} of the gel composites is longer than the gels. The decreased q_{ve} is not a desirable property for a candidate material for use as a tissue expander.

The swelling behavior of VP/HEMA gels enveloped by various polydimethylsiloxane (PDMS) or polybutadiene (PB) elastomer films was also investigated.

The VP/HEMA gels encapsulated with the (PDMS) elastomeric films having optimal properties, which are the ratios of PDMS precursor and crosslinker (F_{PC}) of 10:0.8 and film thickness (d_e) of 550 μm , showed smaller t_{max} , R_s and even q_{ve} than the gels encapsulated with PB elastomer films with various d_e s (15, 75, 145, 275, and 300 μm). The decrease the film thickness of elastomeric films encapsulating gels, their R_s of the gels decreases and their t_{max} increases while maintaining the degree of swelling. The VP/HEMA gels encapsulated with 15 μm thickness PB elastomer film swelled 3 times slower and they took 3 times longer to reach fully swollen state than those of uncoated VP/HEMA gels even though they have similar equilibrium degree of swelling (q_{ve}). The encapsulation of gels with sufficiently thin elastomeric films decreases R_s and lengthens t_{max} without depressing the q_{ve} , which is desirable method for the development of a candidate hydrogel for use in tissue expansion.

The 1-dimensional swelling rates, R_s , of multilayers of alternating VP/HEMA gels and PB elastomer films were studied. It was found that the 1-dimensional R_s was reduced by introducing a rubber membrane layer alternatively between hydrogel layers. The R_s of multilayer systems was determined to be 200~400 times slower than that of the gels. It was shown that the 1-dimensional R_s values of the multilayer decreases proportionally to the top PB rubber layer thickness. Reduction of the elastomer top layer thickness by half produced a reduction of R_s by 2. Although the multilayer structure is very effective in decreasing the R_s and increasing the t_{max} , it does not maintain the equilibrium degree of swelling. These swelling features are not desirable for a candidate material for use in tissue expansion.

References

- [1]. L. Mahadevan, S. Daniel, and M. K. Chaudhury, “Biomimetic ratcheting motion of a soft, slender, sessile gel”, *PANS*, vol. 101, pp. 23-26, 2001.
- [2]. Nicholas A. Peppas, J. Zach Hilt, Ali Khademhosseini and Robert Langer, “Hydrogels in biology and medicine: From molecular principles to bionanotechnology”, *Advanced Materials*, vol. 18, pp. 1345-1360, 2001.
- [3]. Jan Hoffmann, Matthias Plotner, Dirk Kukling, and Wolf-Joachim Fischer, “Photopatterning of thermally sensitive hydrogels useful for microactuators”, *Sensors and Actuators*, vol. 77, pp. 139-144, 1999.
- [4]. Namjin Baek, Kiman Park, Jae Hyung Park, and You han Bae, “Control of the swelling rate of superporous hydrogels”, *Journal of Bioactive and Compatible Polymers*, vol. 16, pp. 47-57, 2001.
- [5]. Hossein Omidian, Jose G. Rocca, and Kiman Park, “Elastic, superporous hydrogel hybrids of polyacrylamide and sodium alginate”, *Macromol. Biosci.*, vol. 6, pp. 703-710, 2006.
- [6]. Nicholas A. Peppas and Robert Langer, “Origins and development of biomedical engineering within chemical engineering”, *AIChE Journal; Bioengineering, Food, and Natural Products*, vol. 50, pp. 536-546, 2004.
- [7]. Gordon L. Amidon, Ping I. Lee, and Elizabeth M. Topp, Edited, *Drug and the Pharmaceutical Science Vol.102, Transport Processes in Pharmaceutical Systems*. 2000.
- [8]. D. J. T Hill, N. G. Moss, P. J. Pometry, and A. K. Whittaker, “Copolymer hydrogels of 2-hydroxyethyl methacrylate with n-butyl methacrylate and cyclohexyl methacrylate: synthesis, characterization and uptake of water”, *Polymers*, vol.41, pp. 1287-1296, 2000.
- [9]. Robert Langer and Nicholas A. Peppas, “Advances in biomaterial, drug delivery and bionanotechnology”, *AIChE Journal; Bioengineering, Food, and Natural Products*, vol. 49, pp. 2990-3006, 2003.

- [10]. Neide A Blaz Vieira, Joao Ruggiero Neto, and Marcio Jose Tiera, "Synthesis, characterization and solution properties of amphiphilic N-isopropylacrylamide-poly(ethylene glycol)-dodecyl methacrylate thermosensitive polymers", *Colloids and Surfaces A: Physiochem. Eng. Aspects*, vol. 262, pp. 251-259, 2005.
- [11]. Yi Luo, Kelly R. Kirker, and Glenn D. Prestwich, "Crosslinked hyaluronic acid hydrogel films: New biomaterials for drug delivery", *Journal of Controlled Release*, vol. 69, pp. 169-184, 2000.
- [12]. M. Rubinstein, R. H. Colby, *Polymer Physics*, Oxford University Press, New York, 2003.
- [13]. J. Flory, *Principles of Polymer Chemistry*, Cornell University Press: New York, 1969.
- [14]. Kazutoshi Haraguchi, Toru Takehisa, and Simon Fan, "Effect of clay content on the properties of nanocomposite hydrogels composed of poly(N-isopropylacrylamide) and clay", *Macromolecules* vol. 35, pp. 10162-10171, 2002.
- [15]. Torsten Meyer, Tomas Hellweg, Stefan Spange, Stephanie hesse, chridtian jager, Cornelia Bellmann, "Synthesis and properties of crosslinked polyvinylformamine and polyvinylamine hydrogels in conjunction with silica particles", *Journal of Polymer Scicence: Part A: Polymer Chemistry*, vol. 40, pp. 3144-3152, 2002.
- [16]. Wen-Fu Lee and Kai-Tai Tsao, "Preparation and properties of nanocompososite hydrogels containing silver nanoparticles by ex-situ polymerization", *Journal of Applided Polymer Scicence*, vol.100, pp. 3654-3661, (8pp), 2007.
- [17]. Ivan. Sondi and Branka Salopek-Sondi, "Silver nanoparticles as antimicrobial agent: a case study on E. coli as a model for Gram-negative bacteria", *Journal of Colloid and Interface Science*, vol. 275 pp. 177–182, 2004.
- [18]. Fang Zeng, Chao Hou, Shuizhu Wu, Xinxing Liu, Zheng Tong and Shuning Yu, "Silver nanoparticles directly formed on natural macroporous matrixa dn their anti-microbial activities", *Nanotechnology*, vol.18, pp. 055605 (8pp), 2007.
- [19]. Kyle N. Plunkett and Jeffrey S. Moore, "Patterned dual pH-responsive core-shell hydrogels with controllable swelling kinetics and volume", *Langmuir*, vol. 20, pp. 6535-6537, 2004.

- [20]. N. A Peppas and P. S. Ritger, “A Simple equation for description of solute release I. fickian and Non-fickian release from non-swellable devices in the form of slabs, spheres, cylinders of disc”, *Journal of Controlled Release*, vol. 5, pp. 23, 1987.
- [21]. Weili Wu and Dajun Chen, “Thermal and mechanical properties of silicone rubber, polybutadiene rubber, and ethylene–propylene–diene monomer blends”, *Journal of Applied Polymer Science*, vol. 101, pp. 4462-4467, 2006.
- [22]. Veronika Kozlovskaya and Svetlana A. Sukhishvili, “Amphoteric hydrogel capsules: multiple encapsulation and release Route”, *Macromolecules*, vol. 39, pp. 6191-6199, 2006.
- [23]. Zengshe Liu and Paul Calvert, “Multilayer hydrogels as muscle-like Actuators”, *Advanced Materials*, vol. 12, pp. 288-291, 2000.

CHAPTER VII

CONTROL OVER SWELLING DIRECTION : CONTROLLED ANISOTROPIC SWELLING

Attempts to control the degree and rate of swelling of gels have been discussed not only using the VP/HEMA and VP/AA gels prepared by UV-initiated and thermal polymerizations but also by manipulating the preparation conditions of gel systems in the previous chapters IV, V and VI. The target applications for these gels are to use in hypoplasia surgeries such as the closure of cleft palate defects, syndactyly (congenitally fused fingers or toes) repair and facial reconstruction (ears, nose, eyelid, lips). To use the hydrogel tissue expander in such applications, control over swelling direction or shape is another important key feature for the tissue expander. For example, for the repair of cleft palate defects [1], the skin expander needs to enlarge the skin around the split bones and should not give any pressure to bones next the inserted expander during the hydrogel swelling. Therefore an understanding of such anisotropic swelling and efforts to control the swelling direction (or anisotropy of swelling) were carried out in this study.

Studies on anisotropic swelling of hydrogels are reviewed in Chapter 2. However, studies on the control of the anisotropic swelling of hydrogels have not been widely reported. In this work, methodologies to systematically control anisotropic swelling of gels were developed. Initially VP/HEMA gels with gradient crosslinking densities created with controlled UV-initiated polymerization using photomasks were tested for anisotropic swelling and their swelling behavior was investigated. Subsequently, using an optimized VP/AA gels thermally polymerized, compressed gels were prepared with different processing conditions and the produced anisotropic swelling was investigated as functions of controlling parameters.

7.1. Swelling of Gradient Hydrogels

Recently, studies on gradient hydrogels have been undertaken because the hydrogels can be beneficial as matrixes for cell migration and spreading [2, 3] caused by the interaction between cells and the matrix which is achieved by surface chemistry, topology and mechanics [4, 5]. Although the gradient hydrogels has been studied for the use for cells, the purpose of the fabrication of gradient hydrogels in this study is to verify their anisotropic swelling behavior.

7.1.1. Assumption of Gradient Morphology-Induced Anisotropic Swelling

It was assumed (see Figure 7.1) that a dry gel with a controlled gradient crosslinking density in (before swelling) can produce the hydrogel with architecturally or positionally varied and controlled swollen state (after swelling) via anisotropic swelling. The mesh density expresses the crosslinking density and the δx is the thickness of the each section of gradient prepared by the section of patterned photomasks. Each section of the gel swells by different amount, although the total degree of swelling is expected to be an average value of all degree of swelling from all the sections. As shown in Figure 7.1, during the process of gel swelling, the gel section with lower density of crosslinking (or coarse mesh) will absorb more amount of water due to larger mesh size and the section with higher crosslinking density (or dense mesh) will absorb less amount of water due to smaller mesh size. Thus the fully swollen hydrogel will have the anisotropic swollen shape which depends on the gradient of the crosslinking density. For the crosslinking gradient shown in the figure, the hydrogels with the shape bulgy in the middle of the hydrogel would be obtained.

For the swelling kinetics of the gradient gels, it was also assumed that the diffusion coefficient (D) of the gels with the gradient network structure can be calculated

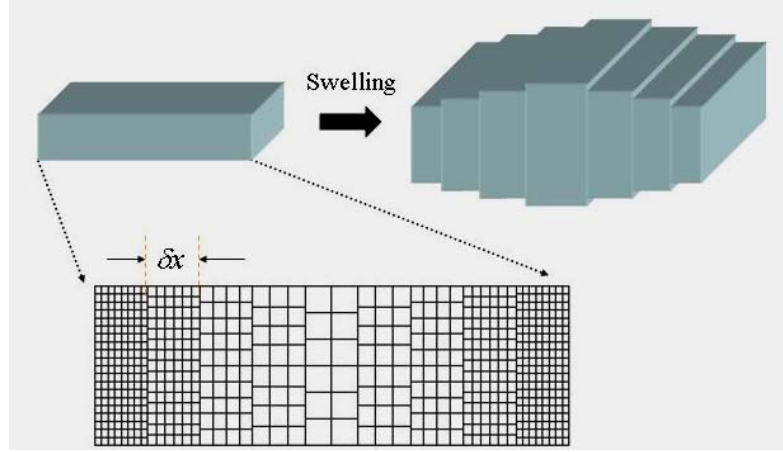


Figure 7.1. The schematic of expected structural gradient in a gel (left) obtained using a DGrad-Mask 1 and its fully swollen state (right).

using Equation (43). If the gradient in the gel is discrete and the total D is expected to be an averaged value of all the D values obtained from all sections.

$$\overline{D} = \frac{\sum_{m=0}^l D_m dx}{l} \quad (43)$$

Here, l is the length of the gel in the direction of gradient, dx is the thickness of the each section in gradient, and m indicates each section in gradient.

It is also assumed that this type of equation can be used to determine collective parameters. Accordingly, for the gels with discrete gradient prepared in this study, the characteristic parameters such as total equilibrium mass and volume swelling ratios (q_{me} and q_{me}), swelling exponent (n) average initial swelling rate (R_s) and time to reach to equilibrium state (t_{max}) are expected to be evaluated from averaging of all values obtained from all section.

7.1.2. Swelling Studies

To obtain the VP/HEMA gels with a designed gradient morphology, photomasks were used during the UV irradiation for gelation. Gradient VP/HEMA gels, DGrad-UVHIB3 gels and DGrad3-UVHIB3 gels, were successfully synthesized with VP and HEMA feed weight ratio of 9:1, 0.2 wt. % BIS and 0.8 wt. % Irgacure 651 and by UV-initiated free-radical polymerization with two different discrete gradient photomasks, DGrad-Mask1 and 2, respectively (see Figures A3 and A4). These photomasks can locally control the UV irradiation intensity (see Appendix I). To obtain the hydrogel with the bulgy shape in the middle based on the previous work [6] the middle part of the photomasks was designed to allow more UV intensity. In addition, according to Beebe and his coworkers [7], a patterned photomask produces high definition of pattern. Thus it was expected that the network structure of the VP/HEMA gels obtained using a patterned photomask discretely changes for each section. Attempts to verify this using magnetic resonance imaging (MRI) image were carried out (described below). Hydrogels with various shapes, which are very useful to various hypoplasia surgeries, are thought to be possible prepared by manipulating the pattern of photomask.

The mass swelling ratio (q_m) values of DGrad-UVHIB3 and UVHIB3 gels as a function of time are shown in Figure 7.2. The DGrad-UVHIB3 gels swell somewhat slower and to a lower extent than the UVHIB3 gels, however the DGrad-UVHIB3 gels take slightly longer time to approach a fully swollen state. The average initial swelling rate (R_s) and time to reach the equilibrium state (t_{max}) of DGrad-UVHIB3 gels and UVHIB3 gels are shown in Figure 7.3. The R_s of DGrad-UVHIB3 gels (0.054 min^{-1}) is about two times slower than that of UVHIB3 gels (0.133 min^{-1}). This result is unexpected since based on the hydrogel design, the two edge parts of the DGrad-UVHIB3 gel have the same crosslinking density as the UVHIB3 gel and the initial swelling rates of the edges are expected to be slower than the middle parts due to their

higher crosslinking density expected. The reason of the unexpected result is considered because the discrete gradient pattern might hinder the swelling rate and even slightly depress the degree of swelling. The extent of hindrance and depression of swelling is going to be dependent on the gradient pattern. The t_{max} of the DGrad-UVHIB3 gels (7 hours) is somewhat longer than that of UVHIB3 gel (6 hours).

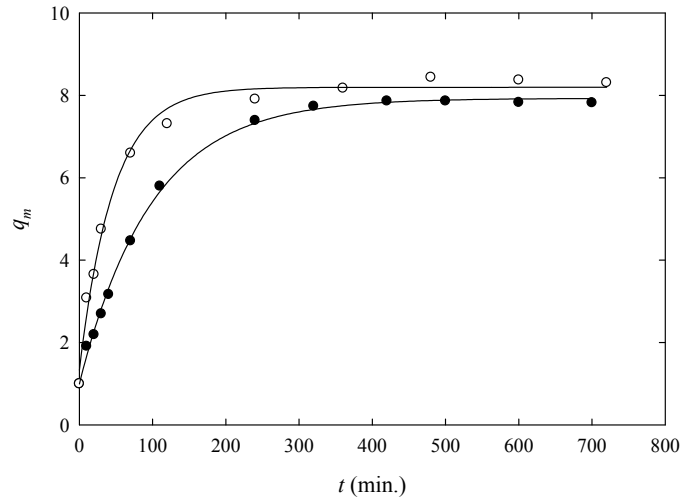


Figure 7.2. The mass swelling ratio (q_m) of DGrad-UVHIB3 gels and UVHIB3 gels as a function of time

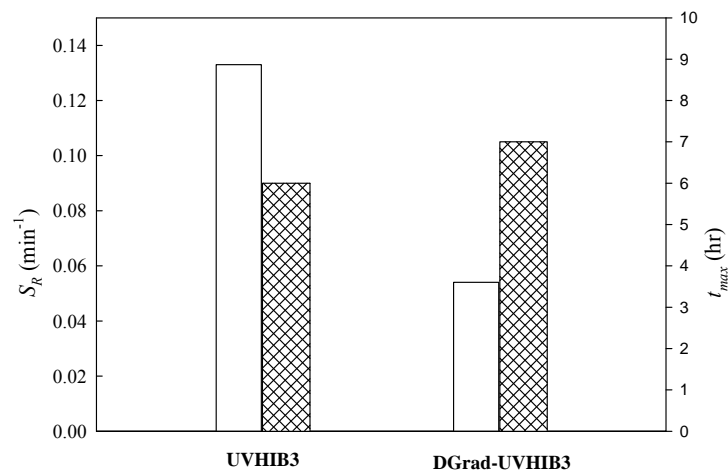


Figure 7.3. The R_s (\square) and t_{max} (\boxtimes) of DGrad-UVHIB3 gels and UVHIB3 gels

The diffusion coefficient (D) and the exponent (n) defining the diffusion mechanism of the swelling of both gel systems with and without gradient were calculated using their swelling data. The D of DGrad-UVHIB3 gels ($(5.21 \pm 0.06) \times 10^{-7}$ cm/s) is smaller than that of UVHIB3 gels ($(6.73 \pm 0.34) \times 10^{-7}$ cm/s). This result is different from the assumption on collective properties mentioned in previous section. If the assumption were correct, the D of DGrad-UVHIB3 gels would be the average value of each gradient section. These sections correspond to UVHIB3e, UVHIB3d, and UVHIB3c, UVHIB3 gels from the middle toward edge part, respectively, with the D values of 7.85×10^{-7} cm/s, 7.23×10^{-7} cm/s, 6.87×10^{-7} cm/s, and 6.73×10^{-7} cm/s, respectively. Therefore the average D would be 7.07×10^{-7} cm/s, which is larger than that of DGrad-UVHIB3 gel. Clearly, the mathematical assumption is not applicable for expecting characteristic parameters of swelling. This might be due to the geometry-limited mobility of solvent molecules within discontinuous (discrete) gradient hydrogels.

The values of diffusion characteristic exponent n of DGrad-UVHIB3 hydrogels are 0.71 ± 0.1 , which indicates the diffusion of a saline solution into DGrad-UVHIB3 gel follows non-Fickian diffusion mode. The value is higher than the n values of UVHIB3e, UVHIB3d, and UVHIB3c and UVHIB3 gels ($0.54 \sim 6.00$), which indicates that diffusion mode of solvent into gradient gels is more deviated from Fickian. This explains that the morphology of gels affects the diffusion behavior. The n values for gradient can not be obtained using the equation (43), which supports that the equation is not applicable for obtaining characteristic parameters of swelling.

The DGrad-UVHIB3 gel was characterized using stereo optical microscopic imaging not only to verify whether the gradient gel obtained using the designed photomask swells as expected, but also to investigate the anisotropy of swelling of the gradient hydrogel. Figure 7.4 shows an image of a fully swollen DGrad-UVHIB3 hydrogel. The thickness of the hydrogel gradually changes along the gradient direction. The gel does display gradient morphology, which creates anisotropic swelling. However,

the variation in the thickness across the gradient is not very significant and therefore impractical for preparing the hydrogel for use in tissue expansion.

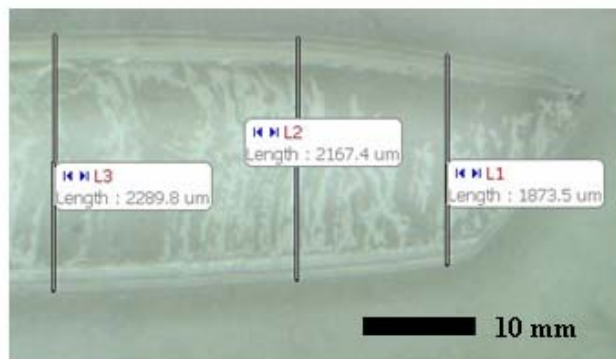


Figure 7.4. Stereo-optical micrograph of a fully swollen DGrad-UVHIB3 hydrogel

To verify a spatial morphology variation existed in the gradient gel, gels were prepared using the photomask with three discrete gradients (Dgrad-Mask2, see Figure A4), which are DGrad3-UVHIB3 gels. In addition, the gradient in the fully swollen DGrad3-UVHIB3 hydrogels were visualized by magnetic resonance imaging (MRI) techniques. It is well known that the mobility of a water molecule can be monitored by using MRI techniques. Its mobility is dependent on the morphology of the hydrogels, resulting in morphology dependent self diffusion coefficient (D_s). Three D_s (called diffusion tensors $D_s(x)$, $D_s(y)$, and $D_s(z)$) along the principal directions (x, y, and z) can be obtained and degree of anisotropy of D_s can be determined using nuclear magnetic resonance (NMR) or MRI [8, 9]. The diffusion tensor $D_s(x)$, $D_s(y)$ and $D_s(z)$ and the anisotropy of D_s of DGrad3-UVHIB3 hydrogels is discussed in Appendix II. Here the morphology gradient in the fully swollen DGrad3-UVHIB3 hydrogels obtained using the photomask with 3 discrete sections was investigated by monitoring the $D_s(x)$ where x is the direction along

the gradient) (see Figure 7.5). The hydrogel specimens were cut into small slices for the examination. The small hydrogel specimen included the middle part designed to have a loose network structure and the edge part designed to have a dense network structure. From the grey scale values, the higher D_s appear as white and the lower end toward black. As expected, the gel obtained via higher intensity irradiation has lower crosslinking density, resulting in a higher degree of swelling and thus higher $D_s(x)$ (bright). The edge parts obtained by lower UV intensity irradiation have higher crosslinking density, resulting in the lower degree of swelling and lower $D_s(x)$ (darker). The $D_s(x)$ imaging of gradient hydrogels could assure that the gradient photomask produces gels with gradient (morphology variation) as designed, which induces anisotropic swelling.

However, as shown in Figure 7.5 (a), the sections of the hydrogel are not precisely divided and some mixing occurs between sections most probably due to the molecular connectivity in the network structure. This is different from the result of the polyacrylamide (PAAm) hydrogel systems observed by Beebe *et al.* [7], which might be because the scale of specimens used in this work is much larger than theirs (micron scale).

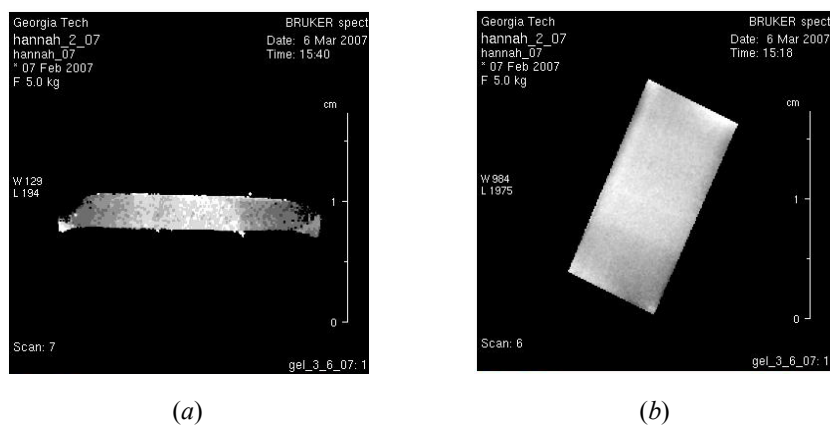


Figure 7.5. The $D_s(x)$ images of (a) the cross-sectional view and (b) the planar view of the DGrad3-UVHIB3 gel determined by MRI technique. The diffusion coefficient is encoded by the grayscale (light: high D_s and dark: low D_s).

7.2. Compressed Force-Induced Anisotropic Swelling of Compressed Gels

A number of studies performed on anisotropic swelling of hydrogels without any intrinsic anisotropy of their structure are on the stress-induced anisotropic swelling of the hydrogels [10-12]. Most of these studies related thin film with nano-scale or micron-scale thickness prepared on a substrate and placed under a mechanical constraint [11]. Sometimes buckling patterns [12] are obtained because of different swelling behavior of the free surface part compared to the interface constrained by the substrate.

Recently, Swan and co-workers [13] reported an attempt to obtain anisotropic swelling of gels compressed in the bulk state for the medical use. The compressed gels swell in the direction opposite to the compression direction with an ultimate expansion ratio up to approximately 15 in expansion direction. Despite these developments, several problems remain unresolved such as poor mechanical integrity of swollen hydrogels due to damage that occurs during the compression process and limited ultimate expansion.

In this study, using an optimized VP/AA gel system (Chapter 5), the compressed gels were prepared with the controlled processing conditions to systematically improve their anisotropy and their characteristic properties were investigated as functions of controlled processing parameters as well as anisotropic swelling behavior. .

7.2.1. VP/AA Gels Compressing Conditions

Prior to compressing TVAAB5*b* gels, the glass transition temperature (T_g) of VAAB5*b* gel was measured by DSC and found to be 130 ± 3.70 °C from the second heating curve (see Figure 7.6).

The transition temperature obtained at the first heating curve was found to be around 115 °C. The gels need to be compressed at temperatures where molecules in the network are mobile enough to rearrange their confirmation but should have the least

capability (low freedom or energy) to restore to their original state. Therefore, compression temperatures investigated was near T_g . The TVAAB5*b* gels were compressed at temperatures from 100 °C to 150 °C.

The compression strain percent values investigated were chosen to be 70 % to 95 % based on that more stained molecules have higher tendency to restore.

Slow compression gives molecules enough time to reorient and avoid mechanical failure during compression. The stress remained inside the gels after the processing and the inertia effect caused by high rate of compression need to be minimized. Therefore, the compression stain rates investigated were chosen to be in the range between 0.01 s⁻¹ and 0.0001s⁻¹.

The compression creep and recovery tests of the TVAAB5*b* gels were performed using 2 cycles of loading and unloading compressive force at the processing conditions, prior to the compression of gels. The compressions creep and recovery curves for the gels were found to be all similar. Figure 7.7 shows that the compressions creep and recovery curves for a TVAAB5*b* gel obtained at the compression temperature of 130 °C and with the compression strain rate of 0.001 s⁻¹. The stress and strain (s-s) curve of VAAB5*b* gel under compression agrees well with typical stress and strain isothermal curve for natural rubber at room temperature [14, 15]. The large increase in stress (σ) at large stain (ε) is associated with the densification usually found in the network or porous structural materials under an applied compressing force.

The closed stress hysteresis loop of TVAAB5*b* gel under compressive loading and unloading indicates there is no residual strain. The smaller stress of the gel shown in the hysteresis loop during the unloading process is probably due to the molecular reorientation creating less stress and dissipating energy as heat. The area of the loop is proportional to the amount of energy dissipated during the loading and unloading cycle. As seen in Figure 7.7, the s-s curve at the first cycle of loading and unloading is almost the same as the curve at the second cycle, which indicates the processing conditions for

preparing compressed gel do not induce mechanical failure in the gel. Above 65 % strain the stress in the second loading and unloading cycle is slightly higher than the first cycle, which might be caused by the better molecular arrangement (higher densification).

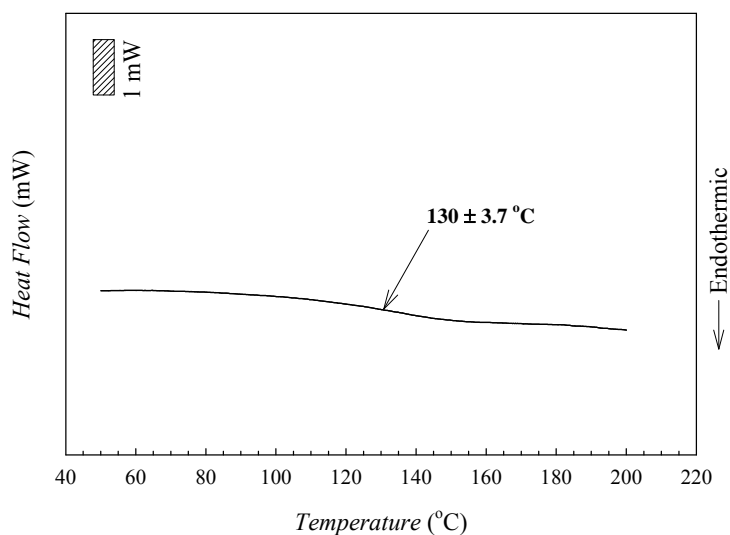


Figure 7.6. Second heating DSC curve of the TVAAB5*b* gel with a heating rate of 10 °C/min under nitrogen gas

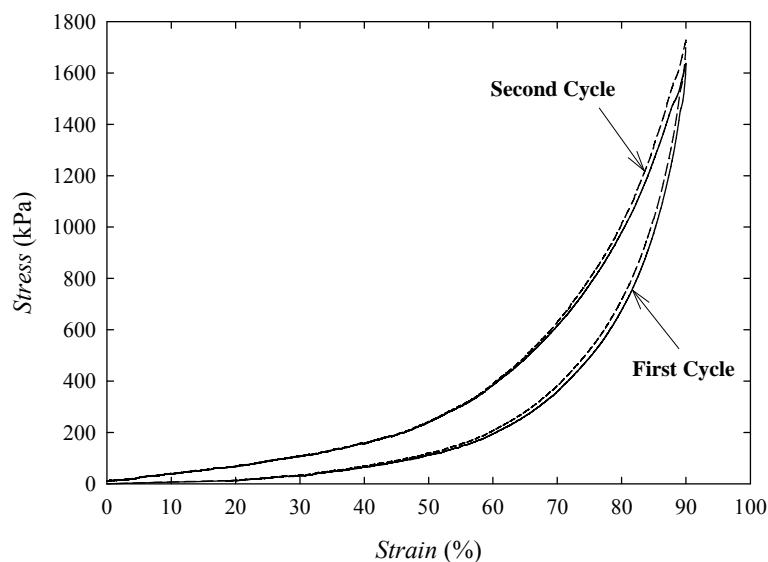


Figure 7.7. The compression and recovery curve of TVAAB5*b* gel at 130 °C and with the strain rate of 0.001 s⁻¹ (the first loading and unloading cycle (—) and second cycle (---))

7.2.2. Gel Network Structure Change under Applied Compression

Unlike solids and liquids that are incompressible, gels can be compressible and allow densification under compressive loads. As illustrated in Figure 7.8, I propose that if the gel having an ideal network structure is compressed with appropriate processing conditions, folding of the molecular chains only in the height direction without changing the top and bottom area may result in the decrease of the mesh void volume and the change in the density of the gel.

For compressible gel processing, the temperature, stain rate and strain should be carefully chosen. Appropriate temperatures and the shear rates must be chosen so that the molecules in the network can have enough mobility and time to rearrange their conformation in the compressed state. Stains must be not only low enough to prevent chains scission in the network during the compression but also high enough to acquire the change of density (decrease in volume). Chain folding is expected to be dominant in the middle part of gel specimens while chain slipping prevails at in the edgiest.

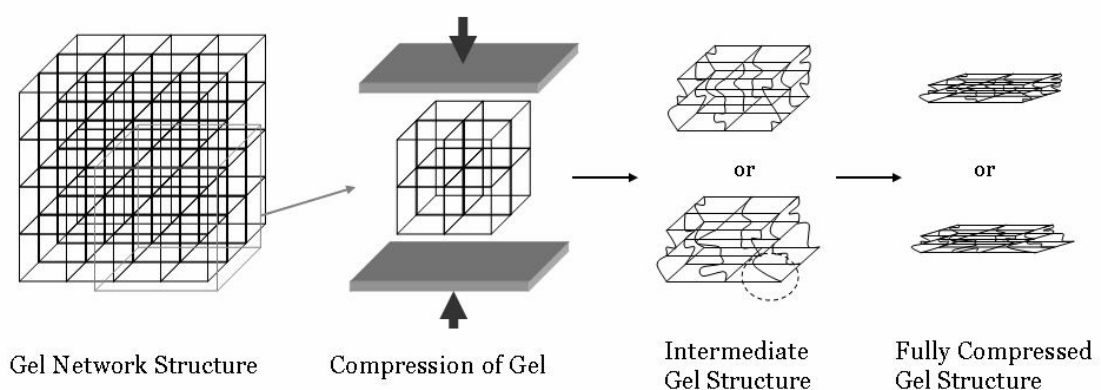


Figure 7.8. Assumed model for the ideal network structure of a gel and the intermediate and fully compressed network structure of the partial gel part (the chain in dotted circle shows slippage due to the friction occurred on the surface)

7.2.3. Fixicity of Gels

For any given applied compressive strain (ε_c), a strain remains in the gel (ε_r) after the compression process (accompanied with cooling and unloading). The difference between ε_c and ε_r are quantified as the fixicity ($=\varepsilon_c / \varepsilon_r \times 100$) [16]. Fixicity of the gels is essential for the anisotropic swelling since more compressed gels should swell more in the direction opposite to the compression direction. The effect of compression temperature, stain, and strain rate on the gel fixicity was investigated.

Figure 7.9 shows the fixicity of the TVAAB5b gels as a function of a temperature. Up to the temperature of 130 °C the fixicity increases with increasing temperature, associated with a higher elasticity and lower mobility of the gel at lower temperature. While above 130 °C the fixicity is approximately independent of temperature.

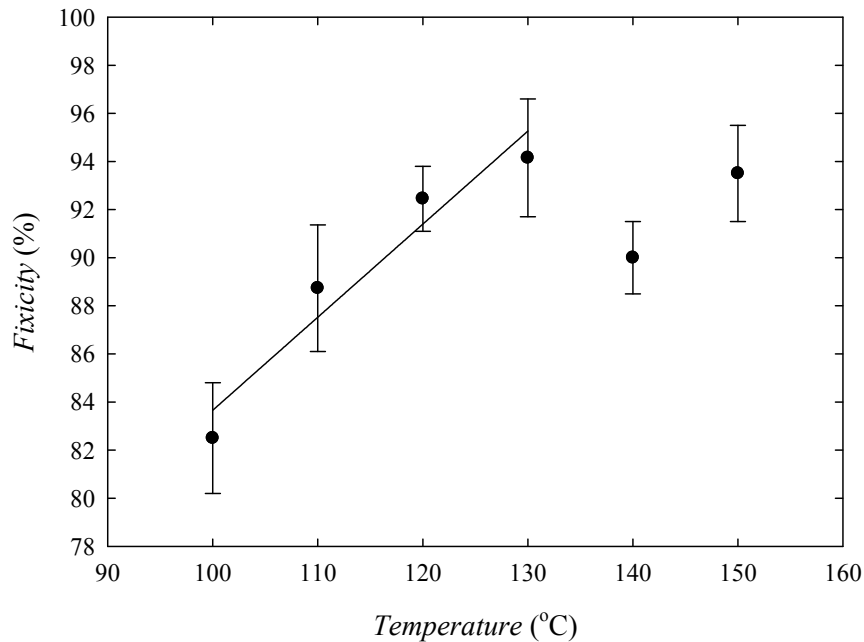


Figure 7.9. The fixicity of TVAAB5b gels compressed at strain rate 0.001 s^{-1} and strain 90 % as a function of temperature

Figures 7.10 (a) and (b) show the fixicity of the TVAAB5b gels as a function of compression stain and stain rate, respectively. More strained gel has more tendencies to

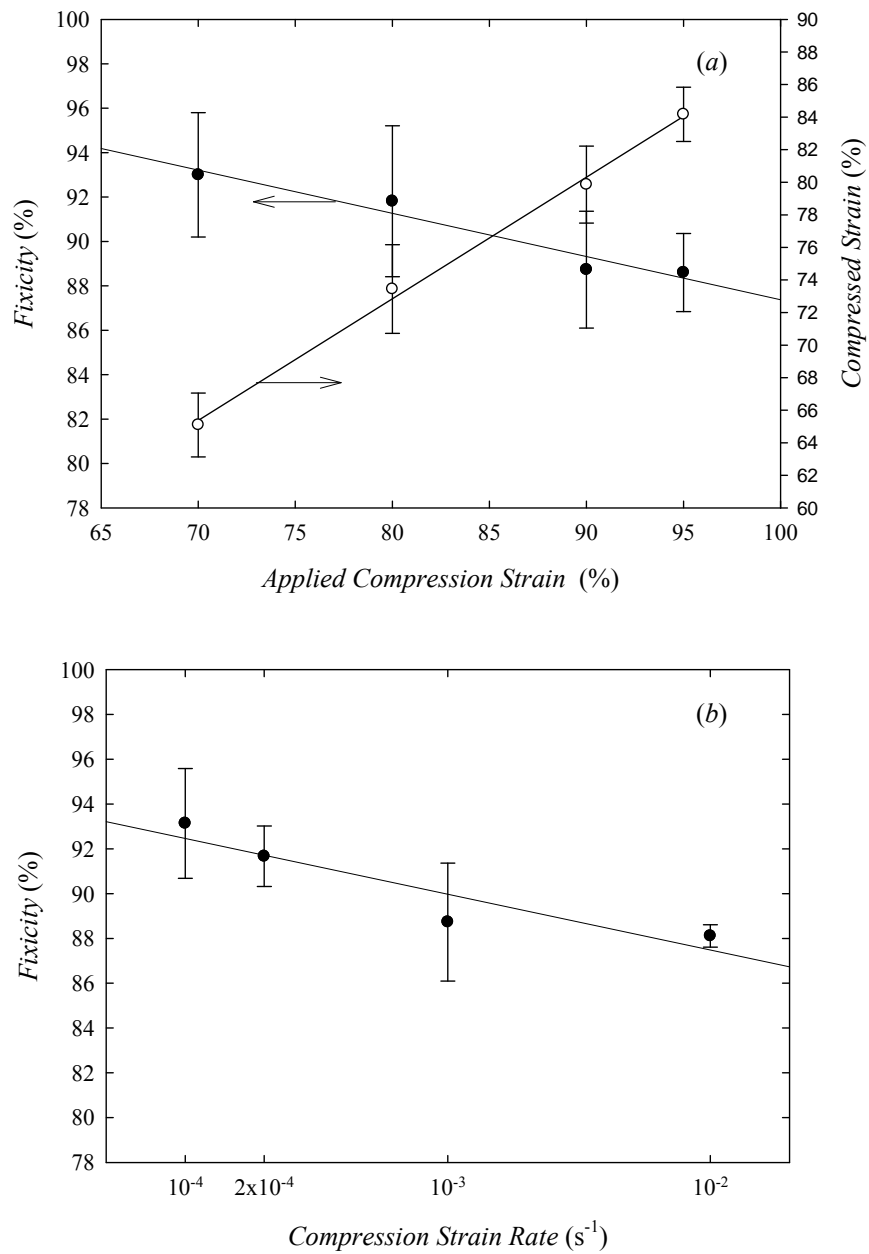


Figure 7.10. The fixicity of TVAAB5b gels compressed (a) at temperature 110 °C and strain rate $0.001 s^{-1}$ a function of strain and (b) at temperature 110 °C and strain 90 % as a function of strain rate

restore to their original conformation, thus it is natural that gels compressed with higher strains have higher restoring force, resulting in lower fixicity. However, the compressive strain values are higher for the gels compressed with higher compressive strain. Therefore, higher compressive strains are required to produce higher swelling ratios unless mechanical damage occurs in the gels.

In addition, slow compression rates give the molecular chains enough time to adjust their compressed structure and also confer more fluidity. This is understandable since the viscoelastic material has less elasticity and more fluidity at longer times and slower strain rates and more restoring force at shorter times and fast rates. Therefore, the gels compressed with high strain rates have high tendencies to restore to their original state, resulting in smaller fixicity.

7.2.4. Morphology

The TVAAB5*b* gels were initially completely transparent and became opaque when they were heated in the period before the compression processing was started. Interestingly the center part of gels became transparent again as a result of the compression. The gels compressed with a strain rate of 0.001 s^{-1} at a temperature of $110\text{ }^{\circ}\text{C}$ up to a strain of 90 % (TVAAB5*b*-2), the difference between the edge and center of the gel are clearly distinguished.

The verification of whether the compressive stress-induced crystallization of molecules in the gels and thus cause loss of transparency was undertaken using the wide angle x-ray scattering (WAXS). Figure 7.11 shows the WAXS pattern of transparent and opaque regions of the VAAB5*b*-2 gel. No change in the diffraction could be observed with an essentially amorphous halo observed for both regions, indicating no development of crystallinity inducing the opaque. .

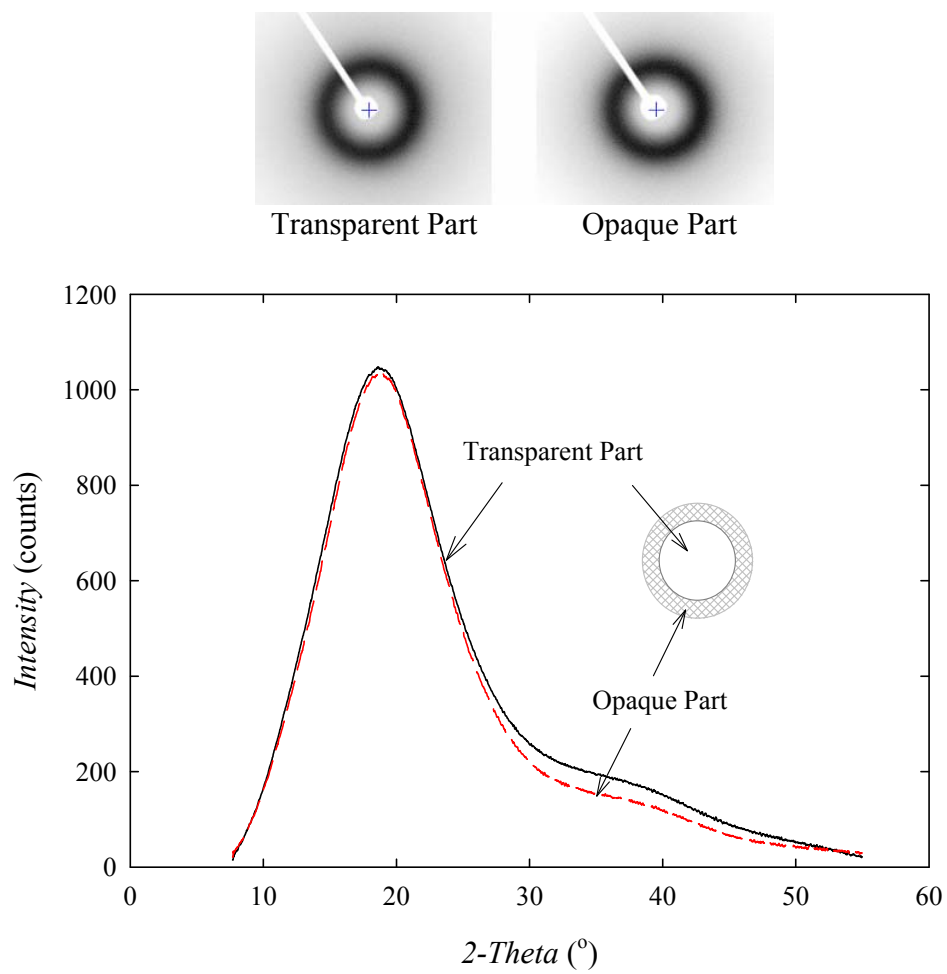


Figure 7.11. WAXS diffraction patterns and their intensity versus 2θ for the transparent and opaque parts of TVAAB5b-2 gel

However, optical microscopy (OM) (Figure 7.12) shows that there are a large number of micro-voids in the edge part of the compressed gel which causes the opacity. No voids are observed in the transparency region. As seen in Figure 7.12 (d), the voids in the compressed gels become more elliptical nearest the edge with a major axis length (l_{ma}) of 10~30 μm and minor axis length (l_{mi}) of 5 ~ 10 μm .

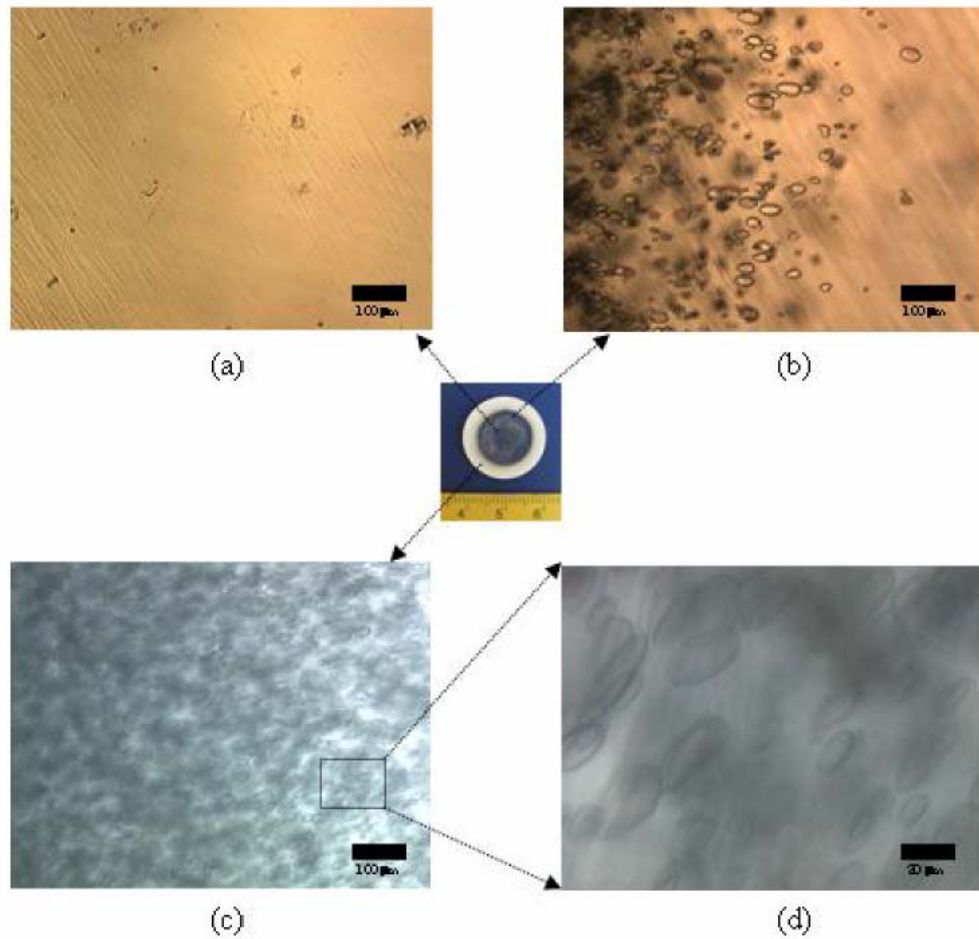
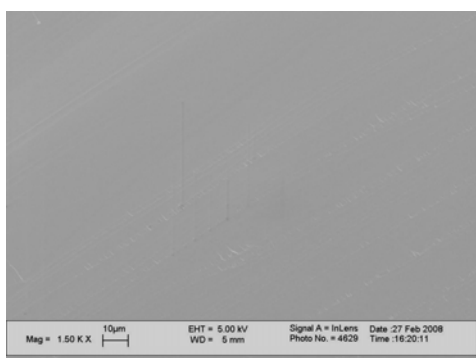


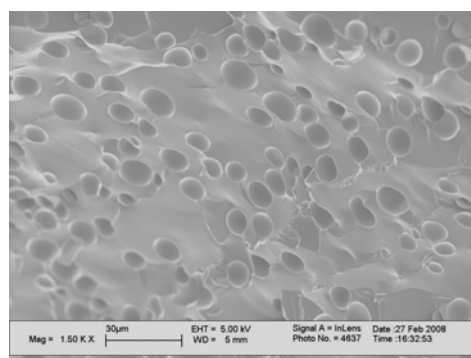
Figure 7.12. OM images of (a) center part, (b) boundary between center and edge, (c) edge part, and (d) magnification of edge part of compressed TVAAB5b-2 gel (scale bars in (a), (b), and (c) images indicate 100 μm and in (d) 20 μm)

The morphologies of the gels before and after annealing in addition to the compressed gels were confirmed by scanning electron microscopy (SEM)

Figure 7.13 shows SEM micrographs of a TVAAB5 gel before and after annealing at 110 °C for 1 hour. No voids were observed in the TVAAB5 gel before annealing. After annealing, the gel displayed a number of voids having an approximately circular shape with diameters in the range of 5 ~ 10 μm . It is thought that these voids may be created either by thermal expansion of trapped N_2 gas used in the gel synthesis [17] or formed by the nucleation and growth of the trapped N_2 gas (phase separation from glassy polymer) caused due to the thermal instability during the heating process [18]. In addition, there is also the possibility of gas formation associated with evaporation of the unreacted VP species. For the voids to form, the chains must be mobile which would only occurring at temperatures above the transition from glassy to rubbery state. However, the measurements to date are unable to distinguish between either of these three voids formation mechanisms.



(a)



(b)

Figure 7.13. SEM micrographs of a TVAAB5 gel before (a) and after (b) the annealing at 110 °C for 1 hour.

The voids trapped in the compressed gels vary across the sample. Figure 7.14 (a) shows SEM micrographs of the edge part and boundary region between edge and center

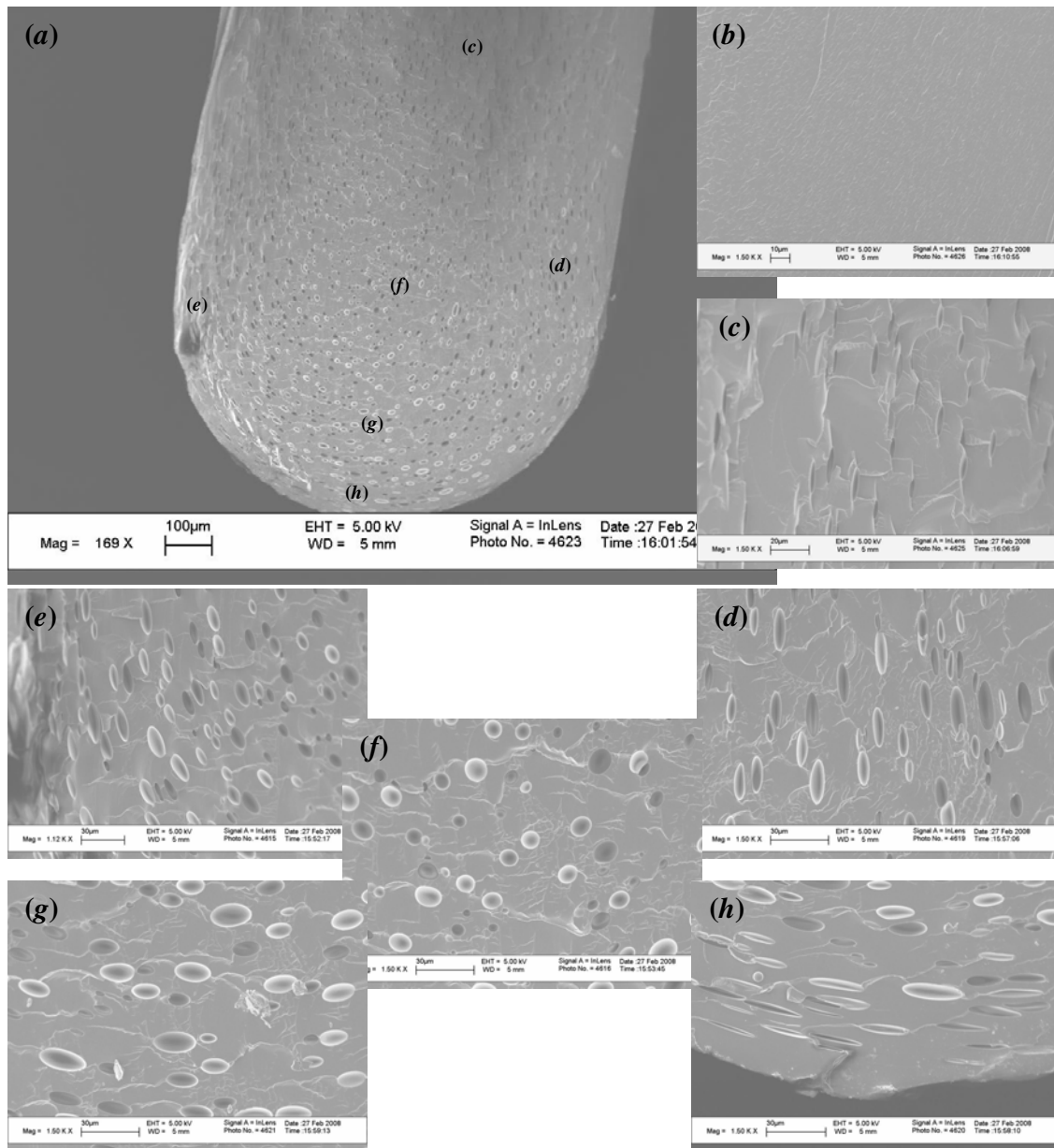


Figure 7.14. SEM micrographs of (a) cross-sectional view of compressed TVAAB5b_2 gel, (b) transparent part, (c) the boundary part between edge and center parts, and (d, e, f, g & h) the edge parts of the compressed gel

parts of the gel.

The cross-section of compressed TVAAB5b_2 gel does not have any void in the center part of the gel (Figure 7.14 (b)), which indicates that the voids are removed during the compression process. From this result, it can be thought to be due to compressive stress and radial normal stress high enough to pull out the voids in the center part.

The shape of the voids in the boundary region between the edge and center parts ((Figure 7.14 (c)) is narrow and elliptical with a l_{ma} of 5~15 μm and l_{mi} of 1~3 μm (high ellipticity). These are thought to be because high compressive stress and radial normal stress are still existed and so applied to the voids in that region.

Voids near the surface (Figures 7.14 (d) and (e)) have high ellipticity (l_{ma} (10~25 μm) and l_{mi} (1.5~5 μm)). In the region nearest the free surface (see Figures 100(h)), no voids are observed, which associated with shear stress. No compressive stress is expected in this region.

Interestingly, the voids shown in the Figure 100(f) remain circular and retain their size (5~ 10 μm) as like the state before the compression process, which indicates that no stress was applied in this region.

By observing the deformation of the voids in the compressed gel, information of stress and displacement within the gel can be inferred. Therefore, based on the observation of voids in a gel through annealing and compression processes, the creation and evolution of voids observed via the processes that have the position-dependent shape and distribution are schematically illustrated in Figure 7.15, relating with expected normal (σ_{rr} and σ_{zz}) and shear stresses (σ_{rz}) along radial direction based on the observed.

The expected σ_{rr} and σ_{zz} and σ_{rz} profile at $z=0$ of the compressed gel are drawn as a function of r in Figure 7.15.

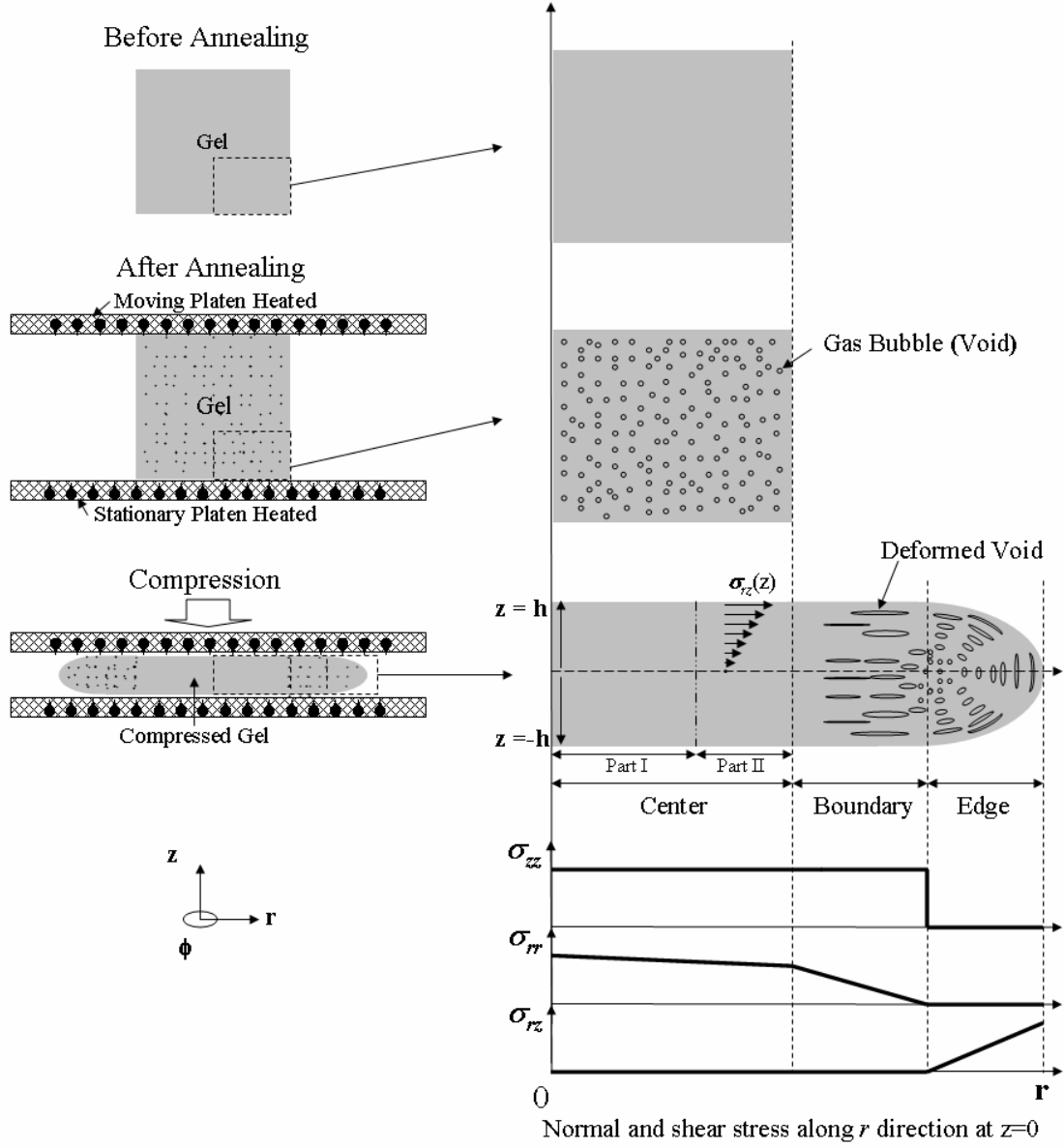


Figure 7.15. The schematics for the formation and evolution of voids in a cylindrical shape gel by annealing process and the extermination and deformation of voids in the center (part I: stationary zone and part II: moving zone), boundary and edge parts of the gel by compression process under no slip condition. The expected normal stress σ_{rr} and σ_{zz} and shear stress (σ_{rz}) profiles along the r direction at $z=0$.

In the center zone of the compressed gel, voids all disappear because the normal stress combined of σ_{zz} built up due to the applied compressive stress, with σ_{rr} developed, so that the voids are pulled away. Development of σ_{rz} having a higher magnitude with increasing distant from the center region is due to the no slip condition since no lubricant was used in the compression studies, causing the slippage of chains next to the edge as assumed (see Figure 7.8). Part I in the center zone is the stationary zone where chains do not experience distinguishable movement toward edge part and Part II is the moving zone where chains move significant toward edge apart resulting from the development of σ_{rz} .

In the boundary zone, there are the regions without and with voids. In the regions with voids, the voids gradient is seen and the voids are ellipsoidal and aligned parallel to the r direction. At $z = 0$, the voids near the edge are less ellipsoidal, which is probably because σ_{rr}/σ_{zz} decreases along the r direction toward the edge in the region and eventually becomes zero at the border point between the boundary and the edge zones, which is consistent with no change in the size and shape of voids at the point.

At the point, the shear stress σ_{rz} is probably zero and increases along z direction toward the surface because a no slip condition exists, which is confirmed by the voids near the surface more ellipsoidal. The finding of the area where no stress is applied is quite interesting and significant since this has not been reported and considered although a number of studies on the squeezing flow of polymeric materials have been reported [19-23]. Engmann and coworkers [22] reviewed and Adams and coworkers [23] reported the studies on the squeezing flow under no slip and slip conditions using compressive deformation of materials. Figure 7.16 shows some results of their work that the velocity field, velocity component fields, the pressure distribution and displacement fields obtained for compressive deformation under no slip wall boundary condition based on the theory. However, any spots which having zero stress and showing no displacement change are not shown and not found even near the free surface region. In addition, such

border between the edge and the boundary parts is not seen. These results are maybe because they used not high strain since many theories for the material deformation have been build up under small strain conditions. Contrarily, in this present study the high compression strain was used to the gel and consequently more area of free surface region was achieved. Thus information of material function in the region could be obtained.

In the edge zone (free surface area), where no σ_{zz} is applied and no σ_{rr} exists, voids are observed with higher ellipticity are aligned normal to the free surface and are found toward the edge. This confirms that shear stress σ_{rz} exists and that σ_{rz} increases toward free surface (Figures 7.14 and 7.15).

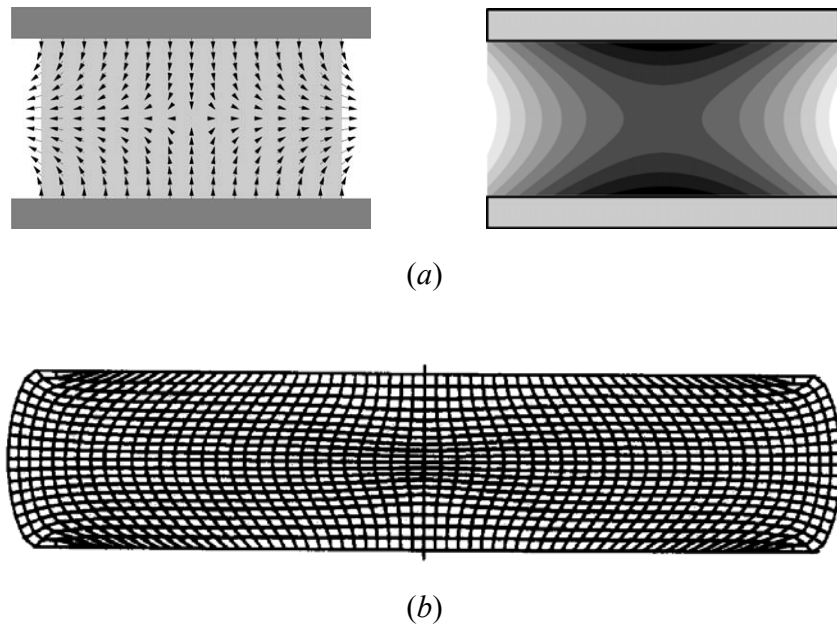


Figure 7.16. (a) Velocity field and velocity component fields (left side) and the pressure distribution (right side, darker regions corresponding to higher values of the pressure) in no slip squeeze flow according to a theoretical equation (Reproduced [22]). (b) The computed displacement fields for a 29 % compressive deformation under no slip wall boundary condition (Reproduced from [23]).

As discussed above, σ_{zz} at $z=0$ is expected to be constant in the center and boundary zone of compressed gel and tend to zero at the border point between the center and boundary zones where the free surface of gel starts (see Figure 7.15). The σ_{rr} at $z=0$ is expected to decrease gradually along the r direction in the center zone, drastic decrease in the boundary zone, which agrees well the result reported by Engmann and coworker [22] (Figure 7.16), and then become zero at the border point of the center and boundary zones (see Figure 7.15). The σ_{rz} at $z=0$ is zero in the center and boundary zones although σ_{rz} gradient are expected to be in the z direction due to the no slip condition, but increases along the radial direction in the edge zone and become so high nearest to the edge to pull away the voids(see Figure 7.15).

7.2.5. Birefringence of the Compressed Gels

Figure 7.17 shows birefringent images of a compressed TVAAB5b gel obtained at room temperature, where two different birefringent zones are observed in each image. The transparent part of the gel shows birefringence, which indicates the alignment of network chains perpendicular to the radial direction. This chain alignment developed through chain displacement and movement generated due to the various force fields induced by applying compressive force. The compressive force is responsible for the anisotropy of the gel. The light intensity pattern provides the information of the spatial distribution of the stress field. In the center of birefringence image of the compressed gel does not show the stress profile reflecting the chain flow/movement along the radial direction. This region is the core part (stationary zone) of the gel (Part I in the center zone, see Figure 7.15) where the molecular chains do not experience distinguishable chain displacement or movement toward the edge part since σ_{zz} is high and no velocity field is developed. The molecular chains in the rest part (not core part) of the gel tend to move toward the edge and aligned well, by which the voids are removed. This

observation that the deformation occurs only in neighborhood of the center is well agreed with the explanation on the squeezing flow in the report by Dealy and Wissbrun [21].

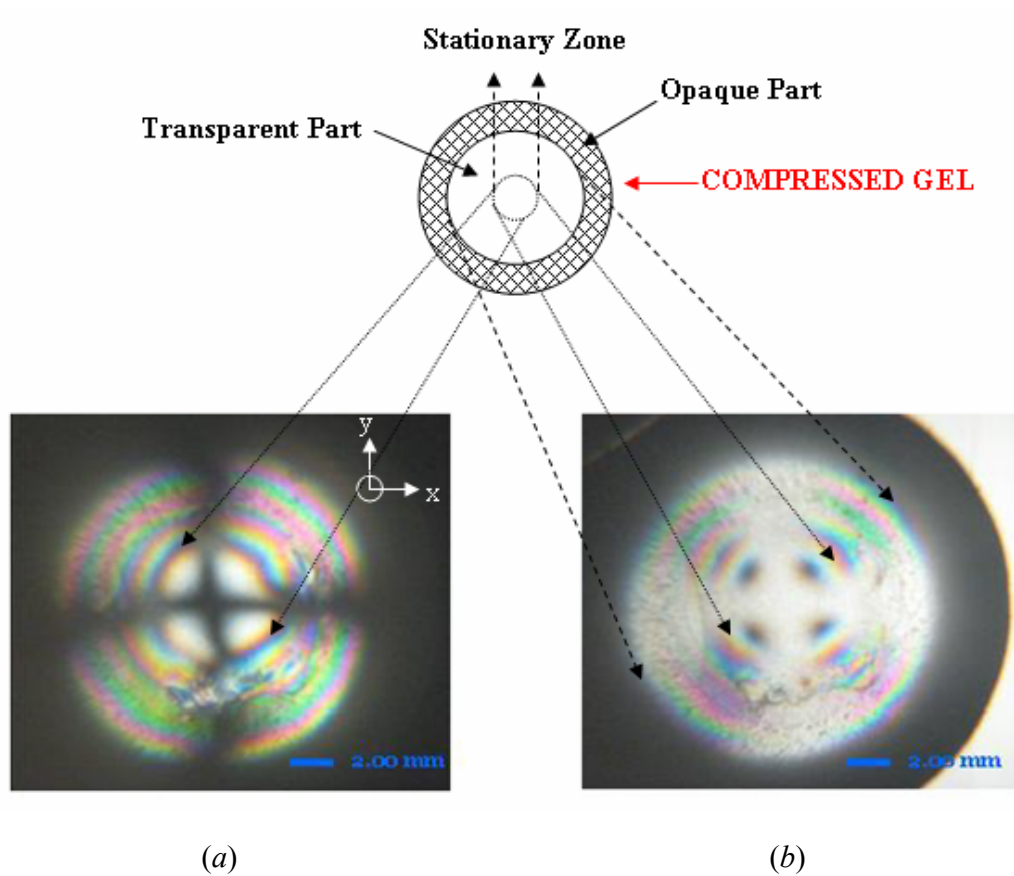


Figure 7.17. Birefringence images of the compressed TVAAB5b gel obtained between (a) crossed polarizers and (b) parallel polarizers at room temperature (light propagates along z axis) (with schematic gel with transparent and opaque parts as well as stationary zone). Arrows note the corresponding part and zone.

7.2.6. A Thermomechanic Cycle of Compression, Anisotropic Swelling and Deswelling of Gels

To understand anisotropic swelling of compressed gels, a thermomechanic cycle of compression, anisotropic swelling and deswelling of a gel is proposed as shown in Figure 7.18. During a gel goes through all the process from A to F, the gel changes its

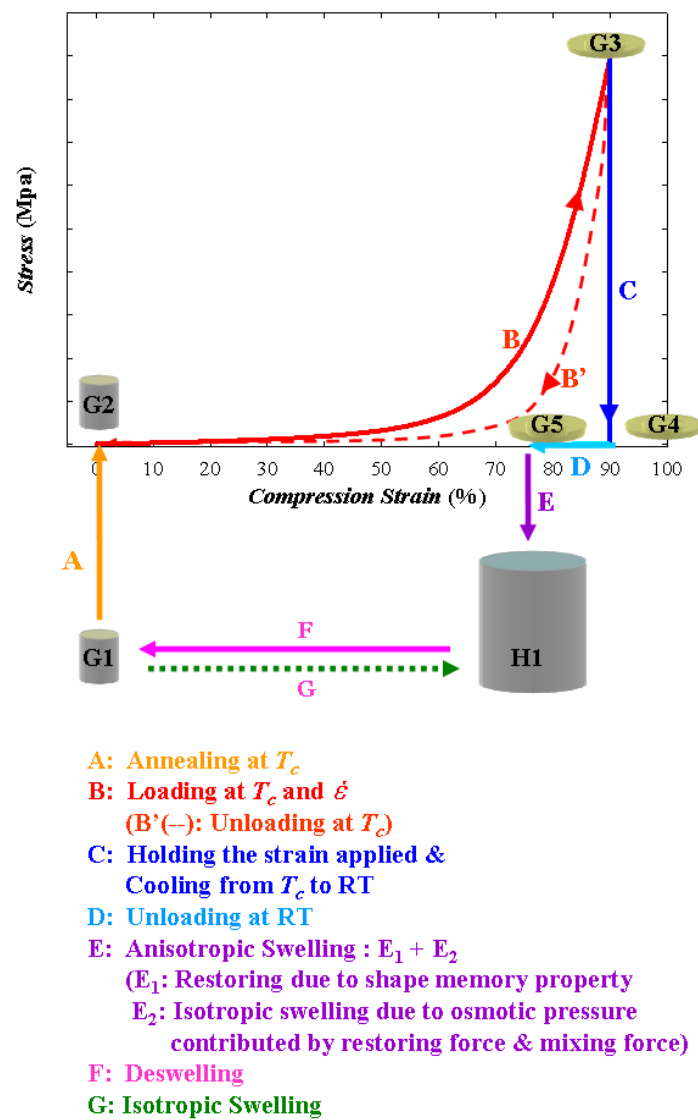


Figure 7.18. The thermomechanic cycle for compression, anisotropic swelling and deswelling of compressed gels (G1-G5 are the gels before and after the compression and H1 is the fully swollen hydrogel)

state from G1 to G5 and then finally return to the G1 again. A well dried cylindrical gel specimen (G1) is annealed (process A) at the processing temperature T_c (compression temperature) for a certain time (1 hour was used in this study) and the annealed gel (G2) is compressed by applying a set load (process B) at T_c and with chosen compression strain rate ($\dot{\epsilon}_c$) up to the set compression strain (ϵ_c). During this process, the stress initially slowly increases and then exponentially later with increasing compression strain, as expected for elastomers. If no mechanical failure occurs in the gel during the process B, when the load is removed at T_c (process B') the compressed gel (G3) would recover to the G2 state. While the G3 gel held at ϵ_c and T_c is cooled down to room temperature (RT) while holding the strain applied the G3 gel (process C). During this process, stress also decreases with cooling, to yield the compressed and cooled G4 gel in a transient state. As soon as the stain is removed (process D), the gel recovers some strain due to the shape memory property of gel giving G5 gel with only residual strain (ϵ_r). The ratio of applied strain ($\dot{\epsilon}_c$) and residual stain (ϵ_r) (the fixicity, see Section 7.2.3) was found to be affected by the compression temperature, stain and stain rate. When the G5 gel swells (process E), anisotropic swelling behavior is observed and eventually reaches a fully swollen hydrogel state (H1). It is thought that this anisotropic swelling of the compressed gel (G5) is the result of the combination of the restoring process (E_1) caused due to the shape memory property of the material and isotropic swelling process (E_2) which is due to the osmotic pressure. In other words, the compression-induced anisotropic swelling is caused by the anisotropic movement of chain molecules in the gel due to the nature of gel having shape memory and by the isotropic motion of the chains due to osmotic pressure. In principle, if the gel maintains their network structure without any thermomechanical failure in the gel during all processes (A to E), when the H1 ideally deswells (process F) the hydrogel would return to the G1 gel state. In addition, if

G1 swells isotropically (process G), H1 hydrogel would be obtained. This was confirmed by anisotropic swelling studies of various TVAAB5*b* gels.

7.2.7. Swelling Studies-Anisotropic Swelling

Figure 7.19 shows the q_{me} and q_{ve} of various TVAAB5*b* gels compressed at different T_c values. It was found that the gels compressed at 140 °C and 150 °C (TVAAB5*b*_5 and TVAAB5*b*_6 gels, respectively) become slightly yellowish color, indicating occurrence of some degradation in the gel. Accordingly although their q_{me} and q_{ve} values were found to be higher, these temperatures (140 °C and 150 °C), which are above the T_g of TVAAB5*b* gel, are not appropriate for obtaining compressed gels. This degradation might be the reason that not only the fixicity (Figure 7.9) but also the q_{He} and degree of swelling anisotropy (DSA) values (Figure 7.20) of these gels are independent of the temperature at $T_c > T_g$. Interestingly, while the q_{me} values ($\sim 74 \pm 4.3$) are not affected by the T_c , the q_{ve} values decrease from 92 ± 2.1 to 73 ± 1.6 with increasing the T_c from 100 °C up to T_g (130 °C) of TVAAB5*b* gel. It is thought that the decrease in q_{ve} is because of the decrease of density (increase in volume) which might be caused by the formation of voids in the gel during annealing process before the compression of gels. The formation of voids is easier at higher temperatures, thus more (or larger) voids are expected with increasing temperature, resulting in the reduction in the density of the gel. The density values of the TVAAB5*b* gels were determined to be 1.21~1.36 before the annealing and reduced to 0.95~1.15 after the annealing and compression process. The compression makes the gel more dense, thus the density of the gel just after the annealing is expected to be even lower than 0.95~1.15. This is contradictory to the assumption of the gel morphology under compression discussed in the section 7.2.2. The increase of density of gel by an applied compression was only assumed since the formation of voids in the gel and the effect of T_c , which often occur in the experiments, were not considered.

From the q_{me} and q_{ve} of the gels, the use of a lower T_c (here 100 °C) is thought to be most appropriate approach to obtain larger swelling gels. However with increasing T_c (at $T_c \leq T_g$), the q_{De} of the gels also slightly decreases from 1.9 ± 0.1 to 1.3 ± 0.1 and their q_{He} values increase from 14 ± 2.1 to 32 ± 5.6 . This is caused by an increase of fixicity due to a reduction in elasticity and an increase in mobility obtained at higher temperatures. Consequently the DSA values increase from 8.6 ± 0.1 to 25 ± 3.2 with increasing the T_c (at $T_c \leq T_g$). The temperatures of 110 °C and 120 °C (20°C and 10 °C below T_g) are the most appropriate temperature range to compress to maximize both the degree of swelling and the degree of swelling anisotropy. For all subsequent work, a temperature of 110 oC was used for preparing the compressed gels.

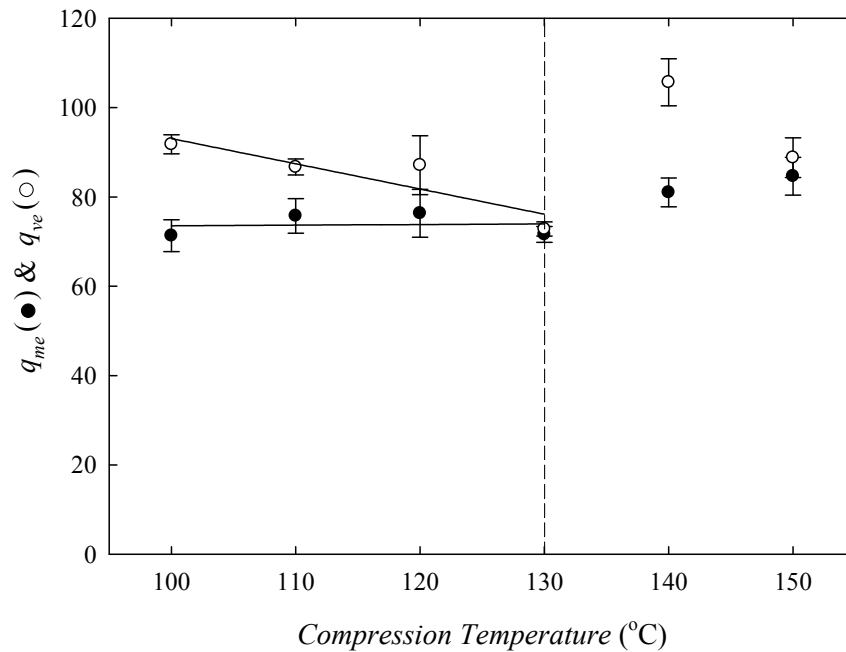


Figure 7.19. The q_{me} and q_{ve} of various TVAAB5b gels compressed at various temperatures of 100 °C, 110 °C, 120 °C, 130 °C, 140 °C and 150 °C (the used $\dot{\epsilon}_c$ and ϵ_c are 0.001 s⁻¹ and 90 %, respectively).

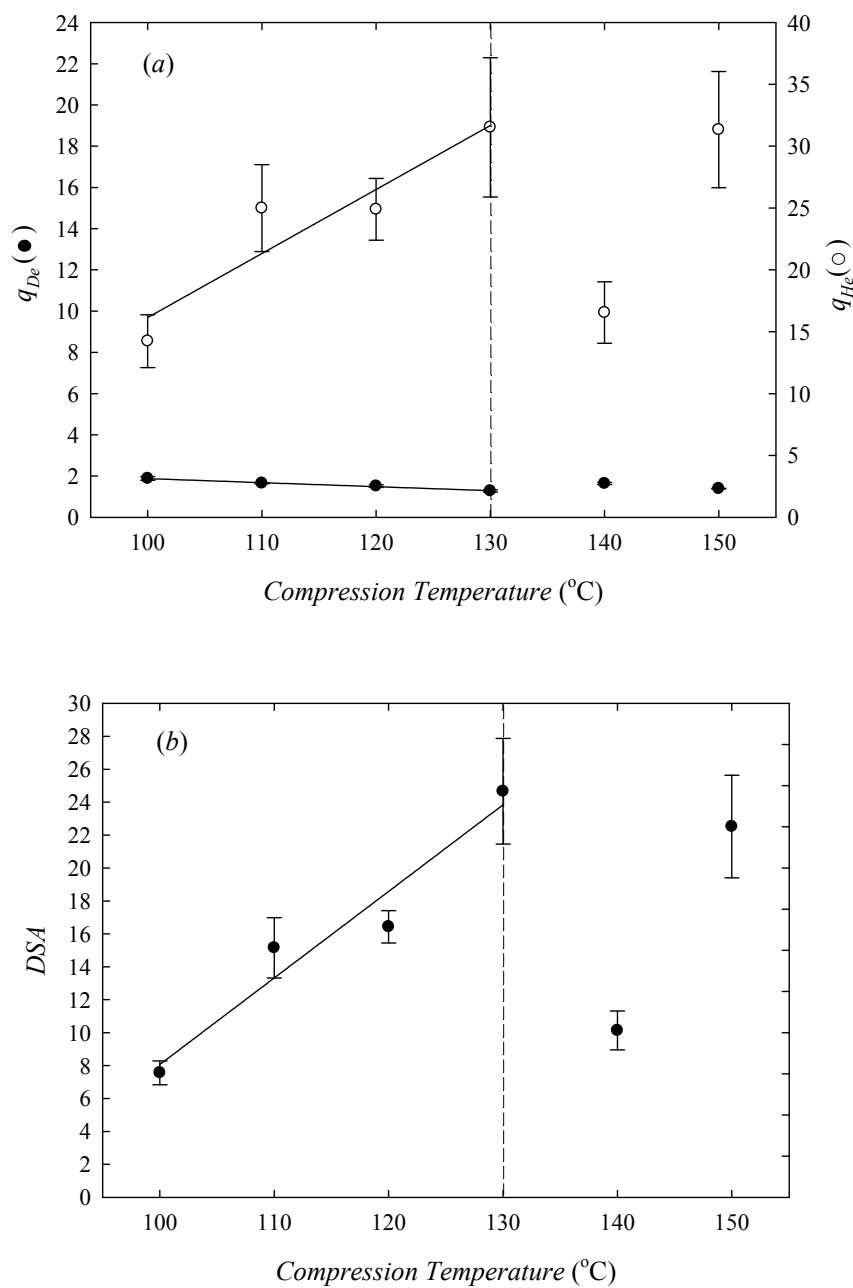


Figure 7.20. (a) the q_{De} and q_{He} and (b) $DSA (= q_{He}/q_{De})$ of various TVAAB5b gels compressed at the temperature of 100 °C, 110 °C, 120 °C, 130 °C, 140 °C and 150 °C (the used $\dot{\epsilon}_c$ and ϵ_c are 0.001 s⁻¹ and 90 %, respectively).

Figure 7.21 shows the effect of applied compression strain (ε_c) on the q_{me} and q_{ve} values of various compressed TVAAB5b gels. It is seen that the q_{me} values ($\sim 76 \pm 3.1$) of the gels are independent of the ε_c , and their q_{ve} values only slightly increase from 83 ± 2.2 to 86 ± 2.6 with increasing the ε_c from 70 % to 95 %. Although the compressed (residual) strain (ε_r) increases with increasing the ε_c , the fixicity of the gels decreases with increasing the ε_c , leading to a small increment in q_{ve} .

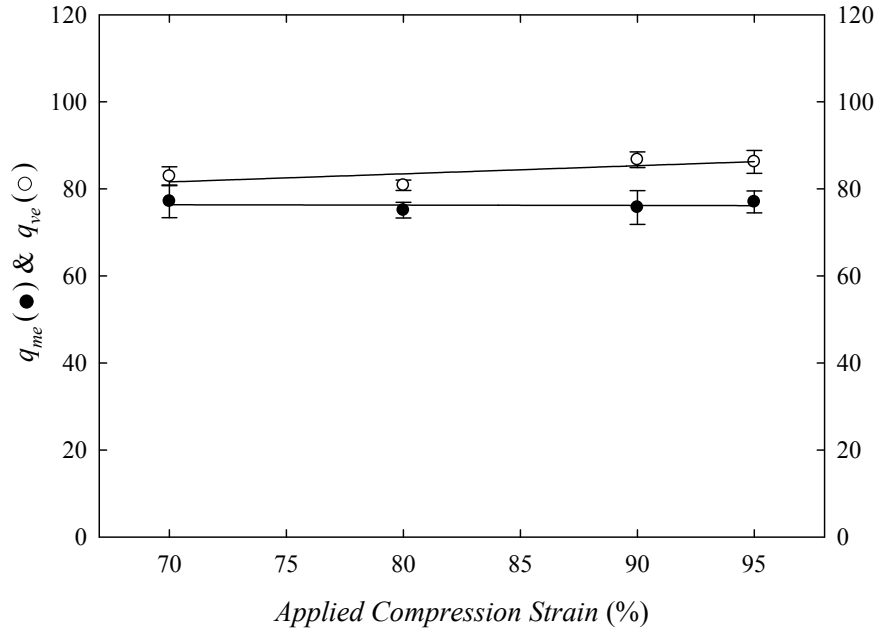


Figure 7.21. The q_{me} and q_{ve} of various TVAAB5b gels compressed up to the strain of 70 %, 80 %, 90 % and 95 % (the used $\dot{\varepsilon}_c$ and T_c are 0.001 s^{-1} and $110 \text{ }^\circ\text{C}$, respectively).

As shown in Figure 7.22 (a), the q_{He} values of the gels exponentially increase from 18 ± 2.9 to 29 ± 3.0 with increasing applied ε_c from 70 % to 95 %. At the same time, the q_{De} values slightly decreases from 1.8 ± 0.1 to 1.4 ± 0.1 , which results in larger increases of DSA from 10 ± 0.2 to 21 ± 1.1 with increasing the ε_c (Figure 7.22 (b)).

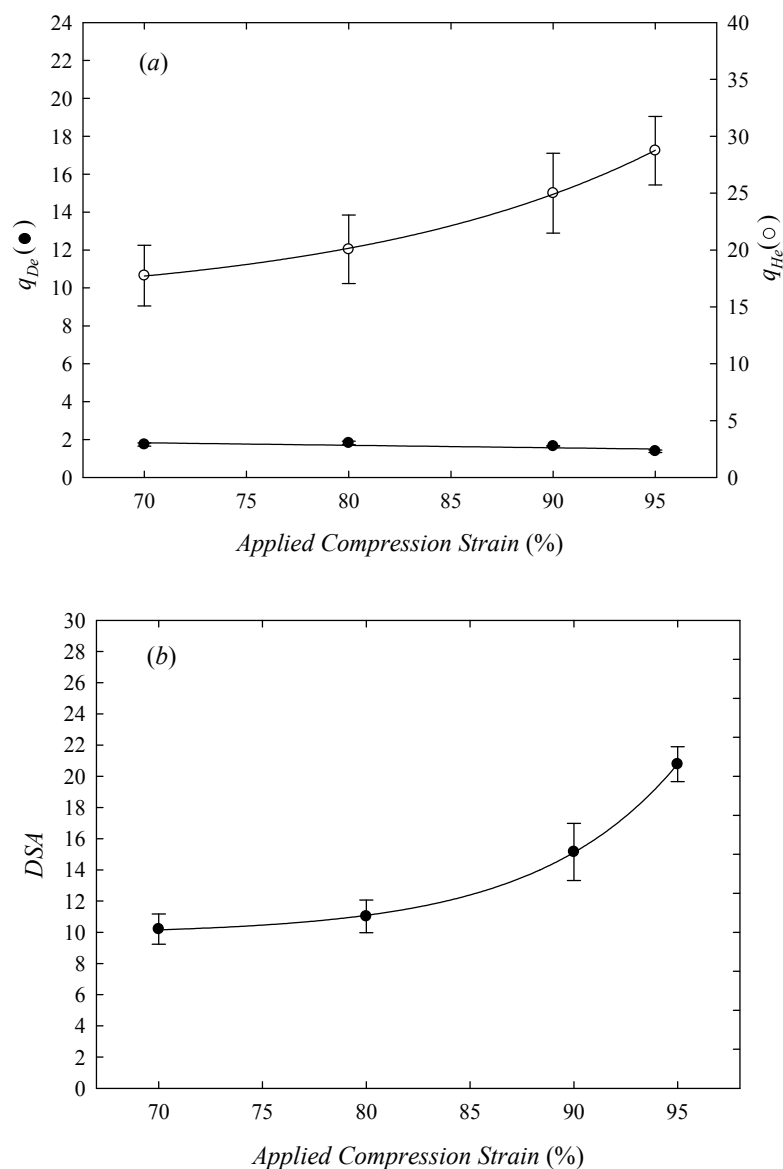


Figure 7.22. (a) the q_{De} and q_{He} and (b) DSA of various TVAAB5b gels compressed up to the strain of 70 %, 80 %, 90 % and 95 % (the used $\dot{\varepsilon}_c$ and T_c are 0.001 s^{-1} and 110°C , respectively).

The q_{me} and q_{ve} values of various TVAAB5b gels compressed with different compression strain rates ($\dot{\epsilon}_c$) of 0.0001 s^{-1} to 0.01 s^{-1} are shown in Figure 7.23. Both q_{me} and q_{ve} show a weak maxima in their values of 82 ± 3.5 and 90 ± 4.0 , respectively, at 0.0002 s^{-1} and then decrease to 73 ± 1.5 and 76 ± 8.0 , respectively, with increasing the $\dot{\epsilon}_c$. The observation of a maximum can not be accounted for at present, however the decrease in swelling degree is thought to be due to the decrease in fixicity with increasing $\dot{\epsilon}_c$ which also affect q_{He} and eventually DSA values. As shown in Figure 7.24 (a), the q_{He} values of gels decrease from 30 ± 1.0 to 20 ± 3.2 with increasing $\dot{\epsilon}_c$ from 0.0001 s^{-1} to 0.01 s^{-1} while the q_{De} values slightly increase from 1.4 ± 0.02 to 1.6 ± 0.1 , which results in a decrease of DSA from 22 ± 0.3 to 12 ± 1.4 with increasing the $\dot{\epsilon}_c$ (Figure 7.24 (b)). Slow compression can give enough time to rearrange chain conformation during the compression and produce higher fixicity and consequently higher DSA .

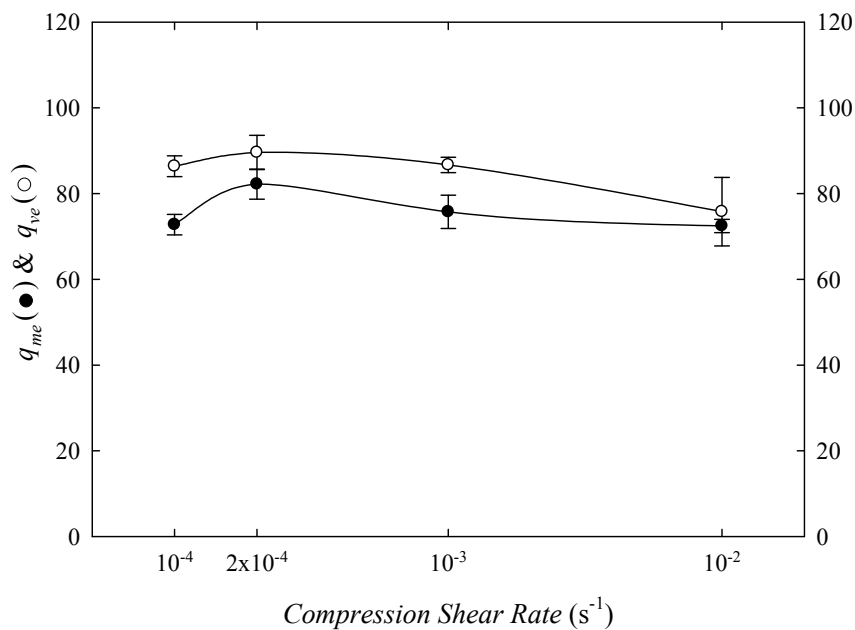


Figure 7.23. The q_{me} and q_{ve} of various TVAAB5b gels compressed with the $\dot{\epsilon}_c$ of 0.0001 s^{-1} , 0.0002 s^{-1} , 0.001 s^{-1} , and 0.01 s^{-1} (the used ϵ_c and T_c are 0.001 s^{-1} and 110°C , respectively).

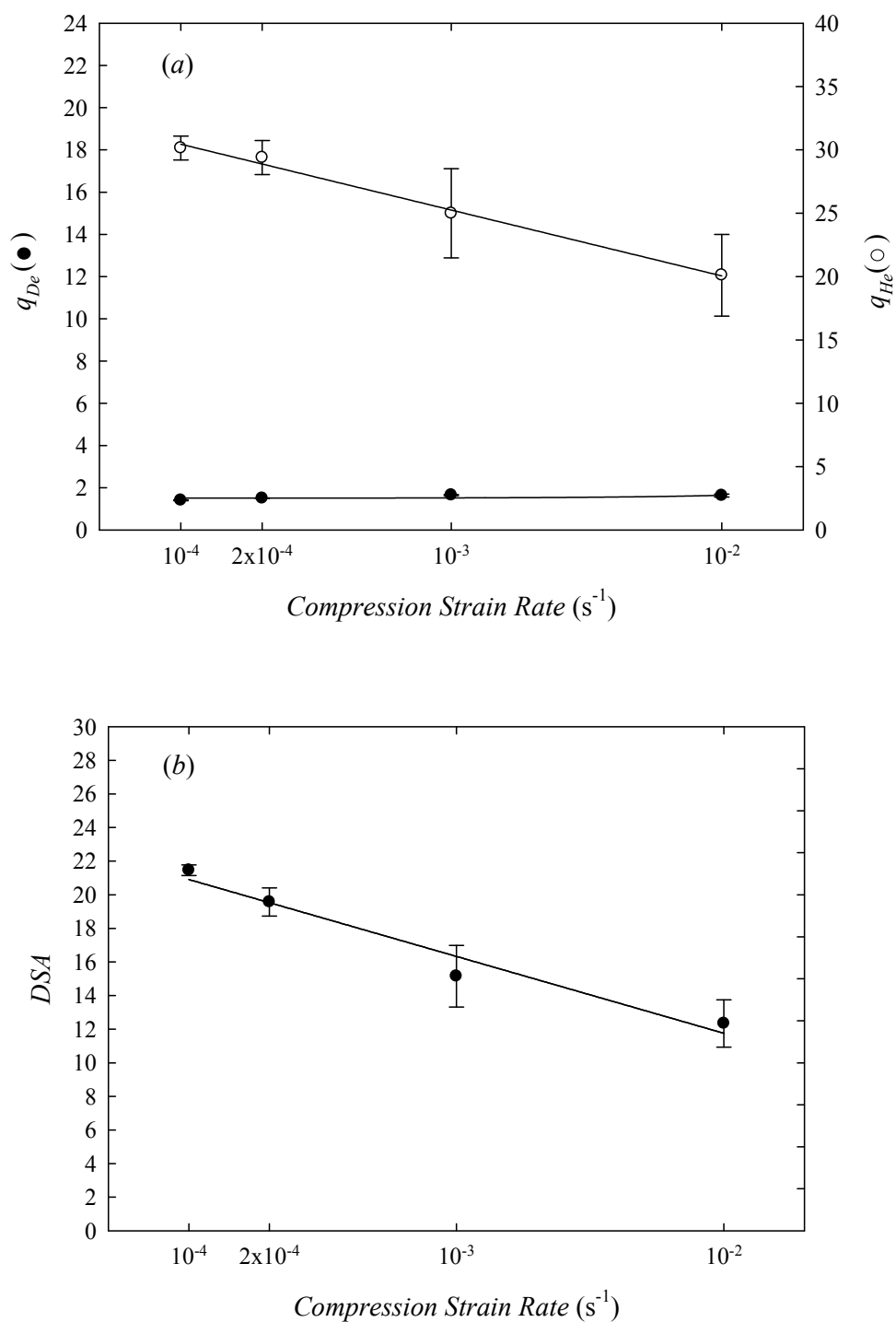


Figure 7.24. (a) the q_{De} and q_{He} and (b) DSA of various TVAAB5b gels compressed with the $\dot{\epsilon}_c$ of 0.0001 s^{-1} , 0.0002 s^{-1} , 0.001 s^{-1} , and 0.01 s^{-1} (the used ϵ_c and T_c are 0.001 s^{-1} and 110°C , respectively).

Figure 7.25 shows the TVAAB5*b* gel compressed with the smallest $\dot{\epsilon}_c$ of 0.0001 s^{-1} (the used ϵ_c and T_c are 0.001 s^{-1} and 110°C , respectively) (TVAAB5*b*_11 gel) and the same sample in the fully swollen state (the TVAAB5*b*_11 hydrogel). As seen, the thickness and diameter of the compressed gel are 0.88 mm and 21.4 mm, respectively. After swelling, the thickness and diameter of the fully swollen hydrogel became 25.7 mm and 30.5 mm. Clearly the swelling is highly anisotropic. The time to reach the fully equilibrium state (t_{max}) of the gel was 14.4 days, which is slightly longer than that of an isotropic TVAAB5*b* gel (i.e. an uncompressed gel) (~ 13.4 days). The q_{me} , and q_{ve} values of the TVAAB5*b*_11 gel are 73 ± 2.4 and 86 ± 2.4 , respectively. These values are similar to those for isotropic TVAAB5*b* gel. The q_{He} , and q_{De} values of the gel are 29.2 and 1.43, respectively, resulting in a *DSA* of 20.4

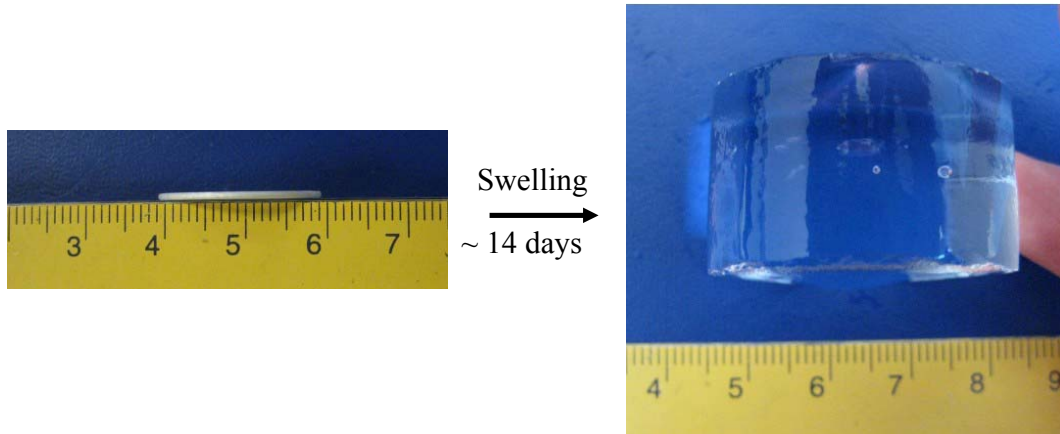


Figure 7.25. The TVAAB5*b* gel compressed with 0.0001 s^{-1} at 110°C up to 90 % (left) and the hydrogel fully swollen in saline solution at room temperature for 14.4 days (right).

The TVAAB5b gels without compression produce the q_{ve} of 91.7 ± 13.6 , which is similar values to that of compressed TVAAB5b gels ($73 \pm 1.6 \sim 92 \pm 2.1$). Comparison between q_{ve} values of the gels with and without compression shows that the gels restore almost all their original volume after the anisotropic swelling. This result is significant useful information since its DSA value is able to be expected from swelling ratios of isotropic gels and the dimensions of a compressed gel. In addition, this confirmed the processes (F and G) in the thermomechanic cycle proposed in Section 7.2.6.

The swelling rate of the compressed TVAAB5b gels was also investigated as functions of T_c (at $T_c \leq T_g$), ε_c and $\dot{\varepsilon}_c$. Figures 7.26 (a), (b) and (c) show the R_s and t_{max} of various TVAAB5b gels compressed at various T_c , with $\dot{\varepsilon}_c$ and up to ε_c . With increasing T_c , the R_s values increase from $0.0017 \pm 0.0003 \text{ min}^{-1}$ to $0.0026 \pm 0.0001 \text{ min}^{-1}$ and the t_{max} values decrease from 14.5 ± 0.10 days to 10.3 ± 0.7 days. With increasing ε_c , the R_s values slightly increase from $0.0021 \pm 0.0003 \text{ min}^{-1}$ to $0.0025 \pm 0.0003 \text{ min}^{-1}$ and the t_{max} values increase from 11.7 ± 0.15 days to 15.0 ± 1.00 days, which indicates that the effect of ε_c on R_s is not very significant compared to the T_c effect, but on t_{max} is quite noticeable. With increasing $\dot{\varepsilon}_c$, the R_s values slightly increase from $0.0019 \pm 0.00002 \text{ min}^{-1}$ to $0.0022 \pm 0.00002 \text{ min}^{-1}$ and the t_{max} values decrease from 14.4 ± 0.10 days to 12.7 ± 0.11 days. The effect of $\dot{\varepsilon}_c$ on the R_s is also less obvious than that of T_c . The effect of $\dot{\varepsilon}_c$ on the t_{max} is not as large as the effects of T_c and ε_c . The R_s values of compressed TVAAB5b gels are the range between $0.0017 \pm 0.0003 \text{ min}^{-1}$ and $0.0026 \pm 0.003 \text{ min}^{-1}$, which are almost twice smaller than those of not compressed TVAAB5b gels ($0.0052 \pm 0.009 \text{ min}^{-1}$). These results from the compression causing the densification of the gel and therefore a smaller mesh size which hinders the water diffusion into the gel at the beginning of the swelling process. The t_{max} values of the compressed TVAAB5b gels are in the range between 10.3 ± 0.7 days and 14.5 ± 0.10 days. The t_{max} values of not compressed TVAAB5b gels are 13.0 ± 0.40 days, which is in the range of values of the compressed

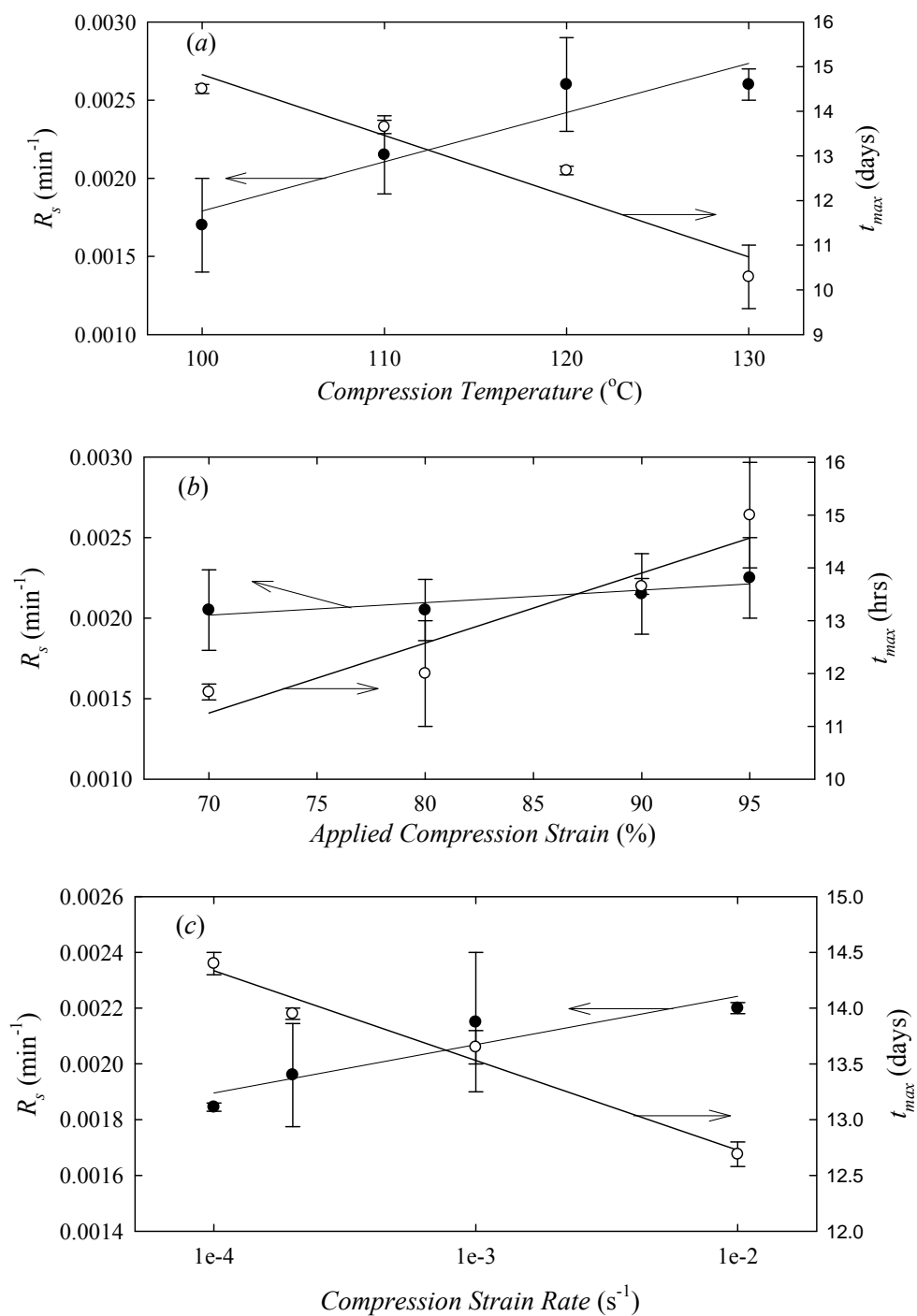


Figure 7.26. The R_s and t_{max} of various TVAAB5b gels compressed (a) at various T_c (with the $\dot{\epsilon}_c$ of 0.001 s^{-1} and up to the ϵ_c of 90 %), (b) up to various ϵ_c (with the $\dot{\epsilon}_c$ of 0.001 s^{-1} and at T_c of 110°C), and (c) with various $\dot{\epsilon}_c$ (at T_c of 110°C and up to the ϵ_c of 90 %).

gels. Only the compressed gels obtained at the T_c of 100 °C and 110 °C, with the ε_c of 90 % and 95 % and the $\dot{\varepsilon}_c$ of 0.0001 s⁻¹, 0.0002 s⁻¹ and 0.001 s⁻¹ have the longest t_{max} . Gels prepared at smaller T_c , larger ε_c and smaller $\dot{\varepsilon}_c$ have longer t_{max} and smaller R_s (except for ε_c). The processing conditions for producing longer t_{max} and smaller R_s are desirable for preparation of the gels to be used for tissue expansion. However these conditions need to be checked whether these can produce higher DSA and q_{ve} . With reference to the results of various swelling ratios, higher T_c , larger ε_c and smaller $\dot{\varepsilon}_c$ are required to obtain higher DSA , and smaller T_c and larger ε_c and smaller $\dot{\varepsilon}_c$ can yield the gels having higher q_{ve} .

Finally the modulus (G) values of the anisotropically fully swollen state of various TVAAB5b gels compressed with various conditions were determined. It was found that all G values are in the range between 3.88 ± 0.70 and 9.72 ± 0.41 kPa, which are quite similar to the values of the uncompressed TVAAB5b gels (7.50 ± 1.75 kPa) and the values of the annealed gels (7.19 ± 0.71 kPa). Clearly the gels maintain their mechanical stiffness and structure, which is consistent with having the same degree of swelling after the compression. Gels obtained at $\dot{\varepsilon} < 0.001$ s⁻¹ and $T_c > T_g$ have slightly lower G values, which might be caused by small degree of mechanical failure of the chains in gel network during the compression process.

7. 3. Conclusions

Two different gel systems producing controlled anisotropic swelling were developed via different methods.

One system is a gel with positional gradient in crosslinking density (a gradient gel), which was prepared using the photopolymerization with a gradient photomask and able to control UV irradiation intensity as a function of position. A VP/HEMA gel system (UVHIB3) was used for these studies. It was found that the degree of swelling of each section of the morphology gradient in the gel network was different, resulting in anisotropically swollen hydrogel with thickness variation. However, due to the small difference in degree of swelling between each section in the system, it was not considered to be not usable for tissue expansion.

Compressed gels were prepared with varying compression temperatures, stains, and stain rate, and show compressive stress induced anisotropic swelling behavior. The VP/AA gel synthesized by thermal polymerization (TVAAB5b) was used for these studies.

Under compression, the molecular chains in the gel network rearrange, resulting in a dense network structure. By varying compression conditions, different compressed gels with various densities, fixicity values and residual stain values were obtained. The higher stain and lower strain rate is appropriate for obtaining higher compressed strain. The temperature to be used for obtaining higher fixicity and higher compressed strain is needed to be high enough to have mobility to arrange chain structure in the network under the compression but not too high to have high entropy that cause more difficulty in having arranged structure.

The formation and deformation of voids observed during the preparation of compressed gel specimens can provide detailed information of stress or displacement distributing in materials including even the free surface area. When there is no slip

between the material and the plates, it is very difficult to obtain fundamental material functions for analyzing the material response to applied force unless some prior constitutive assumptions are made. Thus this visualization of the material deformation obtained by using the voids distributed in a gel are significant meaningful.

These compressed gels expand anisotropically in the direction opposite to the compression direction with swelling ratios 14 ± 2.1 to 32 ± 5.6 and in the radial direction with small ratio 1.3 ± 0.1 to 1.9 ± 0.1 . Consequently, the degree of swelling anisotropy (*DSA*) of compressed gels was determined to be in the range between 7.6 ± 0.7 and 25 ± 3.2 . The anisotropic swelling of compressed gels was explained with the combination of the restoring force caused by their shape memory property and osmotic pressure by proposing a thermomechanic cycles. The finding that the diameter of the compressed gels expands as well as the height shows some possibility of risk for the use of tissue expansion for specific application such as cleft repair since the radial expansion might cause pressure to the split bone during the expansion of the implant gels, however the expansion degree in radial direction is relatively quite small and in height direction is very high thus these gels are considered to be quite desirable as candidate materials for the use of tissue expansion. From the investigation of various swelling ratios, it was found that higher compression temperature (T_c), larger compressive stain (ε_c) and smaller compressions strain rate ($\dot{\varepsilon}_c$) are required to obtain higher *DSA*, and smaller T_c and larger ε_c and smaller $\dot{\varepsilon}_c$ can yield the gels having higher q_{ve} .

It was also found that the initial swelling rate of the compressed gel ($0.0017 \pm 0.0003 \text{ min}^{-1}$ and $0.0026 \pm 0.003 \text{ min}^{-1}$) is about twice slower than the not compressed gel due to denser network structure formed by the compression, however the time to reach the equilibrium swelling state is about two weeks, which means the compression only affects the initial swelling rate. The interesting finding in this study on swelling kinetics of compressed gels is that the compressed gel with higher degree of densification swell

slower (smaller R_s) and the compressed gel with higher remaining stain (ε_r) takes more time to be fully swollen. For the effect of temperature on R_s , the result that the compressed gel obtained at higher temperature produced higher R_s , was contradictory to the expectation. It is probably due to the more number of voids or larger voids formed at higher temperature. The importance of the gel network structure affecting the swelling behavior is perceived. The anisotropic swelling of a compressed gel is expected to be significantly affected by the shape memory property of the gel, the effects of fixicity (or degree of densification) and ε_r on the swelling kinetics is an understandable result.

Although the swelling ratio and kinetics of the compressed gel were controlled, the gels maintained their mechanical stiffness (3.88 ± 0.70 and 9.72 ± 0.41 kPa) after annealing and compression processes.

Based on the considerations for the desirable properties required for the gel to be applied in a specific medical application such cleft repair, the gel compressed at T_c of 110 °C up to the ε_c of 90 % with 0.0001 s^{-1} (TVAAB5b-11 gel) are determined to be most optimized system in this anisotropic swelling work.

Due to the controlled morphology of the gel by adjusting the compression conditions, the swelling ratio of compressed gels could be directionally controlled and their anisotropic swelling properties (DSA) could be controlled. Therefore, it is believed that these systematically compressed gels showing controlled stress induced anisotropic swelling can be a very good candidate for tissue or skin expansion needed in a specific application such as cleft repair.

References

- [1] Kazimierz F. Kobus., “Cleft palate repair with the use of osmotic expanders: a preliminary report”, *Journal of Plastic, Reconstructive & Aesthetic Surgery*, vol. 60, pp. 414-421, 2007.
- [2] Jason A. Burdick, Ali Khademhosseini and Robert Langer, “Fabrication of gradient hydrogels using a microfluidics/ photopolymerization process”, *Langmuir*, vol. 20, pp. 5153-5156, 2004.
- [3] N. Zaari, P. Rajagopalan, S. K. Kim, A. J. Engler, and J. Y. Wong, “Photopolymerization in Microfluidic Gradient Generators: Microscale control of substrate compliance to manipulate cell response”, *Advanced Materials*, vol. 16, pp. 2133-2137, 2004.
- [4]. Joyce Y. Wong, Jennie B. Leach, and Xin Q. Brown. “Balance of chemistry, topology, and mechanics at the cell-biomaterial interface: issues and challenges for assessing the role of substrate mechanics on cell response,” *Surface Science*, vol. 570, pp. 119–133, 2004.
- [5]. Joyce Y. Wong, Alan Veasco, Padmavathy Rajagopalan and Quynh Pham, “Directed movement of vascular smooth muscle cells on gradient-compliant hydrogels,” *Langmuir*, vol. 19, pp. 1908-1913, 2003.
- [6]. J. Hannah Lee and David Bucknall, “Swelling behaviour of hydrogels synthesized using controlled UV-initiated free radical polymerization”, *Journal of Polymer Science B: Polymer Physics*, vol. 46(14), pp. 1450-1462, 2008
- [7]. D. J. Beebe, J. S. Moore, J. M. Bauer, Qing-Yu, R. H. Liu, C. Devadoss, B. H. Jo, “Functional hydrogel structures for autonomous flow control inside microfluidic channels” *Nature*, vol. 404, pp. 588–590, 2000.
- [8]. D. L. Bihan and P. V. Zijl, “From the diffusion coefficient to the diffusion tensor” *NMR Biomed.*, vol. 15, pp. 431–434, 2002.
- [9]. Denis Le Bihan, Jean-Francois Mangin, Cyril Poupon, Chris A. Clark, Sabina Pappata, Nicolas Molko, and Hughes Chabriat, “Diffusion tensor imaging: concepts and applications”, *Journal of Magnetic Resonance Imaging*, vol. 13, pp. 534-546, 2001.

- [10]. Toyochi Tanaka, Shao-Tang Sun, and Shizue Ueno-Nishio, "Collapse of gels in an electric field", *Science*, vol. 218, pp. 467-469, 1982.
- [11]. M. E. Harmon, D. Kuckling, P. Pareek and C. W. Frank, "Photo-cross-linkable PNIPAAm copolymers. 4. Effects of copolymerization and cross-linking on the volume-phase transition in constrained hydrogel layers", *Langmuir*, vol. 19, pp. 10947-10956, 2003.
- [12]. Toyochi Tanaka, Shao-Tang Sun.; Yoshitsugu Hirokawa, Siji Katayama, John Kucera, Yoshiharu Hirose, and Takayuki Amiya, "Mechanical instability of gels at the phase transition", *Nature*, vol. 325, pp. 796-798, 1987.
- [13]. M. Swan, D. G. Bucknall, T. Goodacre, J. Meakins and J. Czernuszka, Soft Anisotropic Tissue Expander, *UK Patent*, 0600336.2, 2006
- [14]. Flory, P. J., in *Principles of Polymer Chemistry*; Cornell University Press: New York; 1969.
- [15]. James E. Mark and B. Erman, *Rubberlike Elasticity: A Molecular Primer*, John Wiley and Sons, Inc, 1988.
- [16]. Jasmeet Kaursoin, Ashwini K. Agrawal, "Melt spun thermoresponsive shape memory fibers based on polyurethanes: Effect of drawing and heat-setting on fiber morphology and properties", *Journal of Applied Polymer Science*, vol. 103, pp. 2172-2182, 2007.
- [17]. Kelyn A. Arora, Alan J. Lesser and Tomas J. McCarthy, "Compressive behavior of microcellular polystyrene foams processed in supercritical carbon Dioxide", *Polymer Engineering and Science*, vol. 38, pp. 2055-2062, 1998.
- [18]. M. Wessling, Z. Borneman, Th. Van Den Boomgaard and C. A. Smolders, "Carbon dioxide foaming of glassy polymers", *Journal of Applied Polymer Science*, vol. 53, pp. 1497-1512, 1997.
- [19]. R. Byron Bird, Robert C. Armstrong, and Ole Hassager, *Dynamics of Polymeric Liquids: Vol .1 Fluid Mechanics*, John Wiley & Sons Inc., 1987.
- [20]. Christopher W. Macosko, *Rheology: Principles, Measurements, and Applications*, Wiley-Vch Inc., 1994.

- [21]. John M Dealy and Kurt F. Wissbrun, *Melt Rheology and Its Roles in Plastics Processing: Theory and Application*, Van Nostrand Reinhold, 1990.
- [22]. Jan Engmann, Colin Servais, and Adam S. Burbidge, "Squeeze flow theory and applications to rheometry: A review", *J. Non-Newtonian Fluid Mech.*, vol. 132, pp. 1-27, 2005.
- [23]. M. J. Adams, I. Aydin, B. J. Briscoe, and S. K. Sinha, "Finite element analysis of the squeeze flow of an elasto-viscoplastic paste material", *J. Non-Newtonian Fluid Mech.*, vol. 71, pp. 41-57, 1997.

CHAPTER VIII

CONCLUDING REMARKS AND FUTURE WORK

In this dissertation work, development of an anisotropic swelling hydrogel system to use in reconstructive surgeries such as the closure of cleft palate defects and syndactyly repair was accomplished by systematically controlling the degree, rate, and direction of gel swelling. Since a hydrogel inserted in the body expands by absorbing aqueous body fluid and ultimately induces the tissue expansion, the choice of gel system and the control of such swelling behaviors through the manipulation of network structure are significantly essential keys for development of these devices. Using a neutral gel system (VP/HEMA copolymeric gel) and an ionizable gel system (VP/AA copolymeric gel), prepared using thermal and UV-initiated polymerization, various approaches to control swelling degree and rate were studied. These resulted in not only understanding how to control the parameters that control such swelling behavior but also obtaining an optimized gel system with large degree of swelling to minimize the number of surgical operations and with slow enough swelling to avoid skin cell necrosis while maintaining their mechanical integrity. Two methods to induce large scale anisotropic swelling of hydrogels were investigated. Preparation of morphology-gradient VP/HEMA hydrogel system using unique photomasks was not successful. The VP/AA gel system with the most optimal properties was utilized and compressed. Significant anisotropic swelling could be obtained by systematically controlling compression temperature, strain and strain rate, which is due to the controlled anisotropy of network morphology. Therefore this system is believed to be good candidate for tissue or skin expansion. Although an anisotropic swelling hydrogel system for reconstructive surgeries such as the cleft palate repair was successfully achieved, further work is required in developing these hydrogels before such devices can be used in medical applications.

Before the hydrogels are used in human body their biocompatibility needs to be tested. Both cytotoxic and monocyte differentiation tests need to be carried out for *in vitro* tests. MTT assay can be used for determining the cytotoxicity of the hydrogels. In these assays, cells are seeded into a hydrogel, which has been incubated in cell culture medium with serum before the seeding. The cells seeded in the hydrogel would be stained by (3-(4,5-dimethylthiazol-2-yl)-2,5-diphenyltetrazolium bromide) (MTT). The MTT molecules yield a purple color in the presence of viable cells. The viability of cells in the hydrogel can be visualized using confocal microscopy. To obtain information of inflammatory cell response to a hydrogel, monocyte differentiation test can be used. When the monocyte cells seeded in the hydrogel differentiate and turn into normal macrophages and dendritic cells with proper morphology not into giant cells, the hydrogel can be considered as a bio-benign material. For *in vivo* tests, a hydrogel would be inserted under subcutaneous layer in mice or rabbits for several weeks. Histology of the tissue surrounding the hydrogel is then performed after euthanizing the animals. Cytotoxic and leukocyte assays would provide the necessary information of the interaction between cells and the hydrogels and any inflammatory cell response to the hydrogels identified.

Moreover, although the highly anisotropic swelling hydrogel was successfully developed by systematic controlling the compression parameters, this approach requires further studies. By establishing the relationship between compression processing parameters and characteristic parameters of swelling or morphologies of gel under compression, the key parameters would be quantified and eventually the desired properties can be estimated prior to series of experiments. The use of other hydrogel system would be helpful to found these relationships.

APPENDIX A

DEVELOPMENT OF PHOTOMASKS

Several photomasks were prepared to manipulate the UV irradiation intensity, and thereby control crosslinking density and morphology in the gels. The photomasks were made of carbon-printed PET transparency films and the density of the carbon layer (darkness) printed on the film varied to alter the UV transmission intensity from 0 to 100 % as shown in Figure A1. UV transmission intensities for the photomasks used in this work listed in Table A1. The UV transmittance through the photomasks depends on the darkness. The transmittance (T) was calculated by the relationships; $A = 2 - \log_{10}(T \times 100) = -\log I_l/I_0$, where A is the absorbance and I_0 & I_l is the light intensity of incident light and after passing the medium material. Figure A2 shows the UV spectra of Irgacure 615 photoinitiator, monomer mixture of VP/HEMA, standard slide glass, and photomasks A-E. To excite a photo-initiator (a UV sensitive compound and usually including a chromophore) and create initiator radicals able to initiate the polymerization, the photo-initiator needs to absorb the UV light. Although the Irgacure 651 possesses absorption peaks (λ_{max}) at 295 nm and at 340 nm as shown in Figure A2, it will only

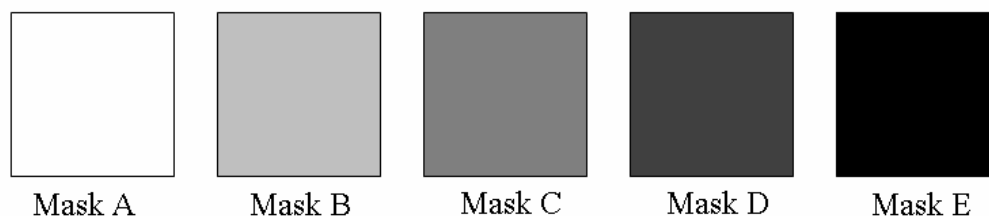


Figure A1. Various photomasks with different UV transmittance from 0 % to 100 % (from Mask E to Mask A)

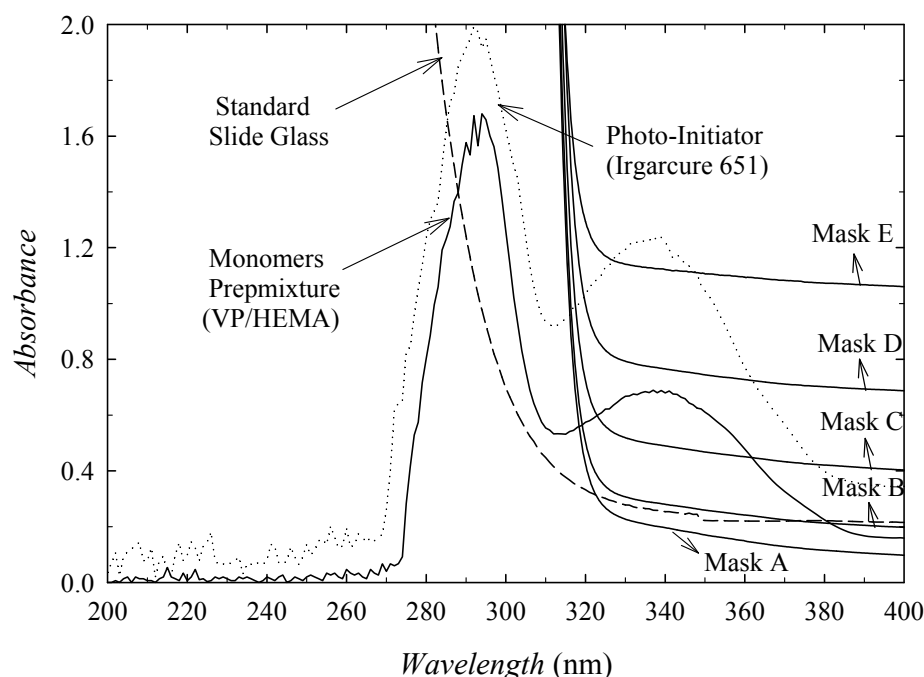


Figure A2. UV spectra of photoinitiator (Irgacure 615), monomer mixture of VP/HEMA, standard slide glass, and photomasks A-E.

absorb in the range of the wavelengths (λ) above 320 nm since a photomasks absorbs almost all incident UV light at the λ below 320 nm. Consequently, the transmittance of photomasks at the wavelength $\lambda = 340$ nm (λ_p) was determined for obtaining UV intensity irradiating for the polymerization using UV spectroscopy. The photomasks used for polymerizing the VP/HEMA and VP/AA gels were prepared by the process explained above. The UV transmittance values through the photomasks and the obtained UV intensity irradiating the pregel mixture for the gelation are shown in Table A1. Discrete Gradient photomasks (DGrad-Masks), which were developed to locally control the UV irradiation intensity for preparing the gradient gels, have gradient darkness as shown in Figures A3 and A4. Each section of the gradient allows different amount of

Table A1. Characteristics of the photomasks used

Photomask code	Transmittance of Photomask (%)	UV Intensity Irradiated (mW/cm^2)
Mask 1	0.2380	0.0075
Mask 2	0.9200	0.0530
Mask 3	0.476	0.2380
Mask 4	1.840	0.9200
Mask 5	3.250	1.6300
Mask 6	5.340	2.6500
DGrad-Mask1	Discrete Gradient	Discrete Gradient (0.2380, 0.9200, 1.6300, 2.6500)
DGrad-Mask2	DGRAD	Discrete Gradient (0.2380, 2.6500)

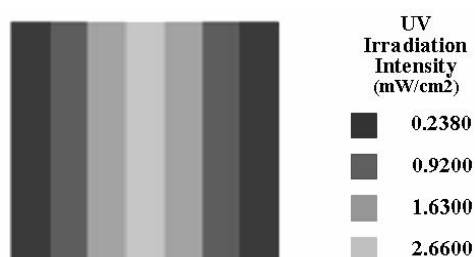


Figure A3. The schematic of the discrete gradient photomask (DGrad-Mask1) developed in our lab and the UV irradiation intensity through each section in the mask



Figure A4. The schematic of three discrete gradient photomask (Dgrad-Mask2) developed in our lab and the UV irradiation intensity through each section in the mask

UV light transmittance. Unlike the most results [1], it was found that with increasing UV intensity the equilibrium swelling ratio increases due to the more number of dangling chains that occur at faster reaction caused by higher UV intensity (see Section 4.1.6.2, [2]). Thus, to obtain the fully swollen hydrogels with oval shape, as like the DGrad-Mask1 and 2, the middle part and the edge part of the photomasks were designed to allow higher and lower UV irradiation respectively to the pregel mixture during the gelation.

References

- [1]. Joyce Y. Wong, Alan Veasco, Padmavathy Rajagopalan and Quynh Pham, "Directed movement of vascular smooth muscle cells on gradient-compliant hydrogels," *Langmuir*, vol. 19, pp. 1908-1913, 2003.
- [2]. J. Hannah Lee and David G. Bucknall, "Swelling behaviour of hydrogels synthesized using controlled UV-initiated free radical polymerization", *Journal of Polymer Science B: Polymer Physics*, vol. 46(14), pp. 1450-1462, 2008.

APPENDIX B

SPATIAL DISTRIBUTION OF SELF-DIFFUSION COEFFICIENTS (D_s) OF WATER IN GRADIENT HYDROGELS

To verify the spatial variation in the crosslinking density of the gradient gel, DGrad3-UVHIB3 gel was prepared with a designed photomask Dgrad-Mask2 (Figure A4) with three discrete gradients as shown schematically in Figure B1. Anisotropic swelling associated with a controlled morphology was investigated by monitoring the self diffusion coefficient (D_s) images in the fully swollen DGrad3-UVHIB3 hydrogel along the x, y, and z directions ($D_s(x)$, $D_s(y)$ and $D_s(z)$ images (x, the direction of along the gradient)) using magnetic resonance imaging (MRI) techniques.

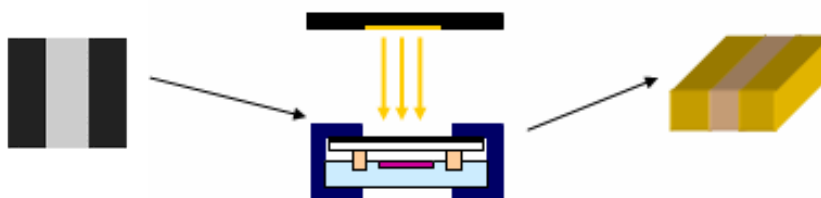


Figure B1. Schematic diagram of DGrad3-UVHIB3 gel (right) obtained by UV initiated polymerization using the photomask Dgrad-Mask2 (left).

The mobility of solvent molecules in a hydrogel has been monitored using MRI techniques [1, 2]. The mobility is very dependent on its environment created by the morphology of hydrogels, resulting in morphology dependent D_s . The three positional

D_s (called diffusion tensors $D_s(x)$, $D_s(y)$, and $D_s(z)$) along the principal directions (x, y, and z)) (see Figure B2) can be monitored using MRI technique [3, 4]. Moseley and coworkers [5] reported that the D_s in the parallel direction ($D_{s\parallel}$) and the D_s orthogonal to the gradient direction ($D_{s\perp}$) were determined using MRI and the degree of anisotropy ($D_{s\parallel}/D_{s\perp}$) [5] could be also calculated for hydrated materials with anisotropic morphology.

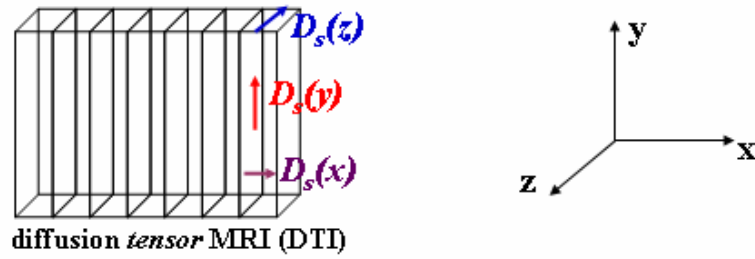


Figure B2. The D_s values of water in material having anisotropic structure along the x, y, and z directions ($D_s(x)$, $D_s(y)$ and $D_s(z)$, respectively) determined by diffusion tensor MRI (DTI, Redrawn from [3]).

The $D_s(x)$, $D_s(y)$, and $D_s(z)$ MRI images in DGrad3-UVHIB3 gel were observed in both cross-sectional and planar views using MRI where diffusion was encoded with gradients during a stimulated echo sequence. The $D_s(y)$, and $D_s(z)$ images did not show any gradient with respect to D_s . However, diffusion coefficient gradient was observed in $D_s(x)$ image (see Figure 7.5 and Section 7.1.2), which indicates crosslinking density gradient. This is probably due to limitations on the water mobility which is caused by the morphological variation in the gradient direction (x).

References

- [1]. J. L. Koenig, Spectroscopy of Polymers: Chapter 11. NMR Imaging of Polymeric Materials, American Chemical Society, Washington DC, 1992.
- [2]. N. Tanaka, S. Matsukawa, H. Kurosu and Isao Ando, "A study on dynamics of water in crosslinked poly (N- sopropylacrylamide) gel by NMR spectroscopy" *Polymer*, vol. 39, pp. 4703-4706, 1998.
- [3]. D. L. Bihan and P. V. Zijl, "From the diffusion coefficient to the diffusion tensor" *NMR Biomed.*, vol. 15, pp. 431–434, 2002.
- [4]. Denis Le Bihan, MD, PhD, Jean-Francois Mangin, PhD, Cyril Poupon, PhD, Chris A. Clark, PhD, Sabina Pappata, MD, PhD, Nicolas Molko, MD, and Hughes Chabriat, MD, "Diffusion tensor imaging: concepts and applications", *Journal of Magnetic Resonance Imaging*, vol. 13, pp. 534-546, 2001.
- [5]. M. E. Moseley, Y. Cohen, J. Kucharczyk, J. Mintorovitch, H. S. Asgari, M. R. Wendland, J. Tsuruda, and D. Norman, "Diffusion-weighted MR imaging of anisotropic water diffusion in cat central nervous system," *Radiology*, vol. 176, pp. 439-446, 1990.